University of Bath

PHD

Concentration and recovery of nitric acid via electro-membrane processes

Robbins, Brian J.

Award date:
1996

Awarding institution:
University of Bath

Link to publication

Alternative formats
If you require this document in an alternative format, please contact:
openaccess@bath.ac.uk

Copyright of this thesis rests with the author. Access is subject to the above licence, if given. If no licence is specified above, original content in this thesis is licensed under the terms of the Creative Commons Attribution-NonCommercial 4.0 International (CC BY-NC-ND 4.0) Licence (https://creativecommons.org/licenses/by-nc-nd/4.0/). Any third-party copyright material present remains the property of its respective owner(s) and is licensed under its existing terms.

Take down policy
If you consider content within Bath's Research Portal to be in breach of UK law, please contact: openaccess@bath.ac.uk with the details. Your claim will be investigated and, where appropriate, the item will be removed from public view as soon as possible.

Download date: 05. May. 2023

Concentration and recovery of nitric acid via electro-membrane processes

submitted by Brian J Robbins
for the degree of PhD
of the University of Bath
1996

COPYRIGHT

Attention is drawn to the fact that the copyright of this thesis rests with its author. This copy of the thesis has been supplied on condition that anyone who consults it is understood to recognise that its copyright rests with its author and that no quotation from the thesis and no information derived from it may be published without prior written consent of the author.

This thesis may not be consulted, photocopied or lent to other libraries without permission of the author for three years from the date of acceptance of the thesis.

UMI Number: U602151

All rights reserved

INFORMATION TO ALL USERS
The quality of this reproduction is dependent upon the quality of the copy submitted.

In the unlikely event that the author did not send a complete manuscript
and there are missing pages, these will be noted. Also, if material had to be removed,
a note will indicate the deletion.

UMI U602151
Published by ProQuest LLC 2014. Copyright in the Dissertation held by the Author.
Microform Edition © ProQuest LLC.
All rights reserved. This work is protected against
unauthorized copying under Title 17, United States Code.

ProQuest LLC
789 East Eisenhower Parkway
P.O. Box 1346
Ann Arbor, MI 48106-1346

UNIVERSITY OF BATH
LIBRARY
34 - 7 JAN '97
5107985

Acknowledgements

The list of people who have assisted my research is long and so I apologise in advance for any omissions from this page - thank you.

Firstly, I would like to thank the DRA Chemical Process Research for funding this project, particularly Greville Bagg and Anthony Arber for inspiring my work since I first met them as a budding Chemical Engineer in 1990.

I am sincerely grateful to my three supervisors: Stan Kolaczkowski, Robert Field and Tony Lockett who have given me their full support throughout my time at Bath. They have advised me in all areas of my work from practical to advanced theoretical and on to the strategies and schemes of Chemical Engineering research!

I am indebted to John Hammond who, as a consultant Electrochemical Engineer, has acted as my personal mentor throughout this research, and whose role rapidly developed from one of teacher to that of learned colleague willing to discuss the finer points of theory pertinent to my work.

I would also like to thank all the technical staff under the helm of Mac Forsyth, Mike Lock the University Glass-blower and those in the inter-schools workshop lead by Les Steele.

Finally, I would like to thank my family and especially Karen for their tremendous support without which this thesis would not have been possible.

Summary

Acid recovery technology is needed to be able to concentrate nitric acid back to a form which can re-enter the dinitrogen pentoxide production cycle. Established extractive distillation processes are unattractive for low volume applications and so the model requirement for this post graduate research was thus to extract and concentrate the nitric acid from a nominal 5 wt% spent acid stream and to investigate the characteristics and potential of electro-membrane processes.

A literature search into electro-membrane processes and their application to acid processing found that little/no process-based research had been undertaken in this area. Consequently it was decided to construct a laboratory pilot rig capable of being configured for both electrodialysis and electro-electrodialysis in a flow-through cell operating in batch recirculation mode. Experimental runs were undertaken using a two-compartment electro-electrodialysis configuration and the study focused on anion exchange membranes. At the low pH values and the relatively high current densities employed in the experiments, it was found that nitrate reduction at the cathode could be significant.

A trade-off was observed in membrane performance in that a decrease in current efficiency appeared to be coupled with a decrease in the water flux. This interesting relationship was the focus of much theoretical work which lead to the proposal of a consolidated proton leakage and water flux theory. Further understanding of membrane performance was gained from detailed analysis of the experimental data. This knowledge could be used either to develop new membranes or to optimise the performance of a process based on existing membrane capabilities. Avenues for further research in order to fully understand process performance have been revealed and this work should lead to the increased possibility of an industrially viable process.

Table of contents

Acknowledgements ii

Summary iii

Table of contents iv

Nomenclature xiii

List of figures xviii

Executive summary xxv

1. Introduction to electromembrane processes 2

1.1 Background to project 2

1.2 Ion exchange membranes 3

1.2.1 History and applications 3

1.2.2 Functionality and operation 5

1.2.2.1 Fixed and mobile ions 6

1.2.2.2 Effect of Donnan potential 7

1.2.2.3 Effect of osmotic pressure 8

1.3 Ion exchange membrane process descriptions 9

1.3.1 Diffusion dialysis (D) 9

1.3.2 Electrodialysis (ED) 10

1.3.3 Electro-electrodialysis (EED) 12

1.4 Basic electromembrane theory 14

1.4.1 Ions in solution 14

1.4.1.1 Solvation shells 14

1.4.1.2 Proton tunnelling 16

1.4.1.3 Proton leakage 17

1.4.2 Fundamental electrochemistry 18

1.5 Framework for research 21

1.5.1 Electro-membrane process uncertainties 21

1.5.2 Structure of thesis 22

2. Literature review 25

2.1 Electro-membrane processes for low-concentration nitrate 25

2.2 Application of electro-membrane processes to acids 27

2.2.1 Diffusion dialysis (D) 27

2.2.2 Electrodialysis (ED) 29

2.2.3 Electrodialysis with bipolar membranes (BP-ED) 31

2.2.4 Electro-electrodialysis (EED) 32

2.3 Experimental apparatus 34

2.3.1 Electrodialysis 35

2.3.2 Electro-electrodialysis 38

2.4 Concentration analysis 41

2.5 Performance measurement 42

2.5.1 Ion transport 42

2.5.1.1 Transference number 42

2.5.1.2 Current efficiency 44

2.5.1.3 Transport numbers 45

2.5.2 Water transport 47

2.5.3 Mass transfer 48

2.6 Performance improvement 51

2.6.1 Temperature effects 52

2.6.2 Distance between membranes 52

2.6.3 Ion conducting spacers 52

2.6.4 Combination ion exchange membranes 53
2.6.5 Electro-osmosis of the second kind 53
2.7 Ion transport and membrane modelling 53
2.7.1 Nernst-Planck equation 54
2.7.2 Electroneutrality 57
2.7.3 Novel modelling techniques 57
2.8 Membrane performance 58
2.8.1 Cation exchange membranes 59
2.8.1.1 Selectivity 59
2.8.1.2 Water transport 60
2.8.2 Anion exchange membranes 60
2.8.2.1 Proton leakage 60
2.8.2.2 Water transport 62
2.8.3 Bi-polar membranes 63
2.8.3.1 Fundamental BPM studies 63
2.8.3.2 BPM applications 65
2.9 Conclusions 66

3. Experimental 70
3.1 Experimental rig design 70
3.1.1 Operating mode 70
3.1.1.1 Continuous operation 70
3.1.1.2 Batch operation 71
3.1.2 Electro-membrane stack design 72
3.1.2.1 Spreadsheet model of cell 72
3.1.2.2 Specification of commercial stacks 74
3.1.2.3 Electrode materials 78

3.1.2.4 Estimation of voltage drop across stack 78
3.1.3 Flowsheet of experimental rig 79
3.1.4 Materials of construction 80
3.1.5 Line sizing 81
3.1.6 Pump sizing 82
3.1.7 Temperature control 84
3.1.7.1 Cooling 85
3.1.7.2 Heat exchangers 86
3.1.8 On-line concentration analysis 86
3.1.9 Flow measurement 88
3.1.10 Data logging 88
3.1.11 Vessel sizing 89
3.1.12 Incorporation of reference electrodes 90
3.1.13 Views of rig 90
3.1.14 Safety 92
3.2 Experimental protocol 92
3.2.1 Operation of rig 92
3.2.1.1 Cell configuration 92
3.2.1.2 Power control 93
3.2.2 Experimental procedure 93
3.2.3 Chemical analysis 95
3.2.3.1 Total acid determination 95
3.2.3.1.1 Simple volumetric 95
3.2.3.1.2 Reverse volumetric 96
3.2.3.1.3 Acid concentration units of measurement 97
3.2.3.2 Nitrite determination 97
3.2.3.2.1 Volumetric 98

3.2.3.2.2 High pressure liquid chromatography (HPLC) 99
3.2.3.2.3 Indicator tests 99
3.2.3.3 Ammonium determination 99
3.2.4 Experimental rationale 101
3.2.4.1 Membrane evaluation 101
3.2.4.2 Electrochemistry 104
3.2.4.2.1 Additional process measurements 104
3.2.4.2.2 Independent cell trials 104
3.2.4.3 Detailed individual membrane study 105
3.3 Summary of experimental work 105

4. Experimental results and data analysis 108
4.1 Determination of performance data 108
4.1.1 Membrane current efficiencies 108
4.1.1.1 Integral current efficiency 109
4.1.1.2 Differential current efficiency 110
4.1.1.3 Current efficiency data manipulation 110
4.1.2 Water transport 111
4.1.2.1 Water transport number 112
4.1.2.2 Specific water transport number 112
4.2 Qualitative electrochemical reaction study 113
4.2.1 Review of publications on nitrate reduction 114
4.2.2 Gas evolution 115
4.2.3 Current sweeps 118
4.2.3.1 Qualitative reaction kinetics 121
4.2.3.2 Mass transfer 123
4.2.4 Species analysis 127

4.2.5 Discussion and conclusions 130

4.3 Membrane performance 133

4.3.1 Membrane screening 134

4.3.1.1 Current efficiencies 135

4.3.1.1.1 Abscissa parameter 136

4.3.1.1.2 Differential current efficiency data 138

4.3.1.2 Water transport 140

4.3.1.2.1 Water transport numbers 140

4.3.1.2.2 Specific water transport number 141

4.3.2 Detailed individual membrane study 143

4.3.2.1 Effect of initial concentration 143

4.3.2.2 Effect of current density 146

4.4 Conclusions of experimental programme 148

5. Membrane performance - extended discussion 151

5.1 Relationship between proton leakage and water flux 151

5.1.1 Observed trade-off 151

5.1.2 Importance of trade-off 152

5.1.3 Previous studies 153

5.1.3.1 Proton leakage in AEMs 153

5.1.3.2 Heterogeneous nature of ion exchange membranes 155

5.1.4 Consolidated model for proton leakage and water flux 157

5.1.4.1 Model conclusions 161

5.1.4.2 Summary of model 161

5.2 Advanced understanding of the membrane 162

5.2.1 Water transport 163

5.2.1.1 Water transport and ion co-ordination 163

5.2.1.2 Limitations of process measurements 164
5.2.1.3 Deductions from limiting cases 166
5.2.1.4 Further fundamental studies 169
5.2.2 Ion transport 170
5.2.2.1 Membrane resistance to proton transport 170
5.2.2.2 Limitations of process measurements 177
5.2.2.3 Further fundamental studies 178
5.2.3 Summary of improved understanding 178

6. Model of EED process 181
6.1 Process performance 182
6.1.1 Electrochemical phenomena 183
6.1.1.1 Electrode reactions 183
6.1.1.2 Reduction efficiency assumption 184
6.1.2 Membrane performance 187
6.1.2.1 Performance equations 188
6.1.2.2 Current efficiency evaluation 190
6.1.3 Other considerations 191
6.1.3.1 Purge air stripping and vent gas 191
6.1.3.2 Membrane water transport 192
6.1.3.3 Batch reactor model 192
6.2 Model system 193
6.2.1 Electrode reactions 194
6.2.2 Membrane transport 195
6.2.3 Electrolyte mass balance equations 195
6.3 Solution of model 196
6.4 Comparison with experimental data 198

6.5 Example application of model 201

6.6 Conclusions of modelling 203

7. Process evaluation 206

7.1 Sources of waste nitric acid 206

7.2 Conventional technology 207

7.3 General process considerations 208

7.3.1 Electro-membrane stack design 209

7.3.2 Electrodes and electrode reactions 209

7.3.3 Membrane fouling 209

7.3.4 Contaminants 210

7.3.5 Post-treatment 210

7.4 Cell configurations 211

7.4.1 Two-compartment EED 211

7.4.2 Three-compartment EED 212

7.4.3 Four-compartment EED 213

7.4.4 ED configuration 214

7.5 Possible process configurations 215

7.5.1 Case 1 - weak acid feed to concentrated product 216

7.5.2 Case 2 - weak acid feed to concentrated product 217

7.5.3 Case 3 - intermediate acid feed to concentrated product 218

7.5.4 Case 4 - intermediate acid feed to 100% product 219

7.6 Conclusions of process evaluation 220

8. Conclusions and recommendations 223

8.1 Nitrate reduction 223

8.2 Membrane performance 224

8.3 Process evaluation **225**

References **227**

Appendix 1 Spreadsheet model of cell **241**

Appendix 2 Estimation of cell power **244**

Appendix 3 Nitrate reduction literature **247**

Appendix 4 Error analysis **255**

Appendix 5 Anolyte mass balance **263**

Appendix 6 Fortran model of process **266**

Appendix 7 Completed publications **274**

Nomenclature

a,b	Tafel coefficients (V)
A_m	membrane area (m^2)
C	concentration (mol m^{-3})
C_a	anolyte acid concentration (mol m^{-3}) (unless M stated)
C_b	bulk solution concentration (mol m^{-3})
C_c	catholyte acid concentration (mol m^{-3}) (unless M stated)
C_X	concentration of fixed ion exchange groups (mol m^{-3})
d	pipe diameter (m)
D	molecular diffusivity (m^2 s^{-1})
E	specific energy consumption (W s m^{-2} mol^{-1})
E_{cell}	voltage drop across entire cell stack (V)
E_{IR}	voltage drop due to solution (V)
E_m	voltage drop across membrane (V)
E_{OP}	overpotential (V)
E_{SHE}	standard hydrogen reference electrode voltage (V)
f	frictional loss (m^2 s^{-2})
f(t)	curve fit function to η_{ICE} data (s^{-1})
F	Faradays of charge passed
$\Im$	Faraday constant (96485 A s mol^{-1})
g	acceleration due to gravity (m s^{-2})
g(x,y,z)	general function, invariant with time
h	peak height from mass spectrometer analysis (mm)
h_f	head loss due to friction in suction line (m)
h_{H2}/h_{Ar}	hydrogen evolution rate relative to argon flowrate

h_o	head of liquid above inlet to pump (m)
i	current (A)
j	current density (A m^{-2}) (unless mA cm^{-2} stated)
j_{exp}	current density used in experiment determining R_m therefore not a variable (A m^{-2})
j_{lim}	limiting current density (A m^{-2})
J	molecular flux (mol m^{-2} s^{-1})
J_{conv}	ionic flux due to convection (mol m^{-2} s^{-1})
J_{diff}	ionic flux due to diffusion (mol m^{-2} s^{-1})
J_i	species flux (mol m^{-2} s^{-1})
J_{mig}	ionic flux due to electrical migration (mol m^{-2} s^{-1})
k_m	mass transfer coefficient (m s^{-1})
L	length of pipe (m)
M_r	molecular mass
n_{H2O}	specific water transport number
$\tilde{n}_{H2O}$	differential specific water transport number
$\tilde{n}_{H2O/H+}$	differential specific water transport number relative to proton transport
N	number of moles transferred or produced (mol)
N_A	amount of acid (mol)
N_W	amount of water (mol)
pNH_3	partial pressure of ammonia (atmos)
P	system or inlet pressure (N m^{-2})
P_v	liquid vapour pressure (N m^{-2})
q	charge passed (A s)
Q	total charge passed (A s)
R	resistance of system (Ω)

Re	Reynolds number
R_m	membrane resistance to proton transport (s m^{-1})
$\Re$	ideal gas constant (J mol^{-1} K^{-1})
t	time (s)
t^-	true transport number ($^-$ cation, $^+$ anion)
t_{H+}	proton transport number
t_{H2O}	water transport number
t_i	transference number
T	temperature (K)
u	fluid velocity (m s^{-1})
V	volume (m^3)
W_{A-}	anion co-ordination number
W_{H+}	proton co-ordination number
W_S	shaft work (W)
x	unit length along axis of motion (m)
X	liquid mole fraction
X_s	nitrate reduction efficiency modification factor
z	species charge (unless vertical height (m) stated)
Z	sum of all charges

Greek symbols

α	flow coefficient (α=1 laminar, α=0.5 turbulent)
γ	molecular activity
δ	thickness of concentration boundary layer (m)
δ_m	membrane thickness (m)
Δ	change in a variable
ΔM_w	change in mass due to water transport (g)

ε	number of protons per water molecule in solution
η	theoretical current efficiency
η_{CE}	experimental current efficiency
η_{DCE}	differential current efficiency
η_{ICE}	integral current efficiency
η_r	nitrate reduction efficiency
η'_r	former value of η_r (prior to modification)
θ^-	effective transfer number
ρ	density (kg m^{-3})
ω	fixed charge sign
τ_m	reservoir residence time (s)
τ_r	cell residence time (s)
υ	velocity of electro-osmotic flow (m s^{-1})
φ	electrical field potential (V)
Φ	friction factor

Subscripts

0	initial value
a	anolyte value
A	acid
c	catholyte value
conv	convection term
diff	diffusion term
f	final value
i	species i
m	membrane
max	maximum value

mig	migration term
ref	reference electrode
W	water
+	anion
-	cation

Abbreviations

AEM	anion exchange membrane
BP-ED	bipolar membrane electrodialysis
BPM	bipolar membrane
CEM	cation exchange membrane
D	dialysis
ED	electrodialysis
EED	electro-electrodialysis
EIX	electrochemical ion exchange
IEM	ion exchange membrane
SCE	standard calomel electrode
SHE	standard hydrogen electrode
NPSH	net positive suction head

List of figures

Figure 1.1: Anion exchange membrane 6

Figure 1.2: Ion imbalance giving rise to Donnan potential in a CEM 7

Figure 1.3: Diffusion dialysis 10

Figure 1.4: Electrodialysis 11

Figure 1.5: Electro-electrodialysis 13

Figure 1.6: A water molecule 15

Figure 1.7: Electron dipole in water 15

Figure 1.8: Possible chloride ion solvation shell 15

Figure 1.9: Proton tunnelling 16

Figure 1.10: Illustration of proton leakage 17

Figure 1.11: Chain of ion movement in electro-membrane processing of nitric acid 20

Figure 2.1: Coupling of D with ED 28

Figure 2.2: Reported acid concentration against year of publication for ED 29

Figure 2.3: Reported acid concentrations against year of publication for EED 33

Figure 2.4: Typical static laboratory cell configuration 35

Figure 2.5: Typical flow cell configuration 35

Figure 2.6: Concentration analysis techniques used by other workers 41

Figure 2.7: Ionic fluxes through a membrane 43

Figure 2.8: Representation of actual and theoretical maximum ionic fluxes 44

Figure 2.9: Concentration polarisation at membrane surface 49

Figure 2.10: Current versus voltage curve showing plateau at limiting current 51

Figure 2.11: Illustration of possible mechanism in which acid dissociation controls proton leakage 62

Figure 2.12: Bipolar membrane water splitting 63

Figure 3.1: Illustration of a continuous electro-membrane process 71

Figure 3.2: Illustration of an electro-membrane process operating in batch recycle mode 72

Figure 3.3: Illustration of a spacer in an FM01 cell 75

Figure 3.4: Representation of the flows in an FM01 configured for EED 76

Figure 3.5: Representation of the flows in an FM01 configured for ED 76

Figure 3.6: Equivalent circuit used to estimated voltage drop across cell 78

Figure 3.7: Line diagram of experimental rig 79

Figure 3.8: Minimisation of volume hold-up and pressure drop in line sizing 81

Figure 3.9: Cooling circuit 86

Figure 3.10: Comparison of concentration measures for nitric acid 97

Figure 3.11: Apparatus used for ammonium analysis 100

Figure 4.1: Typical peak height against molecular mass histogram taken from mass spectroscopy data 116

Figure 4.2: Variation of relative hydrogen evolution rate with operating current and catholyte acid concentration 117

Figure 4.3: Typical current density against time profile for current sweeps of EED stack 119

Figure 4.4: Typical total cell voltage drop against current density

for current sweep experiments 119

Figure 4.5: Reference electrode voltage against logarithm of current density (0.47M catholyte) 120

Figure 4.6: Reference electrode voltage against logarithm of current density showing linear region of curve (1.16M catholyte) 122

Figure 4.7: Resistance term against reciprocal of current density used to determine limiting current (1.16M catholyte) 124

Figure 4.8: Normalised resistance term against reciprocal of current density corrected for catholyte acid concentration 125

Figure 4.9: Species profile for experiment initially with 1M acid electrolyte 127

Figure 4.10: Species profile for experiment initially with 1.5M acid electrolyte 128

Figure 4.11: Species profile for experiment initially with 2M acid catholyte 128

Figure 4.12: Species profile for experiment operated at 150 mA cm^{-2} 129

Figure 4.13: Species profile for experiment operated at 300 mA cm^{-2} 129

Figure 4.14: Species profile for experiment operated at 450 mA cm^{-2} 130

Figure 4.15: Acid concentration profiles for ADP2 experimental run 134

Figure 4.16: Acid concentration profiles for ARA2 experimental run 135

Figure 4.17: Integral current efficiency profile for experimental run ADP2 135

Figure 4.18: Integral current efficiency profile for experimental run ARA2 136

Figure 4.19: Differential current efficiency against trans-membrane concentration difference 137

Figure 4.20: Differential current efficiency against catholyte acid concentration 137

Figure 4.21: Differential current efficiency against anolyte acid

concentration 138
Figure 4.22: Differential current efficiency against anolyte acid concentration for 1M initial electrolytes 139
Figure 4.23: Differential current efficiency against anolyte acid concentration for 2M initial electrolytes 139
Figure 4.24: Overall water transport number for different membrane types 141
Figure 4.25: Specific water transport numbers for AW membrane with minimum error evaluation 142
Figure 4.26: Specific water transport numbers for ARA membrane with minimum error evaluation 142
Figure 4.27: Specific water transport numbers for ADP membrane with minimum error evaluation 142
Figure 4.28: Specific water transport numbers for RAI membrane with minimum error evaluation 143
Figure 4.29: Differential current efficiency against anolyte acid concentration for AW membrane 144
Figure 4.30: Specific water transport numbers against anolyte acid concentration for AW membrane showing minimum error evaluation 145
Figure 4.31: Differential current efficiency against anolyte acid concentration for AW002 run 146
Figure 4.32: Differential current efficiency against anolyte acid concentration for AW membrane 146
Figure 4.33: Differential current efficiency against anolyte acid concentration for AW membrane 147
Figure 4.34: Overall specific water transport numbers against

operating current density showing minimum error evaluation for AW membrane 148

Figure 5.1: Illustration of hydrophobic IEM showing polymer, active and interstitial zones 156

Figure 5.2: Illustration of model applied to AEM in low concentration acid 158

Figure 5.3: Illustration of model applied to AEM in high concentration acid 159

Figure 5.4: Differential specific water transport number against anolyte acid concentration [AW002] 165

Figure 5.5: Differential specific water transport number relative to proton transport [AW002] 166

Figure 5.6: Estimated anion co-ordination number against anolyte acid concentration for WH+=1.0 168

Figure 5.7: Estimated proton co-ordination number against anolyte acid concentration for WA-=3.5 169

Figure 5.8: Illustration of membrane transport terms 171

Figure 5.9: Voltage drops across cell showing membrane voltage drop Em 172

Figure 5.10: Voltage drop across membrane and boundary layers against anolyte acid concentration 173

Figure 5.11: Membrane resistance to proton transport against catholyte acid concentration 174

Figure 5.12: Membrane resistance to proton transport against anolyte acid concentration 175

Figure 5.13: Membrane resistance to proton transport against membrane and boundary layer voltage drop 176

Figure 6.1: Predicted fraction of current going to hydrogen evolution against current and catholyte acid concentration 186

Figure 6.2: Relative hydrogen evolution rates obtained from mass spectrometer analysis 186

Figure 6.3: Membrane voltage drop against anolyte acid concentration for AW membrane showing curve fit 188

Figure 6.4: Membrane resistance to proton transport against membrane voltage drop for AW membrane showing curve fit 189

Figure 6.5: Variation of anion co-ordination number with acid concentration showing curve fit 192

Figure 6.6: Illustration of system described by model 194

Figure 6.7: Solution algorithm used in numerical solution of the model 197

Figure 6.8: Comparison of measured and predicted ammonium concentration profiles 199

Figure 6.9: Comparison of measured and predicted current efficiency data 200

Figure 6.10: Comparison of measured and predicted acid concentration profiles 201

Figure 6.11: Species and ηDCE profiles predicted by the model for a base case industrial process 202

Figure 7.1: Two-compartment EED cell 212

Figure 7.2: Three-compartment EED 212

Figure 7.3: Four-compartment EED 213

Figure 7.4: ED configuration 214

Figure 7.5: Flowsheet showing recovery of nitric acid via

2-compartment EED and distillation 217

Figure 7.6: Flowsheet showing recovery of nitric acid via 3-compartment EED and distillation 218

Figure 7.7: Flowsheet showing direct nitric acid recovery via distillation 219

Figure 7.8: Flowsheet showing breaking of azeotrope by electromembrane process 220

Executive summary

The DRA have been researching novel techniques for the nitration of complex organics employing solutions of dinitrogen pentoxide as the nitrating system. These nitrations proceed rapidly and can be effected continuously without the requirement for additional dehydrating modifiers such as sulphuric acid. The resultant dilute nitric acid stream, after separation of the nitro-organic, is contaminated with organic contaminates and requires further processing.

Acid recovery technology is needed to be able to concentrate the nitric acid back to a form which can re-enter the dinitrogen pentoxide production cycle. Established extractive distillation processes, e.g. with magnesium nitrate, could be used to break the nitric acid azeotrope, but the economics of such processes are unattractive for low volume applications. For low volume speciality nitration processes, therefore, there may be a case for considering novel acid recovery technologies that would be inappropriate for bulk or semi-bulk nitrations. On-site membrane processes, for example, may become economic when compared with on-site extractive distillation or off-site treatment at a specialist acid recovery plant.

The model requirement for this post graduate research was thus to extract and concentrate the nitric acid from a nominal 5 wt% spent acid stream, presuming that all organics have been previously removed, and to investigate the characteristics and potential of electro-membrane processes. The target product concentration for this research project was specified to be at least 30 wt% in order to demonstrate technical feasibility. The concentration of residual acid in

the spent stream should be low to allow minimal post-treatment prior to discharge.

A literature search into electro-membrane processes and their application to acid processing found that little/no process-based research had been undertaken in this area. Consequently it was decided to construct a laboratory pilot rig capable of being configured for both electrodialysis and electro-electrodialysis in a flow-through cell operating in batch recirculation mode. In order to avoid the de-coupling problems associated with electrodialysis, which result from the presence both anion and cation exchange membranes, experimental runs were undertaken using a two-compartment electro-electrodialysis configuration and the system performance was determined throughout each experiment. The study focused on anion exchange membranes and the reasons for their low electrical efficiency in acid processing which results from their ability to transport protons (proton leakage).

On-line measurements were taken both sides of the membrane and recorded along with other relevant variables using a data logger. The key process parameters varied were: initial concentration, operating current density and membrane type. Ultimately, up to 50 wt% acid product was achieved which was dictated by experimental rather than membrane limitations. At the low pH values and the relatively high current densities employed in the experiments, it was found that nitrate reduction at the cathode could be significant. This interesting electrochemistry was studied qualitatively using additional process measurements.

A trade-off was observed in membrane performance in that a decrease in current efficiency appeared to be coupled with a decrease in the water flux. Consequently the same membrane, when operated less efficiently, potentially yields a stronger acid product. This interesting relationship was the focus of much theoretical work which lead to the proposal of a consolidated proton leakage and water flux theory. The consolidated theory was based on the fundamental membrane properties studied by other workers and explains why a balance must be made between electrical cost and product concentration. Further understanding of membrane performance was gained from detailed analysis of the experimental process data. This understanding could be used either to develop new membranes or to optimise the performance of a process based on existing membrane capabilities.

Whilst the electro-electrodialysis configuration employed in the experimental programme was found unlikely to be commercially viable except for very dilute acid feeds (e.g. < 1 wt%), the improved understanding of membrane performance has lead to several new avenues for further research and the increased possibility of an industrially sucessful process.

Chapter 1:
Introduction

1. Introduction to electro-membrane processes

This introductory chapter is intended to give a brief background to the research project along with some elementary theory. It describes electro-membrane processes and introduces some of the main principles behind their operation. The structure of the thesis is described at the end of this chapter.

1.1 Background to project

The Defence Research Agency (DRA) have been researching novel techniques for the nitration of complex organics employing solutions of dinitrogen pentoxide, N_2O_5, as the nitrating system. These nitrations proceed rapidly and can be effected continuously without the requirement for additional dehydrating modifiers such as sulphuric acid. Reactions proceed at ambient conditions and so the extremes of temperature and pressure encountered in traditional nitration processes are avoided. After separation of the nitro-organics, the resultant aqueous stream consists of relatively pure nitric acid with some organic contaminants which require further treatment.

Acid recovery techniques are desired to be able to concentrate the nitric acid back to a form which can re-enter the dinitrogen pentoxide production cycle. This could be achieved by using a conventional extractive distillation process with sulphuric acid or magnesium nitrate to break the nitric acid-water azeotrope. Alternatively non-conventional technologies might be employed which avoid the azeotropic limitations. These could be electro-membrane processes.

The specialist nature, relatively high value and low volume requirement of the complex nitro-organics permits the consideration of novel recovery techniques for on site use, which may thus compete economically with conventional tankering to specialist acid recovery units.

The model requirement for this research project was thus to extract and concentrate nitric acid from a nominal 5 wt% spent acid stream using an electro-membrane process, presuming that all organics had been previously removed. The target product concentration in the first instance was at least 30 wt% in order to demonstrate technical feasibility. The concentration of residual acid in the spent stream should be low to allow minimal post-treatment prior to discharge.

1.2 Ion exchange membranes

At the heart of an electro-membrane process are the ion exchange membranes which effect selective ion transport. The two main types of ion exchange membrane are cation exchange membranes (CEMs) and anion exchange membranes (AEMs) which are named according to the ions transported.

1.2.1 History and applications

Ion exchange membranes were discovered in 1948 at Harvard University (McRae, 1993). Since then they have undergone much development and are used commercially in many applications. Using the data given by McRae the areas of membranes used in industrial applications in 1993 are summarised as in Table 1.1.

Application	**Membrane area** m^2
Desalination of brackish or potable water by electrodialysis	3,000,000
Concentration of sea water by electrodialysis for salt production	600,000
Electrolysis of sodium chloride brine to chlorine, caustic and hydrogen	200,000
Separators in electrical batteries/cells	750,000 *per annum*
Miscellaneous:	
• Demineralisation of whey and non-fat milk for food and feed applications	
• Electrohydrodimerization of acrlyonitrile to adiponitrile for nylon manufacture	
New applications:	
• De-ashing of beet, cane or other sugar juices and molasses	
• De-acidification/ acidification of fruit juices	
• De-salting of soy sauce, amino acid solutions and fermentation broths	
• De-mineralisation of blood plasma	
• Recovery of valuable components from metal plating or treating effluents (recovery of acids from spent steel pickle liquor)	

Table 1.1: Ion exchange membrane usage and applications in 1993 (McRae, 1993)

Development work at present is improving membrane characteristics for specific applications. Some examples of membrane developments for acidic applications are given by: (Cherif & Gavach, 1988), (Indusekhar, Triveldi & Shah, 1991), (Elmidaoui, Belcadi, Houdus, Cohen & Gavach,1992a) and (Elmidaoui, Cherif, Brunea, Duclert, Cohen & Gavach, 1992b). These papers will be discussed in the literature review.

Membrane process are increasingly being studied for applications that minimise process waste. As environmental legislation becomes tighter conventional treatment techniques can be found to be inadequate. The three main electro-membrane separation processes are: diffusion dialysis, electrodialysis and electro-electrodialysis. They are described later in this chapter. Membrane technologies can allow pure products to be obtained from waste streams in order to recycle (or sell) them as (sometimes valuable) by-products. An ideal membrane process produces no effluent and allows complete recycle of components. In practice however a clean effluent requiring only minimal post-treatment is generally specified.

1.2.2 Functionality and operation

Ion exchange membranes (IEMs) are dense membranes which selectively distinguish between different ions for active membrane transport. There are three common types of ion exchange membrane: cation exchange membrane (CEM), anion exchange membrane (AEM) and the more novel bipolar membrane (BPM) which is a composite of AEM and CEM.

The operation of a typical ion exchange membrane has been reviewed in the literature (Kuppinger, Neubrand & Eigenberger, 1993) and is briefly summarised below.

1.2.2.1 Fixed and mobile ions

An ion exchange membrane is a cross-linked polymer matrix onto which charged functional groups are fixed. To maintain overall electro-neutrality the fixed charges are compensated by ions of the opposite charge which are held in place by strong Coulomb (electrical) forces as illustrated in Figure 1.1. For nitric acid the mobile counter-ion would be nitrate, NO_3^-. The exchange capacity of a membrane is the amount of fixed charges per unit volume or mass of membrane. This is commonly expressed in equivalents (or milli-equivalents) per gramme of dry membrane.

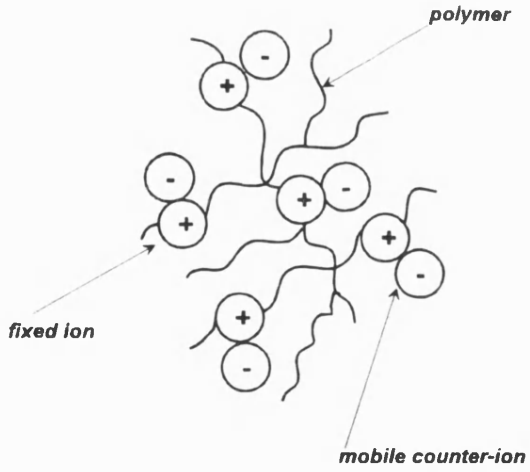

Figure 1.1: Anion exchange membrane (adapted from Kuppinger et al, 1993)

If an IEM is placed into a solution the mobile counterions may be replaced (exchanged) by similar ions from solution. For example, if a CEM were to be placed into an acidic solution the positive mobile counterions would exchange

with the hydronium ions (H_3O^+) from the acid. The hydronium ions will remain in the membrane if it is removed from solution because of the magnitude of the Coulomb forces. Should the hydronium ion form of the CEM be placed into a common salt solution, the H_3O^+ would swap with the Na^+ cation until an equilibrium was reached. Thus the Na^+ becomes the new mobile counter-ion held in the membrane by Coulomb forces. If the H_3O^+ form of the membrane were instead to be placed into pure water, little/no exchange would occur as there would be no similar ions present. The water would remain close to neutral charge.

1.2.2.2 Effect of Donnan potential

When an ion exchange membrane is placed into solution some mobile ions may move out into the liquid phase. This ion imbalance gives rise to a slight potential difference between the membrane and the solution. This is known as the Donnan potential and is illustrated below for a CEM.

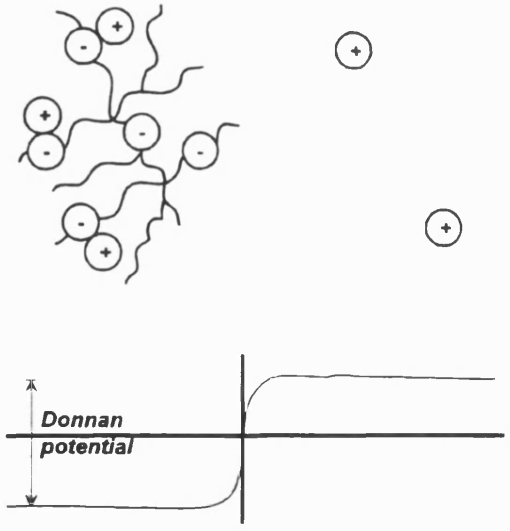

Figure 1.2: Ion imbalance giving rise to Donnan potential in a CEM (adapted from Kuppinger et al, 1993)

The Donnan potential illustrated in Figure 1.2 prevents any further cations from moving into solution and additionally prevents anions from entering the CEM. The Donnan potential acts so as to selectively reject co-ions whilst allowing counter-ions to enter (and be transported across) the polymer matrix. It should be noted that, despite being a highly regarded theory, the classical Donnan model does not always hold for real systems as was found for the case of HCl sorption in various anion exchange membranes (Tugas, Pourcelly & Gavach, 1993a).

1.2.2.3 Effect of osmotic pressure

As the concentration of ions held in the membrane is high, water molecules diffuse into the polymer matrix to effectively 'dilute' the internal ions. This gives rise to ion hydration and leads to swelling of the polymer. Swelling increases the space within the polymer matrix which aids counter-ion movement. An equilibrium is reached between the osmotic pressure and the tensile forces of the polymer. Osmotic pressures can amount to several hundred bars and are able to destroy insufficiently cross-linked polymer matrices (Kuppinger et al, 1993).

The internal osmotic pressure of the membrane can effect ion selectivity. For example, if Na^+ were to be exchanged by Ca^{2+} the osmotic pressure could drop by a factor of two. Thus by exchanging Ca^{2+} for Na^+ the internal energy of the membrane has been reduced. Exploitation of this osmotic pressure effect is used to develop membranes which are selective with respect to ions of the same charge (e.g. different cations such as Na^+ or H^+ and Ca^{2+}).

In summary, the Donnan potential is responsible for the exclusion of co-ions from the polymer matrix giving the membrane its ion rejection properties. Swelling aids ion transport and the osmotic pressure effects can give rise to selectivity between different counter-ions.

1.3 Ion exchange membrane process descriptions

There are three main membrane processes that use ion exchange membranes: diffusion dialysis, electrodialysis and electro-electrodialysis. The key features of their operation and cell configurations are discussed in this section.

1.3.1 Diffusion dialysis (D)

Diffusion dialysis has been applied for many years to the recovery of waste acids. The contaminated waste stream is contacted with a clean water stream via an anion exchange membrane. No electrical field is applied. Instead, the driving force is the concentration difference between the feed and the receiving stream. Operation is reliant on the fact that metal ions are rejected by the membrane but protons can leak through the membrane to enable acid anion transport. This technique effectively separates acids from their metal salts and is illustrated in Figure 1.3 (Latagne & Velin, 1992). For nitric acid X^- would represent NO_3^- whereas H^+ and M^+ represent protons and metal ions respectively.

In order to maximise acid recovery the process is usually operated counter-currently to maintain a reasonable concentration gradient. Recovery of acids can be quite high at around 80% (Latagne & Velin, 1992) and the process has been studied for acids up to 4M (Cohen, Dagard, Molenat, Brun & Gavach,

1986). A typical application of D is in the metal pickling industry (Latagne & Velin, 1992), (Kobuchi, Motomura, Noma & Hanada, 1986). The process is suitable for purifying concentrated spent acids but the product can never be more concentrated than the feed stream. This makes D unsuitable for weak acid feeds or for acid concentration applications, but it could have an important role as a decontamination stage in a hybrid treatment process (Wisniewska, Wisniewski & Winnicki, 1993).

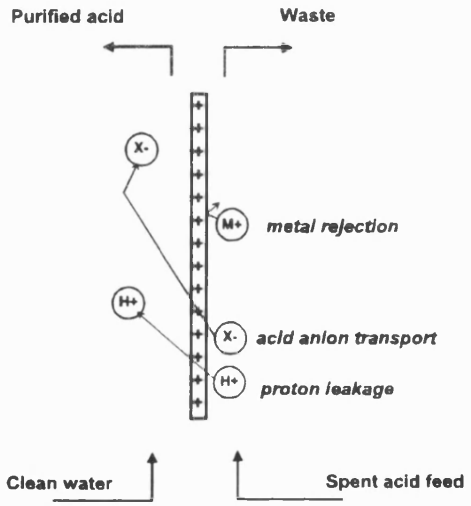

Figure 1.3: Diffusion dialysis

1.3.2 Electrodialysis (ED)

Electrodialysis employs an electrical field as the driving force to drive even dilute waste streams against a concentration gradient (Latagne & Velin, 1992). An electrodialysis stack is made up of alternating cation and anion exchange membranes between two electrodes. Many tens of unit cells are placed between a single pair of electrodes in a typical industrial stack. It will be shown later however that laboratory stacks usually employ less than twenty unit cells.

Ions migrate through the stack to their respective poles of the electric field and are selectively rejected or transported by the ion exchange membranes. This gives rise to alternate concentrated and dilute nitric acid channels which are illustrated in Figure 1.4.

Proton leakage through the AEM, although exploited in diffusion dialysis, is detrimental to electrodialysis as it reduces the efficiency of the process. Consequently much work has been undertaken recently to develop of AEMs with low proton leakage. A large proportion of this work has been carried out by researchers in France (Cherif & Gavach, 1988), (Cherif & Gavach,1989), (Elmidaoui et al, 1992a) and (Elmidaoui et al, 1992b). Membrane development is discussed in the literature review.

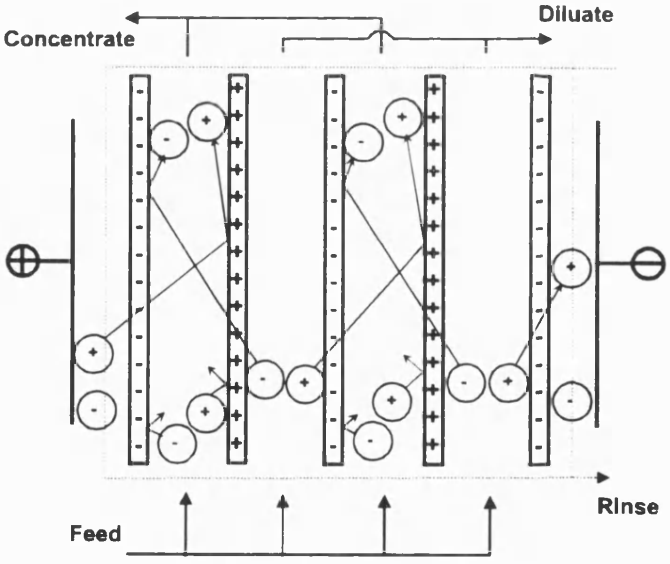

Figure 1.4: Electrodialysis
(adapted from Kuppinger et al, 1993)

Bipolar membranes can also be used to replace one of the membrane types in the stack (AEM or CEM) to effect water splitting within the BPM structure. This creates a source of H^+ and OH^- ions at the CEM and AEM faces of the

membrane respectively. This arrangement forms an alternative to the EED process for salt splitting. BPMs have been successfully used in salt splitting applications (Greben, Pivarov & Latskov, 1988), (Mani, Chlanda & Byzewski, 1988), (Jörissen & Simmrock, 1991), (Greben, Pivovarov, Rodzik & Kovarskii, 1993) and (Simons, 1993).

1.3.3 Electro-electrodialysis (EED)

An extreme case of ED might be regarded as the process of electro-electrodialysis (or electrohydrolysis). The correct definition of electro-electrodialysis incorporates ion separation coupled with a cathodic metal deposition, whereas electrohydrolysis exploits only the common gas evolution reactions (H_2 and O_2) found in aqueous systems. Thus the correct definition depends on whether valuable cations are being reduced in the process simultaneously with ion recovery. However some confusion arose when many papers defined any electro-membrane separation directly exploiting the electrochemical reactions to be electro-electrodialysis (e.g. Raucq, Pourcelly & Gavach, 1993). For convenience, and to take note of the importance of contaminants in a real industrial waste treatment process, all of these processes have been called electro-electrodialysis (EED) in this thesis.

In EED electrochemical reactions are exploited and as such there is a requirement for a pair of electrodes for every unit cell. This is opposite to ED where many unit cells can be arranged between a single electrode pair. Consequently EED is more costly than ED in terms of both capital and power requirements.

Either two-, three- or four-compartment unit cells can be employed depending on the application. If two pure product streams are required, then three compartments with a central feed are favoured. Three compartment EED can also be used in salt-splitting applications for acid and base recovery in a similar way to ED with BPMs. A basic two compartment configuration for nitric acid recovery is shown in Figure 1.5.

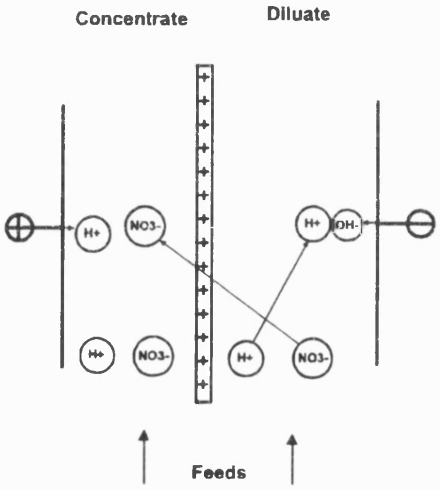

Figure 1.5: Electro-electrodialysis

Waste acid is fed into the catholyte compartment where protons are reduced at the cathode and hydrogen gas is produced (or valuable metals are recovered via electro-plating (Cohen, 1991)). The anion (e.g. nitrate) passes across the AEM to the anolyte compartment where it combines with a proton resulting from the anodic oxidation of water. The chain of ion transfers is described later in the text.

EED is theoretically capable of generating high purity acid at a high concentration. One of the reasons for this is the fact that is there only a single ion exchange membrane over which water transport can occur. This limits the

total water flux associated with ion transport in the system. A high concentration difference can promote back-diffusion of acid from the anolyte to the catholyte stream, but most significantly, increased proton leakage occurs at high acid concentrations. This decreases the current efficiency of the process. Therefore an AEM is required which has both low proton leakage and a low water flux to maximise the overall process performance. EED has previously been shown to be capable of concentrating sulphuric acid to 7.5M (Elmidaoui et al, 1992b) but the high costs associated with EED have made it unattractive for many waste treatment problems.

1.4 Basic electro-membrane theory

The fundamental concepts of ion interactions and basic electrochemical phenomena are highlighted in this section prior to the detailed literature review in the next chapter.

1.4.1 Ions in solution

It is necessary to understand ion interactions in aqueous solution in order to understand the membrane transport characteristics. These chemical and physical interactions can be extremely complex. The general principles have been clearly illustrated previously (Kuppinger et al, 1993) and so are summarised below.

1.4.1.1 Solvation shells

Water (H_2O) has the molecular structure as shown in Figure 1.6. A cluster of electrons is found around the electrophilic oxygen atom which causes the electron cloud not to be uniform. This gives rise to an electron dipole illustrated in Figure 1.7.

When ions are in solution (solvated) they tend to attract adjacent water molecules which form an aggregate with the ion. This aggregation or co-ordination varies with ionic charge. For example, a chloride ion in solution could be surrounded by water as shown in Figure 1.8. This formation would be similar for other anions such as nitrate.

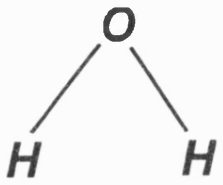

Figure 1.6: A water molecule

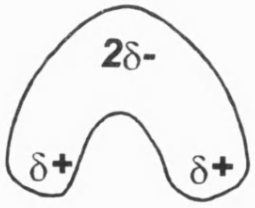

Figure 1.7: Electron dipole in water

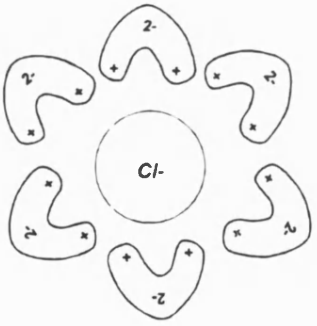

Figure 1.8: Possible chloride ion solvation shell

The solvated ion moves throughout the solution as an aggregate of solute and solvent. It retains the overall negative charge which is distributed across all the

water molecules. The water molecules are known as the ion solvation shell and the number of water molecules per ion is defined as the co-ordination number. Ion solvation explains why water passes through ion exchange membranes with ion transport. The observed effect is of neutral water migrating with the electrical field.

1.4.1.2 Proton tunnelling

The electron dipole of water allows molecules to readily combine with protons in solution to form a more stable hydronium (H_3O^+) ion. Here the positive charge is distributed evenly over the entire molecule. A dynamic equilibrium is reached which is represented by:

$$H^+ + H_2O \leftrightarrow H_3O^+ \qquad [1.1]$$

Protons can move from a hydronium ion to an adjacent water molecule to create another hydronium ion whilst the original H_3O^+ returns to a simple water molecule. This occurs extremely rapidly and is illustrated in Figure 1.9.

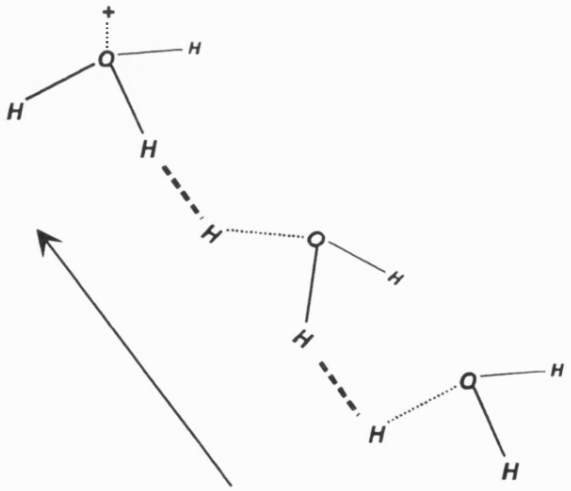

Figure 1.9: Proton tunnelling

The hydronium ion appears to have moved through the solution but no molecular movement has occurred. This is known as proton tunnelling and accounts for the extraordinary mobility of protons in water. The rapid nature of this gives rise to the phenomenon that all water molecules have a small positive charge given by $H_{2+\varepsilon}O^{\varepsilon+}$ where ε is the number of protons per water molecule in solution (Samoilov, 1965).

1.4.1.3 Proton leakage

Proton leakage can be simply illustrated using the ion solvation and proton tunnelling concepts introduced previously. Although the diagram may not be mechanistically correct, it helps to visualise a possible mechanism for this important phenomenon and so it is shown in Figure 1.10. Ion⁻ could represent nitrate ions within the membrane.

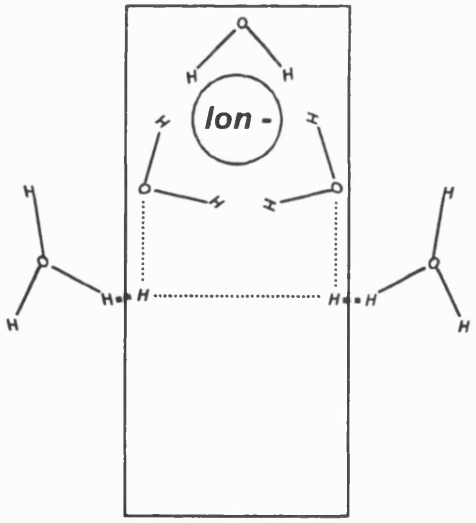

Figure 1.10: Illustration of proton leakage

It can be seen that the hydronium ion on one side of the membrane could use the solvation shell of the ion in the membrane to effectively 'leap' across the structure. This would result in a proton being effectively transported by the

AEM. The probability of this occurring would be a function of the number of hydronium ions present in solution and the number of anions within the membrane. This is supported by macroscopic observations made in the literature.

Proton leakage is a real problem in electro-membrane processes operating in low pH acidic conditions and consequently much work is being undertaken to reduce proton transport in AEMs. Proton leakage is discussed in detail throughout this thesis.

1.4.2 Fundamental electrochemistry

The 'Faradays' of charge passed over a given time can be defined by Equation 1.2 which becomes Equation 1.3 under constant current (galvanostatic) operation. F represents the number of moles of electrons that have been transferred around the process over a time t.

$$F = \frac{\int_0^t idt}{\mathfrak{F}} \qquad [1.2]$$

$$F = \frac{it}{\mathfrak{F}} \qquad [1.3]$$

This useful measure can be used to determine the moles of a particular species that have been transported as a function of its charge and an efficiency term to account for non idealities in the system according to:

$$N = \eta \frac{F}{z} \qquad [1.4]$$

F Faradays of charge passed

$\Im$ Faraday constant (96485 A s mol^{-1})

i current (A)

N number of moles transferred (mol)

t time (s)

z species charge

η theoretical current efficiency

The efficiency term, η, is known as the current efficiency and relates the performance of the process to a theoretical maximum. It can either be used to describe how the current is distributed between different electrochemical reactions or to describe the relative transport of different ions across a membrane. Current efficiency is therefore extremely useful for process evaluation. Other performance measures are discussed later in the text.

The sequence of charge transfer in electro-membrane processing of nitric acid is shown in Figure 1.11. It represents single-cell ED with rinse streams (or four-compartment EED).

As a result of H^+ being consumed by electrochemical reaction shown in Equation 1.5, there is an ion imbalance in the rinse stream adjacent to the cathode. This causes a proton to migrate across the CEM to compensate the negative charge. The resultant effect of this compensation causes the NO_3^- to be transported across the AEM to maintain electro-neutrality in the diluate.

cathode $H^+ + e^- \rightarrow {}^1/_2 H_2$ [1.5]

At the anode H^+ is generated (via reaction in Equation 1.6) and crosses the CEM to combine with the transported NO_3^-. The electron generated in Equation 1.6 then returns via the external electrical circuit to the cathode in order to initiate the reaction in Equation 1.5. In this way the negative charge is in effect passed from cathode to anode giving rise to ion transport in the process. The total current flowing around the process at any instant is constant.

anode $^1/_2 H_2O \rightarrow H^+ + {}^1/_4 O_2 + e^-$ [1.6]

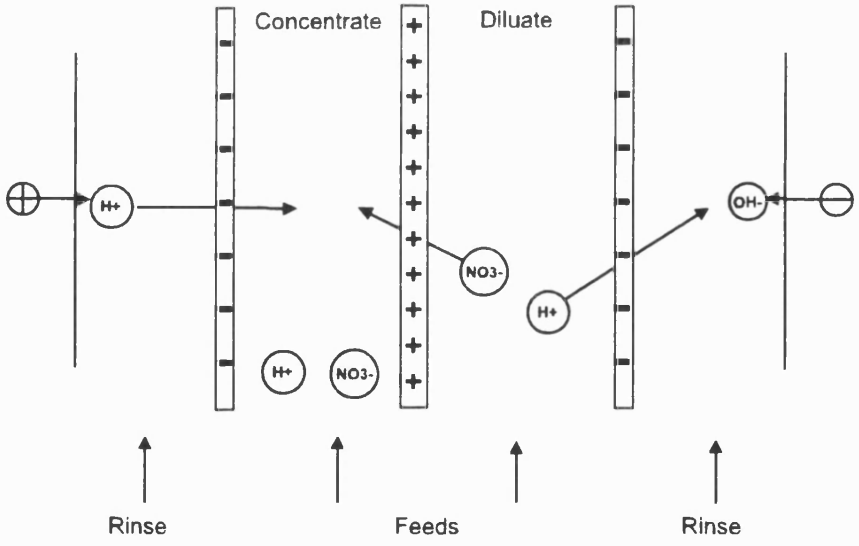

Figure 1.11: Chain of ion movement in electro-membrane processing of nitric acid

Due to the number of repeated cells in a typical ED stack (up to hundreds of units) the passage of a single electron can result in many ions being transported across the membranes.

1.5 Framework for research

Having introduced electro-membrane processes and established a general background to this project, it is possible to highlight the uncertainties that existed at the beginning of the project, and to describe the structure of the thesis.

1.5.1 Electro-membrane process uncertainties

There were many questions to be answered at the beginning of the project on all aspects of electro-membrane processes and their application to acid recovery. It is useful to list the key uncertainties as points of reference for the thesis. They were updated/ extended throughout the course of this research. For simplicity they are given as numbered questions.

1. What are the main electro-membrane processes and to what extent have they been applied to acidic/ acid recovery processes? Which acids/ mixtures of acids have been studied? What feed and product concentration were used and what industrial applications/ trials have been reported?

2. What types of experimental apparatus have been used and what are the advantages and disadvantages of these? Were the experiments laboratory or pilot based and which analytical techniques were used?

3. What are the key issues regarding ion exchange membranes in this area of acid processing and what is the commercial availability of such membranes?

4. Is there a limit of concentration attainable by current ion exchange membranes and how does their performance vary with process conditions?

5. What mathematical models have been developed to describe membrane transport in these applications and can they be applied to experimental data?

It can be seen that many of the initial uncertainties could be divided into two main areas, firstly, those relating to the scarcity of knowledge of previous studies of the application of electro-membrane processes to acidic conditions and, secondly, those matters which could only be resolved by an experimental programme. A literature review was instigated in order to satisfy the former knowledge-based issue and to give an insight into the equipment and techniques that are needed to undertake a fundamental experimental study of the process. The literature review and its conclusions are is discussed in Chapter 2.

1.5.2 Structure of thesis

The structure and layout of the thesis are explained in this section. The chapters and sections have been arranged to logically discuss the research and so do not necessarily represent the chronological progress of the project. Notwithstanding this, the chapters are organised to demonstrate how fundamental understanding was built-up and improved throughout the course of the research culminating in the conclusions and recommendations made at the end of the thesis.

Following the introduction to electro-membrane processes in Chapter 1, Chapter 2 reviews the literature relevant to the project covering processes, performance and mathematical modelling. The experimental protocol and laboratory pilot rig design are covered in Chapter 3 with the results of the experimental programme being presented in Chapter 4.

The performance of anion exchange membranes is discussed in detail in Chapter 5 where theories and data analysis techniques, based on fundamental ion transport models, are introduced to generate a mechanistic understanding of membrane operation.

A basic process model is described in Chapter 6 and the results generated by it compared with experimental data. Whilst the model itself is elementary, the concept of combining both electrochemical and membrane transport expressions provides a useful basis for future work in this area.

Finally, the potential for industrial application of electro-membrane processes in the field of nitric acid recovery is evaluated in Chapter 7 before the conclusions and recommendations of the research are discussed in Chapter 8.

Chapter 2:

Literature review

2. Literature review

This review focuses on publications concerning ion exchange membranes (IEMs) and their application to acid recovery. It is shown that research in this area has been either small-scale laboratory experiments or large industrial pilot studies aiming to apply existing membranes to specific industrial problems (e.g. Voortman, Simpson, Kerr & Buckley, 1992).

Nitric acid concentration has not been studied extensively in electro-membrane processes. Consequently the papers reviewed relating to nitrate recovery generally describe low concentration feed streams as applicable to the water industry. These papers are briefly reviewed before commenting on publications that cover electro-membrane processes for a wide range of other acidic streams.

During the experimental programme, nitrate ions were found to be reduced on the cathode. This is not covered in the main literature review but is discussed at the appropriate point in the thesis.

2.1 Electro-membrane processes for low-concentration nitrate

Nitrates can form nitrites, nitriles and nitrosamines which are carcinogenic or can induce blood poisoning, especially in infants. The EU recommended level of nitrate in drinking water is <25 mg/l (≈0.004M) (Sata, Yamaguchi & Matsusaki, 1995b). This low limit has prompted nitrate recovery via electro-membrane processes to be studied for use in the water industry.

An early study employed electrochemical ion exchange (EIX) to recover nitrate from a 0.005M feed (Kessore, Shaposhnik & Frolich, 1991). EIX utilises an ED type stack but the diluate chambers are filled with an ion exchange resin to enhance performance for low concentration electrolytes. A comparison of dialysis (D), electrodialysis (ED) and EIX for nitrate recovery from hard drinking water using newly commercialised ion exchange membranes (IEMs) has been made (Salem, Sandeaux, Molenat, Sandeaux & Gavach, 1995). ED and EIX were found to be significantly faster than D and both generated a pure water product. Nitrate recovery up to 99% was achieved by EIX. The paper highlighted the need for further improvements in the selectivity of anion exchange membranes (AEMs) towards nitrate transport. Subsequent work described a method of improving the selectivity of an AEM via the introduction of hydrophobic groups into the membrane (Sata, Yamaguchi & Matsusaki, 1995a). The resultant membranes were eighteen times more selective to nitrate than chloride ions.

Although concerned with recovering the nitrate anion, these processes were mainly directed towards nitrate salts that are found at low concentrations in drinking water rather than waste nitric acid. They are not therefore included in the subsequent review of potential electro-membrane processes for nitric acid recovery.

2.2 Application of electro-membrane processes to acids

The literature review focuses on the key processes of dialysis(D), electrodialysis(ED), electrodialysis with bipolar membrane(BP-ED) and

electro-electrodialysis (EED) and their application in acidic conditions. In the majority of cases work was concerned with the removal of trace contaminants from acidic process streams such as those generated by the metal processing industry. Thus acid systems containing H_2SO_4, HCl, H_2CrO_4 and HF/HNO_3 mixtures have been studied. A summary of publications concerning membrane processes for acidic applications is given below. It is divided into different processes and is presented in chronological order within each process group. Where sufficient information was given in the literature acid concentrations have been converted into molarities.

2.2.1 Diffusion dialysis (D)

The table below lists the acids and acid concentrations reported in the literature for the diffusion dialysis process.

Acid	Maximum concentration	Author(s)
HCl	4M	Cohen et al, 1986
HF & HNO_3	2.5M:2.5M mixture	Kobuchi et al, 1986
H_2SO_4	1.86M	Boeteng 1990
H_2SO_4	1M	Elmidaoui et al, 1992a
H_2SO_4		Elmidaoui et al, 1992b
HF & HNO_3	10%:5% mixture	Lantagne & Velin, 1992
HCl	0.32M & 0.15M	Wisniewska et al, 1993

Table 2.1: Application of D to acids

Few overall trends could be seen in the development of the dialysis process although there are some points worth mentioning. The requirement of a

concentration driving force for dialysis results in a lower concentration product stream than the feed. Consequently the acid products are generally of low concentration (e.g. <3M) especially if the system has been cost-optimised in any way. Nitric acid was studied only as part of a mixed acid system containing hydrofluoric and nitric acids from the metal pickling industry (Kobuchi et al, 1986).

One of the most interesting papers is a US patent which described a two-stage process coupling both dialysis with electrodialysis for the removal of metal cation contaminants from an effluent stream (Boetang, 1990). It is illustrated below.

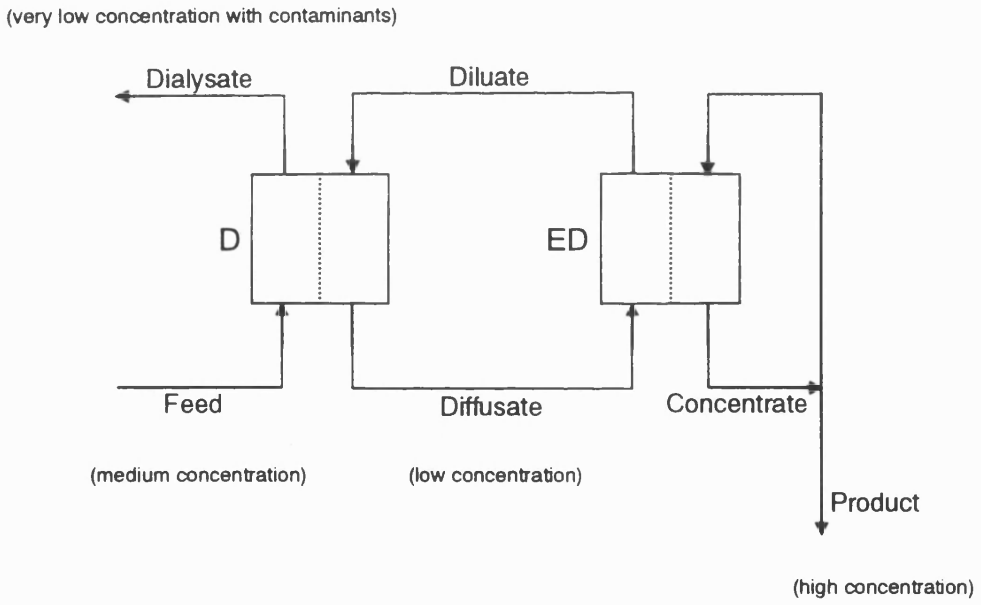

Figure 2.1: Coupling of D with ED (adapted from Boetang, 1990)

Coupling of these processes resulted in the high purity, lower concentration product of D being concentrated via ED to a concentration greater than (or similar to) the initial feed. Hence, the shortfalls of each process were mutually

compensated for by this coupling. Pure sulphuric acid was recovered at just under 2M. This idea could be useful if adopted when optimising complete electro-membrane systems.

2.2.2 Electrodialysis (ED)

General application of ED in the chemical industry has been reviewed in the literature (Strathmann, 1985). For acidic applications, an increase in acid product concentrations was seen over the period 1984 to 1996 and is shown below. The data sources are listed in Table 2.2.

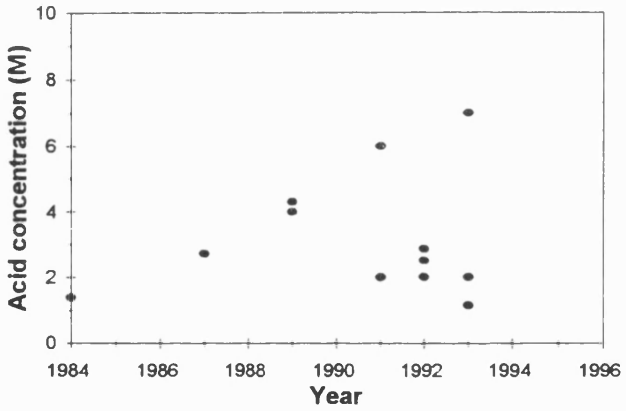

Figure 2.2: Reported acid concentration against year of publication for ED

Since the process began to be applied to acid effluent treatment, the development of new AEMs with lower proton leakage led to considerable improvements in the acid product concentrations reported. One of the ED studies concentrated HCl to 7M (Lindheimer et al, 1993). The increase of interest in ED for acidic applications is also illustrated by the cluster of points for recent years in Figure 2.2.

Acid	Maximum concentration	Author(s)
HCl	1.4M	Kononov, Ponomarev, Shkaraputa, Grebenyuk & Skylar, 1984
HCl	2.72M	Shah & Scamehorn, 1987
nitrates	517 ppm	Kneifel & Luhrs, 1988
malic	21%	Sridhar, 1988
HCl	4.3M	Goldstein, Bayat-Makooi, Sabharwal & Singh, 1989
H_2SO_4	4M	Sridhar, 1989
HCl	6M	Boudet-Dummy, Lindheimer & Gavach, 1991
H_2SO_4	2N	Boudet-Dummy et al, 1991
H_2SO_4	2M	Raucq, Pourcelly & Gavach, 1991
H_2SO_4	2M	Elmidaoui et al, 1992b
H_2SO_4	2.5M	Lantagne & Velin, 1992
H_2SO_4	5%	Baltazar, Harris & White, 1992
H_2SO_4 & HNO_3	0.52M:1.17M mixture	Audinos, Nassr-Alah, Alvarez, Andres & Alvarez, 1993
HCl	7M	Lindheimer, Boudet-Dumy & Gavach, 1993
acetic & HNO_3	10%:1% mixture	Shah, Kovvali, Khan & Khan, 1993
lactic	<2M	Yen & Cheryan, 1993
citric	5%	Novalic et al, 1995

Table 2.2: Application of ED to acids

Until the beginning of this decade, the acid solutions studied were mainly hydrochloric and sulphuric. Some organic acids have been successfully recovered such as malic (Sridhar, 1988) lactic (Yen & Cheryan, 1993) and

citric (Novalic et al, 1995) because these are relatively high value products. The process has also been studied for the selective separation of mixed acid streams such as the separation of nitric from sulphuric (Audinos et al, 1993) or the removal of acetic from nitric (Shah et al, 1993). Nitric acid was not studied other than as part of mixed acid systems.

2.2.3 Electrodialysis with bipolar membranes (BP-ED)

BP-ED has been separated from conventional ED as it is a more novel process which has not been widely adopted by industry. It has been developed mainly for salt splitting applications where there is an acidic, a near-neutral and an alkaline stream in the same cell. This differs from the conventional two-compartment ED unit cell. The papers which cover BP-ED are listed in Table 2.3.

The increase in acid product concentration over the period reviewed was not as evident as seen in the case of ED. Work has been targeted to improve the BPM performance to give lower electrical resistance, higher permselectivity, improved mechanical strength and longer membrane lifetimes (Strathmann, Bauer & Rapp, 1993). Nitric acid was studied in a binary system in order to evaluate performance of a salt splitting/ mixed acid system (Chiao et al, 1991).

Acid	Maximum concentration	Author(s)
H_2SO_4	0.90M	Bobrinskaya, Pavlova & Shatalov, 1985
HCl	3.24M	Greben et al, 1988
H_2SO_4	2M	Mani et al, 1988
HCl	1.64M	Parykin & Vlasova, 1988
HNO_3	3.53M	Chiao, Chlanda & Mani, 1991
H_2SO_4	3.57M	Jörissen & Simmrock, 1991
H_2SO_4	3M	Raucq et al, 1991
HCl	4M	Greben et al, 1993
HCl	2M	Simons, 1993

Table 2.3: Application of BP-ED to acids

2.2.4 Electro-electrodialysis (EED)

EED was found to be a most promising process for acid concentration. Performance was significantly improved by the new AEMs from a product concentration of 2M H_2SO_4 (Cherif & Gavach, 1988) up to 7.5M (Cohen, 1991) (Elmidaoui et al, 1992b), (Lantagne & Velin, 1992), (Raucq et al, 1991) and (Raucq et al, 1993). The reported acid concentrations are plotted in Figure 2.3.

Here the increase with time is not as apparent as was seen in Figure 2.2, but the activity in this area is illustrated by the cluster of points, some of which are super-imposed on each other when identical concentrations were reported in the same year. The data sources are given in Table 2.4.

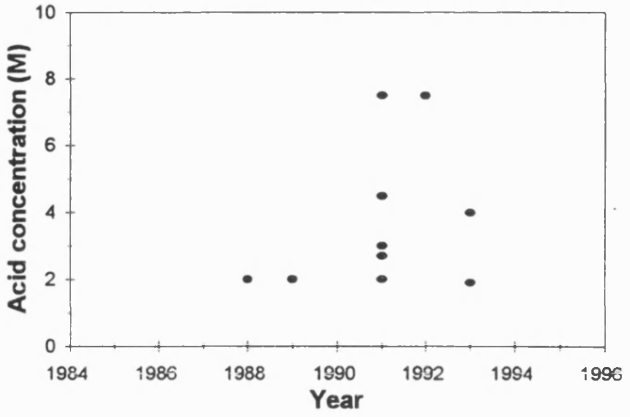

Figure 2.3: Reported acid concentrations against year of publication for EED

Acid	Maximum concentration	Author(s)
H_2SO_4	2M	Cherif & Gavach, 1988
H_2SO_4	2M	Cherif & Gavach, 1989
H_2CrO_4	3M	Audran, Baticle & Letord, 1991
H_2SO_4	2M	Audran et al, 1991
H_2CrO_4	2.7M	Cohen et al, 1991
H_2SO_4	2M	Cohen et al, 1991
HNO_3		Cohen et al, 1991
H_2SO_4 & H_3PO_4	7.5M	Cohen et al, 1991
H_2SO_4	4.5M	Raucq et al, 1991
H_2SO_4 & H_3PO_4	7.5M	Elmidaoui et al, 1992b
H_2SO_4	7.5M	Lantagne & Velin, 1992
propanoic	1.91M	Boyoval, Seta & Gavach, 1993
H_2SO_4	4M	Raucq et al, 1993

Table 2.4: Application of EED to acids

Many of the EED studies were completed in order to compare electrolytic salt splitting with bipolar membrane techniques. Three-compartment EED units were often used as opposed to the simple two-compartment configuration. In one case, a four compartment EED process was used to compare propanoic acid processing with a five-compartment BP-ED process (Boyoval et al, 1993).

A research group based in France at CNRS Montpellier, has taken a key role in the development of new AEMs. At the beginning of this project this group was developing membranes for both hydrochloric and nitric acid under a Brite-Euram programme (Brunea, 1994). The prototype AW membrane that was evaluated for this thesis was a result of that work.

2.3 Experimental apparatus

Particular attention was given to the experimental apparatus used by other workers to study electro-membrane processes. Data on experimental apparatus for both ED and EED is given in this section.

The two most common configurations were static or flow cells. Static cells are used for small-scale laboratory experiments where the electrolytes are mixed via stirring. A typical set-up is illustrated in Figure 2.4. Flow cells utilise external circulation of the electrolytes through the cell stack. These rigs have similar definitions of mass transfer and cell configuration to a commercial stack and therefore can be regarded as a more realistic approximation of an industrial process. A typical flow cell arrangement is shown in Figure 2.5.

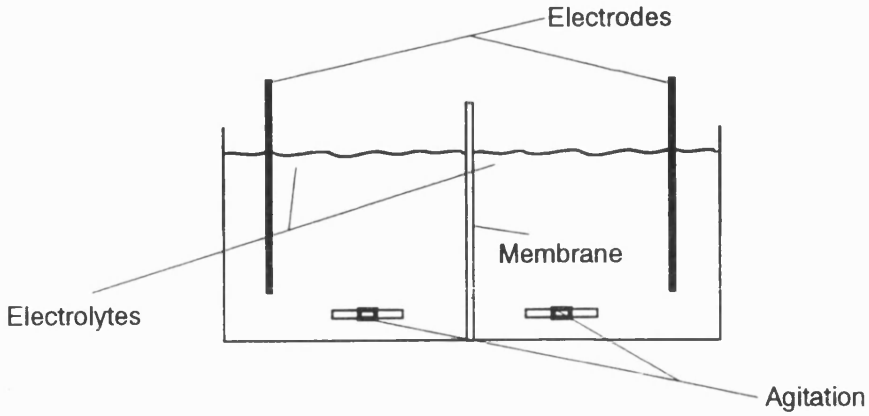

Figure 2.4: Typical static laboratory cell configuration

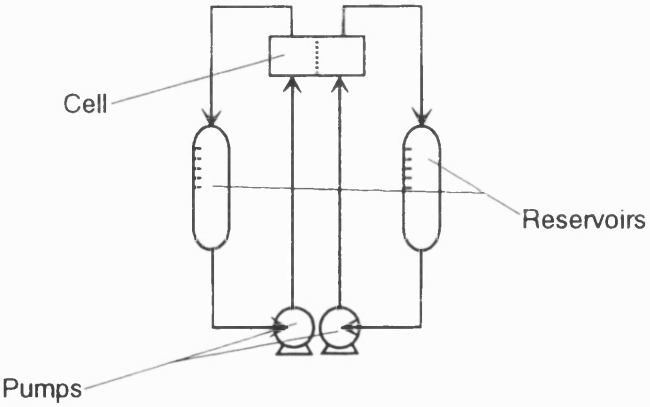

Figure 2.5: Typical flow cell configuration

2.3.1 Electrodialysis

The cell areas and reservoir volumes used in ED experimental studies are shown in Table 2.5. All systems were operated with flow cells.

Flow	Cells	Current	Area	Reservoir volume			Author(s)
				conc.	dil.	rinse	
		mA cm^{-2}	cm^{-2}	cm^3	cm^3	cm^3	
F	2	10	50				Kononov et al, 1984
F	2						Shah & Scamehorn, 1987
F †	120		$5x10^5$		continuous operation		Kneifel & Luhrs, 1988
F	16	20	1600				Sridhar, 1988
F	5		40				Audinos et al, 1989
F	19	45-70	3971				Goldstein et al, 1989
F †	10	50	2000				Andrés et al, 1991
F †	1		61.6				Indusekhar et al, 1991
F	2	250	40	200			Elmidaoui et al, 1992
F	10	120	2000	20,000	20,000	20,000	Baltazar et al, 1992
F	5	20					Audinos et al, 1993
F	3		588	2000	2000	2500	"
F	1	50-200	40	200	5000	1000	Lindheimer et al, 1993
F †	10		2000	1500	2000	5000	Saracco, Zanetti & Onofrio, 1993
F	5	30	684				Shah et al, 1993
F	20	30	4600	460	460		Yen & Cheryan, 1993
F		90	37				Novalic et al, 1995

Cells number of unit cells between the electrode pair
F flow rig
† non acid applications (e.g. desalination, metal recovery, nitrate removal)

Table 2.5: Key parameters in ED experimental studies

Active membrane area varied from $40cm^2$ (Audinos, Alvarez & Alvarez, 1989) up to $5x10^5cm^2$ for a pilot de-nitrating plant trial (Kneifel & Luhrs, 1988). The most common membrane area for an experimental rig was less than $2000cm^2$. This is a reasonable area for membrane experiments without entailing excessive cost. It is also interesting to note that the large pilot plant used by Kneifel & Luhrs was operated continuously, whereas the majority of experimental rigs were run in batch mode. The differences between these modes of operation are discussed later.

There appears to be little trend in the number of unit cells between electrodes, except that multi-unit stacks were preferred usually with somewhere less than twenty repeated cells. This was probably the result of a trade-off between minimising edge effects and increasing the overall flux, by increasing the membrane area, and reducing the cost of the experimental apparatus.

The ED rigs had a reasonable size and were operated in batch re-circulating mode. Since 1993 studies have employed reservoir volumes of the order of litres rather than millilitres and active membrane area has been hundreds of square centimetres. The specific area to initial product volume ($A_m/V_a(0)$ cm^{-1}) has been shown to effect the final product concentration in a batch ED process (Lindheimer et al, 1993).

ED stacks were generally based on a plate and frame construction in a similar way to industrial units. Thus the trend has been towards small scale laboratory pilot (flow) rigs rather than static laboratory cells.

2.3.2 Electro-electrodialysis

The major difference between work on ED and that on EED was that the experimental apparatus for EED was generally configured as a static cell. Such cells are extremely useful for membrane evaluation but do not allow fundamental process data to be generated. The key parameters used in EED experimental studies are shown in Table 2.3.

Out of the flow rigs reported, the first was a two-cell pilot consisting of a central anode with cathodes either side. It was of similar dimensions to an ICI FM21 industrial electrolyser and was operated by EDF, France (Audran et al, 1991). The other flow rig was used to compare bipolar membranes with EED for salt-splitting (Jörissen & Simmrock, 1991). A flow rig was described in a third publication but the results given were somewhat confusing as they appeared to be from a static laboratory cell also described in the paper (Elmidaoui et al, 1992b).

Operating current density increased as the EED process and associated IEMs were developed. The highest current density reported was 300 mA cm^{-2} (Jörissen & Simmrock, 1991), although static cells employed current densities less than 100 mA cm^{-2}.

Flow	Membranes per cell	Unit cells	Current	Area	Reservoir volume		Author(s)
					anolyte	catholyte	
			mA cm^{-2}	cm^2	cm^3	cm^3	
S	1	1	40	7	210	20	Cherif & Gavach, 1988
S	1	1	40	7	210	20	Cherif & Gavach, 1989
F	1	2	50	2840			Audran et al, 1991
S	1	1	50	225			Cohen, 1991
F	1	1	300				Jörissen & Simmrock, 1991
S	2	1	100		250	250	Raucq et al, 1991
S	1	1	120	7	210	20	Elmidaoui et al, 1992
F	1	1			2000	200	"
S	2	1	100	40	250	250	Raucq et al, 1993

S static rig

F flow rig

Table 2.6: Key parameters in EED experimental studies

In order to test new membranes in static cells, relatively small membrane areas (<40 cm^2) were generally used and reservoir volumes were low. Anolyte volumes were approximately 250 cm^3 or less with catholyte volumes either of similar size or an order of magnitude smaller. A small catholyte reservoir allowed acid concentration changes to be monitored whilst maintaining a near-constant acid concentration in the anolyte (Cherif & Gavach, 1988). The only exception to this was the circulating flow rig reported by Elmidaoui which had a large catholyte reservoir (2000 cm^3) and a smaller (200 cm^3) anolyte reservoir (Elmidaoui et al, 1992b). This configuration would allow larger product acid concentrations to be obtained. Unfortunately, results from this rig were not published in isolation from the static cell reported in the same paper.

It was interesting to note that the majority of publications cited in Table 2.6 were from the same research group based in France. Only one of the papers did not have any apparent links with the team (Jörissen & Simmrock, 1991). Consequently much of the work was undertaken on similar if not identical experimental apparatus. The apparatus of Cherif (Cherif & Gavach, 1988), (Cherif & Gavach, 1989) and Elmidaoui (Elmidaoui et al, 1992b) had identical rig dimensions, as were those published in the papers by Raucq (Raucq et al, 1991), (Raucq et al, 1993). Therefore the majority of the EED studies were undertaken using only two or three experimental rigs. This would have the advantage that rig design would not be a variable between these data and that similar methods of interpretation could be used. On the other hand, inherent experimental errors (if any) could perpetuate.

Some studies considered commercially available ion exchange membranes but performance was usually compared over entire experiments using transfer numbers (Cherif & Gavach, 1988), (Elmidaoui et al, 1992b). Variation in performance throughout an experiment should ideally be investigated along with the effect of process conditions. Electro-osmotic water transport should also be studied as this was not considered by any of these workers.

2.4 Concentration analysis

It is important to determine accurately acid concentration in order to assess the performance of a process. The variety of techniques used by other workers is illustrated in Figure 2.6.

It can be seen that the most common technique was titration. Titration can be very accurate although it is strictly off-line even if auto-titrators are used. Additionally, titration is a destructive technique so the volume of liquid in the experimental apparatus must be sufficient to allow samples to be taken during to course of an experiment.

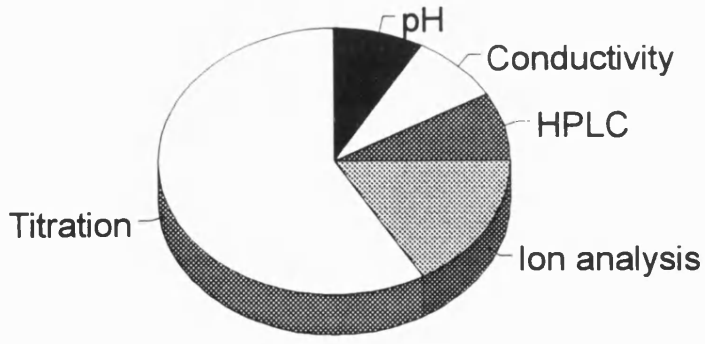

Figure 2.6: Concentration analysis techniques used by other workers

In-line analysis techniques were not generally used with the exception of Leitz who used on-line conductivity detectors (Leitz, 1986).

2.5 Performance measurement

The measures used for performance assessment varied between publications but the main methods are given in this section. The actual performance measures used in this project are discussed at the beginning of the results section later in this thesis.

In an electro-membrane process the key measures of membrane performance are ion transport (ion selectivity) and water transport. These are discussed below.

2.5.1 Ion transport

An ion exchange membrane ideally transports only the counter-ions of interest. In practice, competing counter-ions and co-ion leakage can reduce the efficiency of membrane transport. There are many measures which are used to describe the same fundamental ion transport phenomena. This can give rise to some confusion and so the key measures used to quantify ion transport are highlighted in this section.

2.5.1.1 Transference number

The transference number of an ion is the ratio of the flux of a particular ion to the total ionic flux of the system at a particular instant (Kuppinger et al, 1993). The transference number is a function of many system variables.

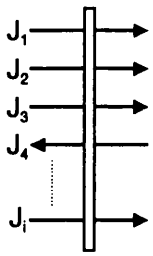

Figure 2.7: Ionic fluxes through a membrane

The individual ionic fluxes through a membrane are illustrated Figure 2.7 and the transference number is defined as:

$$\text{Transference number of particular ion} = \frac{\text{Flux of particular ion}}{\text{Total ionic flux}}$$

which on substitution gives:

$$t_i = \frac{z_i J_i}{\sum z_i J_i} \qquad [2.1]$$

The total system flux ideally follows the Faradaic relationship:

$$\sum z_i J_i = \frac{j}{\mathfrak{F}} \qquad [2.2]$$

The transference number, t_i, consequently becomes:

$$t_i = \frac{\Im z_i J_i}{j} \qquad [2.3]$$

j current density (A m^{-2})

J_i species flux (mol m^{-2} s^{-1})

t_i transference number

2.5.1.2 Current efficiency

Current efficiency is a good measure of membrane performance as it is the ratio of the amount of a particular ion transported to a theoretical maximum.

$$\text{Current efficiency} = \frac{\text{Actual ion transport}}{\text{Maximum theoretical ion transport}}$$

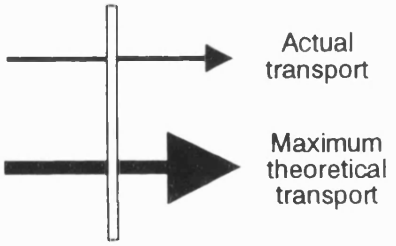

Figure 2.8: Representation of actual and theoretical maximum ionic fluxes

The concept is illustrated in Figure 2.8. Over a given time period the current efficiency is given mathematically by:

$$\eta = \frac{N_i z_i}{\frac{\int_0^t i dt}{\Im}} \qquad [2.4]$$

Under constant current (galvanostatic) operation the current efficiency from experimental data is found via (Lindheimer et al, 1993):

$$\eta_{CE} = \frac{z_i[N_i(t) - N_i(0)]\Im}{jA_m t} \qquad [2.5]$$

A_m membrane area (m^2)

η_{CE} experimental current efficiency

The term η_{CE} is used to denote that the current efficiency has been calculated from experimental data over a time period, t. It is not necessarily equal to the theoretical, instantaneous, current efficiency, η, unless $t \rightarrow 0$. The current efficiency can also be related to the specific energy consumption which is the amount of energy required per unit of product/ treated effluent:

$$E = \frac{jR\Im}{\eta} \qquad [2.6]$$

E specific energy consumption (W s m^{-2} mol^{-1})

R resistance of system (Ω)

2.5.1.3 Transport numbers

Transport numbers are similar to current efficiency but have a sign definition according to the direction of motion and the membrane type. They are similar to the transference numbers given in Section 2.5.1.1 but are not determined at a particular instant. Transport numbers are usually determined over the duration of an experiment and are given by:

$$t^- = \frac{z_i\left(C_f V_f - C_0 V_0\right)\Im}{Q} \qquad [2.7]$$

C concentration (mol m^{-3})

Q total charge passed (A s)

t^- true transport number ($^-$ cation, $^+$ anion)

V volume (m^3)

Radiotracers can be used in practice to determine unidirectional transport numbers but, as the transport number does not account for back diffusion (osmosis), they can only take values such that $0 \leq t^- \leq 1.0$. In order to avoid the complicated experimental techniques associated with determining unidirectional fluxes, an effective transfer number, θ^-, has been proposed for use in real applications (Cherif & Gavach, 1988). The effective transfer number is calculated in the same way as the transport number but the definition is relaxed so that the effect of back-diffusion is acknowledged and considered when evaluating the data. It is therefore given by:

$$\theta^- = \frac{z_i\left(C_f V_f - C_0 V_0\right)\Im}{Q} \qquad [2.8]$$

θ^- effective transfer number

The effective transfer number can take values outside of the range of the true transport number, for example:

$\theta^- > 1.0$ diffusion in direction of electric field

$\theta^- < 0$ back-diffusion greater than electrical migration

Although the effective transfer number is a good measure for system comparisons, it is not strictly a novel parameter. It is little more than the value of the current efficiency at the end of the experiment which is shown by:

$$\eta_{CEf} = \frac{z_i\left(C_f V_f - C_0 V_0\right)\Im}{Q} = \theta^- \qquad [2.9]$$

Rather than being introduced as a new term in some papers (Cherif & Gavach, 1988), (Cherif & Gavach, 1989), (Elmidaoui et al, 1992b) it should therefore more appropriately have been labelled the overall or ultimate current efficiency. Current efficiencies of electro-membrane processes have been reported for many years.

2.5.2 Water transport

It is useful to quantify the water transport through an ion exchange membrane as this has a non-electrical effect on the overall process performance. Despite this, only one paper reported data for water transport in an electro-membrane process for acid processing (Cherif & Gavach, 1988), although water flux in IEMs has begun to attract some interest (Okada, Kjelstrup-Ratkje, Moller-Holst, Jerdal, Friestad, Xie & Holmen, 1991), (Reboiras, 1996).

Water fluxes were given in the form of a water transport number (or water transference number) which relates the water flux to the total ionic (electron) flux and is defined as:

$$\text{Water transport number} = \frac{\text{Moles of water transported}}{\text{Moles of electrons transferred}}$$

which on substitution gives:

$$t_{H2O} = \frac{N_w(t) - N_w(0)}{\frac{\int_0^t i dt}{\mathfrak{F}}} \qquad [2.10]$$

N_W amount of water (mol)

t_{H2O} water transport number

2.5.3 Mass transfer

In an electro-membrane process ions move from the bulk solution across the boundary layer to the membrane surface. At the membrane surface the ion is sorbed into the ion exchange membrane. This gives rise to a lower ionic concentration at the membrane surface than in the bulk, Figure 2.9. If the ion flux is increased then the situation can be reached where the membrane surface is depleted of ions and a near-zero surface concentration exists. This is known as the limiting current of the process.

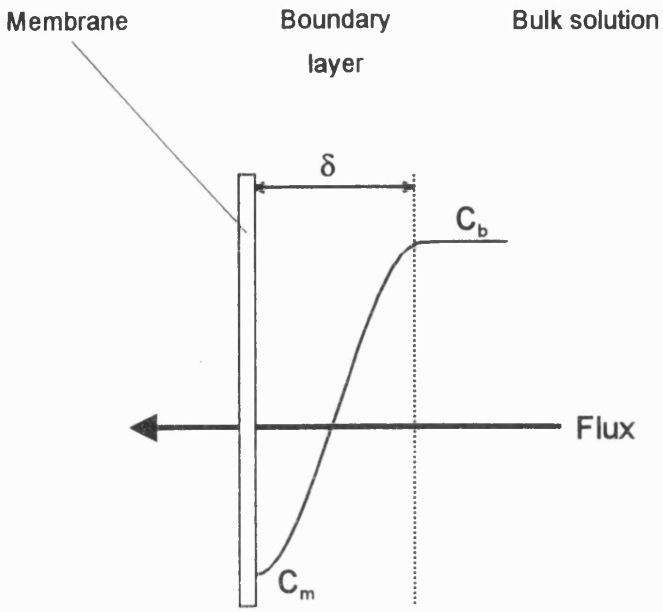

Figure 2.9: Concentration polarisation at membrane surface

The limiting current depends on many factors such as: bulk concentration, boundary layer thickness, membrane properties, hydrodynamic permeability, electrical resistance and electro-osmotic permeability. Consequently it is specific to the particular system studied. It can be difficult to determine the limiting current in practice and many techniques have been developed for its identification. The technique adopted for use in this work is discussed later in the thesis.

At the limiting current mass transfer to the membrane surface is equal to ionic migration and, as C_m is close to zero, they are related by:

$$\frac{D}{\delta}C_b = \frac{j_{lim}}{z\Im} = k_m C_b \qquad [2.11]$$

C_b bulk solution concentration (mol m^{-3})

D molecular diffusivity (m^2 s^{-1})

j_{lim} limiting current density (A m^{-2})

k_m mass transfer coefficient (m s^{-1})

δ thickness of concentration boundary layer (m)

The current against voltage curve of the above system would be almost linear initially before decreasing to a plateau at the limiting current. This point can sometimes be determined graphically from experimental measurements (Spiegler & Laird, 1980). Advanced studies have extended the curve to a threshold point where the current increases again (Rubinstein & Maletzki, 1991). This is illustrated in Figure 2.10. Above the threshold point the system operates chaotically with low frequency electrical noise being observed. Processes are not generally operated in this region although it has been the focus of some academic study (Maletzki, Rosler & Staude, 1992), (Rosler, Maletski & Staude, 1992).

In 1978 the proposed over-limiting current conduction mechanism was via convection currents which injected electrolyte into the boundary layer (Gavish & Lifson, 1978). It was said that, convection became turbulent in the over-limiting current range which explained current noise and the increase in conductance. Further work suggested that the over-limiting current conductance could be a result of local electroneutrality not being observed. Charge could be distributed via a Poisson relationship and the resultant regions of space charge

would trigger new conductance mechanisms (Kedem & Rubinstein, 1983). Water splitting has also been suggested as a possible charge transport mechanism in the over-limiting current range (Mavirov, Pusch, Kominek & Wheelwright, 1983) but there is some doubt as to whether sufficient splitting rates could be achieved to carry all the current (Kedem & Rubinstein, 1983). The latest work employed fast-logging electronics to monitor membrane potentials after the current was stopped in the hope of developing a technique for the prediction of boundary layer characteristics (Judd, Solt & Wen, 1993).

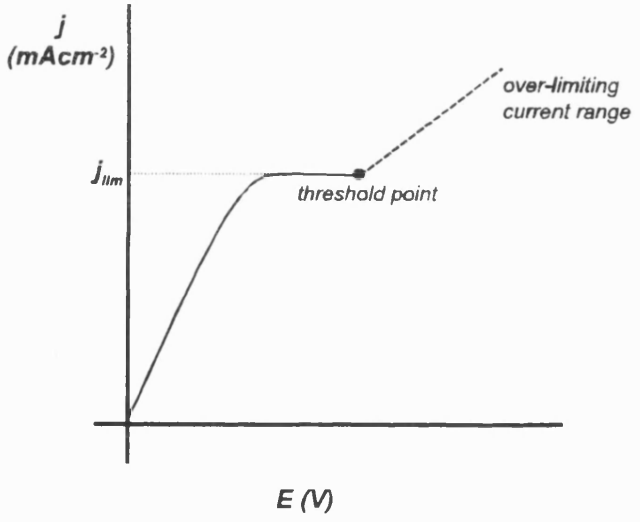

Figure 2.10: Current versus voltage curve showing plateau at limiting current (adapted from Rubinstein & Maletzki, 1991)

2.6 Performance improvement

There have been many attempts to increase the performance of electrodialysis processes or of commercial ED stacks. Some of these are highlighted here.

2.6.1 Temperature effects

The variation of temperature on an ED system has been studied over the range 15→90°C (Hwang & Lai, 1987). It was shown that both ion fluxes and the limiting current increased with increasing temperature. This was attributed to increased pore sizes at higher temperatures combined with an increase in permeability and diffusivity through the membrane.

2.6.2 Distance between membranes

Two key geometrical parameters in an electrodialysis stack are the path length for solution flow and the inter-membrane distance. For mass transfer intensification, the distance between membranes is most important. If the distance between membranes exceeds the total thickness of the boundary layers there is a region in the centre of the solution where little/ no concentration change occurs and energy is expended on unproductive ion transport. Concentration profiles were measured using laser inferometry and a 145% improvement in efficiency was obtained with an optimised inter-membrane distance (Praslov & Shaposhnik 1988).

2.6.3 Ion conducting spacers

The inert turbulence promoting spacers found in ED stacks were exchanged for ion conducting spacers (Kedem & Maoz, 1976). These were made of anion exchange and cation exchange fibres. The net effect of these spacers was to increase the current efficiency. Many commercial cells still use inert spacers because efficiency improvements with ion conducting spacers are only moderate (Dukhin & Mishchuk, 1993).

2.6.4 Combination ion exchange membranes

Composite membranes which consist of an anion exchange membrane with a perforated cation exchanger on the surface have been tested for an aluminium anodising process (Greben, Pivovarov, Rodzik & Kovarskii, 1993). The transport number for Al^{3+} was reduced by a factor of fifty which gave rise to improved proton transport.

2.6.5 Electro-osmosis of the second kind

Under a strong electrical field a bulk charge can appear in the concentration polarisation zone adjacent to a membrane. A tangential electrical field was applied to this zone and the bulk charge moved along the surface of the membrane. This phenomena was called electro-osmotic slip or electro-osmosis of the second kind. A theoretical study concluded that mass transfer could be improved using this technique (Dukhin & Mishchuk, 1993) but it remains to be applied industrially.

2.7 Ion transport and membrane modelling

It is useful to develop an engineering model of a process for design purposes and so that its operation can be further studied via computational techniques. This section covers the mathematical models which have been applied in this area. Numerical solution techniques are not discussed.

2.7.1 Nernst-Planck equation

The most common models for ion transfer across an ion exchange membrane are based on the Nernst-Plank equation which has two terms, one for diffusion and the other for electrical migration.

Diffusion due to a chemical potential gradient (concentration and molecular activity difference) is given by:

$$J_{diff} = -D_i\left[\frac{\partial C_i}{\partial x} + C_i\frac{\partial \ln \gamma_i}{\partial x}\right] \qquad [2.12]$$

J_{diff} ionic flux due to diffusion (mol m^{-2} s^{-1})

x unit length along axis of motion (m)

γ molecular activity

Migration in an electrical field was determined from Faraday's law with the inclusion of the Einstein relationship which relates ionic mobility to diffusion in dilute systems, to give:

$$J_{mig} = -D_i\frac{z\Im}{\Re T}C_i\frac{\partial \varphi}{\partial x} \qquad [2.13]$$

J_{mig} ionic flux due to electrical migration (mol m^{-2} s^{-1})

$\Re$ ideal gas constant (J mol^{-1} K^{-1})

T temperature (K)

φ electrical field potential (V)

Combining Equations 2.12 and 2.13 gives the Nernst-Planck equation:

$$J_i = -D_i\left[\frac{\partial C_i}{\partial x} + C_i\frac{\partial \ln \gamma_i}{\partial x} + \frac{z_i \Im}{\Re T} C_i \frac{\partial \varphi}{\partial x}\right] \qquad [2.14]$$

ionic flux = diffusion + migration

In dilute solutions γ_i is assumed invariant with x and so this term is neglected to give the dilute-solution version of the Nernst-Planck equation:

$$J_i = -D_i\left[\frac{\partial C_i}{\partial x} + \frac{z_i \Im}{\Re T} C_i \frac{\partial \varphi}{\partial x}\right] \qquad [2.15]$$

For concentrated solutions however this assumption is not valid and activities must be retained as they can vary with distance. Diffusivity will also vary in concentrated solutions.

A third term can be added to the Nernst-Planck equation to account for electro-osmotic convection which is given by:

$$J_{conv} = C_i \upsilon \qquad [2.16]$$

J_{conv} ionic flux due to convection (mol m^{-2} s^{-1})

υ velocity of electro-osmotic flow (m s^{-1})

When combined with a three-dimensional version of Equation 2.14 this gives the equation for ionic motion as (Helfferich, 1962):

$$J_i = -D_i\left[\nabla C_i + z_i C_i \frac{\mathfrak{I}}{\Re T}\nabla\varphi + C_i \nabla \ln \gamma_i\right] + C_i \upsilon \qquad [2.17]$$

ionic flux = diffusion + migration + convection

There have been many criticisms of the Nernst-Planck model when applied to membrane systems which were reviewed in the literature (Buck, 1984). In summary, there are two main arguments. Firstly, the model assumes a uniform membrane composition and therefore ignores edge effects and the heterogeneous nature of ion exchange membranes. Secondly, the model cannot account for interaction between charges within a membrane. These interactions can become significant in concentrated solutions.

Several new equations have been proposed as alternatives to the Nernst-Plank model such as the Onsager or the Stefan-Maxwell relationships. However, despite being more thorough, these models also have inherent problems and do not always yield an improvement over the Nernst-Plank equation (Buck, 1984).

Despite its limitations, the Nernst-Plank equation remains extremely useful and is still used by workers in this area (Cherif & Gavach, 1988), (Mavarov et al, 1993). Accurate values of system parameters such as ionic diffusivities and activities are required in order to apply the model satisfactorily.

2.7.2 Electroneutrality

The total charge in a system must be net neutral. This gives rise to the electroneutrality constraint which implies that at a particular point all charges summate to zero. It is given by:

$$\sum z_i C_i + \omega C_x = 0 \qquad [2.18]$$

C_X concentration of fixed ion exchange groups (mol m^{-3})

ω fixed charge sign

Electroneutrality is sometimes relaxed in practice if regions of different space charge are said to exist providing that the overall total charge remains zero. Space charges would therefore be distributed, for example, according to a Laplace or Poisson relationship, where:

$$\nabla^2 Z = 0 \quad \text{or} \quad \nabla^2 Z = g(x, y, z) \qquad [2.19]$$

g(x,y,z) general function, invariant with time

Z sum of all charges

2.7.3 Novel modelling techniques

A model of ion transport in cation exchange membranes (CEMs) was used to study counter-ion selectivity between H^+, Na^+ and Ca^{2+} (Karlin, 1993). Thermodynamic equilibrium was assumed at the membrane solution interface (equal standard electrochemical potentials) and overall neutrality was maintained via either the electroneutrality constraint or the Poisson equation.

Agreement was good for the Na^+/Ca^{2+} system for which experimental data was available.

More recently a model for facilitated transport in a pressure driven membrane process was proposed using an electrical analogy (Kang, Hong, Jang & Kim, 1996). A parallel resistor-capacitor (RC) circuit was used to describe the membrane. The resistive term represented the membrane matrix and the capacitance term the fixed site carriers. Excellent agreement was found using parallel RC Circuits in series. It would be interesting to extend this approach for transport in IEMs under an electrical driving force. In this case the analogy is likely to be even closer as the ion transfer would be analogous to electron transfer in a parallel RC circuit.

2.8 Membrane performance

The remainder of this chapter is devoted to reviewing the publications which directly concern the performance limitations of ion exchange membranes (IEMs). The main problems associated with IEMs were given to be: proton leakage through AEMs, poor selectivity of CEMs, cation leakage through BPMs and poisoning of CEMs due to organic fouling (Gavach, Bribes, Chapotot, Maillois, Pourcelly, Sandeaux, Sandeaux & Tugas, 1994). These four areas have been the focus of much research for membrane development. All three membrane types (AEM, CEM and BPM) are reviewed in this section.

2.8.1 Cation exchange membranes

CEMs form part of the unit cell membrane pair in ED stacks and, although they are not the largest source of inefficiency in acid processing (Lindheimer et al, 1993), their performance is reviewed below.

2.8.1.1 Selectivity

Process streams often contain many species especially if it is an effluent. CEMs are being developed which preferentially transport monovalent cations, for use in effluent applications. For example, to recover acid from metal processing, monovalent protons in the effluent should be transported in preference to multivalent metal ions.

The diffusive fluxes of many metal cations in a CEM membrane system were studied using a rotating diffusion cell (Xue, Longwell & Osseo-Asare, 1991). At low metal concentrations the transfer process was controlled by boundary layer diffusion whilst for high metal concentrations it was controlled by membrane diffusion. Analysis of the data found that at low concentrations the flux of an ion was governed by the hydration size of the ion and its properties in the aqueous phase, whereas at high concentrations it was related to ionic size and charge and therefore a function of membrane properties.

State-of-the-art commercial CEMs with improved selectivity were evaluated in an experimental study (Chapatot, Pourcelly & Gavach, 1994). At zero-current divalent ions sorbed preferentially into a CEM but under applied potential the CEMs became several hundred times more selective to monovalent ions. This was explained by Kedem who stated that divalent ion depletion in the Nernst

layer would give rise to monovalent ions being sorbed in greater amounts within the membrane (Kedem & Rubinstein, 1983). Further work involved adsorption of polymers onto the surface of CEMs to improve the selectivity (Chapatot, Pourcelly, Gavach & Lebon, 1995).

2.8.1.2 Water transport

The mechanisms of water transport have not been studied in detail by workers in this field. Water transport was found to be generally larger through CEMs than AEMs. This was attributed to the larger hydration radius of cations and the importance of polarisability in AEMs (Reboiras, 1996). It was also observed that water transport followed a similar trend to the hydration of ions in solution. Other work showed that water transport was not a linear function of ion transfer and that the transport number of water decreased with increasing electrolyte concentration (Okada et al, 1996).

2.8.2 Anion exchange membranes

AEMs were found to be the largest source of inefficiency in an ED cell membrane pair (Lindheimer et al, 1993). This is due mainly to proton leakage which is discussed below along with the limited water transport studies that have been carried out.

2.8.2.1 Proton leakage

In an acidic environment the permselectivity of AEMs is reduced due to the extraordinary mobility of protons discussed in Section 1.4.1.2. This is exploited in the application of acid recovery via diffusion dialysis, but it is not desirable in electro-membrane processes where good permselectivity is required. Much work

has been undertaken to elucidate the mechanisms of proton leakage and these are highlighted below.

One of the earlier studies prepared four different membranes via a radiation induced grafting technique and compared the effect of various membrane parameters on proton leakage (Cohen et al, 1986). A low exchange capacity resulted in a lower proton diffusive flux up to a threshold concentration beyond which the flux became linear with acid concentration. Along with this important observation, the molality of fixed ions appeared to remain approximately constant. Consequently it was shown that proton leakage was linked with increased sorption of acid and not the molarity of fixed sites within the membrane.

Further studies were carried out in a static laboratory electro-electrodialysis cell (Cherif & Gavach, 1989). The aim of this work was to elucidate the mechanisms of proton leakage. A radiotracer technique was used to allow unidirectional fluxes to be measured along with the amount of acid sorbed in the membrane. Back-diffusion of acid increased with sorbed acid but could be overcome to some extent by increasing the operating current density. The results were modelled using the Nernst-Plank equation and reasonable agreement was obtained. It was noted that the observed phenomena could not be accounted for by classic Donnan theory.

Additional work compared CEM transport with that occurring in AEMs (Pourcelly, Boudet-Dumy, Lindheimer & Gavach, 1991). It was found that sorbed acid was much greater than theoretical predictions which could account

for the poor permselectivity (Boudet-Dumy et al, 1991). A high amount of sorbed acid in relation to sorbed water was found in a low proton leakage AEM and so the amount of acid dissociation was thought important. An illustration of a possible mechanism in which acid dissociation controls proton transport is given in Figure 2.11. This simple picture of membrane transport has been significantly improved by further fundamental studies and detailed analysis of these results during the course of this project. Proton leakage is therefore discussed in detail later on in the thesis.

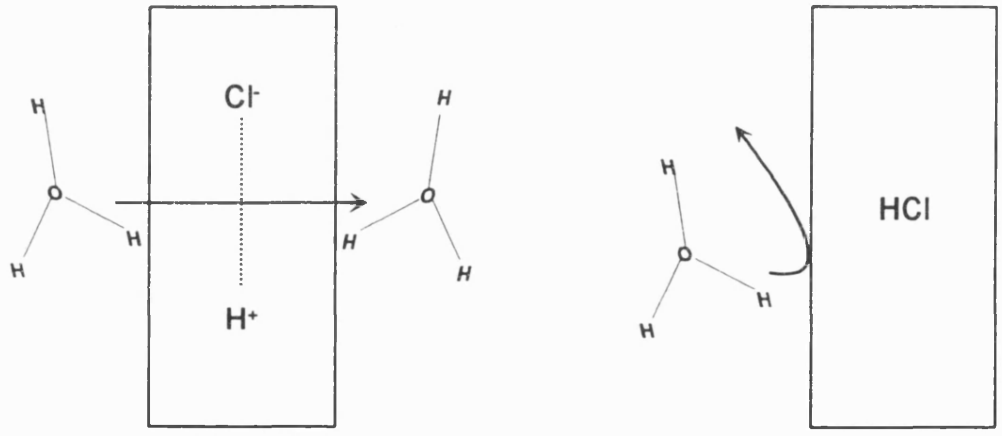

Figure 2.11: Illustration of possible mechanism in which acid dissociation controls proton leakage

2.8.2.2 Water transport

Little/ no water transport data has been reported for AEMs especially for acid processing applications. In various salt solutions, the hydration of anions in the aqueous phase was found to affect water flux and smaller hydrated anions were preferentially transported (Reboiras, 1996).

2.8.3 Bi-polar membranes

Bipolar membranes have attracted interest due to their potential application to salt splitting for acid and alkali recovery. A bipolar membrane comprises of a layer of AEM and a layer of CEM fixed together with an appropriate binding agent. Water diffuses into the central region where it splits and the resultant hydrogen and hydroxyl ions migrate from either side due to the action of the electrical field as illustrated below.

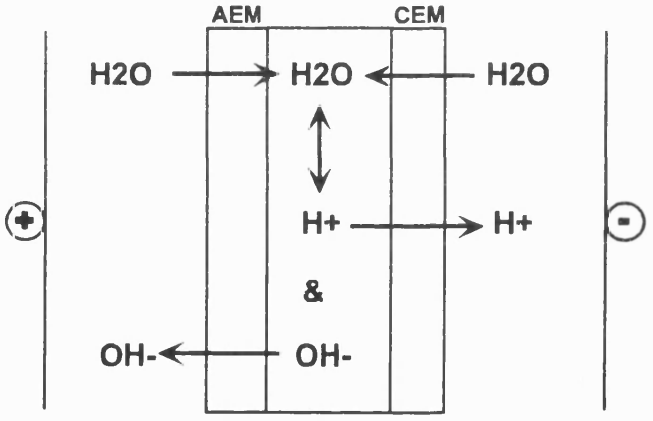

Figure 2.12: Bipolar membrane water splitting (adapted from McArdle et al, 1991)

A bipolar membrane induces water splitting in the absence of electrode reactions. Thus energy is not wasted on gas generation. Electrodialysis incorporating BPMs could therefore compete with an electrochemical method of salt splitting such as EED.

2.8.3.1 Fundamental BPM studies

Fundamental studies lagged behind the rate of progress made by the early commercialisation of BPMs. Consequently many of the early applications could

not take advantage of improved membrane understanding. Fundamental work is highlighted in this section before the BPM applications are given.

The main focus of fundamental research on BPMs has been to elucidate the mechanism of water splitting. It was thought that water splitting was either due to high localised electrical fields within the membrane (Second Wien effect) or due to enhanced chemical dissociation (Chemical Reaction model). The Chemical Reaction model gave the closest agreement with experimental findings (Ramírez, Aguilella, Manzanares & Mafe, 1992).

Further work highlighted the possibility that water splitting was induced by the ammonium groups found in IEMs (Strathmann et al, 1993a). A new membrane was made using a binder incorporating ammonium groups and enhanced water splitting was observed, however these membranes could only be operated to 50 mA cm^{-2} (Strathmann, Rapp, Bauer & Bell, 1993b). The drive for improved membrane performance led to the development of a BPM with a low voltage drop that was stable up to 6M HCl in a laboratory cell (Simons, 1993).

The advances in BPM technology are still some way from full commercialisation. It is difficult to obtain small samples of BPMs for experimental trials which suggests that larger quantities could be even more elusive. This availability could reduce the rate of uptake of BPM technology by industry.

2.8.3.2 BPM applications

The efficiency of a BPM process was found to be dependent, not only on the BPM properties, but on the physical configuration of the unit cell (Greben et al, 1988). In a novel set-up the BPMs were separated from the concentrated acid and alkali solutions by additional AEMs and CEMs. This configuration gave better overall efficiencies and contamination was reduced. This does not appear to have been adopted by industry but work continued in this area to produce a flow-cell for this configuration (Greben et al, 1993a). Efficiency was increased by a factor of four (≈0.13 to 0.50) along with reduced product contamination.

Commercialisation of bipolar membranes was lead by Aquatech Inc which promoted acid/ alkali recovery from salt streams (Mani et al, 1988). Successful 100-day pilot trials indicated good process reliability but the product concentrations were no more than 1M. Similar work was undertaken by other workers concerned with ion exchange resin regeneration but product concentrations were not given in this paper treatment (Parykin & Vlasova, 1988). Batch operation and alternative cell arrangements were studied in further work (Mani, 1991).

The application of BPMs in conventional ED stacks has been considered. This is known as bipolar membrane electrodialysis (BP-ED). In one case the CEMs in the unit cells were replaced by BPMs and the stack used for direct acid purification (Chiao et al, 1991). Contaminants remained in the feed and a 1.8M nitric acid product was produced. BP-ED was also compared with EED for salt splitting applications using new bipolar membranes (Raucq et al, 1993). A 4M, slightly contaminated, caustic product was obtained which was less than

the 6M caustic product achieved via EED. Water transport through the CEMs limited the product concentration in both cases. It was thought that the lower capital charges of BP-ED could make it commercially more attractive (Chiao et al, 1991).

2.9 Conclusions

This section presents the conclusions of the literature review and proposes areas for further work which are required in order to answer the questions raised during the study.

The main performance constraint of IEMs was found to be poor selectivity in terms of monovalent/ divalent ion transport in CEMs and counter-ion/ co-ion leakage in AEMs. Performance was measured mainly using small-scale experimental cells rather than process-based laboratory rigs. An acid concentration limit was not reported.

Very little work has been undertaken to specifically study nitric acid, although publications by workers considering other mineral acids allow various analogies to be made. Acid product concentrations were low (e.g.<7M) and far below the concentration of commercial technical grades for the acids concerned. This is perhaps one of the reasons why there are no industrial applications at present.

For the most part, the key uncertainties raised at the end of Chapter 1 have been addressed during the course of the literature review. The questions regarding previous work on electro-membrane processes for acid recovery have therefore been answered. A detailed understanding of membrane and electro-membrane

process performance for nitric acid processing can only be gained via experimental research focused on this area. This is the next phase of the research.

It is logical to conclude that EED process trials should be undertaken using a circulating flow rig rather than the static laboratory cells favoured by preliminary studies. The work should study the new-generation of commercially available anion exchange membranes such as those available from: Asahi Glass, Japan; Solvay SA, France and Tokuyama Corporation, Japan. Analysis of process streams should be carried out off-line via titration but the availability of in-line techniques such as pH, refractive index and density allows these to be considered in a new flow rig.

Mathematical models of ion transport are reasonably well developed. However detailed data on membrane properties are required for their solution. Although techniques exist to measure these properties, this data has not been published (and often has been not measured) for many membrane systems. The Nernst-Plank model will be adopted for preliminary work in this area and its applicability to experimental data evaluated.

The focus of the research should be to understand how membranes function in the nitric acid-water system, whilst studying the the factors that limit product acid concentration and the variation of performance with process conditions. Performance measures should consider both ion and water transport and so figures of merit such as current efficiency and water transport numbers will be used. As a result of the research, the improved understanding of IEMs should

allow either application of electro-membrane processes using existing membranes or the development of improved membranes for future applications. Wherever possible potential electro-membrane processes should be evaluated against alternative technologies.

Chapter 3:

Experimental

3. Experimental

Having reviewed the previous work on electro-membrane processes, it was necessary to devise an experimental programme to study their application and performance in nitric acid processing. Experimental rig design and experimental protocol are discussed in this chapter. The first section of the chapter is devoted to a detailed description of the laboratory pilot rig and its design and the remainder of the chapter focuses on experimental techniques.

3.1 Experimental rig design

This section discusses the main points that were considered when designing the laboratory pilot rig to study electro-membrane processes.

3.1.1 Operating mode

There are two common modes of operation of an electro-membrane process: batch and continuous. Industrial electrochemical processes are often operated continuously but experimental rigs are usually operated batch-wise. The differences between these two options are discussed below.

3.1.1.1 Continuous operation

In a continuous process the electrolyte streams flow through the electro-membrane stack and then onwards to the next unit operation. For some membrane systems this is accomplished using a recycle system with feed-and-bleed operation. As a result the electro-membrane cell must effect complete conversion/ separation in a single pass. A detailed knowledge of the feed and product streams is therefore required in order to design a continuous electro-

membrane stack. As a result of this such units are often less flexible for experimental studies because they are designed to operate within tight constraints. Additionally, large feed reservoirs and in-line post-treatment techniques are required to allow continuous operation in a laboratory. The diagram below shows a continuous electro-membrane process for a waste treatment application such as nitric acid recovery.

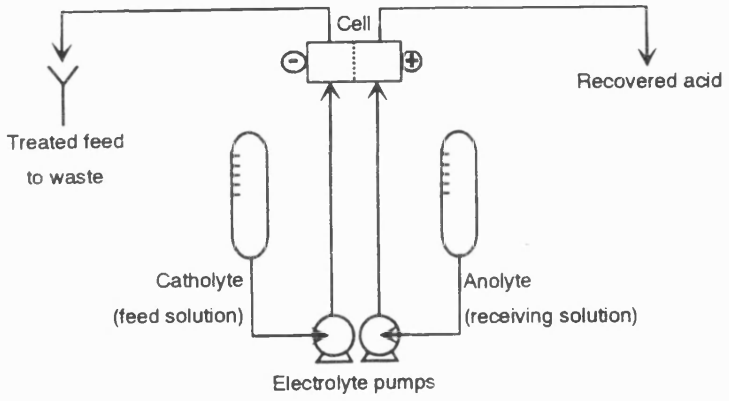

Figure 3.1: Illustration of a continuous electro-membrane process

Continuous operation is favoured by many processes where a constant product quality is required from a controlled feed. For effluent treatment applications, where there can be a variation in feed concentrations, batch operation is often favoured unless a complex process control system is to be used.

3.1.1.2 Batch operation

In batch operation of an electro-membrane process the electrolytes are re-circulated until the desired product concentrations are obtained. In this way the concentration changes per pass of the cell do not have to be significant. A variety of feed concentrations can be studied without altering any of the key process parameters; experiments are simply undertaken for different time periods as required. Many effluent treatment processes favour batch operation so that

sufficient processing can be ensured prior to discharging the treated stream. This enhanced flexibility led to batch recycle mode being adopted for the laboratory pilot rig which is illustrated below.

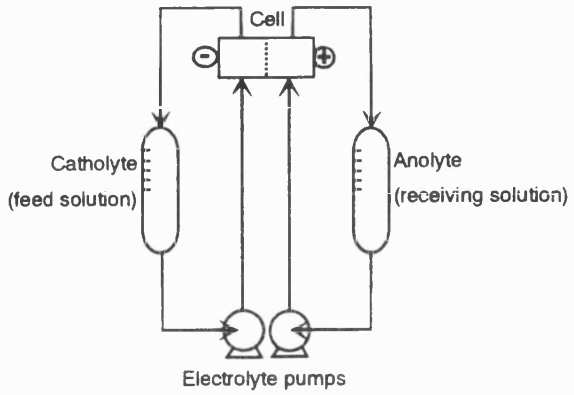

Figure 3.2: Illustration of an electro-membrane process operating in batch recycle mode

3.1.2 Electro-membrane stack design

This section highlights the main features that were considered when designing the electro-membrane stack. Both the model used to size the cell and the stack configuration based on an ICI FM01 laboratory electrolyser are covered here.

3.1.2.1 Spreadsheet model of cell

In order to design the cell for the experimental rig, a simple spreadsheet model was developed. This can be seen in Appendix 1. The model allowed estimation of ionic and water fluxes to predict electrolyte concentration and volume changes throughout a run. In this way the effect of membrane area, reservoir volumes and acid concentrations could be studied to allow optimisation of the rig design. For example, a large electrode area would give rapid concentration changes in a short time period but would require a large stack and membrane area. The resultant experiments would be fast but the cost of the laboratory rig and membrane samples would be high.

It was also decided to design the electro-membrane stack using a standard commercial cell. Utilisation of an off-the-shelf commercial stack saved significant time and effort required to design an in-house unit. Additionally, scale-up between laboratory and industrial cells is facilitated if a commercial laboratory stack is used. The spreadsheet model therefore allowed stack variables, such as electrode and membrane area, to be fixed according to commercial cell specifications. The effect of reservoir volumes was also studied to allow sufficient flexibility to be incorporated into the experimental apparatus for both duration of experimental runs and allowance for electro-osmotic water flux. The model was used to specify the size of the electro-membrane stacks to be incorporated into the experimental apparatus.

Movement of nitric acid from catholyte to anolyte was estimated assuming that osmosis was not significant. A simple Faradaic relationship was used as the basis for the model, such that:

$$N = \frac{jA_m t}{z\Im} \qquad [3.1]$$

At the concentrations being examined nitric acid dissociates almost completely to $H^+$and NO_3^-. For every mole of NO_3^- passing across an anion exchange membrane the equivalent moles of nitric acid were assumed to be transported because the nitrate ion would combine with a proton from either cation exchange membrane transport (electrodialysis) or electrochemical generation (electro-electrodialysis). The model also included provision for water transport through the membrane via ion solvation shells. This was effected by assuming a constant

co-ordination number for nitrate transport (2-3 mol water per mol acid was estimated).

Gas evolution at the electrodes was calculated from the electrochemical reactions:

$$\text{cathode} \quad H^+ + e^- \rightarrow {}^1/_2 H_2 \qquad [3.2]$$

$$\text{anode} \quad {}^1/_2 H_2O \rightarrow H^+ + {}^1/_4 O_2 + e^- \qquad [3.3]$$

The resultant hydrogen evolution rate was used to determine the amount of purge-air required to dilute the gas to below its lower explosive limit. A safety factor of four was used as is commonly used in industry.

3.1.2.2 Specification of commercial stacks

As a result of the simple modelling, two electro-membrane units were selected and then procured from ICI Chemicals & Polymers Ltd. They were based on the standard ICI FM01 laboratory electrolysers which are scaled-down versions of the FM21 industrial cell.

The FM01 cell is based on a filter-press or plate-and frame construction so the flows are conducted through the stack via spacers with internal manifolds. This configuration is explained in detail in the FM01 data manual (ICI, 1993) and a representation of a spacer is given in Figure 3.3.

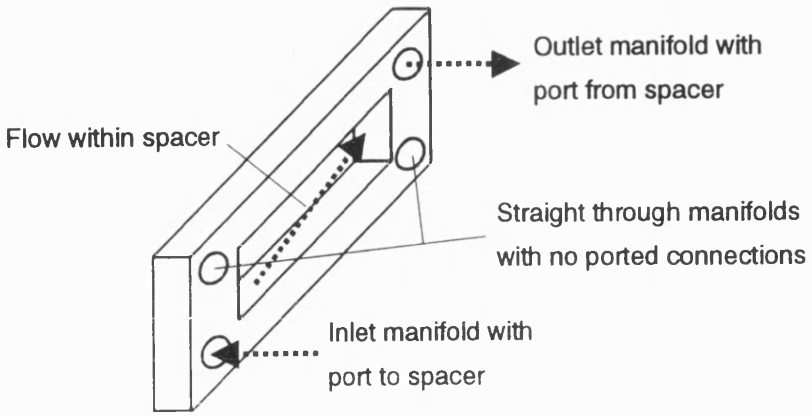

Figure 3.3: Illustration of a spacer in an FM01 cell

The electrolyte enters from the manifold at the bottom of the spacer, passes within the spacer across the face of the electrode or membrane, and exits via the port diagonally opposite the feed. The straight manifolds allow a second electrolyte to pass through the spacer in order to reach a subsequent chamber in the stack where it flows across the cell. Careful arrangement of spacers allows separate electrolytes to flow each side of a membrane without any contact of the two streams. This is suitable for electro-electrodialysis (EED) and the representation of the internal flows is illustrated in Figure 3.4. In this figure a stream enters a spacer and flows across the surface of the membrane before leaving at the same end of the stack as the feed.

In electrodialysis there are four process streams which means that a standard FM01 configuration cannot be used. A modification was therefore implemented by fitting connections to both ends of the stack (rather than the standard single end ports). The internal spacers were arranged to create four discrete cell compartments (anode rinse, concentrate, diluate and cathode rinse) and an illustration of this configuration is shown in Figure 3.5.

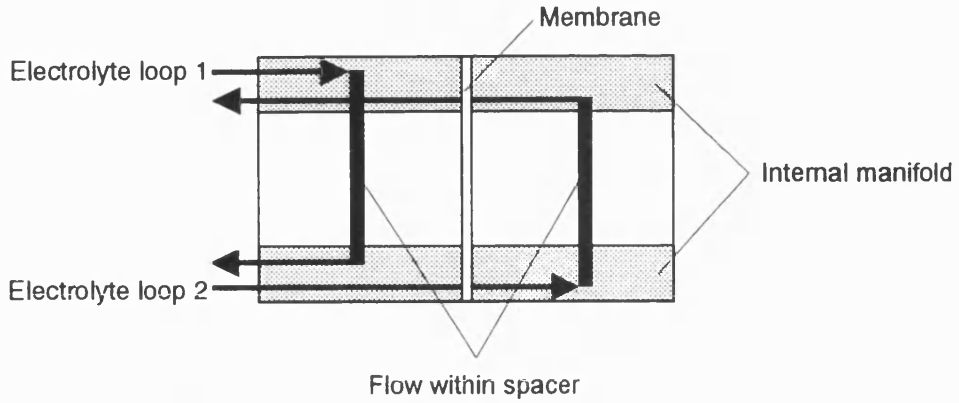

Figure 3.4: Representation of the flows in an FM01 configured for EED

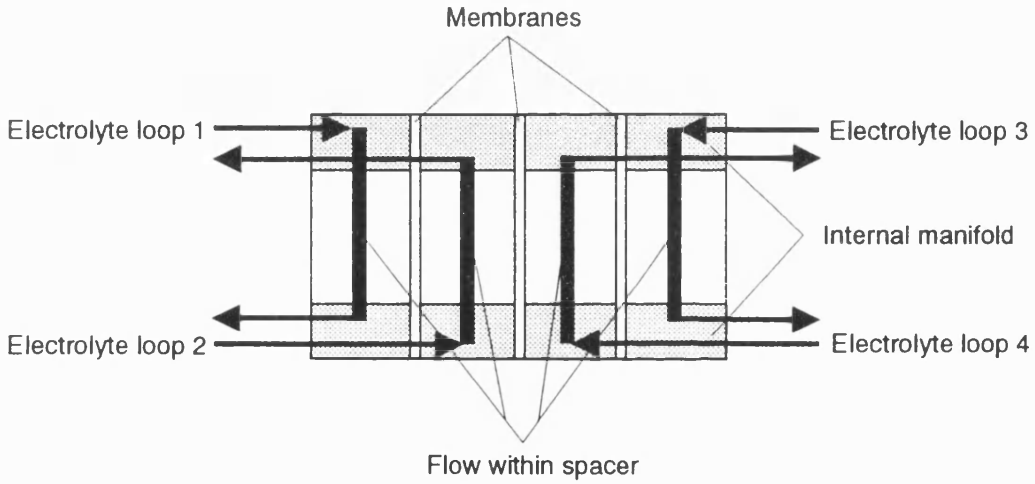

Figure 3.5: Representation of the flows in an FM01 configured for ED

The active cross-sectional area of a unit cell in the FM01 electrolyser is 64 cm^2. Consequently the membrane area employed in an experiment is a multiple of 64 depending on how many repeated cells are employed. For example, the experimental electro-electrodialysis configuration had two unit cells giving a total membrane area of 128 cm^2. A membrane-electrode gap of 7 mm was used. In a commercial cell the membrane-electrode gap would be much smaller and this would be achieved by the use of lantern-blade electrodes and/ or tortuous path spacers. Although the adopted configuration was sufficient for the experimental

programme, it would be necessary to optimise stack design for industrial application of this technology.

3.1.2.3 Electrode materials

The electrodes for the electro-membrane stacks were specified according to advice given by ICI when procuring the cells. Due to the proprietary nature of electrocatalysts the exact content of the precious metal anode coating was not divulged although the main electrocatalyst was given. For electrodialysis both electrodes operate in rinse streams and so they did not have to withstand the acidic environment whereas the electrodes for EED had to withstand nitric acid. The electrodes were therefore specified as in Table 3.1.

Electrode	Substrate	ICI coating reference	Electrode coating
ED			
anode	Ti	ES2	IrO_2
cathode	316 stainless steel	n/a	
EED			
anode	Nb	ES4	Pt(MA)
cathode	Hastalloy grade C22	n/a	

Table 3.1: Electrode materials for ED and EED showing electrode substrates and coatings

3.1.2.4 Estimation of voltage drop across stack

In order to estimate the size of the power supply, the voltage drop across the electro-membrane units was predicted using a short-cut calculation. An equivalent electrical circuit for voltage drop across the cell is shown in Figure

3.6. It is applicable to either ED or EED as only the number of repeated cells is the variable.

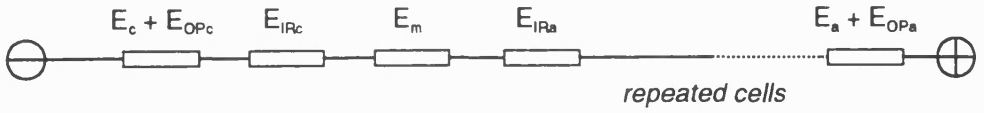

Figure 3.6: Equivalent circuit used to estimated voltage drop across cell

Individual components of the voltage drop were estimated and summated to give the total cell voltage drop according to:

$$E_{cell} = E_c - E_{OPc} - E_{IRc} - E_m - E_{IRa} - \ldots - E_{OPa} - E_a \qquad [3.4]$$

E_a anode potential (V)

E_c cathode potential (V)

E_{cell} voltage drop across entire cell stack (V), <0 for a cell

E_{IR} voltage drop due to solution (V)

E_m voltage drop across membrane (V)

E_{OP} overpotential (V)

The assumptions made in order to estimate the voltage drop across the cell using this technique are given in Appendix 2. A power supply capable of providing 30V and 40A was specified as a result of this calculation. A 3 kW powerpack capable of supplying 60V and 150A in either potentiostatic or galvanostatic operation was obtained from the DRA. This unit was rated higher than estimated but afforded greater flexibility in operation for the experimental programme.

3.1.3 Flowsheet of experimental rig

Having considered the electro-membrane cell which is the heart of the experimental rig, a detailed line diagram was produced for use in design and ultimately construction of the apparatus. This is shown in Figure 3.7.

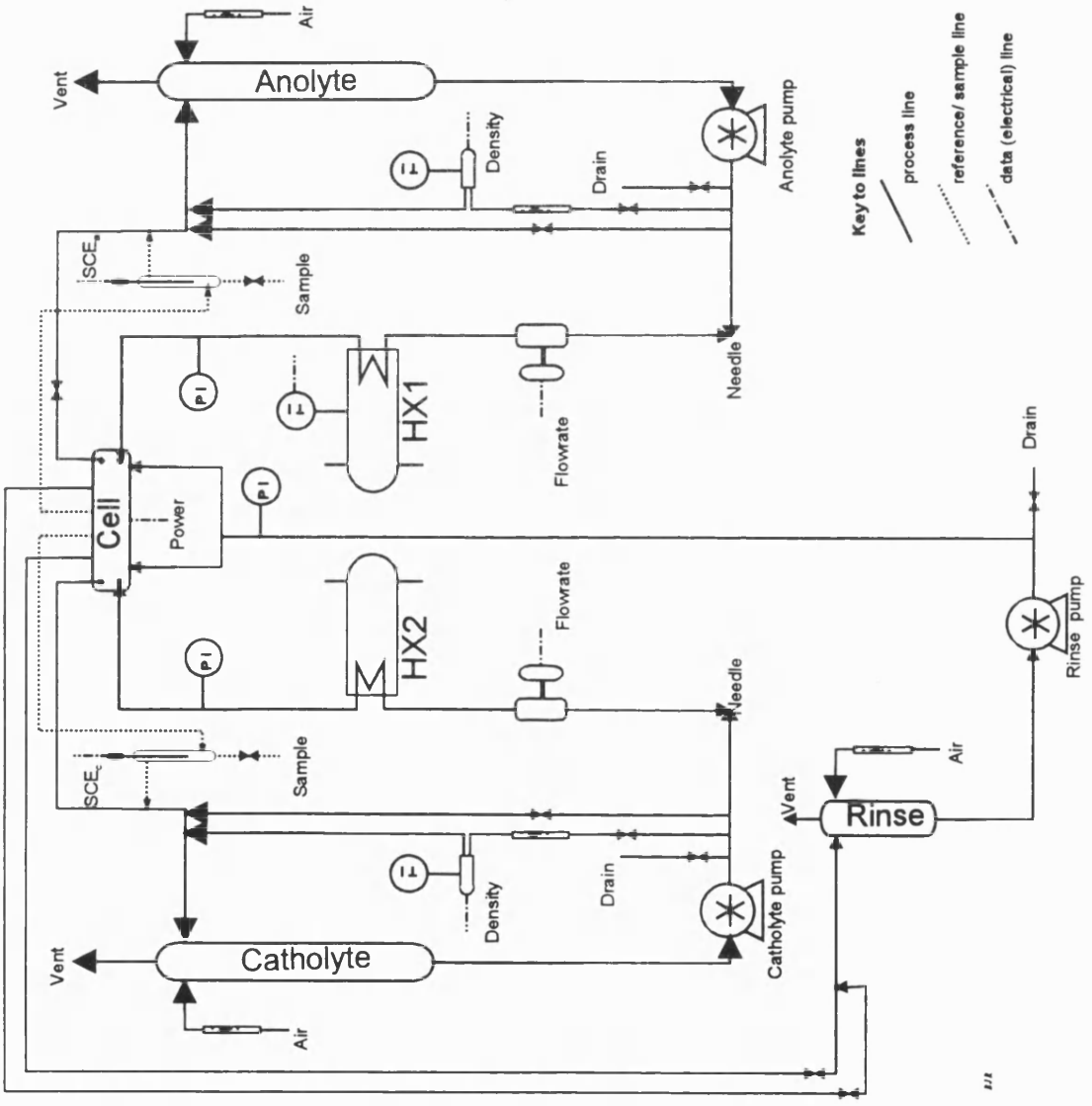

Figure 3.7: Line diagram of experimental rig

There are three main electrolyte loops shown on the line diagram: the anolyte circuit, the catholyte circuit and the electrode rinse circuit. The latter of these would only be used for an electrodialysis configuration of the cell. Its role is to sweep away electrode gases and to maintain conductivity of the electrode compartments in ED.

The anolyte and catholyte circuits are essentially similar and so are discussed simultaneously here. Electrolyte is pumped from the reservoir via a flowmeter and a heat exchanger and on to the cell. It then returns to the reservoir to mix with the bulk. A bypass line in this circuit facilitates flow control by taking a portion of electrolyte from the pump discharge directly back to the reservoir. Two other by-passes are seen on the diagram. The first of these allows a feed of electrolyte to be taken via a rotameter to the density/ temperature transmitters before being returned to the reservoir. The second takes a stream directly from the cell via a small reservoir where a reference electrode is housed back to the main reservoir. Liquid samples are taken from the reference electrode reservoirs.

Purge-air streams are fed into the head-space of the electrolyte reservoirs to dilute and sweep-away gases to the vent. These are fitted with rotameters to monitor the air flow and a trip switch is fitted to the main air supply which stops the power to the electro-membrane cell if the air flow fails.

3.1.4 Materials of construction

It was initially decided to construct the experimental rig out of materials with excellent chemical stability, such as boro-silicate glass or PTFE, to enable many different acids to be studied in future work. This specification was later relaxed to allow the incorporation of Paar in-line density meters which were made from

316 stainless steel. Consequently the fittings in the density meter lines were also made of 316 stainless steel. This meant that the limit of nitric acid concentration in the experimental rig was approximately 60 wt% at ambient conditions. Significant corrosion would occur above this point.

3.1.5 Line sizing

The diameter of the lines in the experimental rig was intentially small in order to reduce the volume hold-up of the apparatus so that concentration changes could be observed in a reasonable period of time. As a result, the pressure drop throughout the system was greater than the commonly used 'optimum'. This trade-off is sketched in below.

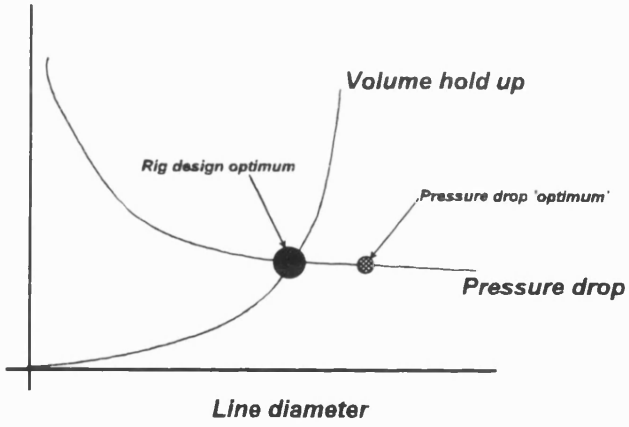

Figure 3.8: Minimisation of volume hold-up and pressure drop in line sizing

Standard sized (12 mm OD/ 9 mm ID) PTFE lines from Chemcon were chosen due to their good chemical stability and their compatibility with existing rigs operated by the DRA.

3.1.6 Pump sizing

As discussed above, the lines in the experimental rig were designed with a small diameter to minimise the hold-up volume of process fluid. This gave rise to a relatively high pressure drop.

The pressure drop around the system was estimated using a simple spreadsheet routine based on the energy equation:

$$\frac{\Delta u^2}{2\alpha g} + \Delta z + \frac{\Delta P}{\rho g} + \frac{W_s}{g} + \frac{f}{g} = 0 \qquad [3.5]$$

f	energy loss due to friction ($m^2 s^{-2}$)
g	acceleration due to gravity ($m s^{-2}$)
P	system pressure ($N m^{-2}$)
u	fluid velocity ($m s^{-1}$)
W_S	shaft work (W)
z	vertical height (m)
α	flow coefficient ($\alpha = 1$ laminar, $\alpha = 0.5$ turbulent)
Δ	change in a variable
ρ	density ($kg m^{-3}$)

The friction factor, Φ, was estimated using the expression for turbulent flow in smooth (PTFE) pipes given by (Coulson & Richardson, 1988):

$$\Phi = 0.0396 Re^{-0.25} \qquad 2.5x10^3 \leq Re \leq 10^5 \qquad [3.6]$$

Re Reynolds number

Φ friction factor

Thus the energy loss due to friction, f, (not the friction factor Φ) could be obtained from the expression given by:

$$f = 4\Phi \frac{L}{d} u^2 \qquad [3.7]$$

d pipe diameter (m)

L length of pipe (m)

The number of fittings and length of pipework around the system was estimated from the flowsheet and their contribution to the total pressure drop was estimated in terms of equivalent velocity heads. Pressure drop data for the electro-membrane stack and heat exchangers were also included to give a total system pressure drop. For the case of water circulated at 13 dm^3 min^{-1} around the rig, the pressure drop was estimated to be 3.5 bar. The contribution of the main components to this pressure drop was broken down as follows: heat exchanger 49%, lines and fittings 36% and cell 15%. As pump manufacturers' data are usually based on water, the 13 dm^3 min^{-1} @ 3.5 bar was taken as the specification for the electrolyte pumps.

A net positive suction head (NPSH) check was included to monitor the risk of cavitation using (Coulson & Richardson, 1986):

$$NPSH = \frac{P_0}{\rho g} - \frac{P_v}{\rho g} + h_0 + h_f \qquad [3.8]$$

h_f head loss due to friction in suction line (m)

h_0 head of liquid above inlet to pump (m)

P_v liquid vapour pressure (N m^{-2})

This was compared with NPSH requirements specified by the pump manufacturers. A typical value of NPSH of 1.5m was used for a centrifugal pump. The value calculated for the rig was sufficiently high to give a good margin of safety in the design.

In order to achieve the required duty, whilst maintaining a low liquid hold-up in the pumps, positive displacement pumps were chosen. The first type tested were Vanton rotating flexi-liners. These gave a pulsating flow and had poor continuous running characteristics. They were therefore exchanged for gear pumps with Ryton gears in a 316 stainless steel body from Tuthill. Although a better pumping performance was achieved by the gear pumps, some chemical stability was sacrificed which meant that operation could only be carried out at ambient temperatures.

3.1.7 Temperature control

Heat is input to the system via electrical heating in the electro-membrane cell and from the energy of pumping. Although this would not cause a large temperature rise per pass through the unit, if not removed it would cause a significant temperature rise over the duration of an experimental run. In addition to maintaining a constant temperature it might have been desirable to

look at the effects of temperature on the system performance. Thus a certain degree of flexibility was required in the heat exchange design. Subsequent constraints on replacement pumps meant that temperature effects could not however be studied.

Temperature control of the experimental rig was divided into two areas for the purpose of design. The first stage was to calculate the required cooling duty and to specify an appropriate refrigeration unit, whilst the second stage was to undertake heat exchanger design.

3.1.7.1 Cooling

The maximum possible heat input to the system was estimated from the electrical and pumping duties taking the cell power requirements estimated in section 3.1.2.4. This gave an over-estimation of the cooling duty but allowed flexibility. The heat duty was determined as:

Cell power	= 657W (mean value)
Pumps (×2)	= 750W
TOTAL	**= 1407W**

A laboratory chiller unit was specified which was capable of removing this heat. A Grant RC1400 was chosen as this could remove 1100W of heat at 20°C and was accurately controlled using an integral heater. At higher temperatures the cooling capacity increased exponentially to 5000W at 50°C. For the duty specified above, the steady-state temperature of the coolant was therefore estimated to be 22°C by linear interpolation of the performance data. In practice it was found that the unit maintained a constant temperature of around

25°C which deviated by a maximum of 5C° under extreme operating conditions.

3.1.7.2 Heat exchangers

The controlled coolant supply and the near-constant temperature of the process fluid facilitated the design of the heat exchangers. Specialist laboratory exchangers were specified.

One of the key objectives was not to include metal in the electrolyte system. Consequently PTFE heat exchangers were chosen as they have significantly better heat transfer characteristics than glass whilst retaining good chemical stability. Spiral tube heat exchangers from Polymer Exchangers Ltd (Type S10-1.9) were chosen. The process fluid volume hold-up and pressure drop of these units is relatively high but compensated by their low cost. As there is only a small temperature rise per pass, the heat exchangers are operated close-coupled in series with respect to the coolant to make connections easier. The cooling circuit is shown below.

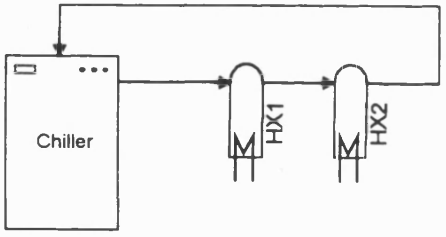

Figure 3.9: Cooling circuit

3.1.8 On-line concentration analysis

As shown in Chapter 2 many researchers working on electro-membrane processes have favoured titration to analyse the composition of the electrolytes. Although accurate, this technique is strictly off-line and the volume of the system

has to be sufficient to allow periodic sampling. On-line techniques were desired as they could aid future process control strategies. The techniques considered for on-line concentration analysis were: pH, conductivity, refractive index and density.

pH has been used by workers studying low concentration electrolytes but for high concentration acids the pH is very low. This can often be off the scale of standard commercial detectors. Conductivity probes and ion specific electrodes have been used along similar lines but again the high conductivity of nitric acid exceeds that of most commercial on-line probes which have been developed primarily for water testing. Glass probes with a high cell constant exist but they have a large liquid hold-up, are fragile and are difficult to operate.

Refractive index (RI) gives an accurate physical measurement with which to infer concentration and is linear over a wide range at a constant temperature. Unfortunately RI measuring devices cost in excess of £10,000 which was somewhat prohibitive for this project!

Finally, density measurement was considered. Density meters have an accuracy of $\pm 1 \times 10^{-3}$ g cm^{-3} or better. On-line Paar digital density transmitters were chosen as they had an accuracy equivalent to $\pm 1/7$ wt% nitric acid (based on manufacturers and nitric acid data). The output was processed using a device constructed within the School of Chemical Engineering to allow analogue data logging of the digital signals. The density meters performed satisfactorily for binary nitric acid-water mixtures. In subsequent work however, the catholyte was found not to be a binary mixture due to nitrate reduction. Despite this phenomena not occurring in the anolyte, the density measurements were used

only to determine the mass of the electrolytes and not to infer the acid concentrations. Concentrations were always determined periodically by titration.

3.1.9 Flow measurement

In order to ensure an adequate feed flowrate for good mass transfer in the electro-membrane cell the flows had to be monitored. Many types of flow measuring devices were considered such as: variable area, pelton wheel, ultrasonic and electromagnetic. Electromagnetic flowmeters from Endress & Hauser were chosen capable of reading 0-20 dm^3 min^{-1}. These meters were PTFE lined and thus suitable for nitric acid. An analogue output signal could be used for data logging.

3.1.10 Data logging

A self-contained analogue data logger was purchased to allow simple and accurate recording of the process variables. This device could be used in the laboratory and allowed subsequent read-back into a personal computer. Thus the dedicated use of a computer in the laboratory was avoided. A Grant Squirrel 1250 was chosen having 16 data inputs for variables such as thermocouples, voltage and current. For example, the power supply to the electro-membrane unit was recorded using two data logger channels. The first monitored the current via a 75 mV shunt rated for currents up to 100A and the second measured the voltage using a ÷3 potential divider rated for cell voltages up to 60V.

3.1.11 Vessel sizing

Gas bubbles generated at the electrodes had to be separated from the process streams. It was not desirable to have separate knock-out pots due to the additional complexity of process piping and operation. Thus the vessel diameters had to be designed to allow disengagement of the bubbles against the direction of liquid circulation to effect the gas-liquid separation.

A correlation for air bubbles rising in water was used and the rise velocity of a bubble in a stagnant liquid was estimated (Clift, Grace & Weber, 1978). Taking a nominal 1 mm bubble diameter the stagnant rise velocity was calculated to be 20 cm s^{-1}. For various diameter reservoirs the net rise velocity, U-v, due to the downwards liquid motion was determined using various standard glass vessel diameters. This is shown in below.

Diameter mm	**U-v** cm s^{-1}
50	3
80	13.4
120	17
150	18†

† 90% of unhindered rise velocity

Table 3.2: Rise velocity of bubbles

A 150 mm diameter vessel was chosen for the catholyte and electrode rinse reservoirs. For the anolyte reservoir the design had to take into account other factors such as the accuracy of volume reading on the vessel wall (for water flux measurements) and the physical height limit of the apparatus. For this case, an

80 mm diameter column was chosen which would give a scale accuracy of approximately 5 ml per 1 mm of column height. Assuming readings were possible to ±2.5 mm this would give in an accuracy of ±25 ml. The catholyte, anolyte and rinse reservoir volumes were 10 dm^3, 5 dm^3 and 5 dm^3 respectively.

3.1.12 Incorporation of reference electrodes

In order to study the electrical phenomena in the system, the experimental rig was modified to incorporate calomel reference electrodes. Improved on-line liquid sampling of each electrolyte loop was also included in this modification. Capillary tubes were chosen that could be fitted to a spacer unit in the electro-membrane cell and allow a flow of liquid from the stack to an external reservoir housing the reference electrode. The liquid returned to the appropriate electrolyte reservoir. It was found when designing this system that there was sufficient pressure in the stack to generate a flow through the capillary tubes of approximately 250 ml min^{-1} without the need for additional pumping. Refillable calomel reference electrodes were obtained from ABB Kent-Taylor. The KCl filling solution was replaced after each experimental run to minimise the effect of process acid leaching into the electrode. This modification is included in the line diagram given in Figure 3.7.

3.1.13 Views of rig

The plates below depict views of the experimental rig prior to comissioning.

General view of experimental rig and bench area

Close-up of experimental rig (safety screens removed)

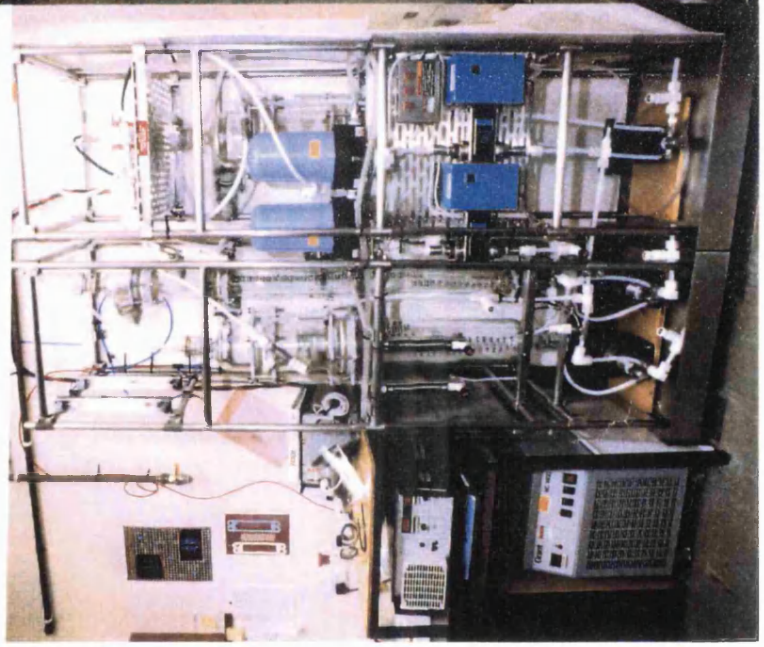

Close-up of bench area showing titration apparatus

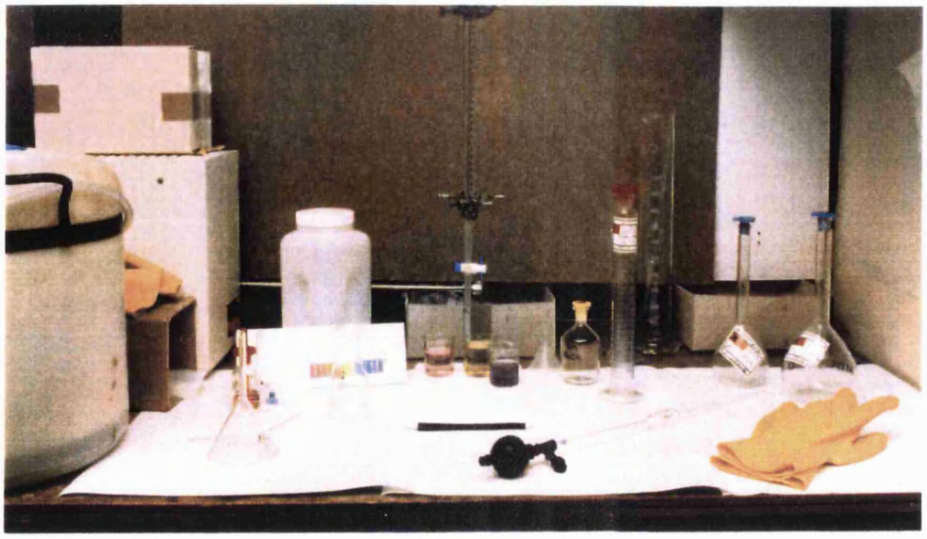

3.1.14 Safety

A full risk assessment of experimental apparatus and procedures was completed in order to satisfy the safety regulations. This included HAZOP and COSHH studies. Amongst other recommendations, the report highlighted the need for a purge-air trip switch to cut the power supply to the cell in the event of air failure in order to stop hydrogen evolution and prevent an explosive mixture from occuring. A copy of this risk assessment is held within the School of Chemical Engineering.

3.2 Experimental protocol

The protocol adopted for the experimental programme is discussed in this section. Cell configuration, chemical analysis techniques and the matrices of experiments are discussed.

3.2.1 Operation of rig

As mentioned in section 3.1.1 the experimental rig was designed to operate in batch recycle mode configured for either electrodialysis (ED) or electro-electrodialysis (EED). Potentiostatic or galvanostatic power control could be adopted. The decisions as to the most appropriate configuration and mode of power control are discussed here.

3.2.1.1 Cell configuration

It is difficult to study the performance of a particular membrane via data obtained in an ED stack due to the combination of alternating anion and cation exchange membranes; performance measurements represent performance of the

membrane pair. An EED configuration (which allows membranes to be studied individually) was therefore used for the experimental study. The literature review in Chapter 2 revealed that the most significant loss of efficiency in ion exchange membranes used for acid processing was due to the transport of protons by anion exchange membranes (proton leakage). Consequently the experimental programme focused on the performance of anion exchange membranes in the EED stack.

3.2.1.2 Power control

In order to study the variation in performance of a particular membrane with process conditions it is desirable to maintain either a constant total flux or a constant driving force across it. When operating in batch mode many variables alter throughout the course of an experimental run. This makes it difficult to maintain a constant driving force. Even if the voltage driving force across the membrane were to be maintained constant, the concentration driving force would be continually changing. Galvanostatic operation was therefore adopted which maintains a constant total ion flux across the membrane. By operating in this way the variation of relative fluxes (counter ions against co-ions) could be studied.

3.2.2 Experimental procedure

Membranes were soaked for at least 24 hours prior to cutting and assembling the electro-membrane unit. New membrane samples were used in each experimental run. The active membrane area used in the experiments was 128 cm^2. For the majority of experimental runs the concentrations of each electrolyte were initially equal. This was achieved by adding accurately prepared acid solutions to a known volume of pure water already in the electrolyte reservoirs.

In this way concentrated (68 wt%) acid was only used in a fume cupboard to prepare solutions prior to transferring them to the experimental rig. Pure ($<20\mu S\ cm^{-1}$) reverse osmosis water was used for all solutions and for the rig make-up and cleaning water.

Both electrolytes were circulated for at least 10 minutes (equivalent to approximately 5 residence times) to ensure good mixing before samples were taken. During this time, the flowrates of the electrolytes and of the purge air were regulated. The power was slowly applied to the cell until the operating current was reached. The key process parameters are listed below for the two-cell EED configuration.

Electrolyte flowrates:	$4.8\ dm^3\ min^{-1}$
Cell inlet pressures:	≈ 0.8 barg
Operating current:	$58\ A \equiv 450\ mA\ cm^{-2}$
	$39\ A \equiv 300\ mA\ cm^{-2}$
	$19\ A \equiv 150\ mA\ cm^{-2}$
Operating temperature:	$25°C \pm 2C°$ normal operation
	$25°C \pm 5C°$ extremes of operation
Purge-air:	$35\ dm^3\ min^{-1}$ catholyte
	$2\ dm^3\ min^{-1}$ anolyte

Throughout an experiment periodic samples were taken for chemical analysis and the rig was shut-down to allow volume readings to be taken. For long experimental runs the rig was stopped overnight for safety reasons before restarting the following morning. Upon shut-down the cell drained completely to the reservoirs so that no membrane transport occurred during this period. It

was found that sufficient humidity remained in the cell for the membranes to be held overnight without being fully wetted - only minimal membrane re-conditioning was observed the following day. At the end of an experiment the rig was stopped and the electrolytes discharged to a neutralisation tank. The rig was washed thoroughly with pure water before dismantling the cell.

3.2.3 Chemical analysis

Nitrate reduction was found to occur at the cathode. Consequently it was necessary to analyse for three main species in the liquid phase: nitrate (NO_3^-), nitrite (NO_2^-) and ammonium (NH_4^+). These represent the reactant, the intermediate and the end product of the reduction pathway which is discussed later in the thesis. The analytical techniques are given below.

3.2.3.1 Total acid determination

As the focus of the project is recovery and concentration of nitric acid, the total acid determination is the most important measure required in order to assess the performance of the process. This measure includes both nitric and nitrous acids and can be undertaken using the relatively simple volumetric techniques discussed in this section.

3.2.3.1.1 Simple volumetric

The simplest form of total acid analysis is via direct titration with a standard alkali solution such as sodium hydroxide (NaOH). In this method a known volume of sample is titrated with the standard alkali and the amount of acid in the sample determined directly from the moles of alkali added. The reaction for this technique is given by:

$$HNO_3 + NaOH \rightarrow NaNO_3 + H_2O \qquad [3.9]$$

3.2.3.1.2 Reverse volumetric

The reverse volumetric method exploits the same reaction described above but, instead of titrating the sample directly with alkali, the sample is first treated with a known amount of standard alkali in excess before being titrated with a standard acid solution such as nitric acid (HNO_3). Thus the two-step reaction scenario proceeds according to:

$$HNO_3 + NaOH \rightarrow NaNO_3 + H_2O + xsNaOH \qquad [3.10]$$

$$xsNaOH + HNO_3 \rightarrow NaNO_3 + H_2O \qquad [3.11]$$

The reverse technique was adopted by the DRA to minimise NOx loss from concentrated acid samples prior to analysis. Additionaly, the resultant liquor is suitable for further volumetric analysis such as nitrite determination as described in the next section. This technique was used throughout the experimental programme.

It should be noted that ammonium present in a sample can effect the results obtained for both of the techniques described above. Either total nitrate or total acid values are modified by the presence of NH_4^+ and this should be considered when interpreting experimental data.

3.2.3.1.3 Acid concentration units of measurement

Although molarities are the most useful unit of concentration when studying acid transport and proton leakage, other measures such as weight percent (wt%) or liquid mole fraction (X) are sometimes used by other workers. The relationship between these three measures is illustrated below for the nitric acid water system. It should be noted that solution interactions such as volume changes upon mixing were neglected. As the chart below is for illustrative purposes only the calculation technique was not refined.

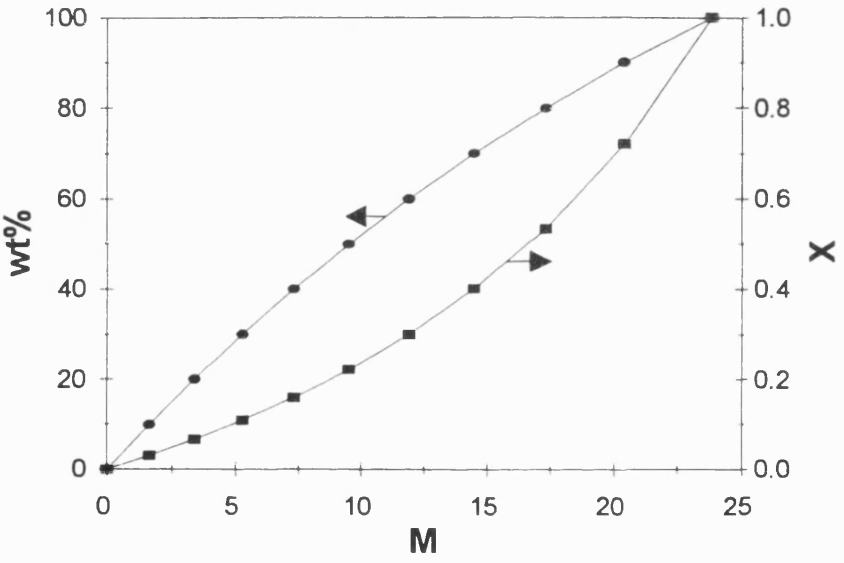

Figure 3.10: Comparison of concentration measures for nitric acid

3.2.3.2 Nitrite determination

It was possible that nitrite could be present in catholyte as an intermediate of the nitrate reduction to ammonium reaction pathway. Liquid samples were therefore analysed to determine their nitrite content throughout an experimental run. This was carried out using the three techniques described below.

3.2.3.2.1 Volumetric

The volumetric technique used for nitrite determination was adapted from a method developed by the DRA for analysing N_2O_4, N_2O_5, HNO_3 and H_2O mixtures (Cumming, 1995). The chemical reactions exploited by this method are the oxidation/ reduction of cerium and subsequent detection using a starch-iodine titration.

A known amount of standard alkali was added to the sample and the total acid determined by titration with standard acid as in Section 3.2.3.1.2. A known amount of ammonium cerium sulphate was subsequently shaken with the liquor to allow Equation 3.12 to proceed. This reduced the cerium by oxidising any nitrite to nitrate. Following this a known amount of potassium iodide was added in excess to reduce any remaining cerium by liberating iodine, Equation 3.13. The iodine was detected using a starch indicator and titrated to a clear end-point with standard sodium thiosulphate as Equation 3.14. Whilst the accuracy of this technique was good, it was laborious to analyse each sample and the cost of reagents was high. This technique was used initially for nitrite determination prior to the use of HPLC described in the next section.

$$2Ce^{4+} + NO_2^- + H_2O \rightarrow 2Ce^{3+} + NO_3^- + 2H^+ \qquad [3.12]$$

$$Ce^{4+} + I^- \rightarrow Ce^{3+} + {}^1/_2I_2 \qquad [3.13]$$

$$I_2 + 2S_2O_3^{2-} \rightarrow 2I^- + S_4O_6^{2-} \qquad [3.14]$$

3.2.3.2.2 *High pressure liquid chromatography (HPLC)*

In order to decrease the time taken to run samples and to reduce the reagent cost per sample, without reducing the accuracy of the analysis, an HPLC technique was used to analyse nitrate and nitrite simultaneously. The HPLC system was configured using a Shodex IC-524A column from Phenomenex operating at 40℃. The eluant was 2.5 mM potassium hydrogen phthalate (pH=4) flowing at 1.5 ml min^{-1}. Loading was via a Rheodyne 7010 valve fitted with a 20 µl injection loop. Detection was via a multiwavelength detector set at 301 nm. This HPLC configuration allowed detection of nitrite concentrations above 100 ppm which could have been improved further using a conductivity detector. HPLC was used for the majority of experimental runs which required nitrite analysis. It produced results agreeing with the volumetric techniques for both total acid and nitrite determination and therefore also provided a double-check of the titration results.

3.2.3.2.3 *Indicator tests*

At rather a late stage in the experimental programme a simple test was discovered for low-level nitrite in nitric acid media. This involved dipping an indicator spill briefly into the acid sample. The resultant colour change at the tip of the spill (grey to bright purple) allowed nitrite to be clearly detected at concentrations above 10 ppm. These indicator spills were used on samples from the latter experimental runs to confirm zero (<100 ppm) results from the HPLC analysis.

3.2.3.3 Ammonium determination

Ammonium was analysed using a classical preparative volumetric technique based on the method given by Basset (Basset, Denney, Geoffries & Mendham,

1978). This method involved adding excess alkali to a sample in a closed vessel which caused any ammonium to be converted to ammonia gas. The sample was boiled and the ammonia vapours trapped in a known amount of standard acid. The acid solution was then titrated with standard alkali to determine the excess acid and hence ammonium concentration in the original sample. The apparatus used for this technique is illustrated below because it was a modified version of that described by Basset et al.

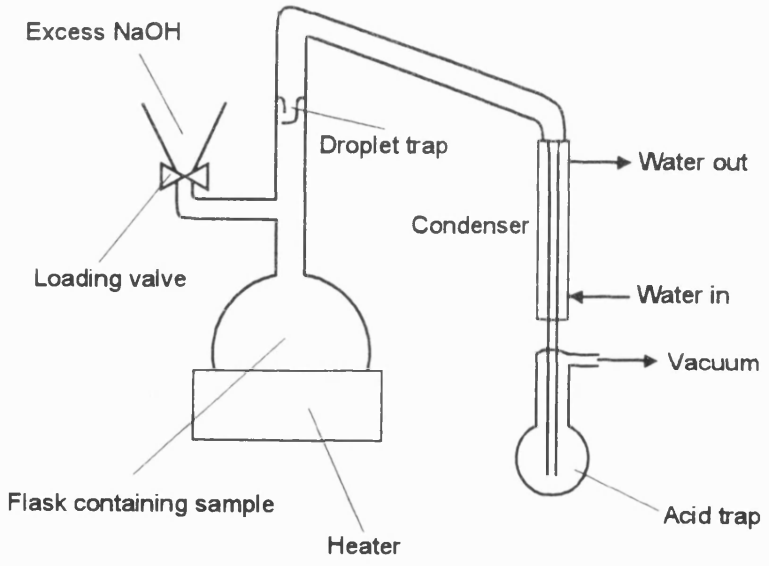

Figure 3.11: Apparatus used for ammonium analysis

All samples were analysed twice to minimise the possibility of spurious experimental data resulting from alkali carry-over into the acid trap. Ammonium analysis was carried out for all catholyte samples where nitrite analysis was undertaken.

3.2.4 Experimental rationale

The experimental programme focused on three main areas: an evaluation of different membranes, a qualitative study of the electrochemical phenomena and a more detailed study of a specific ion exchange membrane. Each of these areas of the study are discussed below along with the appropriate experimental matrices.

3.2.4.1 Membrane evaluation

In order to compare the performance of different commercially available anion exchange membranes samples were procured from various suppliers. The membranes that were evaluated are listed in Table 3.3.

For the membrane evaluation experiments the rig was loaded with equal acid concentrations in both the anolyte and the catholyte reservoirs. The membrane to be evaluated was soaked in pure 1M nitric acid solution for at least 24 hours prior to assembling the stack. Throughout these experiments the current density was maintained at 300 mA cm^{-2}. Variables were recorded at one minute intervals using the data logger. Periodic liquid samples and volume readings taken throughout the experimental run.

Membrane type	Polymer substrate	Basic specifications			Manufacturer
		Thickness μm	Exchange capacity meq g^{-1} †	Resistance Ω cm^{-2}	
ADP	ETFE	160±10	0.9-1.3	1.5-4.5	Solvay SA, France
ARA	ETFE	150±10	0.9-1.3	3-7	"
AW	ETFE	*experimental prototype*			"
AAV	perfluorinated	125±15	N/A	3-4	Asahi Glass, Japan
MA3475	non-perfluorinated	400	0.7	8-17	Ionac, USA
R5035	LDPE	≈200	0.8-0.9	5-16	Rai Research, USA
CRA *cation*	ETFE	160±10	1.4-2.2	1-4	Solvay SA, France

† *milli-equivalents per gramme of dry membrane*

Table 3.3: Specifications of membranes used in experimental programme

Experimental runs were continued until the catholyte concentration approached zero and/or the voltage increased to a point where the operating temperature rose significantly. The matrix of experiments undertaken in this area of the study is given below. Membrane type, initial electrolyte concentration and run identification code are shown.

Membrane type	**Initial concentration** 1 M	2 M
ADP	ADP1	ADP2
ARA	ARA1	ARA2
AW	AW1	AW2
AAV	AAV1†	AAV2†
MA3475	MA1‡	MA2‡
R5035	RAI1	RAI2

† Membranes repeatedly failed on start-up

‡ Membranes deteriorated during run due to chemical instability

Table 3.4: Membrane evaluation experiments showing run identification codes (including AAV & MA3475 failures)

In addition to these runs, a zero current experiment was undertaken with an acid concentration difference of approximately 6M in order to assess the extent of osmosis in the system. The results of the membrane evaluation experiments are given in the results section later in this thesis. Checks of reproducibility were made not only by comparing data from similar experiments but, where possible, by comparing them with the trends of results produced by other workers (Graillon, 1995), (Maeck, 1995).

3.2.4.2 Electrochemistry

In order to assess the extent of nitrate reduction occurring in the electromembrane cell a range of qualitative experiments were undertaken. These were divided into two main areas. Firstly, additional measurements were taken during the main experimental runs and secondly, trials to evaluate system performance were undertaken independently of the membrane assessment. These are discussed briefly below.

3.2.4.2.1 Additional process measurements

Throughout the experimental runs, on-line measurement of electrode potentials was undertaken using calomel electrodes via capillaries placed close to both the anode and the cathode in the cell. In addition to this, periodic liquid samples were analysed to identify specific chemical species and thus the overall extent of nitrate reduction.

3.2.4.2.2 Independent cell trials

In the first set of experiments, the purge gas system was reconfigured to allow argon tracing instead of purge-air. The catholyte off-gas was analysed using a mass spectrometer. Experiments were undertaken for a range of catholyte concentrations at various current densities. A cation exchange membrane (CRA) was used to minimise concentration changes in the catholyte.

The second set of experiments were current sweeps on the stack. A cation exchange membrane was again used and a range of catholyte concentrations studied. Limiting currents were estimated from this data in order to calculate a mass transfer coefficient which was compared to literature values.

3.2.4.3 *Detailed individual membrane study*

This part of the experimental programme focused on the performance of a single anion exchange membrane (AW). The membrane was evaluated using a similar experimental protocol to that given in Section 3.2.4.1. A wider range of initial starting concentrations was used and, for a given concentration, the effect of current density was also studied. These experiments are listed in Table 3.5 along with the run identification codes. Data from these runs were analysed in detail to allow a more advanced understanding of the membrane performance to be evaluated.

Initial anolyte concentration M	**Current density** 150 mA cm^{-2}	300 mA cm^{-2}	450 mA cm^{-2}
0.2†		AW002	
1.0	AW150	AW1	AW450
1.5		AW1.5	
2.0		AW2	

catholyte and anolyte concentrations initially equal except for † where initial catholyte acid concentration 2M

Table 3.5: Individual AW trials showing run identification codes

3.3 Summary of experimental work

In order to study the performance of electro-membrane processes for the nitric acid-water system an experimental rig was designed which was operated in batch re-cycle mode under galvanostatic power control. Various analytical techniques were adopted to monitor the species present in the system, especially those that might result from nitrate reduction in the catholyte. Experiments were

undertaken using the electro-electrodialysis (EED) configuration so that individual membranes could be studied. The performance of anion exchange membranes was the main focus of the research.

There were three main phases to the experimental programme: evaluation of different anion exchange membranes; a qualitative study of electrochemical nitrate reduction and a detailed study of an individual anion exchange membrane (AW). The results of these experiments are presented in the next chapter.

Chapter 4:

Experimental results and data analysis

4. Experimental results and data analysis

In this chapter the results of experiments in three areas are presented: i) process electrochemistry, ii) anion exchange membrane evaluation, and iii) a detailed study of a specific anion exchange membrane. In order to focus discussion on membrane performance, the process electrochemistry data are presented and discussed in this chapter whereas membrane performance is presented here but is discussed in Chapter 5.

4.1 Determination of performance data

Various methods may be used to quantify system performance as discussed in Section 2.4. The criteria used in this study were based on electrical efficiency and water transport which are two key measures of membrane performance. It was not possible to calculate performance measures directly from measurements made during the course of an experiment. In some cases it was necessary to mathematically manipulate the data in order to generate credible performance measures. The methods of calculation of the various measures are given in this section.

4.1.1 Membrane current efficiencies

Current efficiency relates the electrical performance of a process to a theoretical maximum and is therefore extremely useful for process evaluation. The theoretical relationship for current efficiency, η, was introduced in Section 1.4.2 and is given by:

$$\eta = \frac{Nz}{F} \qquad [4.1]$$

For electro-membrane processes, the current efficiency is a measure of the amount of charge transported across a membrane by a specified counter-ion (e.g. nitrate) in relation to the total charge transported. Factors such as competing counter-ions or co-ion leakage can reduce the efficiency of a membrane.

There are two practical definitions of current efficiency: integral current efficiency (η_{ICE}) and differential current efficiency (η_{DCE}). The relative merits of these measures are discussed below.

4.1.1.1 Integral current efficiency

The integral current efficiency, η_{ICE}, is a performance measure of a process over the duration of its operation and is most appropriate for batch operation. It is a mean value of the current efficiency over a given period of time. The mathematical definition is given by:

$$\eta_{ICE} = \frac{Nz\Im}{\int_0^t idt} \qquad [4.2]$$

This is determined in practice for nitrate ion transport (where N is increasing with time) by:

$$\eta_{ICE} = \frac{N(t) - N(0)}{F(t)} \qquad [4.3]$$

The η_{ICE} is easily determined from experimental measurements, however it is only valid for systems which are geometrically and hydrodynamically similar because of its historical dependance.

4.1.1.2 Differential current efficiency

The differential current efficiency, η_{DCE}, is an instantaneous current efficiency value over a differential element of time. It therefore represents the actual value of current efficiency at a given instant rather than an average over a considerable time. The mathematical formula for η_{DCE} is given by:

$$\eta_{DCE} = \frac{dN}{dt}\frac{z\Im}{i} \qquad [4.4]$$

It is determined from experimental data for nitrate ion transport via:

$$\eta_{DCE} = \frac{N(t+1)-N(t)}{F(t+1)-F(t)} \qquad [4.5]$$

The calculated value of η_{DCE} is very sensitive to small measurement errors and fluctuations. For example, whilst the error in an absolute concentration may be slight it can become significant with respect to small concentration changes. To overcome this problem η_{ICE} data was manipulated to derive credible η_{DCE} values. This technique is described below.

4.1.1.3 Current efficiency data manipulation

It is important to be able to study the η_{DCE} of an electro-membrane system if the performance measure is not to be history dependent. Due to the practical problems associated with determination of η_{DCE} directly, η_{ICE} values were

manipulated mathematically via a smoothing technique to derive credible η_{DCE} values.

A curve, f(t), was fitted to the η_{ICE} values determined directly from experimental data. A linear fit was found to be suitable for the η_{ICE} profile and this technique is illustrated later in this chapter. The fitted curve was manipulated with the definitions of η_{ICE} and η_{DCE} (Equations 4.3 and 4.5 respectively) to yield the equation:

$$\eta_{DCE} = \frac{f(t+1)F(t+1) - f(t)F(t)}{F(t+1) - F(t)} \qquad [4.6]$$

f(t) curve fit function to η_{ICE} data (s^{-1})

which was used sequentially to generate a η_{DCE} profile throughout each experimental run. This mathematical tool was developed in order to rationalise data generated by this research project. It was later found to be similar to a technique recently adopted by another worker in this field (Maeck, 1995).

4.1.2 Water transport

Water transport is associated with ion transport due to the formation of solvation shells as discussed in Section 1.4.1. The amount of water transported across a membrane limits the maximum nitric acid concentration which can be recovered. It is therefore important to consider water transport when assessing the performance of a particular membrane as this has a non-electrical effect on the overall process performance.

4.1.2.1 Water transport number

The simplest way to quantify water transport is by the use of a water transport number which is the ratio of moles of water transported in a given time to the Faradays of charged passed over that period. For the case of EED it is given by:

$$t_{H_2O} = \frac{N_W(t) - N_W(0)}{F(t)} + 0.5 \qquad [4.7]$$

N_W amount of water in anolyte (mol)

The number 0.5 in the equation comes from accounting for water consumption at the anode. It should be noted that the water transport number will decrease with decreasing current efficiency even if the co-ordination number for acid anion transport remains constant. Whilst it is a useful measure for comparing membranes of similar efficiency, it is not possible to draw direct conclusions about ion solvation from water transport numbers. Despite this many workers choose only to report water transport numbers when quantifying electro-osmotic water transport.

4.1.2.2 Specific water transport number

In order to account for the effect of current efficiency on water transport numbers a specific water transport number was used. The specific water transport number used here relates the amount of water transported to the amount of a particular ion transported across a membrane. For the system studied the moles of water per mole of nitric acid transported across the membrane was chosen as

a suitable measure. The specific water transport number was determined from the water transport number and current efficiency by using:

$$n_{H_2O} = \frac{t_{H_2O}}{\eta_{ICE}} \qquad [4.8]$$

n_{H2O} specific water transport number

The specific water transport number is not directly related to the ion co-ordination number as it attributes all water transport to the motion of a particular ion. However it gives a much improved measure over the water transport number and is therefore reported for the membranes studied. Improved measurement of water transport is discussed in detail when analysing membrane performance later in this thesis.

4.2 Qualitative electrochemical reaction study

It was found that nitrate could be reduced at the cathode of the experimental rig. A qualitative study of this phenomenon was undertaken in order to assess the effect of various parameters on the electrochemistry. The study was broken into two parts: off-line experiments which were undertaken independently of membrane trials and on-line experiments that were carried out during the membrane trials. In this way a basic understanding of the electrochemical phenomena was obtained simultaneously with the main experimental programme.

4.2.1 Review of publications on nitrate reduction

A review of the publications concerning nitrate reduction was undertaken in order to understand the background to this subject. This was not included in the main review of literature in Chapter 2 as it was thought that it might detract from the main topic of the research. It is therefore summarised in Appendix 3 and the main conclusions are highlighted below.

Most studies were undertaken in alkaline media with all other studies conducted at pH>1. Nitrate concentrations were generally low (<<1.2M) as found in the water industry. Nitrate salts were more often used as the nitrate source rather than nitric acid. Many electrode materials were studied with high hydrogen evolution overpotential electrodes favouring nitrate reduction. All the processes aimed to destroy rather than recover the nitrate ions and consequently it was common not to employ a cell separator or an ion exchange membrane. Anion exchange membranes were not used.

Various mechanisms were proposed for the reduction pathway depending on the conditions in the catholyte. pH appears to have a large influence on the reduction product. Overall two key reduction products, mainly nitrite and ammonium (or ammonia), were highlighted although gaseous nitrogen was also reported in some cases. Detailed half-cell reactions are also given in Appendix 3 and the simplified reactions that illustrate these phenomena at low pH are illustrated below.

$$NO_3^- + 2H^+ + 2e^- \rightarrow NO_2^- + H_2O \qquad E^\circ=0.835V \quad [4.9]$$

$$NO_2^- + 8H^+ + 6e^- \rightarrow NH_4^+ + 2H_2O \quad E^\circ=0.897V \quad [4.10]$$

The publications reviewed included three recent conference papers and four patent applications from industrialists. This clearly demonstrates that nitrate reduction itself is a topical and relevant research subject that is not yet fully understood.

The qualitative study therefore focused on identifying the conditions under which nitrate reduction occurred and the measurement of species in the system. In this way it was hoped to be able to define the main reduction pathways describing the nitrate reduction under the conditions in the experimental rig, and to observe the effect of operating conditions on the relative rates of reaction. Detailed electrochemical reaction kinetic data would have to be obtained independently via a series of fundamental experiments. The three phases of the study were: i) measurement of species in catholyte vent gas, ii) current sweeps of cell to study electrical phenomena, and iii) measurement of species present in the liquid phase during the experimental runs. The results from these experiments are discussed below.

4.2.2 Gas evolution

Various gaseous products have been reported in the literature which varied according to the process conditions within the electrochemical cells used to study the reactions. In order to identify the gaseous components generated at the cathode of the experimental rig, a series of off-line experiments were undertaken to analyse the vent gas stream from the catholyte reservoir. For these experiments the large throughput of purge-air was replaced with a sweep flow of argon. A sample bomb was installed in the vent line which could be isolated and removed to analyse the contents with a mass spectrometer. A cation

exchange membrane (CRA) was used to minimise catholyte concentration changes during an experiment.

A VG Quadrupoles, Micromass PC, Spectrometer was used to analyse the components present in the sample of vent gas. A typical histogram of data from the mass spectrometer is given in Figure 4.1. The argon sweep gas was seen as the major component at Mr=40 with traces of water vapour and neon (present in the argon supply) at Mr=18 and 20 respectively. A spurious system reading was always seen at Mr=0 whilst any hydrogen present was detected at Mr=2. No other components were detected over the range $0 \leq Mr \leq 100$.

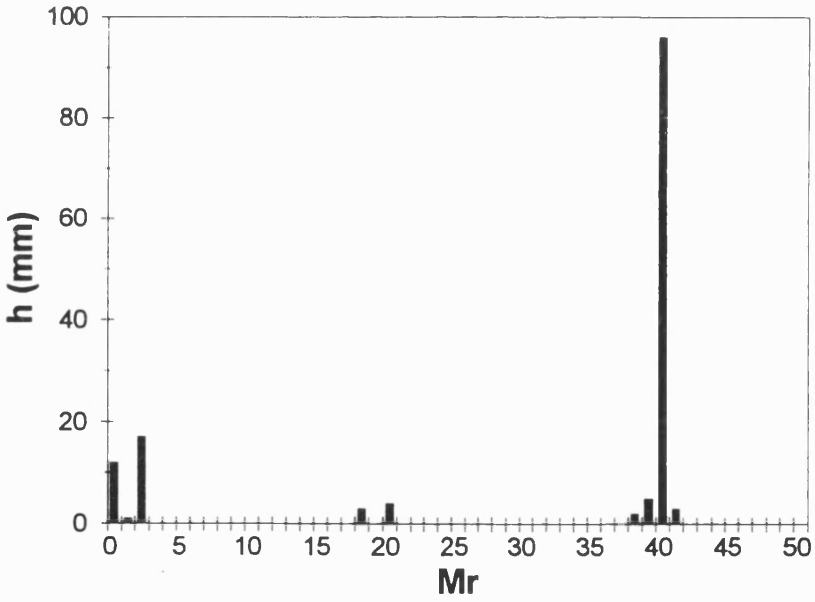

Figure 4.1: Typical peak height against molecular mass histogram taken from mass spectroscopy data

The ratio of hydrogen peak height to argon peak height (h_{H2}/h_{Ar}) was determined for each experiment in order to estimate the relative rates of hydrogen evolution. This could only be regarded as an estimate because the

mass spectrometer was not quantitatively calibrated for the vent gas system. In addition to this, the sweep argon flowrate was maintained only approximately constant for each experiment giving rise to reference case fluctuations. The relative hydrogen evolution rate is plotted against current and catholyte acid concentration in Figure 4.2.

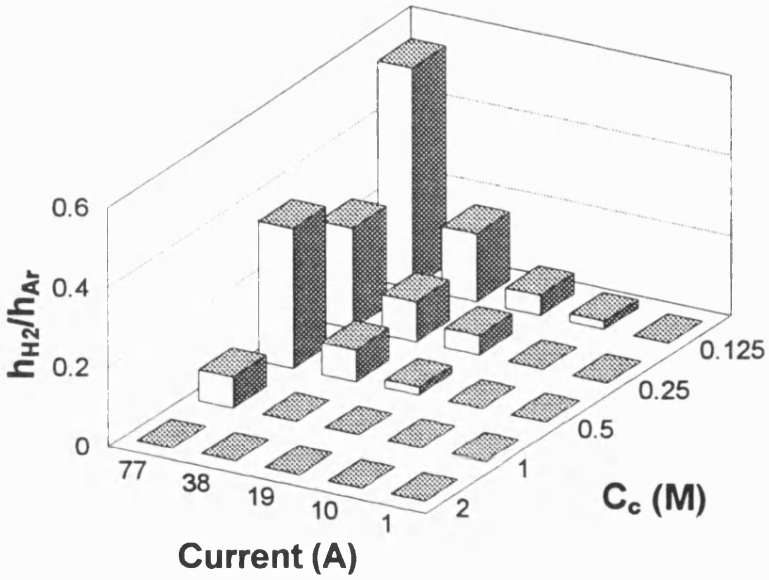

Figure 4.2: Variation of relative hydrogen evolution rate with operating current and catholyte acid concentration

Figure 4.2 shows that the relative hydrogen evolution rate varies under different operating conditions. In a region of mass transfer limitation (low acid concentration and/or high current) significant amounts of hydrogen were evolved. In regions of high mass transfer however no hydrogen was generated which implies that all the current was being consumed by liquid phase electrochemical reactions. The route followed by a typical experimental run for membrane evaluation would start initially in the region of no hydrogen evolution

(e.g. 38A & 2M). As the acid concentration in the catholyte decreased this would change until, at the end of the run, significant amounts of hydrogen would be generated (e.g. 38A & 0.125M). Observations of gas bubble generation during an experimental run agreed closely with this scenario.

It should be noted that hydrogen was usually detected with the mass spectrometer before gas bubbles were visible in the experimental rig. The exception to this was the experiment carried out at 38A and 1M catholyte acid concentration; in this case very small bubbles were visible but no hydrogen was detected in the vent gas.

4.2.3 Current sweeps

The ICI FM01 has been extensively studied elsewhere to determine its mass transfer characteristics, most recently by Brown (Brown, Pletcher, Walsh, Hammond & Robinson, 1992), (Brown et al, 1993), (Brown et al, 1994). Mass transfer data were correlated for a variety of cell configurations based on the reduction of ferricyanide as a model system (Brown et al, 1993).

Rather than simply taking mass transfer data for a model system from the literature, it was decided to undertake current sweeps on the EED stack for several catholyte acid concentrations. Reference electrode measurements were made throughout these experiments so that changes in the cathode potential could be monitored. Typical curves are shown in this section with their subsequent analysis.

A current density against time curve used in the current sweeps is given by Figure 4.3 and the overall cell voltage plotted against current density in Figure 4.4 (both data for 1.16M catholyte acid concentration).

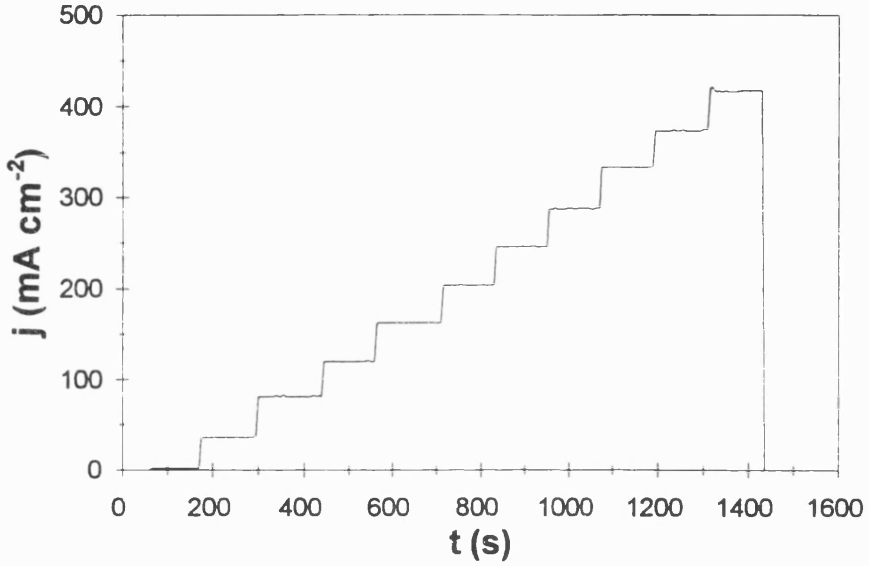

Figure 4.3: Typical current density against time profile for current sweeps of EED stack

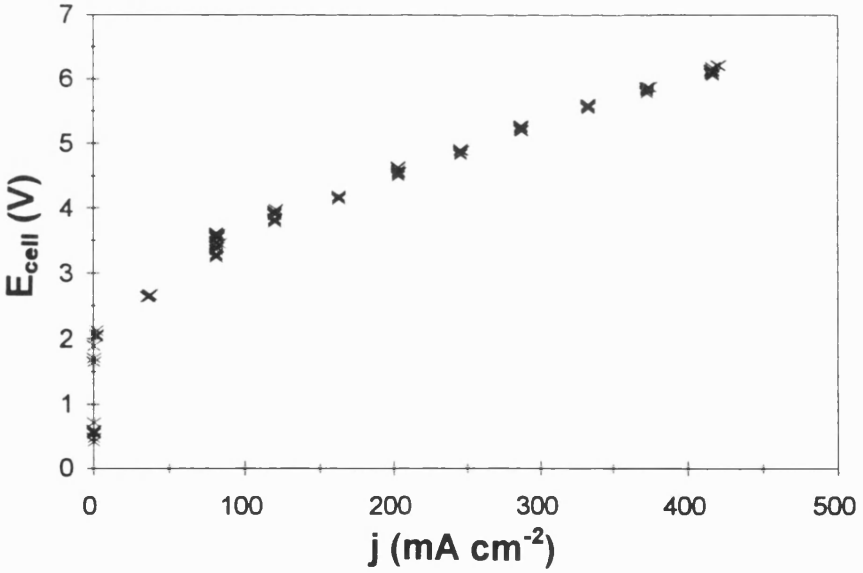

Figure 4.4: Typical total cell voltage drop against current density for current sweep experiments

Figure 4.4 shows the cell voltage against current density and is therefore not the current-potential profile for a specific electrode reaction. It represents the overall effect of electrical phenomema - anode and cathode reactions. There are three regions of the curve: i) the voltage at which current starts to flow which represents the sum of reversible and overpotentials for the cell, ii) the near-linear region of the curve at low current densities (<100 mA cm^{-2}), and iii) the 'Tafel' region of the curve which is discussed later in this section.

For each current setting many measurements were taken by the data logger and these can be seen clearly in Figure 4.4. For subsequent analysis the mean of the measured values for each current was taken.

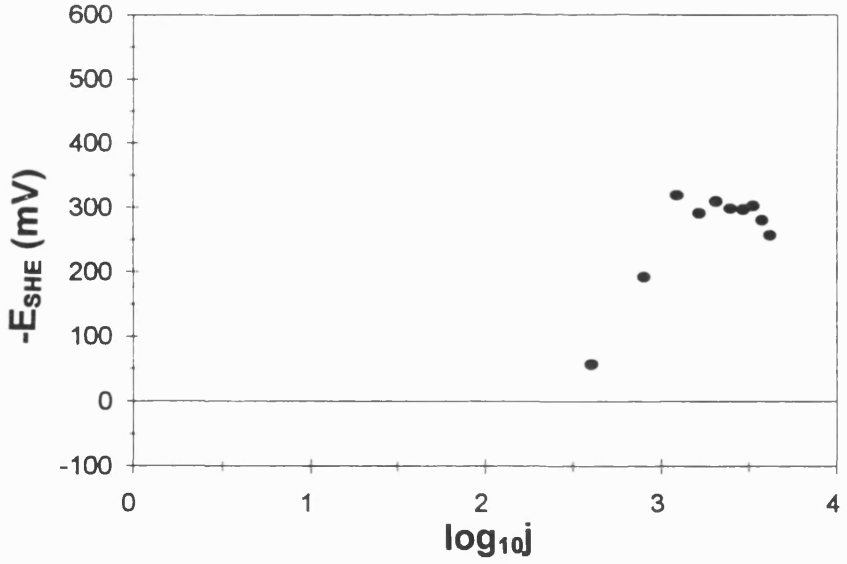

Figure 4.5: Reference electrode voltage against logarithm of current density (0.47M catholyte)

For each successive experiment the catholyte acid concentration was decreased to produce a set of curves giving the characteristics of the EED stack. The reference electrode potential was corrected for voltage drop between the point of measurement and the cathode using conductivity measurements (E_{IR_c}). The

calomel reference electrode voltage was then translated to the standard hydrogen electrode (SHE) scale. The electrode potential against current density can be seen plotted in the classical way in Figure 4.5 for a 0.47M catholyte acid concentration. It should be noted that the system would have become mass transfer limited at the higher currents used in the sweep.

4.2.3.1 Qualitative reaction kinetics

Fundamental studies of electrochemical reaction kinetics are usually undertaken under high mass transfer conditions in order to eliminate mass transfer from the overall rate expression. If an electrochemical reaction is not limited by mass transfer and assumed to be irreversible then the Tafel equation can be used as a good approximation of the reaction kinetics. The Tafel equation is given below and its derivation is discussed in detail along with the significance of the Tafel coefficients a and b in the literature (Scott, 1991), (Walsh, 1993).

$$E_{OP} = a + b\log(i) \qquad [4.11]$$

a,b Tafel coefficients (V)

E_{OP} overpotential (V)

The experimental configuration used for the current sweeps was far from ideal for studying fundamental electrochemical kinetics. However the high mass transfer conditions of one experiment allowed a modified version of the Tafel equation to be used (1.16M nitric acid). The reference electrode potential was plotted against the logarithm of current density in order to identify the linear 'Tafel' region of the curve shown in Figure 4.6.

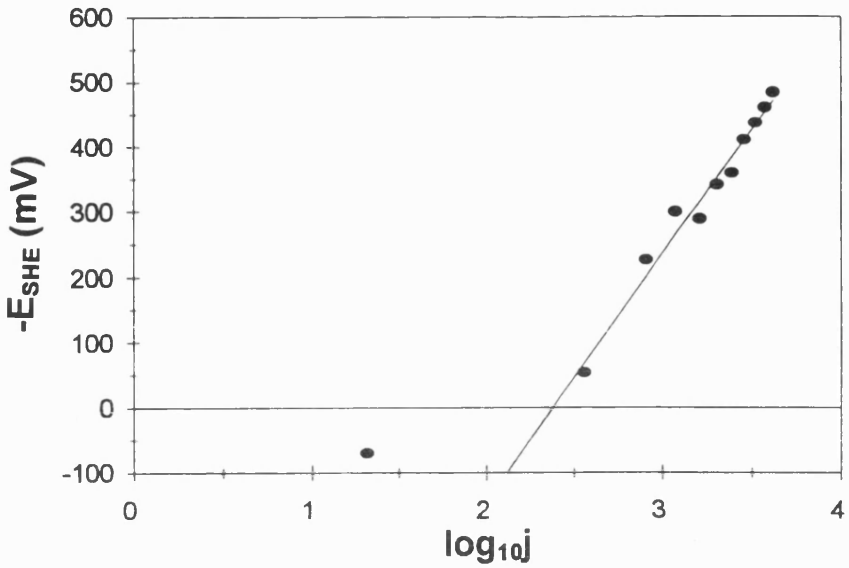

Figure 4.6: Reference electrode voltage against logarithm of current density showing linear region of curve (1.16M catholyte)

The linear slope was calculated to be 380mV/decade where a decade is a factor of ten along a logarithmic scale. A simple 1 electron reaction could be expected to have 118mV/decade Tafel slope. Nitrate reduction is likely to proceed along a complex multi-electron reaction pathway which will alter the Tafel slope however the value calculated here was much higher than the value of 120mV/decade determined by fundamental study of low-concentration (2×10^{-3}M) nitrate reduction (Xing, Scherson & Mak, 1990). The calculated value of the Tafel slope is therefore surprisingly high which should be attributed, in this instance, to the non-ideality of the experiment used to derive this data - in particular, the concentration employed was over two orders of magnitude greater than that of the fundamental experiments carried out by Xing et al. Further interpretation of this data was consequently not undertaken due to the many non-idealities of the experiment. Detailed fundamental electrochemical studies, such as rotating disc electrode experiments, would be required to obtain accurate

kinetic expressions. The overall observed reaction scenario is discussed at the end of this section.

4.2.3.2 Mass transfer

In practice it can be difficult to identify the limiting current from process measurements. In ED it is common to plot the resistance of an entire stack against the reciprocal of current (Cowan & Brown, 1959), (Spiegler & Laird, 1980), (Kuppinger et al, 1993), (Yen & Cheryan, 1993). The point where the gradient of the line changes from positive to negative is the limiting current. This is known as the Cowan & Brown method according to the first researchers to apply it. Some workers have expressed difficulties in applying this technique (Novalic et al, 1995). It appears, however, that the currents used in their experiments might not have been sufficiently high to find the limiting current.

None of the references explain why the minima of the Cowan & Brown curves can be used to determine the limiting current, although the explanation is probably elementary. For example in electrodialysis prior to mass transfer limitation, the resistance of the stack appears to decrease with increasing current showing a deviation from Ohms law. Above the limiting current the resistance would increase significantly due to polarisation effects.

This technique was adapted for use in the EED system to establish whether it could be used to determine the limiting current in the catholyte (i.e. the limiting current of mass transfer to the cathode rather than of membrane transport as applied in the published ED studies). The reference electrode potential divided by the current density was used as the resistance term and this was plotted against the reciprocal of the current density. The change of gradient was easily seen as demonstrated in Figure 4.7. It should be noted that, whilst the data

points to the right of the minimum (the Tafel region of the plot) are reasonably accurate, the data to the left of the minimum are not entirely credible. This is due to the errors which are inherent in the experimental technique at high current densities. When nitrate is mass transfer limited, for instance, gas bubbles reduce the conductivity of the catholyte in the cell and this is not accounted for in the reference electrode voltage correction.

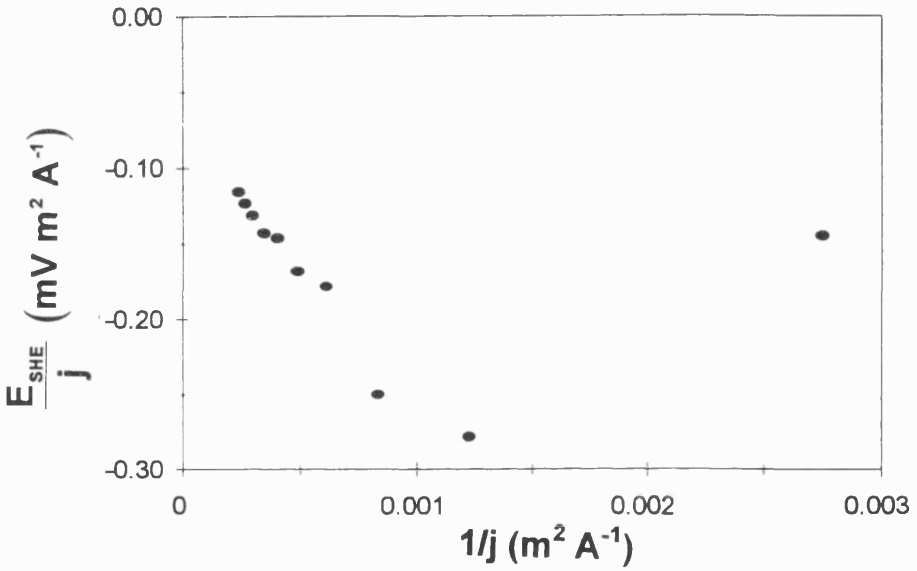

Figure 4.7: Resistance term against reciprocal of current density used to determine limiting current (1.16M catholyte)

Despite its limitations, the Cowan & Brown method appears to provide a potentially attractive technique for determining limiting currents in electrochemical systems because the minima can be easily located. It is therefore discussed here more as an interesting interlude rather than an exhaustive examination of the technique.

The Cowan & Brown method was further modified in order to compare results from experiments at different concentrations. The ordinate was normalised by dividing by the largest modulus value for a given set of data, $(E_{SHE}/j)_{max}$, whilst the abscissa was corrected for catholyte acid concentration by multiplying by the appropriate C_c. This is shown in Figure 4.8.

The minima of these curves should occur at the same position on the abscissa due to the normalisation and correction for concentration. Clearly this is not the case for all five curves. The three lowest concentrations intercept the abscissa in very close proximity, but the data from the higher concentration experiments deviate from this point.

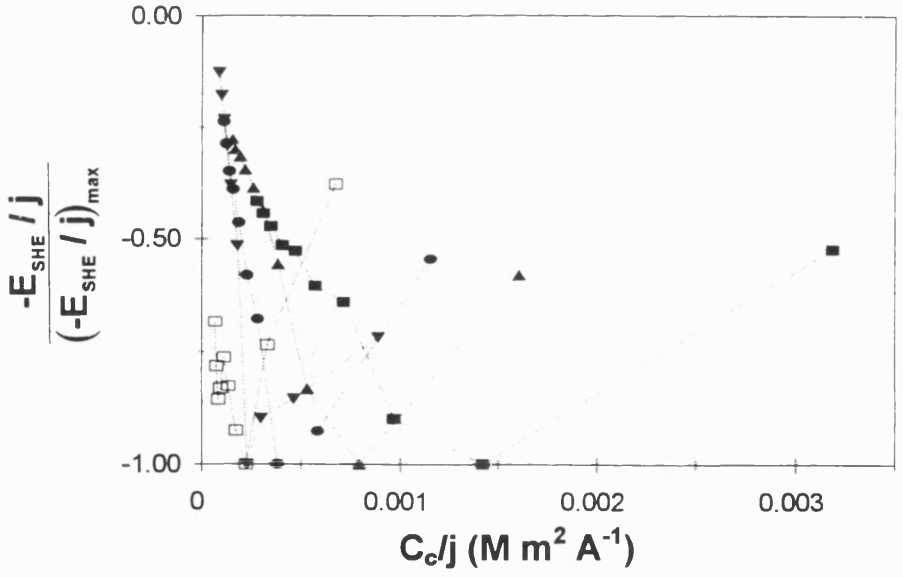

Figure 4.8: Normalised resistance term against reciprocal of current density corrected for catholyte acid concentration (■1.16M, ▲0.64M, ●0.47M, □0.37M, ▼0.28M)

Notwithstanding the fact that there was insufficient data to exactly locate the minima of each curve, the deviation can be explained by studying the Nernst-Plank diffusion term which was introduced in Section 2.7.1 and is given by:

$$J_i = D_i\left[\frac{\partial C_i}{\partial z} + C_i\frac{\partial \ln \gamma_i}{\partial z}\right] \qquad [4.12]$$

In dilute systems the activity coefficient, γ, is often assumed invariant with distance and so the $\partial \ln\gamma/\partial z$ term is deleted. If this is not the case the activity term must be retained and included in the derivation. Over a thin boundary layer ∂z is often approximated by δ, the boundary layer thickness. Thus Equation 4.12 can be manipulated by incorporating the definitions of the limiting current and the mass transfer coefficient to give:

$$\frac{C_c}{j_{\lim}} = \frac{1}{z\Im k_m}\left[\frac{1}{1+\ln(\gamma_b/\gamma_s)}\right] \qquad [4.13]$$

In dilute systems, where $\gamma_b \approx \gamma_s$, the minima of the curves plotted in Figure 4.8 will all occur at the same point on the abscissa. For more concentrated solutions however the point of interception with the abscissa will be altered by the activity term. For example, if $\gamma_b < \gamma_s$ then the intercept would be at a higher value of C_c/j_{lim} than for dilute systems. This is clearly seen in Figure 4.8. If the modified Cowan & Brown method were to be applied to dilute systems this deviation would not be expected.

The mean value of C_c/j for the three most dilute systems was calculated to be 2.24×10^{-4} mol m^2 dm^{-3} A^{-1}, equating to a mass transfer coefficient of 3.7×10^{-5} m

s^{-1}. This compares well to a value of 3×10^{-5} m s^{-1} derived for similar velocity conditions in an FM01 cell (Brown et al, 1993).

4.2.4 Species analysis

Additional measurements were made during the membrane performance experiments in order to detect species present in the catholyte. Nitrate, nitrite and ammonium concentrations were measured as representative of the key species of the nitrate reduction pathway. Figure 4.9, Figure 4.10 and Figure 4.11 show species profiles for experiments undertaken with different initial acid concentrations at a current density of 300 mA cm^{-2}. The species detected were total acid or nitrate (C_a - anolyte, C_c - catholyte) and ammonium (C_{NH4+}). When comparing the species profiles it should be noted that the membranes used in each experiment were not necessarily of the same type. Variations in membrane current efficiency could affect the overall amount of electrochemical reduction that occurred. The variation in catholyte concentration between Figure 4.9, Figure 4.10 and Figure 4.11 would be the most significant factor which is why they are compared.

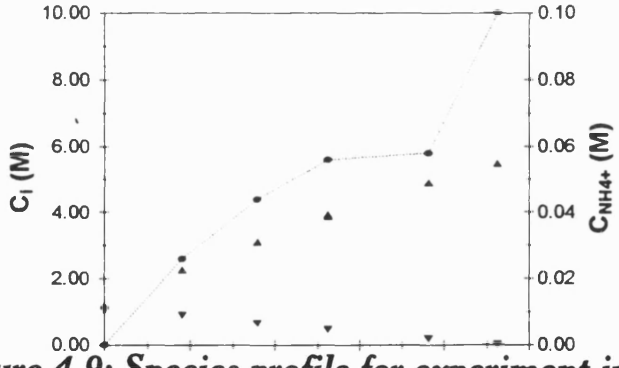

Figure 4.9: Species profile for experiment initially with 1M acid electrolyte ($\bullet C_{NH4+}$, $\blacktriangle C_a$, $\blacktriangledown C_c$)[ADP1] with 1M acid electrolyte ($\bullet C_{NH4+}$, $\blacktriangle C_a$, $\blacktriangledown C_c$)[ADP1]

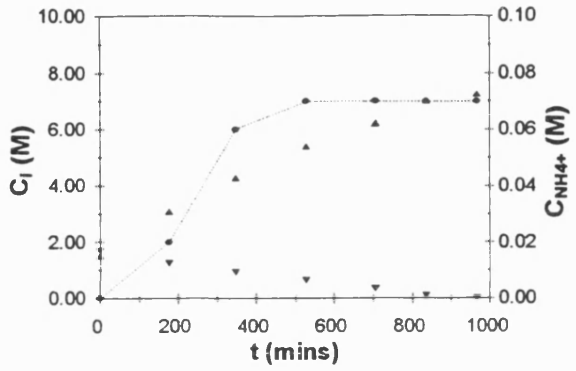

Figure 4.10: Species profile for experiment initially with 1.5M acid electrolyte ($\bullet C_{NH4+}$, $\blacktriangle C_a$, $\blacktriangledown C_c$)[AW1.5]

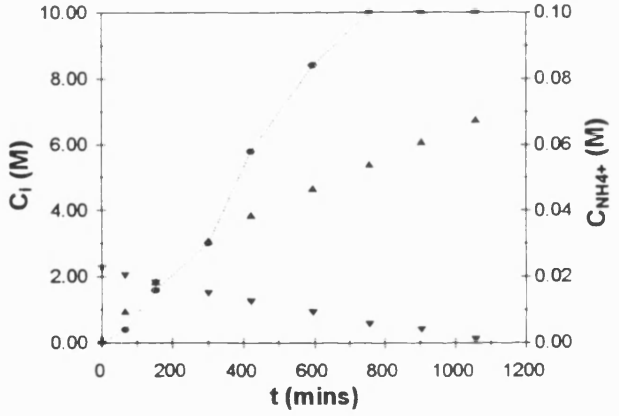

Figure 4.11: Species profile for experiment initially with 2M acid catholyte ($\bullet C_{NH4+}$, $\blacktriangle C_a$, $\blacktriangledown C_c$)[AW002]

The sudden rise in the C_{NH4+} curve shown in Figure 4.9 is discussed later in the text. Process conditions in the catholyte at the end of a run can vary significantly from those encountered during an experiment and so penultimate points are compared. A general trend was observed in that the amount of ammonium present at the penultimate point of a run increased with initial

electrolyte concentration. This is probably due to the increased time taken to reach mass transfer limitation as the catholyte concentration increased which resulted in a larger amount of electrochemical reduction.

In addition to the effect of initial electrolyte concentration, the effect of operating current density can be seen in Figure 4.12, Figure 4.13 and Figure 4.14.

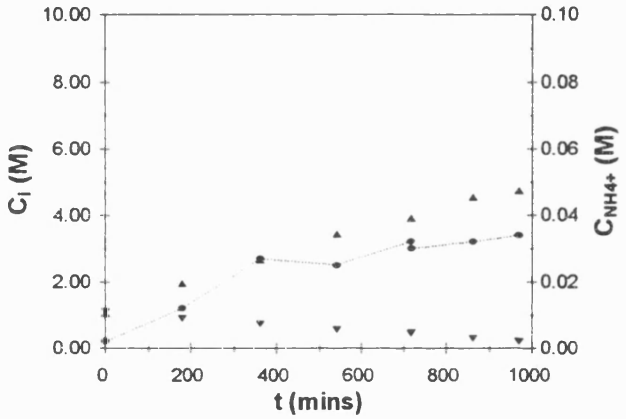

Figure 4.12: Species profile for experiment operated at 150 mA cm^{-2} ($\bullet C_{NH4+}$, $\blacktriangle C_a$, $\blacktriangledown C_c$)[AW150]

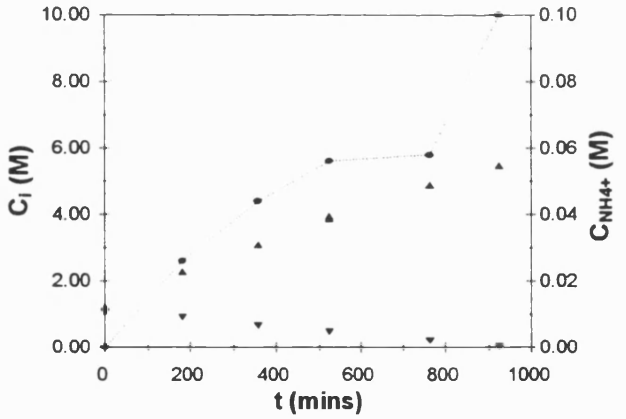

Figure 4.13: Species profile for experiment operated at 300 mA cm^{-2} ($\bullet C_{NH4+}$, $\blacktriangle C_a$, $\blacktriangledown C_c$)[ADP1]

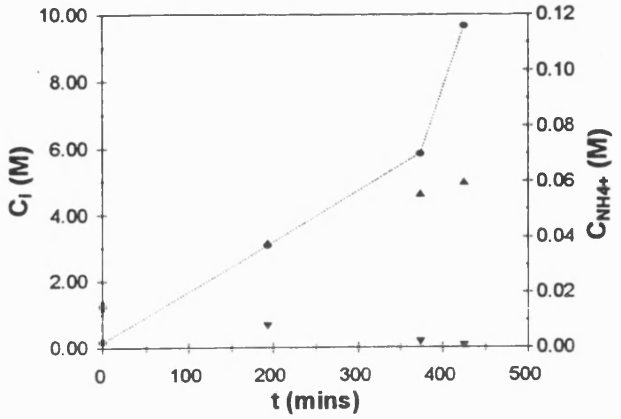

Figure 4.14: Species profile for experiment operated at 450 mA cm^{-2} ($\bullet C_{NH4+}$, $\blacktriangle C_a$, $\blacktriangledown C_c$)[AW450]

Once again a general trend was seen in that the concentration of ammonium given by the penultimate points of a run, increased with increasing current density. If the results are compared at the point where the same number of Faradays of charge have been passed in each experiment (e.g. 150 mA cm^{-2} @ t=1000, 300 mA cm^{-2} @ t=500 and 450 mA cm^{-2} @ t=333) then the measured ammonium concentrations were approximately equal. The experiment undertaken at 450 mA cm^{-2} showed an almost linear increase in ammonium concentration which could be attributed to the high current causing the rate of reaction to be mass transfer limited and therefore proportional to catholyte nitrate concentration. At no point during the experimental runs was any nitrite detected (detection limit 10 ppm). Gas bubbles were observed in the experimental rig at an intermediate point during the runs indicating a switch from liquid phase to gas evolution reactions (or a combination of both).

4.2.5 Discussion and conclusions

The qualitative electrochemical study allowed a basic understanding of the electrochemical nitrate reduction to be generated in order to describe the process. It revealed that in regions of high mass transfer almost all the current was consumed by liquid phase reactions but as the catholyte concentration decreased (or the operating current increased) hydrogen gas was generated. Ammonium was detected at significant levels at the end of an experimental run but at no point was nitrite detected. This implies that the nitrite reduction reaction proceeds more rapidly than nitrate reduction. This agrees with the findings of other workers (Petrii & Safonova, 1992). An overall nitrate to ammonium reaction model could therefore be used for these conditions as indicated by:

$$NO_3^- + 10H^+ + 8e^- \rightarrow NH_4^+ + 3H_2O \qquad [4.14]$$

At the end of the experimental run the pH of the catholyte was found to be almost always pH<1. This pH value was used to calculate the ratio of NH_4OH to NH_4^+ using (Pourbaix, 1974):

$$\log\frac{[NH_4OH]}{[NH_4^+]} = -9.27 + pH \qquad [4.15]$$

The ratio $[NH_4OH]/[NH_4^+]$ was calculated to be 5.37×10^{-9} which implies that little/no NH_4OH can be present under these conditions. Almost all the ammonium must therefore be in the form of NH_4NO_3. If the run were to be continued so that the pH of the catholyte increased dramatically due to a switch

between Equations 4.16 and 4.17, the equilibrium would shift towards NH_4OH.

$$H^+ + e^- \rightarrow {}^1/_2H_2 \qquad \text{acidic reaction} \qquad [4.16]$$

$$H_2O + e^- \rightarrow {}^1/_2H_2 + OH^- \qquad \text{alkaline reaction} \qquad [4.17]$$

Under these conditions ammonia gas would also begin to be liberated as its vapour pressure above the solution increases with increasing pH according to (Pourbaix, 1974):

$$\log\frac{pNH_3}{\left[NH_4^+\right]} = -11.02 + pH \qquad [4.18]$$

$$\log\frac{pNH_3}{\left[NH_4OH\right]} = -1.75 \qquad [4.19]$$

pNH_3 partial pressure of ammonia (atmos)

This was not demonstrated in practice due to the operating voltage becoming prohibitively high at the end of an experimental run.

The reason for the sharp rise in ammonium concentration following the plateau at the end of a run in two out of the five cases is not clear. The analytical technique increases in accuracy as the concentration of ammonia increases and the nitrate available for reduction at the end of a run is limited by mass transfer. There are therefore two possible explainations: i) errors in analysis prior to the final sample give rise to an apparent sharp rise in ammonium concentration or

ii) the conditions at the cathode at the end of a run become favourable for nitrate reduction to proceed more rapidly. As the sharp rise is seen in approximately half of the experiments, the second of these explanations is the most plausible as there should be no observed trend between spurious results. It was found during the nitrate reduction literature review that pH has a strong influence on nitrate reduction which is why many workers operate under alkaline conditions. At the end of a run the rise in pH as the nitric acid becomes depleted could enhance reduction of the remaining nitrate species (e.g. NH_4NO_3) and thus yield a further rise in the ammonium concentration. This would not be seen in experimental runs which were stopped before the pH rise could take effect. A detailed fundamental electrochemical study would afford further understanding of this apparent phenomenon. As mentioned previously, such a study would be required in order to generate accurate electrochemical reaction kinetics for use in a mathematical model of the process. The basic understanding gained from the qualitative study however allowed simple modelling to be undertaken and would help other researchers to plan a fundamental experimental programme.

4.3 Membrane performance

The remainder of this chapter is devoted to the presentation of data relating to the performance of the anion exchange membranes in the nitric acid-water system. It is divided into two sections: i) membrane screening, and ii) a detailed study of an individual membrane (AW). The former covers the general trends observed during the experimental programme and the latter focuses in some detail on the workings of an individual membrane.

4.3.1 Membrane screening

This section covers the series of experiments that were undertaken in order to evaluate the performance of different anion exchange membranes. Raw data is given in a representative form and the performance measures presented for all membranes. The membranes studied were: ADP, ARA, AW, RAI, MA3475 and AAV. The specifications of these membrane types are listed in Section 3.2.4.1. Neither AAV nor MA3475 gave satisfactory performance and so data cannot be presented for these membranes. AAV fractured on several occasions due to the small pressure fluctuations in the experimental rig, whilst the MA3475 became hairline cracked (microchinked) by the end of a run and was later confirmed to be unsuitable for the nitric acid system (Sanderson, 1996). Typical concentration profiles from two experimental runs are shown in the two figures below.

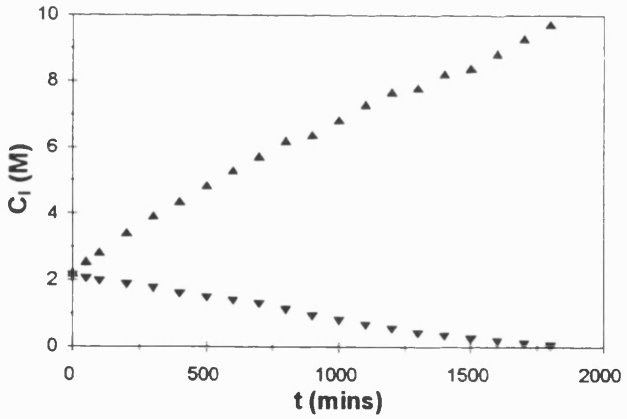

Figure 4.15: Acid concentration profiles for ADP2 experimental run (▲C_a, ▼C_c)

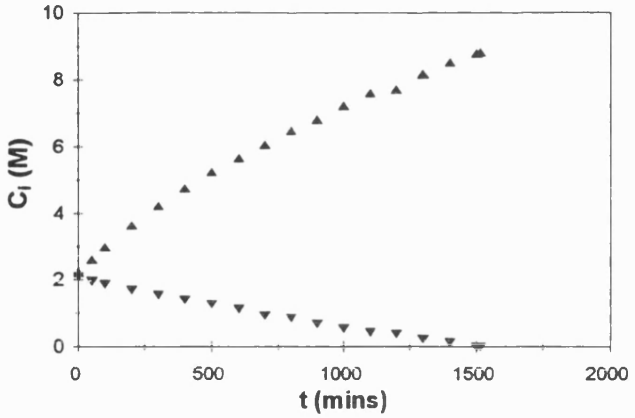

Figure 4.16: Acid concentration profiles for ARA2 experimental run (▲C_a, ▼C_c)

4.3.1.1 Current efficiencies

Integral current efficiency (η_{ICE}) data had to be manipulated in order to generate credible differential current efficiency (η_{DCE}) values. This was discussed in Section 4.1.1.3. The η_{ICE} curves and mathematical curve fits, f(t), are shown in Figure 4.17 and Figure 4.18 for the same experimental runs as given in the previous two figures. The curve fits were used for subsequent η_{DCE} determination.

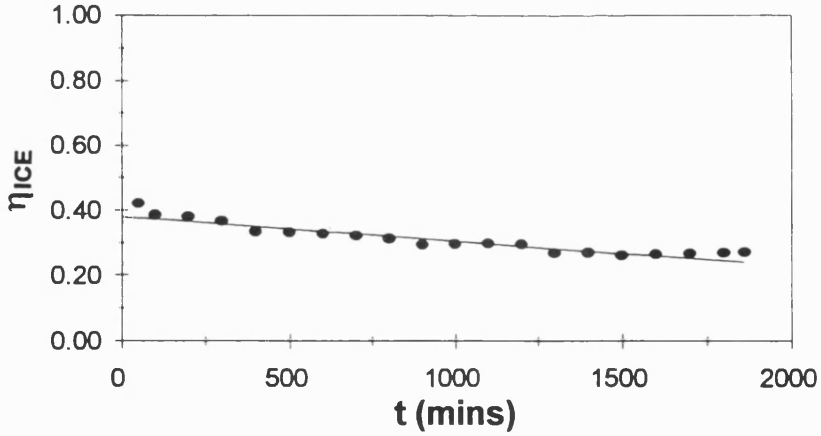

Figure 4.17: Integral current efficiency profile for experimental run ADP2 (●η_{ICE} / f(t))

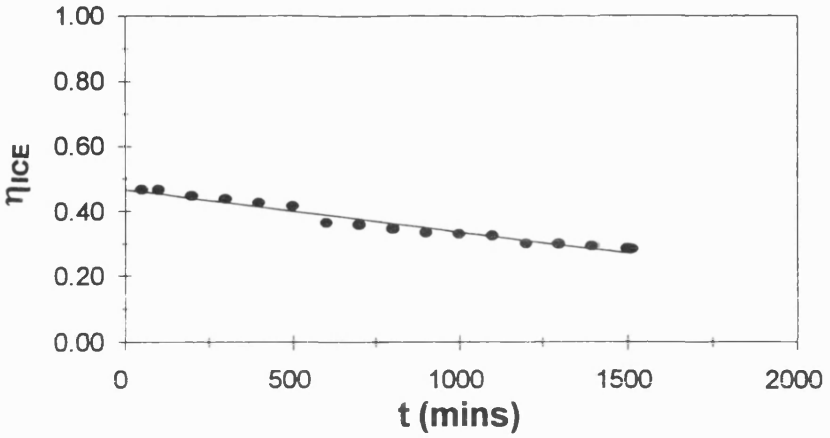

Figure 4.18: Integral current efficiency profile for experimental run ARA2 (●η_{ICE} /f(t))

4.3.1.1.1 Abscissa parameter

It was important to choose an appropriate abscissa against which to plot different sets of performance data so that they could be compared. In the experimental rig both anolyte and catholyte acid concentrations varied simultaneously which meant that the effect of either of these could not be studied in isolation. Other workers have plotted the trans-membrane concentration difference as the key parameter in ED (Lindheimer et al, 1993) and so this was tried initially. The Figure 4.19 shows two sets of η_{DCE} data from different experimental runs using the same membrane type (ARA1, ARA2).

If the abscissa is a key parameter, curves from runs using the same membrane type should have regions of overlap indicating similar performance under similar operating conditions. This was clearly not the case for Figure 4.19. It should be noted that the experiments carried out by Lindheimer et al employed a near-constant catholyte acid concentration which meant that the trans-membrane concentation difference was proportunal to the anolyte acid concentration. Thus

the C_a-C_c abscissa could have fortuitously appeared the key parameter for their experiments.

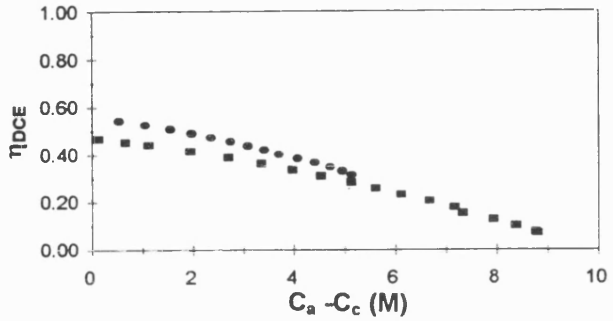

Figure 4.19: Differential current efficiency against trans-membrane concentration difference (●ARA1, ■ARA2)

The next abscissa to be tested was the catholyte acid concentration which is shown in Figure 4.20. Again no overlap of the two curves was seen.

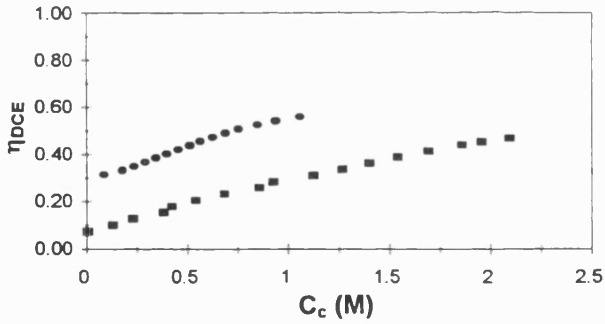

Figure 4.20: Differential current efficiency against catholyte acid concentration (●ARA1, ■ARA2)

Finally, the anolyte acid concentration was used as the abscissa for the η_{DCE} data and this is given in Figure 4.21. For this case there was a significant amount of overlap between the two curves showing the performance of the ARA membrane over a range of acid concentrations from two different experimental runs. This suggests that the anolyte acid concentration might be a key parameter in controlling the efficiency of the membrane. The abscissa

parameter could perhaps be further improved with a better knowledge of membrane properties to give complete overlap of the curves.

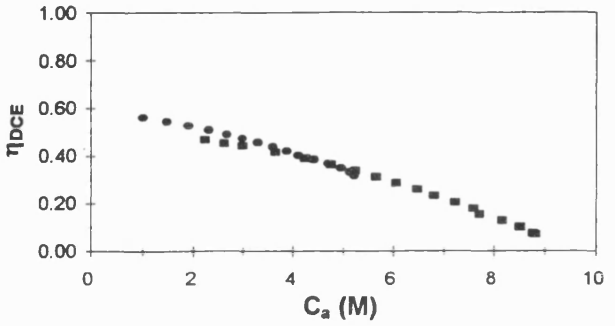

Figure 4.21: Differential current efficiency against anolyte acid concentration(●ARA1, ■ARA2)

4.3.1.1.2 Differential current efficiency data

Having chosen a suitable abscissa parameter, η_{DCE} data were plotted for all the experimental runs. These data are shown in Figure 4.22 and Figure 4.23.

It can be seen that the η_{DCE} decreased with increasing anolyte acid concentration but that the rate of decrease varied between membranes. Whilst there was significant overlap and agreement of data for most membranes between different experimental runs, the RAI membrane showed a surprisingly low current efficiency in the RAI1 run. This was attributed to an anomaly in the RAI samples used and the possible deterioration of membrane performance on standing - these samples were several years old when donated to this project.

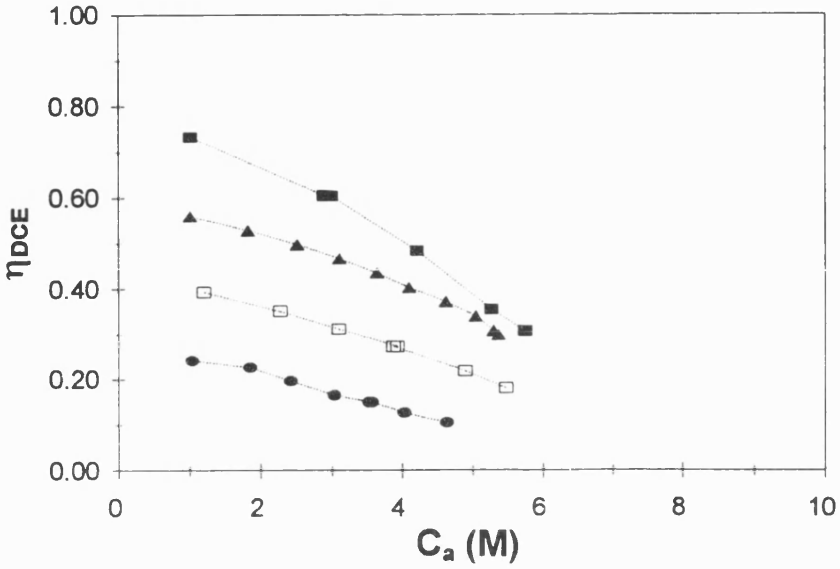

Figure 4.22: Differential current efficiency against anolyte acid concentration for 1M initial electrolytes (■AW1, ●RAI1, ▲ARA1, □ADP1)

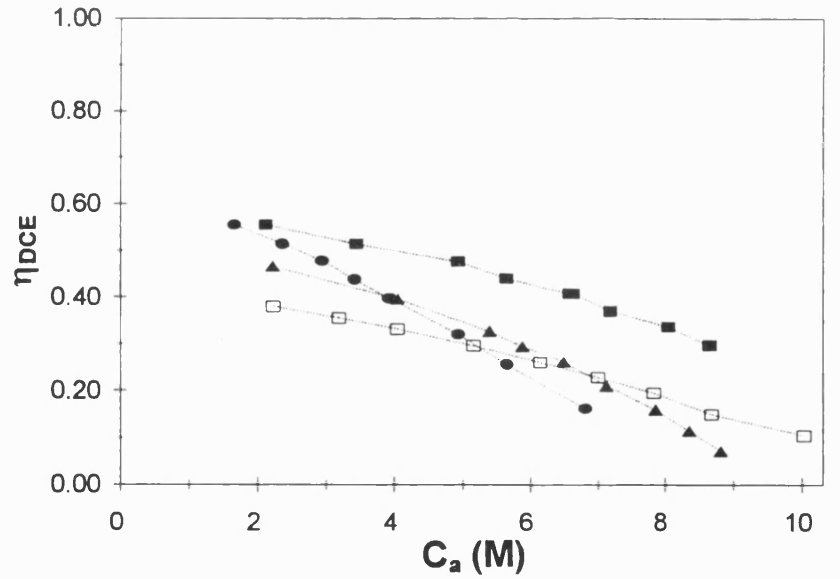

Figure 4.23: Differential current efficiency against anolyte acid concentration for 2M initial electrolytes (■AW2, ●RAI2, ▲ARA2, , □ADP2)

Where possible current efficiency values were compared with similar independent experiments to test for agreement (Graillon, 1995), (Maeck,

1995) although this could not be undertaken for the RAI membrane. Data for the AW and ARA membranes was found to be in close agreement with the results of other workers.

The effect of catholyte concentration between different experimental runs gives rise to complete overlap of data not being observed. This is shown later in the results from the detailed study of the AW membrame.

4.3.1.2 Water transport

In addition to the electrical efficiency, the amount of water transported across the membranes is important as this has a non-electrical effect on overall process performance. The water transport measurements for the membranes evaluated are presented below.

4.3.1.2.1 Water transport numbers

The overall water transport numbers for the experimental runs are plotted in Figure 4.24 for 1M and 2M initial electrolyte concentrations respectively.

Two general trends were observed in Figure 4.24. Firstly, the water transport number decreased with changing membrane type and appeared to be related to the efficiency of the membrane. A high efficiency membrane, such as ARA, had a larger water transport number than a lower efficiency counterpart, such as ADP. The most important relationship was seen when comparing the height of two bars for the same membrane. Here the water transport number decreased with increasing initial electrolyte concentration for all the membranes studied. Once again the trend appeared to be related to current efficiency in that the same membrane operated less efficiently had a lower water transport number.

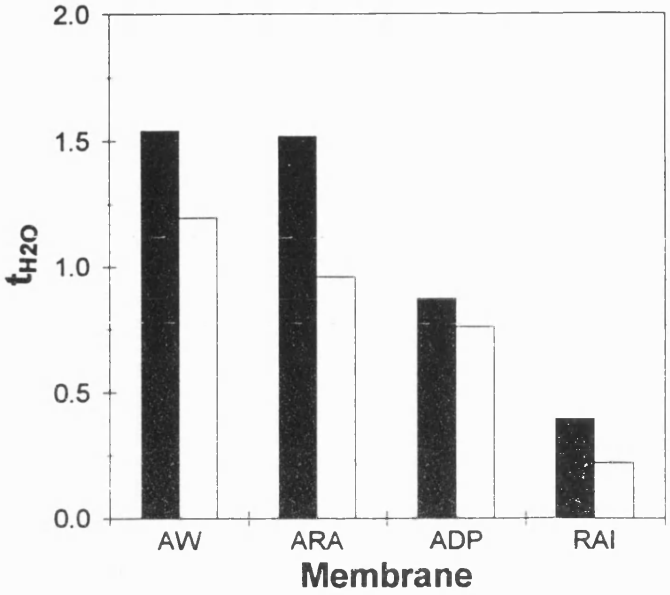

Figure 4.24: Overall water transport number for different membrane types (■1M initial electrolyte, □2M initial electrolyte)

4.3.1.2.2 Specific water transport number

As mentioned in Section 4.1.2.2 the water transport number would be expected to vary with current efficiency even if ion co-ordination numbers remained constant. Consequently specific water transport numbers were determined. Specific water transport numbers are plotted against anolyte acid concentration in the four figures below and a decrease in specific water transport number with increasing acid concentration was observed. The error bounds shown in the figures below are based on the accuracy of volume readings. Calculation of these errors is discussed in Appendix 4.

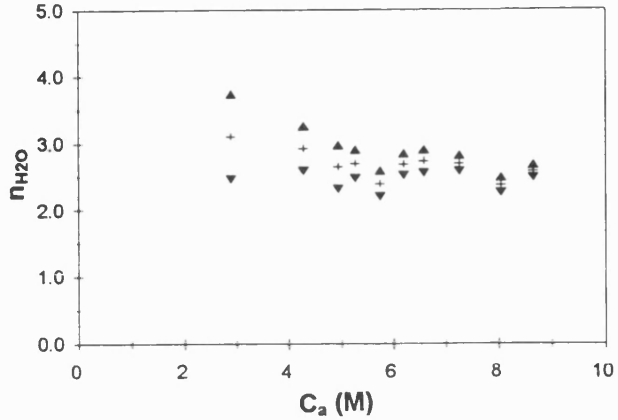

Figure 4.25: Specific water transport numbers for AW membrane with minimum error evaluation

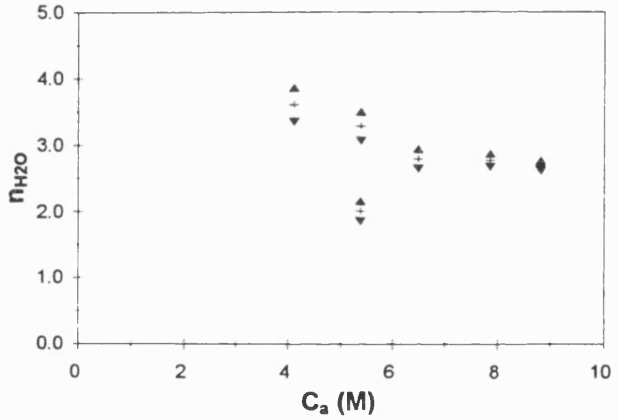

Figure 4.26: Specific water transport numbers for ARA membrane with minimum error evaluation

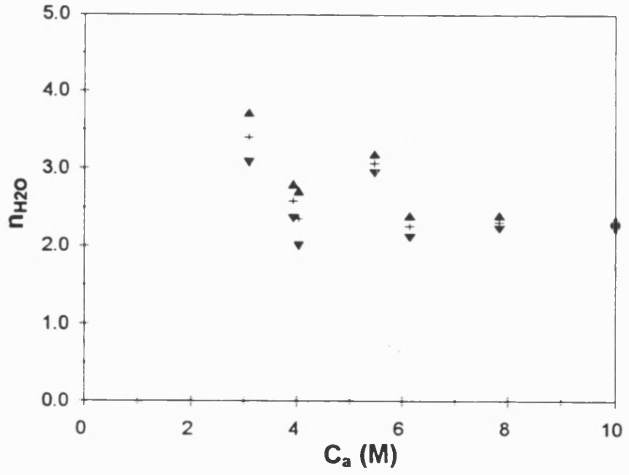

Figure 4.27: Specific water transport numbers for ADP membrane with minimum error evaluation

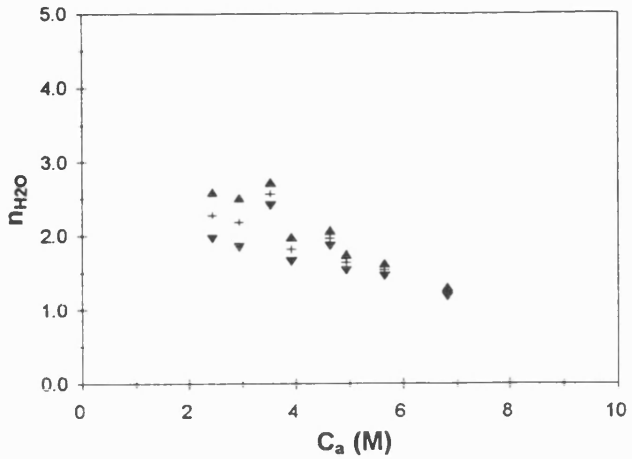

Figure 4.28: Specific water transport numbers for RAI membrane with minimum error evaluation

4.3.2 Detailed individual membrane study

Additional membrane performance experiments were undertaken to allow a more detailed evaluation of the performance characteristics of a specific anion exchange membrane. The high-efficiency AW membrane was chosen for these trials. Significant overlap of performance data from these experiments was expected as they all focused on the same membrane type. The general trends observed by these experiments are presented in this section and a more advanced analysis of the data is presented with the discussion in the next chapter.

4.3.2.1 Effect of initial concentration

Initial electrolyte concentrations of 1M, 1.5M and 2M were used. This allowed the effect of concentration to be studied to a greater extent rather than the simple comparison of two different concentrations as discussed previously. The data are plotted in Figure 4.29.

Initial η_{DCE} values (where both electrolytes were of similar concentration) decreased with increasing electrolyte concentration. The rate of decrease varied between experiments and the curves intercepted before diverging. The catholyte acid concentration could have had a detrimental effect on the measured current efficiency towards the end of the run due to mass transfer limitations as the nitrate was depleted. However reasonable grouping of the data points allows the performance curve of the AW membrane to be visualised within the envelope of scatter. The degree of spread suggests that the anolyte acid concentration is not the only significant parameter.

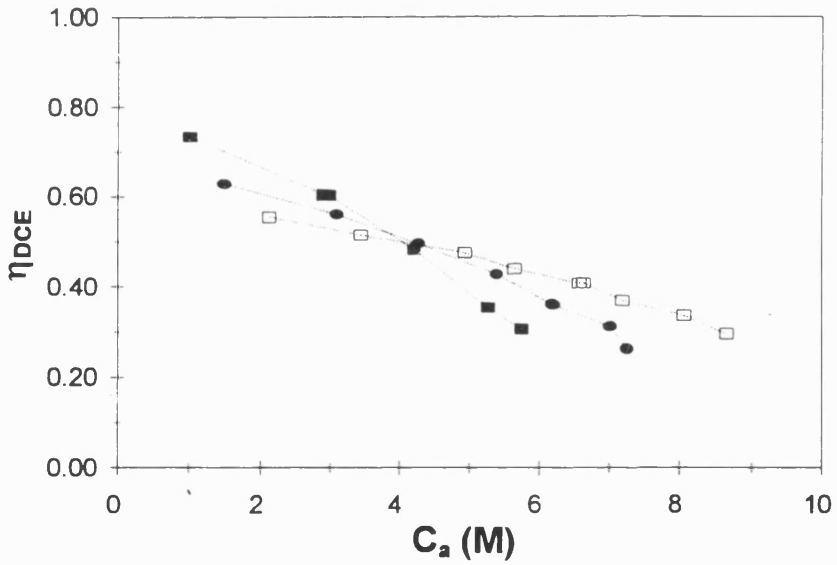

Figure 4.29: Differential current efficiency against anolyte acid concentration for AW membrane (■AW1, ●AW1.5, □AW2)

Specific water transport numbers for the experimental runs are presented in Figure 4.30. Much improved grouping is seen in this data and the decrease with increasing anolyte acid concentration is still apparent.

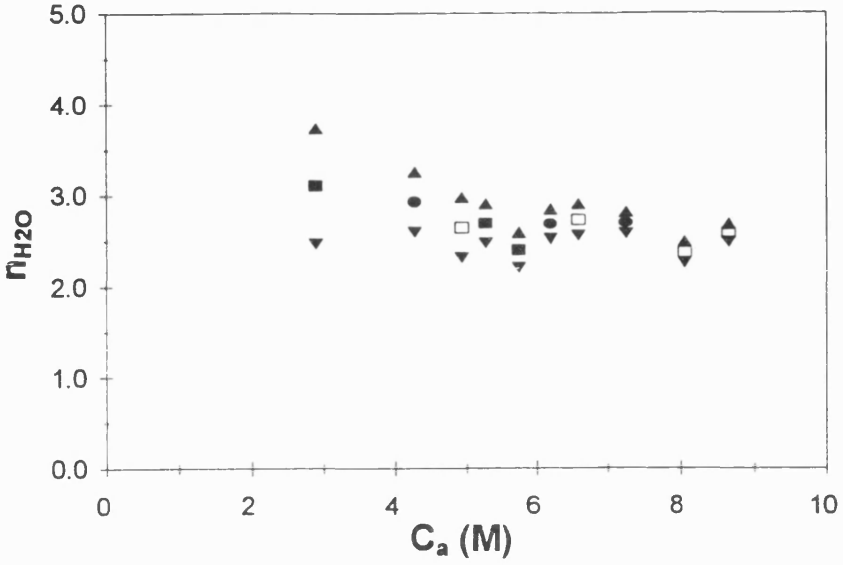

Figure 4.30: Specific water transport numbers against anolyte acid concentration for AW membrane showing minimum error evaluation (■AW1, ●AW1.5, □AW2)

An additional experiment was undertaken in order to study the effect of anolyte concentration. For this experimental run the anolyte was nominally 0.2M and the catholyte 2M. It was hoped that the negative trans-membrane concentration difference and the low anolyte acid concentration would yield a high current efficiency and this was found to be the case. These η_{DCE} data for this run (AW002) are given in Figure 4.31.

These data are combined with the η_{DCE} results from other experimental runs using the AW membrane in Figure 4.32. As expected, an initially high η_{DCE} was found in the AW002 run. Subsequent η_{DCE} values from this run agreed closely with the other performance data for the AW membrane where process conditions became similar.

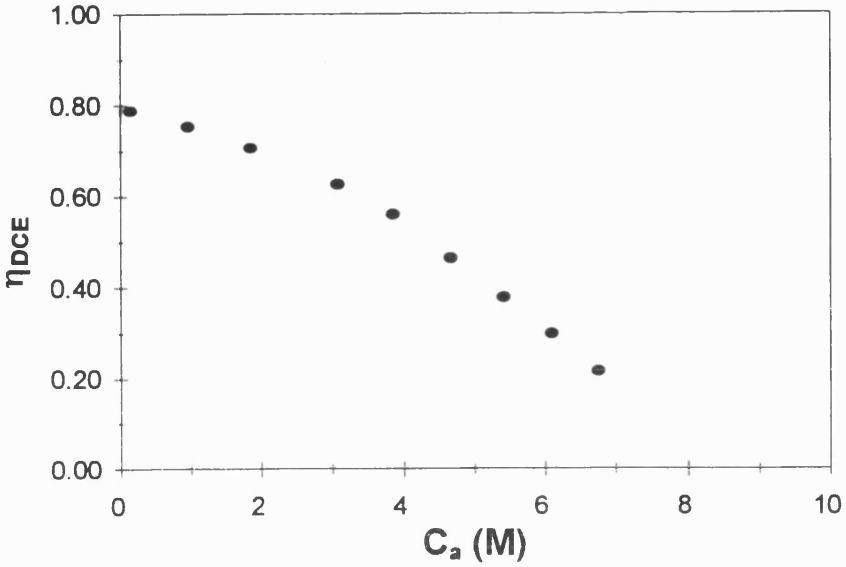

Figure 4.31: Differential current efficiency against anolyte acid concentration for AW002 run

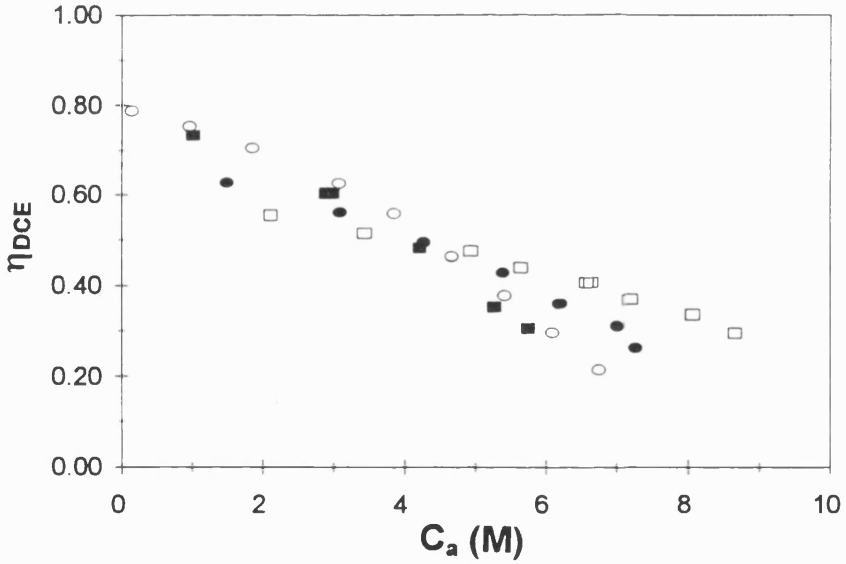

Figure 4.32: Differential current efficiency against anolyte acid concentration for AW membrane (○AW002, ■AW1, ●AW1.5, □AW2)

4.3.2.2 Effect of current density

In addition to the electrolyte concentration, the effect of operating current density was also studied. Current densities of 150, 300 and 450 mA cm^{-2} were

used with the initial electrolyte concentrations 1M in each case. The η_{DCE} values for each run are given in Figure 4.33. There was no apparent trend between the different data sets which all fall in the region of the AW performance curve seen in Figure 4.32. This implies that the current density has very little effect on the current efficiency.

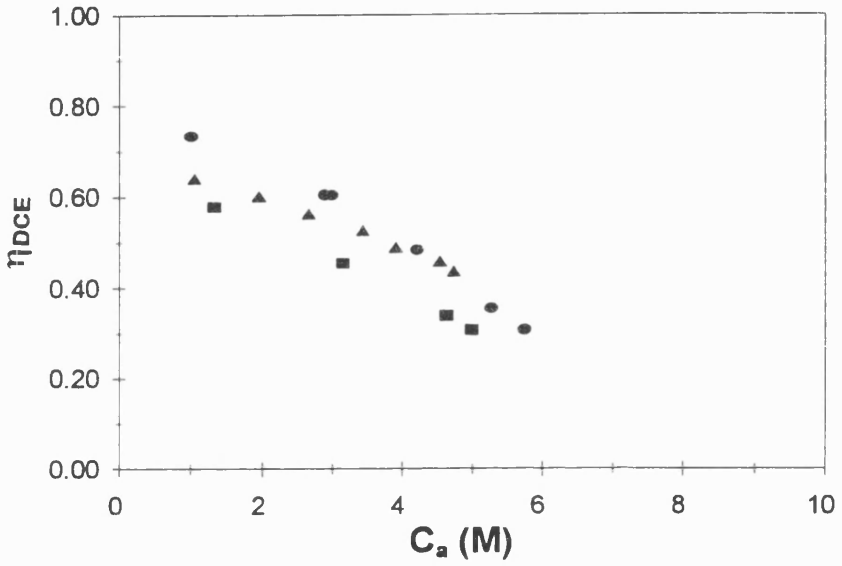

Figure 4.33: Differential current efficiency against anolyte acid concentration for AW membrane (■450 mA cm^{-2}, ●300 mA cm^{-2}, ▲150 mA cm^{-2})

Figure 4.34 shows the effect of current density on overall specific water transport numbers for each of the current densities evaluated. A decrease in the specific water transport number with decreasing current density was observed. This trend was also noticed by other workers working in the field of electrodialysis of sulphuric acid (Baltazar et al, 1993).

4.4 Conclusions of experimental programme

The three phases of the experimental programme produced satisfactory experimental data. A basic understanding of nitrate reduction was generated in order to study its effect on the process performance and this was discussed in Section 4.2.5. Detailed fundamental studies of the electrochemical system would need to be undertaken in order to generate a rigorous description of the electrochemical kinetics.

The Cowan & Brown method for determining limiting currents in electrodialysis stacks was adapted to identify the points of mass transfer limitation for nitrate reduction at the cathode. The mass transfer coefficient estimated via this technique agreed closely with data from literature.

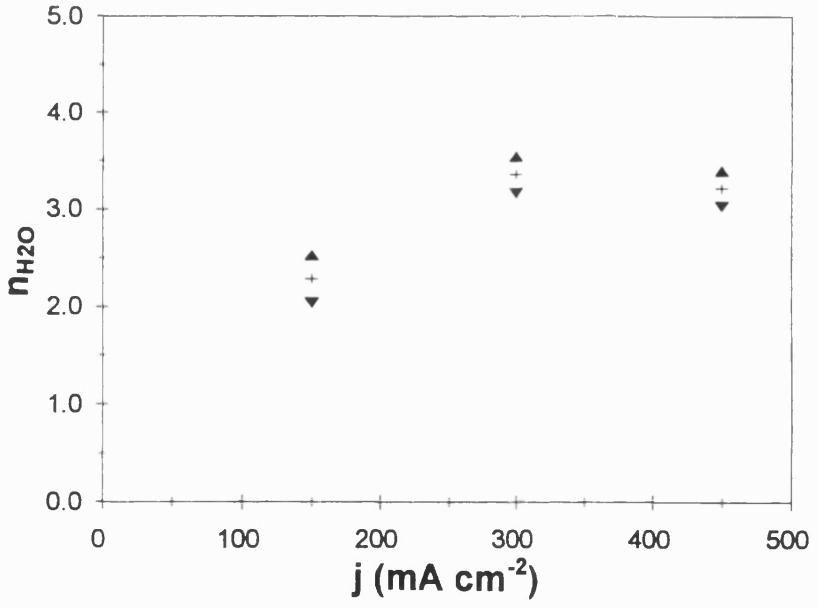

Figure 4.34: Overall specific water transport numbers against operating current density showing minimum error evaluation for AW membrane

Membrane performance studies yielded results showing the variations between different membrane types. The downstream (anolyte) acid concentration was found to be a key parameter in controlling membrane performance.

An interesting relationship between water transport and current efficiency was observed in that the same membrane when operated less efficiently had a lower water transport number. This was found to be the case for all the membranes studied and the phenomenon has been explained using fundamental membrane theories. The resultant theoretical membrane model forms the starting point of the discussion in Chapter 5.

The detailed study of the AW membrane confirmed the findings of the membrane screening experiments and generated data allowing a more detailed analysis of water transport data to be undertaken. This is also discussed in the next chapter which focuses entirely on membrane transport phenomena.

Chapter 5:

Membrane performance - extended discussion

5. Membrane performance - extended discussion

In this chapter membrane performance is discussed in greater detail. The interesting trade-off that was observed between current efficiency and water transport led to the development of a consolidated proton leakage and water flux model which is presented herein. Additionally, a comprehensive analysis of water and ion transport is covered in the second half of the chapter in order to improve understanding of membrane processes, assess the limitations of the experimental measurements and identify areas for further work.

5.1 Relationship between proton leakage and water flux

Previous work on electro-membrane processes has identified proton leakage as the limiting factor in acid concentration, and so has reported current efficiency as the main performance measure (for example Cherif & Gavach, 1989). However at higher concentrations, a further important factor is the water flux associated with ion transport. Ultimately the maximum nitric acid concentration cannot be greater than the concentration of acid being transported through the membrane. If, for example, a single mole of water is transported with every mole of nitric acid, and if electrolytic water consumption and proton solvation are neglected, the mole-fraction of the product cannot exceed 0.5 (or 70 wt%).

5.1.1 Observed trade-off

In Section 4.3 it was shown that differential current efficiency decreased with increasing acid concentration in the anolyte which was attributed mainly to proton leakage. The rate of decrease of efficiency varied between membranes. Additionally, a high efficiency membrane (such as AW) had a relatively high

water transport number ($t_{H2O} \approx 1.1$) whereas a low efficiency membrane (such as RAI), under similar operating conditions, had a much lower water transport number ($t_{H2O} \approx 0.2$). Allowance for water oxidation at the anode was made when determining these values. Osmotic flux was considered to be negligible as zero current experiments showed no detectable water flux for a relatively high trans-membrane concentration difference of approximately 6M.

It should be noted that a change in current efficiency would be expected to alter the water transport number even if the co-ordination number of the acid remained unchanged. Hence specific water transport numbers were determined and were shown to decrease with increasing acid concentration. It appeared that the solvation shell surrounding nitrate ions decreased with increasing acid concentration.

5.1.2 Importance of trade-off

The relationship between current efficiency and water flux is key to the overall performance of an industrial acid recovery processes. A low water flux could give rise to a higher concentration product, but a high acid strength would decrease the electrical efficiency and increase the capital cost. Therefore an optimum must be found between electrical cost, capital charges and product concentration for each application.

It was therefore necessary to understand the processes occurring within an AEM in order to explain this phenomenon. This was undertaken by studying the numerous publications on fundamental membrane properties and analysing the information simultaneously in order to develop a consolidated model. A review of the fundamental work is given below before the model is presented.

5.1.3 Previous studies

Previous work focused on the importance of proton leakage through AEMs but largely ignored the impact of water flux. In order to understand the phenomenon of proton leakage detailed fundamental experimental studies have been undertaken by a number of workers. Analysis of their work has lead to an improved understanding of the factors controlling transport through AEMs and has assisted the development of the consolidated proton leakage and water flux model.

The important trends reported by previous workers are highlighted below and their conclusions have been assembled, in conjunction with data from this project, to postulate an explanation of the relationship between proton leakage and water flux. It should be noted that previous data were published for different membranes and acids. However the IEMs and inorganic acids that were studied were sufficiently similar to allow general conclusions to be drawn in order to validate the proposed mechanisms.

5.1.3.1 Proton leakage in AEMs

An early study demonstrated that the amount of swelling water in a membrane increased linearly with increase in exchange capacity and found that, in acid solutions, the amount of sorbed acid depended on the water content of the membrane (Cohen et al, 1986). Further work found that the amount of sorbed acid (non-exchange sorbed electrolyte) increased approximately linearly with increasing external acid concentration but different anions were sorbed in dissimilar amounts (Cherif & Gavach, 1989). Later studies found that, for a given membrane, the amount of sorbed water decreased with increasing external (and hence sorbed) acid (Pourcelly et al, 1991), (Pourcelly et al, 1994),

(Tugas et al, 1993b). It was also noted that the electro-osmotic water flux decreased with increasing external acid concentration. Subsequent analysis of these results revealed that the total molar hold-up of sorbed species in a given membrane remained approximately constant (±10%). Recent work on IEMs in non-acidic conditions also showed the electro-osmotic water flux to decrease with increasing electrolyte concentration (Okada et al, 1996), (Reboiras, 1996).

Perhaps one of the most significant conclusions to date on the subject of proton leakage was that, for different membranes (1 CEM and 2 AEMs), the loss of proton transport was attributed to an increase in the sorbed acid:water ratio (Pourcelly et al, 1991). Further work showed no undissociated acid to be present in the membrane (Pourcelly et al, 1994), (Tugas et al, 1993b). A mechanistic explanation of the effect of acid:water ratio was not proposed. It should be noted that the proton transport mechanism in AEMs must differ significantly to that found in CEMs which are specifically designed to transport protons via the active ion exchange groups. Protons are the counter-ion in a CEM but a co-ion in an AEM. Additionally, the acid:water ratio appears to have little/no effect on proton transport when a specific AEM is subjected to different operating conditions (Pourcelly et al, 1991), (Tugas et al, 1993b), (Pourcelly et al, 1994).

It is unlikely that transport of protons is accompanied by significant water transport due to their extraordinary mobility via proton tunnelling (Kuppinger et al, 1993). Solvation decreases the mobility of an ion whereas proton leakage is a result of enhanced mobility. For example solvated cations such as Na^+ do not leak anywhere near as readily through anion exchange membranes as protons. It

was also shown that the ratio of ionic mobilities (H^+:Cl^-) in the membrane phase did not differ widely from that in water (Tugas et al, 1993a).

In summary proton leakage is affected both by the absolute and relative amounts of sorbed acid and water in anion exchange membranes.

5.1.3.2 Heterogeneous nature of ion exchange membranes

A simplistic model of an AEM based on a constant electro-osmotic water flux per mole of anions transported would predict a decrease in overall water flux with increased proton leakage. However a more detailed knowledge of the membrane structure is required in order to understand the mechanistic relationship between proton leakage and water transport number or acid co-ordination.

Perfluorinated ion exchange membranes are often regarded as heterogeneous in terms of polymeric and ion transport regions (Timashev, 1991), (Tugas et al, 1993a). Detailed studies on CEMs proposed an essentially two-phase model comprising a hydrophobic polymer backbone and hydrophilic ion exchange groups including sorbed water (Timashev, 1991). A study which specifically focused on AEMs proposed a three-phase membrane model that incorporated co-ion leakage. It comprised of hydrophobic polymer, active ion exchange zone and interstitial sorbed acid zone (Tugas et al, 1993a). Sorbed water was divided between the active and interstitial zones. More recently fundamental experiments confirmed that there appeared to be two mechanisms for acid transport: internal diffusion of sorbed acid and facilitated anion transport (Narebska, Koter & Warsawski, 1995). This heterogeneous representation of

the membrane has been used to develop the consolidated model and is illustrated in Figure 5.1.

In the proposed model it was assumed that sorbed water is partitioned between the active and interstitial zones of the membrane, and that the degree of partition of the water between the zones is governed by interactions within the membrane between hydrophilic ion exchange sites, hydrophobic polymer matrix and solvation of the dissociated sorbed acid. It is this water partition which links proton leakage to electro-osmotic water flux.

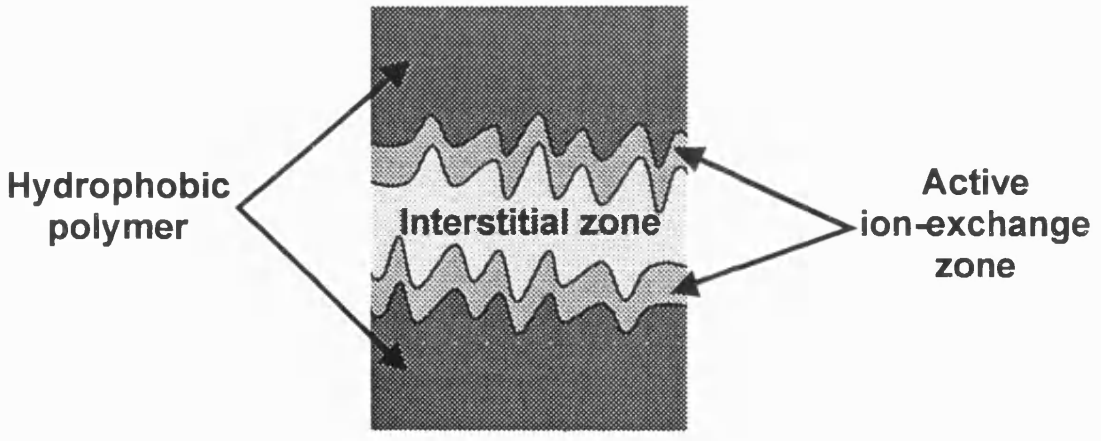

Figure 5.1: Illustration of hydrophobic IEM showing polymer, active and interstitial zones

In order to identify paths for ion transport it was useful to look at individual ion mobilities within the membrane. Using the three-phase membrane model, other workers found the mobility of anions in the active zone of an anion exchange membrane to be greater than the mobility of anions in the interstitial zone (Tugas et al, 1993a). Furthermore they found that, whilst the interstitial anion mobility remained approximately constant, the mobility of the active anions increased with increasing external acid concentration, and was in some cases an

order of magnitude greater than the interstitial anion mobility. Therefore it is reasonable to assume that the majority of acid (anion) transport is via the active zone. On the other hand proton transport would occur mainly through the interstitial zone where repulsion by the ion-exchange sites is minimal and protons can be exchanged with those already sorbed within the matrix. Consequently the electro-osmotic water flux will be governed primarily by the solvation of anions in the active zone whereas proton leakage will depend on the absolute amount of acid sorption in the interstitial zone.

5.1.4 Consolidated model for proton leakage and water flux

Having obtained a good understanding of the fundamental properties of IEMs, particularly from the work studying proton transport in AEMs, it was possible to propose a model which explained the relationship between proton transport and water flux which is given below. Previous workers have not linked these two phenomena in a mechanistic model.

Proton transport is governed by the amount of sorbed acid in the interstitial zone. For a particular membrane, proton transport appears to be most strongly affected by absolute acid sorption but only minimally by variation in the acid:water ratio, for example, typical membrane data presented in the literature suggests that $t_{H+} \propto (N_A)^2$ appears to be a good approximation over a limited range of acid concentrations (Tugas et al, 1993a). Electro-osmotic water flux is governed by the hydration in the active zone and hence the partition of water between the active and interstitial zones.

For a given membrane, as the external acid concentration is increased the acid sorption increases giving rise to a reduction in the overall sorbed water content.

The sorbed water partition shifts towards the interstitial zone because of increased solvation requirements. This reduces the water content of the active zone, thereby increasing the active anion mobility, and decreasing the electro-osmotic water flux. The increase in sorbed acid significantly enhances proton transport.

Figure 5.2 and Figure 5.3 illustrate the model as applied to the same membrane operating in different acid solutions. The acid concentration has been assumed equal on both sides of the membrane for each case. It should be noted that the diagrams in no way represent pore structures.

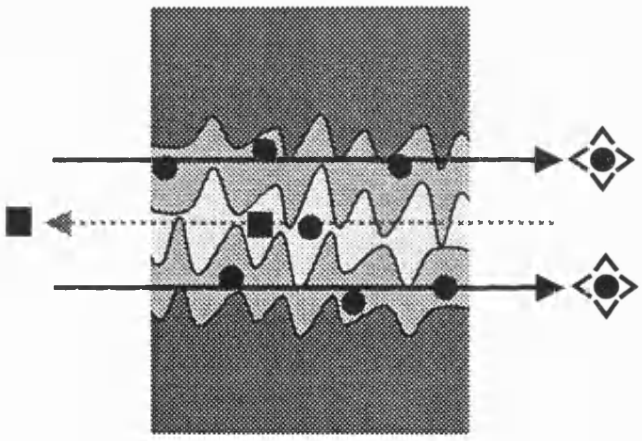

Figure 5.2: Illustration of model applied to AEM in low concentration acid (● anion, ∠ co-ordinated water, ■ proton)

Figure 5.2 shows that a low external acid concentration causes low sorption of acid in the interstitial zone resulting in low proton leakage. The water within the membrane is partitioned towards the active zone which gives rise to a high electro-osmotic water flux. On the other hand in Figure 5.3 the high external acid concentration causes high sorption of acid in the interstitial zone with increased proton leakage. The increased solvation requirements of the sorbed

acid results in a water partition shift towards the interstitial zone. This reduces the electro-osmotic water flux associated with anion transport via the active zone.

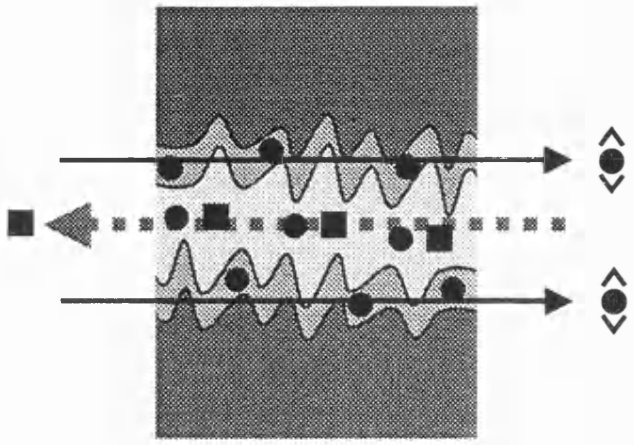

Figure 5.3: Illustration of model applied to AEM in high concentration acid (● anion, ∠ co-ordinated water, ■ proton)

It is difficult to visualise the model when comparing different membranes because of the multivariability introduced by not fixing the membrane properties. However, in general terms, reduced proton leakage would result from a decrease in the absolute acid sorption in the interstitial zone. This in turn might be expected to give rise to increased active zone hydration and hence a greater electro-osmotic water flux.

In order to validate the proposed consolidated proton leakage and water flux model, Table 5.1 lists its main features and the relevant supporting citations. Its applicability to different membranes is further reinforced by the results obtained during this research.

Feature	Characteristics	Author (s)
Membrane structure	Heterogenous three-phase model involving: hydrophobic polymer; active hydrophilic ion exchange groups and interstitial zones .	Tugas et al, 1993a Timashev, 1991
Water sorption	Linear relationship between water content and exchange capacity. Water sorption decreases with increased acid sorption.	Cohen et al, 1986 Pourcelly et al, 1991
Acid sorption	Dependent on amount of sorbed water and increases with increasing external acid concentration.	Cohen et al, 1986 Cherif & Gavach, 1989
Total sorption	Remains approximately constant for a given membrane.	Pourcelly et al, 1991 Pourcelly et al, 1994 Tugas et al, 1993a
Water partition	Water partitioned between active and interstitial zones. Partition varies with amount of sorbed species (Hypothesis of model.).	Tugas et al, 1993a
Proton transport	Increases with external acid concentration and increased acid sorption. As a result of their enhanced mobility proton transport does not involve a solvation shell.	Tugas et al, 1993a Kuppinger et al, 1993
Electro-osmotic water flux	Related to active anion (acid) transport. The smallest solvation shell coincides with the greatest mobility. Electroosmotic flux decreases with increasing external acid because water associated with active anions decreases.	Tugas et al, 1993a Pourcelly et al, 1991 Okada et al, 1996

Table 5.1: Validation of the key features of the model using supporting citations

5.1.4.1 Model conclusions

The consolidated proton leakage and water flux model highlights the need to consider absolute acid sorption rather than sorbed acid:water ratio when assessing proton leakage for a given membrane. It draws together proton leakage theories and describes the relationship between proton transport and electro-osmotic flux via the variation of water partition between the active and interstitial zones of an anion exchange membrane. The consolidated model describes why the same membrane yields a stronger acid product when operated less efficiently, i.e. at high acid concentrations both the current efficiency and water flux are lower than at low acid concentrations.

Whilst the qualitative agreement between the theory and the numerous data sources is extremely strong when considering the performance of a specific AEM, at this stage it is only possible to hypothesise a relationship between different membranes because of the complexity of the problem and the lack of data in this area. Therefore the model has not yet been validated with fundamental measurements to explain the related phenomenon that inefficient membranes appeared to have lower water transport numbers than their higher efficiency counterparts. It nevertheless agrees with qualitative process measurements.

5.1.4.2 Summary of model

In many electro-membrane processes it is important to consider the solvent flux across a membrane as this has a non-electrical effect on the overall process performance. This is certainly the case for acid concentration. For design

purposes therefore, future work in this area should report water flux along with current efficiency as performance measures for membrane evaluation.

The consolidated model propounds that a reduction in proton leakage would lead to increased water flux which is found in practice. The theory explains the variation in proton transport and water flux for a given membrane with different external acid concentrations. When the external concentration increases, proton leakage becomes more significant and current efficiency drops along with the water flux. Water flux is closely linked to proton leakage and an improvement in one of these leads to a deterioration of the other. The same membrane, when operated inefficiently, yields a stronger acid product. Extension of theory to cover the similar trend found between different membranes has yet to be validated with fundamental measurements.

5.2 Advanced understanding of the membrane

Development of the 'proton leakage and water flux' model generated many interesting questions regarding the performance of an AEM under different conditions. In some cases new experimental techniques must be devised in order to generate adequate fundamental membrane data. This section discusses the limitations of experimental techniques used during this project and manipulates the data in order to obtain an advanced understanding of membrane performance. Wherever possible areas for further research are suggested.

5.2.1 Water transport

The importance of water transport in an electro-membrane process has already been highlighted. However the information required to fully understand membrane transport phenomena is not easily obtained from simple experimental measurements. This section highlights which measures are required to fully describe water transport and the limitations of experimental data.

5.2.1.1 Water transport and ion co-ordination

The number of water molecules associated with a particular ion is known as its co-ordination number. As a result of numerous interactions co-ordination numbers vary with solution, and consequently membrane, properties. It is difficult to measure a co-ordination number in the aqueous phase as is illustrated by the spread in values reported. For example, the co-ordination numbers of Na^+ in aqueous solutions have been reported by various workers to be: 71, 66, 44.5, 16.9, 16.2, 6-7, 4.5, 4, 2.5, 2 and 1 (Samoilov, 1965)! Additionally, the formation of hydronium ions leads to the possibility of some degree of proton hydration. For example, H_3O^+ could be regarded as a proton with a co-ordination number of one. Consequently measurement of co-ordination numbers within a membrane is extremely difficult. NMR analysis has been undertaken on CEMs under zero-current conditions with some success (Valuev, 1996). This has yet to be undertaken on-line.

Notwithstanding these comments, the technique used to determine water transport from the experimental data was improved in order to further understand ion co-ordination under process conditions.

5.2.1.2 Limitations of process measurements

Water flux data were derived from volume measurements throughout an experimental run taking into account water oxidation at the anode. Hence, the specific water transport numbers presented in Chapter 4 represented overall rather than instantaneous values.

In order to obtain differential values of the specific transport number over the course of an experiment, a polynomial was fitted to the mass of water present in the anolyte calculated from density and volume measurements. The curve, coupled with an anolyte mass balance, was used to determine the change in mass, ΔM_w, due to water transport over a differential element of time. This is given in Appendix 5. A differential specific water transport number, $\tilde{n}_{H2O}$, was calculated using:

$$\tilde{n}_{H2O} = \frac{\Delta M_w}{18\left[F(t+1) - F(t)\right]\eta_{DCE}} \qquad [5.1]$$

$\tilde{n}_{H2O}$ differential specific water transport number

ΔM_w change in mass due to water transport (g)

This technique was similar to one used to derive credible η_{DCE} values discussed in Chapter 4 and the results are plotted in Figure 5.4

A decrease in $\tilde{n}_{H2O}$ could be seen with increasing acid concentration which indicated reduced water transport relative to acid transport. It should be noted that Equation 5.1 becomes undefined as the η_{DCE} approaches zero and acid transport is very low. Consequently, a second specific water transport number

was defined as the amount of water transported per mole of protons transported across the membrane.

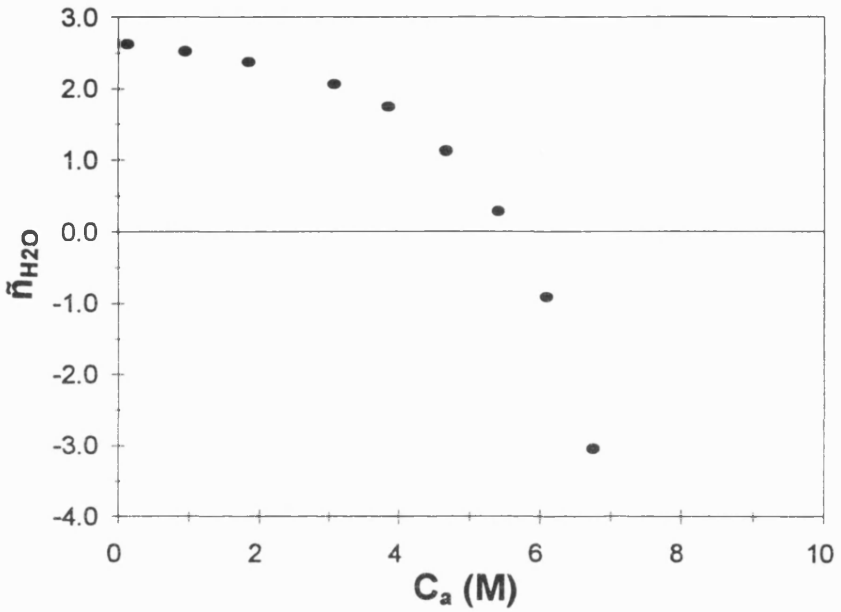

Figure 5.4: Differential specific water transport number against anolyte acid concentration [AW002]

The differential specific water transport number relative to proton transport, $\tilde{n}_{H2O/H+}$, was determined using:

$$\tilde{n}_{H2O/H+} = -\tilde{n}_{H2O}\left(\frac{\eta_{DCE}}{1-\eta_{DCE}}\right) \qquad [5.2]$$

$\tilde{n}_{H2O/H+}$ differential specific water transport number relative to proton transport

The change in sign accounts for the opposite direction of proton transport and the values calculated using this equation are given in Figure 5.5. Equation 5.2

is undefined for high values of η_{DCE} where proton transport is minimal. Therefore $\tilde{n}_{H2O}$ is appropriate for studying water transport at the beginning of an experimental run where current efficiencies are high and $\tilde{n}_{H2O/H+}$ should be used at the end of the run where the current efficiencies are low. Analysis of the curves presented in Figure 5.4 and Figure 5.5 is discussed below.

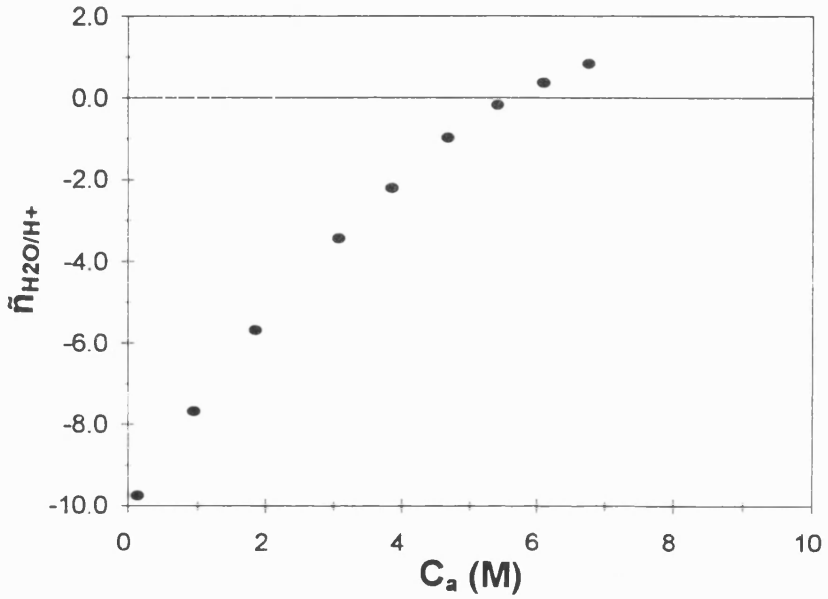

Figure 5.5: Differential specific water transport number relative to proton transport [AW002]

5.2.1.3 Deductions from limiting cases

Using the respective definitions of the differential specific water transport numbers, a mass balance on water in the anolyte yields:

$$\tilde{n}_{H2O} = W_{A-} - W_{H+}\left(\frac{1-\eta_{DCE}}{\eta_{DCE}}\right) - \frac{0.5}{\eta_{DCE}} \qquad [5.3]$$

$$\tilde{n}_{H2O/H+} = -W_{A-}\left(\frac{\eta_{DCE}}{1-\eta_{DCE}}\right) + W_{H+} + \frac{0.5}{(1-\eta_{DCE})} \qquad [5.4]$$

W_{A-} anion co-ordination number

W_{H+} proton co-ordination number

Limiting cases of these equations are $\eta_{DCE} \rightarrow 1$ and $\eta_{DCE} \rightarrow 0$. For these cases Equations 5.3 and 5.4 become Equations 5.5 and 5.6 respectively.

$$\tilde{n}_{H2O} = W_{A-} - 0.5 \qquad \eta_{DCE} \rightarrow 1 \qquad [5.5]$$

$$\tilde{n}_{H2O/H+} = W_{H+} + 0.5 \qquad \eta_{DCE} \rightarrow 0 \qquad [5.6]$$

These expressions allow an estimate of the co-ordination numbers to be made using the data plotted in Figure 5.4 and Figure 5.5. If the limiting cases are assumed to occur where the curves plateau at the beginning or end of a run respectively, then co-ordination numbers of $W_{A-} \approx 3.5 \pm 0.25$ and $W_{H+} \approx 1.0 \pm 0.25$ are estimated from the curves. This implies that, initially, where there is little proton transport, the acid anions are transported with an average of 3.5 molecules of water per acid molecule. At the end of a run, where current efficiency is low, protons are transported with a single water molecule. This agrees with data from other workers studying proton transport in CEMs (Buche, 1996). The limiting cases were not attained completely for either measurement and so the values determined can only be regarded as estimates.

The above analysis allowed the limiting cases of co-ordination numbers to be estimated and showed, at the end of a run at least, some water transport occurs

with proton leakage. It did not allow the variation in ion co-ordination throughout an experimental run to be determined as this requires unidirectional rather than net water flux measurements to be made. However, if the co-ordination number of either anions or protons is assumed constant, a simple visualisation of the variation of the ion co-ordination can be generated. Using the co-ordination numbers estimated above, Figure 5.6 and Figure 5.7 were generated based on this assumption. Figure 5.6 shows a decrease in anion co-ordination whilst Figure 5.7 indicates an increase in proton co-ordination throughout a run.

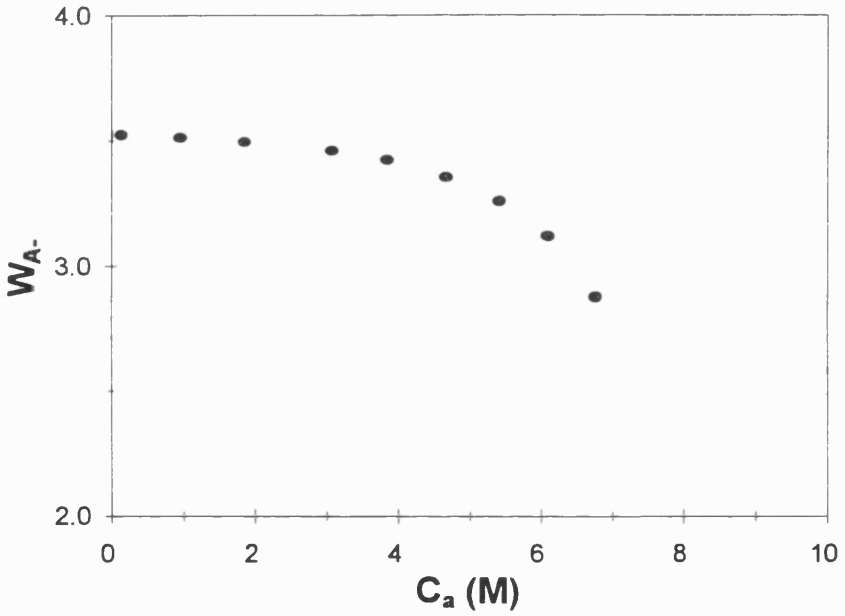

Figure 5.6: Estimated anion co-ordination number against anolyte acid concentration for $W_{H+}=1.0$

It should be noted that Figure 5.6 and Figure 5.7 depend significantly on the assumed value of the co-ordination number and cannot be applied for subsequent theoretical analysis. Further work in this area would require additional experimental techniques to be developed in order to generate better

data. This analysis was therefore only evaluated for the AW002 experimental run.

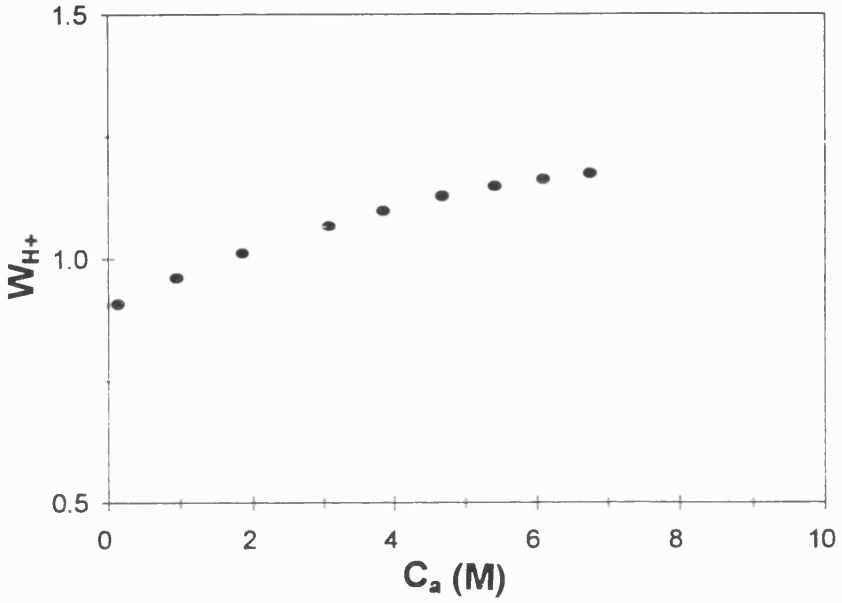

Figure 5.7: Estimated proton co-ordination number against anolyte acid concentration for W_{A^-}=3.5

The limiting case of Figure 5.7 did not agree with the W_{H+} estimated above as it implied that as $\eta_{DCE} \rightarrow 0$, $W_{H+} > 1.0$. Figure 5.6 showed better agreement showing $W_{A^-} \approx 3.5$ as $\eta_{DCE} \rightarrow 1$. This implies that a constant proton co-ordination number of 1.0 is most appropriate with the acid anion co-ordination number decreasing with increasing acid concentration.

5.2.1.4 Further fundamental studies

Unidirectional fluxes have been measured for ions using radiotracer techniques, for example (Cherif & Gavach, 1989). It is more difficult to measure unidirectional fluxes for water. A technique involving heavy water (D_2O) might be adopted in fundamental membrane experiments where one electrolyte is a

D_2O system and the other an H_2O system. This is theoretically possible in a suitable rig with analysis of the D_2O via mass spectrometry (Valuev, 1996).

5.2.2 Ion transport

Having considered water transport in detail, the remainder of this chapter is devoted to the variation in performance of the membrane with regards to ion transport. During the experimental runs a variable concentration profile existed across the membrane rather than the constant profile that was assumed to develop the proton leakage and water model. To account for this, use is made of a novel parameter to characterise the membrane which is discussed below.

5.2.2.1 Membrane resistance to proton transport

Transport of ions through an IEM can be modelled using the Nernst-Plank equation which was discussed in Chapter 2. This theoretical model for ion transport, Equation 2.16, was equated to the measured experimental proton flux to give:

$$J_{H+} = \frac{(1-\eta_{DCE})j}{\Im} = D\left[\frac{\partial C}{\partial x} + \frac{\Im}{\Re T} C \frac{\partial \varphi}{\partial x}\right] \qquad [5.7]$$

The concentration term, C, in Equation 5.7 represents the ions onto which the electrical field acts - this is the anolyte acid concentration, C_a, in the case of proton leakage. Figure 5.8 illustrates the main terms in the ion transport equation.

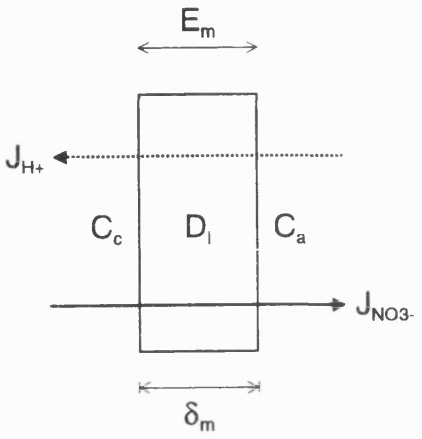

Figure 5.8: Illustration of membrane transport terms

If Equation 5.7 is determined across the membrane thickness, δ_m, then rearrangement and defining R_m gives:

$$\frac{\delta_m}{D} = \frac{C_a\left(1+\frac{E_m\Im}{\Re T}\right)-C_c}{\frac{(1-\eta_{DCE})j}{\Im}} = R_m \qquad [5.8]$$

R_m membrane resistance to proton transport (s m^{-1})

R_m $=\delta_m/D$

R_m can be regarded as the resistance of the membrane to proton transport or an inverse mass transfer coefficient for proton transport across the membrane. As both electrical and concentration driving forces are accounted for, the effect of these on proton transport is effectively included in the R_m value.

R_m can be evaluated from experimental data once all the factors in Equation 5.8 have been determined. Acid concentrations and current efficiency have been discussed previously. The membrane voltage drop, E_m, was calculated from the reference electrode measurements made throughout the experimental runs. These were corrected for the voltage drop of the electrolytes using literature values of conductivity. The voltage components are shown below.

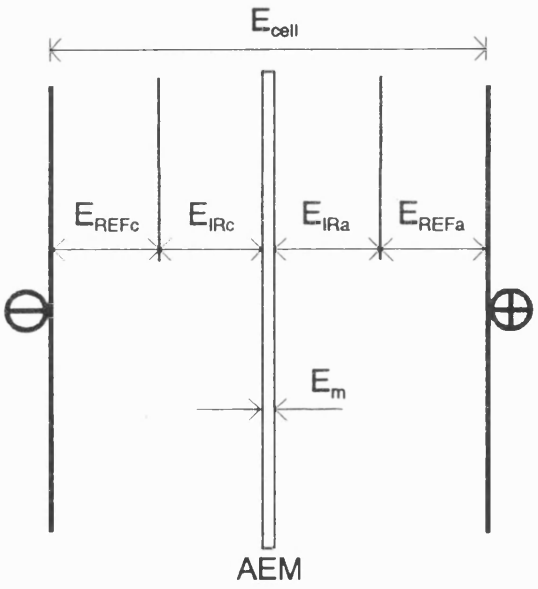

Figure 5.9: Voltage drops across cell showing membrane voltage drop E_m

If the resistances of the boundary layers adjacent to the membrane are different to those of the bulk then the measured E_m would include these. It should therefore be considered as the voltage drop across the membrane and associated Nernst layers. The resultant E_m values are plotted against anolyte acid concentration in Figure 5.10.

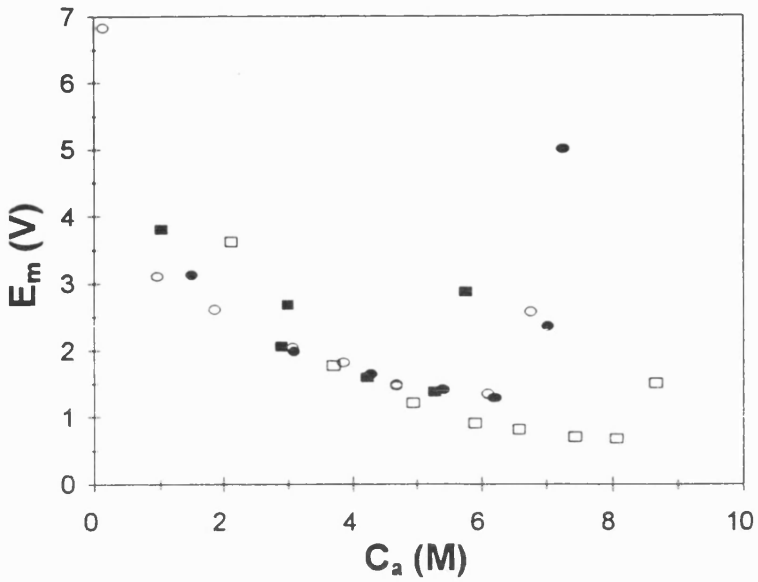

Figure 5.10: Voltage drop across membrane and boundary layers against anolyte acid concentration (○AW002, ■AW1, ●AW1.5, □AW2)

The data showed good grouping apart from some high values which occurred at the end of experimental runs. These were due to the influence of the very low catholyte acid concentration having a similar effect as a very low anolyte concentration at $C_a \rightarrow 0$. Neglecting these points, the membrane voltage drop decreased with increasing acid concentration. This can be explained by the sorption of acid within the membrane that increased with increasing acid concentration and facilitated proton transport. The anolyte acid concentration was again demonstrated to be a key parameter as the effect of catholyte acid concentration only became apparent in the last data point of each run. Anolyte acid concentration is a dominant factor in Equation 5.8 as it is weighted by the ionic migration term which can be two orders of magnitude greater than C_c.

At the beginning of an experimental run, the initial values of E_m were often spuriously high before decreasing to a stable value. This was attributed to start-up phenomena often referred to as 'membrane conditioning'.

The R_m values determined using the above technique are plotted against catholyte acid concentration in Figure 5.11. No clear trend was observed in Figure 5.11 because of the scatter of data for different runs.

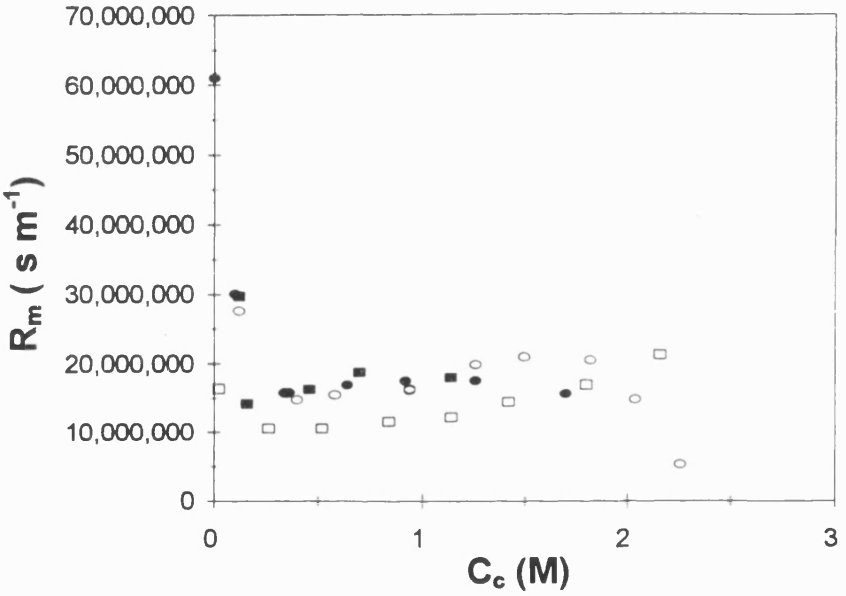

Figure 5.11: Membrane resistance to proton transport against catholyte acid concentration (○AW002, ■AW1, ●AW1.5, □AW2)

At low catholyte concentrations the resistance to membrane transport rapidly increased. This could be due to very low sorption of acid at the catholyte surface of the membrane restricting the flux of protons in an analogous way to the constriction at the exit of a funnel. The total ionic flux remained constant (galvanostatic operation) and this was achieved by a corresponding increase in the membrane voltage drop (electrical driving force). There would be a practical (powerpack) limitation of this power increase after which potentiostatic

operation would be resumed. Figure 5.12 shows the R_m data plotted against anolyte acid concentration.

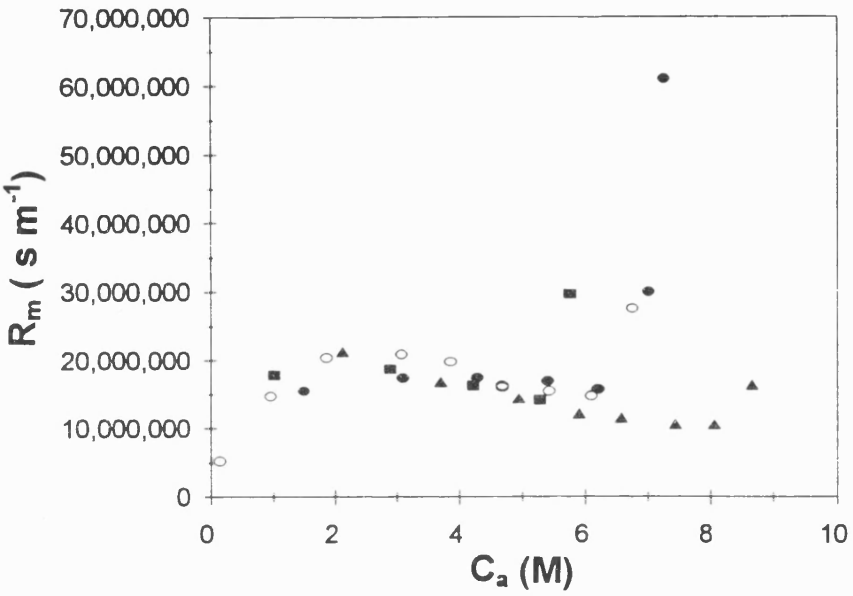

Figure 5.12: Membrane resistance to proton transport against anolyte acid concentration (○AW002, ■AW1, ●AW1.5, □AW2)

Very little scatter was seen in these data which appeared for the most part to describe a single curve. High values were seen at the end of the runs due to low catholyte acid concentrations as was seen in the E_m plot, Figure 5.10. At low values of C_a, R_m is low as the electrical migration term is less significant. As $C_a \rightarrow 0$ then $R_m \rightarrow \leq 0$ (although $R_m < 0$ would only occur at values of C_c high enough to drive protons against the electrical field). High boundary layer resistance or membrane conditioning occurring during this phase would be less apparent due to the low C_a. Once C_a increased to a concentration where the electrical migration term was dominant (and $C_a > C_c$) R_m decreased with increasing anolyte acid concentration. This could be due to increased sorption of acid which would assist proton transport.

It is interesting to observe the relationship between R_m and E_m to see if any observed trend could be explained by the theories proposed previously. These data are plotted in Figure 5.13. The high E_m values occurring at the end of a run are omitted from this chart for clarity.

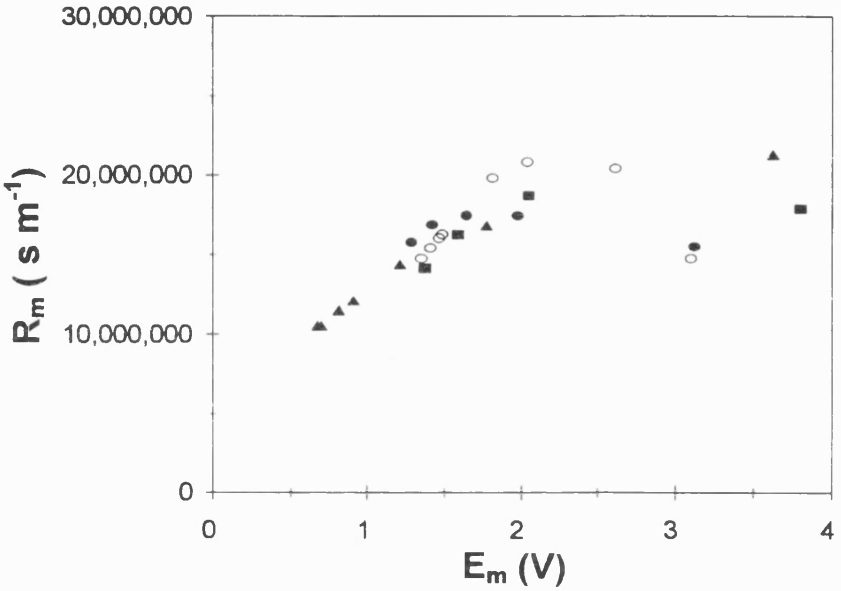

Figure 5.13: Membrane resistance to proton transport against membrane and boundary layer voltage drop
(○AW002, ■AW1, ●AW1.5, □AW2)

The data in the tail of the curve may indicate that there was a deviation towards a maximum resistance to proton transport at high E_m values, although it is not possible to draw conclusions from this area because of the scatter. Therefore, neglecting the scattered tail (as these data were initial values where membrane conditioning was occurring, or in some cases where $C_a<C_c$), the observed trend for the remaining data can be discussed. Good agreement was observed between the data from different runs. Generally there was an almost linear relationship between R_m and E_m. As the electrical resistance of the membrane increases the resistance to proton transport increases. This could be only due to membrane-solution interactions as the membrane type was constant. The

interpretation of this is that increased acid sorption decreased the electrical resistance of the membrane whilst giving rise to the potential for increased proton transport.

In addition to improving understanding of the processes occurring within the membrane, this analysis might prove a useful technique for developing a mathematical model of the membrane process. For example, a set of E_m vs. C_a and R_m vs. E_m data could be used to describe the electrical performance of a particular membrane over a range of concentrations. Fundamental equations could be developed relating E_m and R_m to acid sorption and hence electrolyte concentration, thereby allowing theoretical generation of the above relationships. Present fundamental membrane research is still attempting to understand acid sorption phenomena in IEMs (for example Tugas et al, 1993a), so generation of such theoretical relationships is unlikely to be imminent.

5.2.2.2 Limitations of process measurements

The limitations of the process measurements in quantifying ion transport have been covered concurrently with the above discussion. The main point to emphasise is the potential for spurious data at each end of the experimental runs due to experimental rather than membrane limitations. At the beginning of a run the membranes were equilibrated with acid solution for at least 24 hours prior to being used. Despite this additional membrane conditioning was observed where the voltage drop across the membrane dropped rapidly over an initial period before settling to a pseudo-steady state value. Low electrolyte concentrations also gave rise to high measured membrane voltage drops.

When the concentration of acid in the catholyte became low the transfer of nitrate to the membrane surface became mass transfer limited. Hence, the measured membrane efficiency was affected by this limitation. This does not invalidate the data in this region as the measurements represent true process efficiencies rather than membrane efficiencies in the absence of mass transfer limitations.

5.2.2.3 Further fundamental studies

The evaluation of ion transport in the AW membrane via the R_m term should be extended for other AEMs. Although the performance trends are known to be similar, there may be characteristic parameters that could be used to describe a membrane. For example, the slope of the R_m vs. E_m curve could be compared for many different AEMs.

Additionally, future fundamental membrane studies should be concerned with developing theoretical relationships for acid sorption in AEMs and extending them to describe proton leakage and water transport. At present only a phenomenological model could be developed to describe this process, but this could be a useful technique to determine key membrane parameters (Timashev, 1996).

5.2.3 Summary of improved understanding

It has been shown that proton leakage is related to water transport and a mechanism has been proposed which describes this phenomenon using the fundamental processes occurring within the membrane. Detailed analysis of the experimental data highlighted trends in the membrane resistance to proton transport term introduced in Section 5.2.2.1. The improved membrane

understanding will aid future process evaluation and mathematical modelling of the membrane transport processes. This work could be applied to development of AEMs for acidic applications. For example, a bi-layer membrane consisting of high-efficiency and low-efficiency AEM might enable both proton leakage and water flux to be controlled by exploiting the differences in membrane performance.

The re-arranged version of the Nernst-Plank equation (Equation 5.8) can be used to model membrane transport via the R_m term which can be easily determined from experimental data. This was combined with simple electrochemical assumptions to model the EED process for nitric acid. It is discussed in Chapter 6.

Chapter 6:
Model of EED process

6. Model of EED process

The model developed to describe the EED process is discussed in this chapter and the data generated by the model are compared with experimental results. Emphasis is placed on the importance of combining contemporary electrochemical modelling techniques with those used by membrane scientists in order to develop a detailed process model. The model discussed here employs a re-arranged version of the Nernst-Plank equation to describe membrane transport but the electrochemical reactions are represented by semi-empirical expressions.

Previous modelling work has been focused either on electrochemical phenomena or on the performance of ion exchange membranes, but has not tended to combine the two fields of work. Those studying electrochemical reactions have utilised detailed Butler-Volmer or Tafel data to describe the reaction kinetics, but have modelled an undivided cell or a cell with a porous separator rather than an electro-membrane cell configuration, for example (Scott & Paton, 1993), (Coleman et al, 1996). On the other hand, membrane scientists have applied relationships such as the Nernst-Plank equation to describe ion transport but have not considered the process electrochemistry, for example (Cherif & Gavach, 1989).

It appears that both modelling disciplines are sufficiently advanced that they could be combined to generate a detailed model of a complete electro-membrane process. This would require collaboration between membrane scientists and electrochemical engineers in order to fully describe the system. The resultant set

of equations is likely to be complex. Notwithstanding this, solution is probably feasible using a state-of-the-art computer workstation, and the results would form the basis of a new generation of electro-membrane process models based on theoretical relationships.

The process model described in this chapter has been developed by combining both electrochemical and membrane transport relationships into a complete process model. Simple assumptions were made to describe the electrochemical phenomena and results were produced with reasonable agreement with the experimental data. The model could be significantly enhanced by the incorporation of more detailed electrochemical and membrane transport relationships. Such improvements would not alter the fundamental concept of the model but they would significantly improve its scientific basis.

The assumptions that were made in order to develop the basic model are highlighted in the first section of this chapter. Numerical solution of the model and comparison of model results with experimental data is presented at the end of the chapter.

6.1 Process performance

The techniques and assumptions used to describe the key features of the model are described in this section.

6.1.1 Electrochemical phenomena

A detailed fundamental study of nitrate reduction was not undertaken as part of this research. A semi-empirical approach, therefore, was adopted in order to generate a process model.

6.1.1.1 Electrode reactions

Although individual rate expressions for electrochemical reactions had not been determined, the total rate of reaction could be calculated from the Faraday relationship. The sum of currents of competing reactions can not be greater than the total rate of reaction determined below because the process was operated in galvanostatic mode, thus:

$$\frac{N}{t} = \frac{i}{z\Im} \qquad [6.1]$$

At the anode it was assumed that only electrolysis of water occurred to generate oxygen gas and protons according to the equation:

$$^1/_2H_2O \rightarrow H^+ + {}^1/_4O_2 + e^- \qquad [6.2]$$

This reaction occurs in acidic media and if it is assumed to be charge transfer controlled its rate can be represented using Equation 6.1.

The cathode electrochemistry is more involved as two competing electrochemical reactions were observed (although many more might have occurred in the full nitrate reduction mechanism). The overall reactions are given by:

$$H^+ + e^- \rightarrow {}^1/_2H_2 \qquad [6.3]$$

$$NO_3^- + 10H^+ + 8e^- \rightarrow NH_4^+ + 3H_2O \qquad [6.4]$$

In regions of high nitrate mass transfer, no gas bubbles were detected and so all the current must have been consumed by nitrate reduction reactions. However as mass transfer of nitrate decreased gas evolution was observed which indicated that Equation 6.3 was proceeding. Nitrate reduction (Equation 6.4) could, however, still have been occurring to some extent in this region. It was therefore necessary to determine the relative rates of the two reduction reactions.

There are two approaches that can be used to describe the fraction of current going to hydrogen evolution when nitrate is mass transfer limited: i) both reactions 6.3 and 6.4 proceed at different rates or ii) there is a switch to hydrogen evolution after which no further nitrate reduction occurs. Both of these approaches were tested and the assumptions made in order to describe the two phenomena are described below.

6.1.1.2 Reduction efficiency assumption

The point at which hydrogen began to be evolved appeared to be controlled by the mass transfer of nitrate. It was logical, therefore, to assume that mass transfer characteristics had an influence on the relative rates of Equations 6.3

and 6.4. Therefore, prior to mass transfer limitation it was assumed that only nitrate reduction occurred. After this point both reactions occurred in a ratio equal to the mass transfer flux divided by the total flux of charge. This gave rise to:

$$\eta_r = \frac{k_m A_m C_c}{\left(\frac{j}{\mathfrak{F}}\right)} \qquad 0 \leq \eta_r \leq 1.0 \qquad [6.5]$$

η_r nitrate reduction efficiency (if nitrate is *not* mass transfer limited $\eta_r = 1.0$ by definition)

The mass transfer coefficient, k_m, in this expression was obtained experimentally as described in Section 4.2.3.2. Equation 6.5 implies that nitrate is reduced instantaneously on reaching the electrode. If mass transfer is insufficient to satisfy the total flow of charge then the deficit current will go to hydrogen evolution. Thus η_r can be regarded as a nitrate reduction efficiency.

In order to test the validity this assumption, the predicted fraction of current going to hydrogen evolution ($1-\eta_r$) was plotted for a range of currents and concentrations. This is shown in Figure 6.1.

These data were compared against experimental results for hydrogen evolution which were obtained via mass spectrometer analysis of the vent gas stream as discussed in Section 4.2. The data from the experimental work are presented again below in Figure 6.2 to facilitate comparison of the two figures.

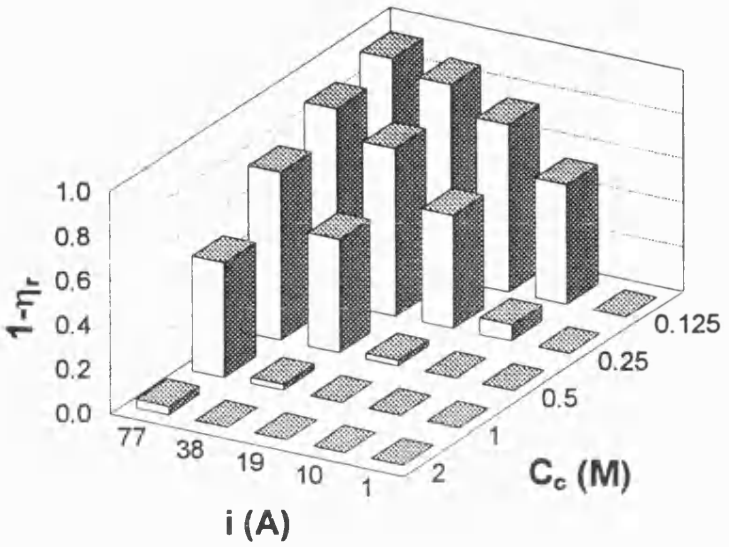

Figure 6.1: Predicted fraction of current going to hydrogen evolution against current and catholyte acid concentration

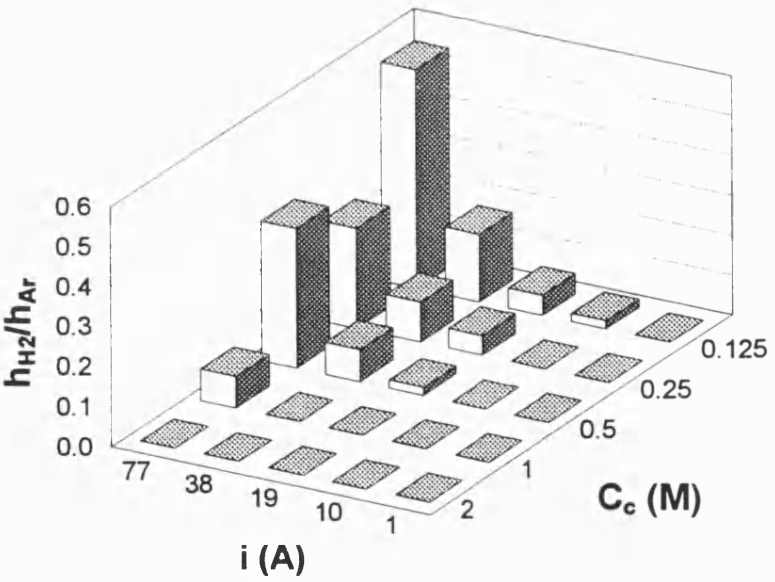

Figure 6.2: Relative hydrogen evolution rates obtained from mass spectrometer analysis

The ordinates of Figure 6.1 and Figure 6.2 are not identical although they are both representative of hydrogen evolution. Complete agreement between the two

figures was not seen. For instance, the model predicted some hydrogen evolution at 38A and 1M but no hydrogen was detected during the experimental hydrogen analysis. For either case this could be due to a number of factors which include errors in the mass transfer coefficient or a false zero reading obtained during experimentation. Despite these discrepancies, the overall shape of the data was similar and therefore taken to be representative of the competing electrochemical reactions in the absence of kinetic data.

In order to include the possibility that there might be a complete switch between the two reduction reactions, and not a gradual transition as implied by Equation 6.5, an additional factor, X_s, was defined which modifies η_r as:

$$\eta_r = \eta'_r(1 - X_s) \qquad [6.6]$$

X_s nitrate reduction efficiency modification factor

η'_r former value of η_r

When X_s is unity there is a complete switch between nitrate reduction and hydrogen evolution when nitrate becomes mass transfer limited, whereas $X_s=0$ implies that there is a gradual transition between the competing reduction reactions. The effect of different values of X_s: $0 \leq X_s \leq 1.0$ in the model predictions is discussed later in this chapter.

6.1.2 Membrane performance

Having studied the resistance of the AW membrane to proton transport in detail in Section 5.2.2, the observed relationships were used as the basis for the model of membrane performance. The data were based on results from four separate

experimental runs and the low scatter reinforced the applicability of this technique. Although the observed trends in the data were explained using membrane theory, the equations employed in the model were mathematical curve fits to the data. Thus the expressions are only valid for the AW membrane. The curve fits represent the effect of electrolyte concentrations on the membrane properties (such as diffusivity and conductivity) and allow application of the re-arranged form of the Nernst-Plank equation. The equations and their validity are given in the following section.

6.1.2.1 Performance equations

The two key parameters required to predict the current efficiency of the membrane were shown in Section 5.2.2 to be the membrane voltage drop as a function of anolyte concentration (E_m vs. C_a) and the resistance of the membrane to proton transport against the membrane voltage drop (R_m vs. E_m). The membrane voltage drop as a function of anolyte acid concentration is given in Figure 6.3.

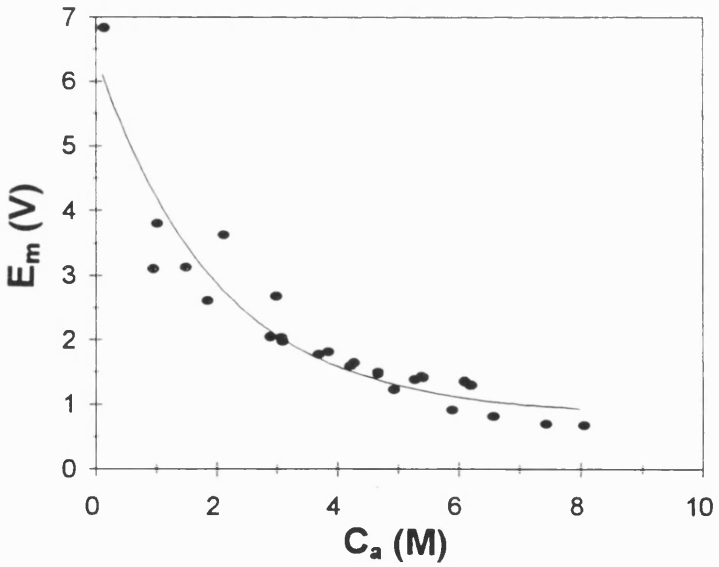

Figure 6.3: Membrane voltage drop against anolyte acid concentration for AW membrane showing curve fit

The mathematical curve fit of these data was obtained using a regression technique and, for the range of conditions indicated, is given by:

$$E_m = 0.83 + 5.56\, e^{(-0.50\, C_a)} \qquad [6.7]$$

AW membrane in nitric acid

$0.2 \leq C_a(M) \leq 8.0$

$C_c > 0.1M$

$j = 300$ mA cm^{-2}

$T = 25°C$

Therefore, providing that all the above conditions were observed, Equation 6.7 allowed prediction of membrane voltage drop from anolyte acid concentration which was essential to the estimation of R_m. The R_m vs. E_m relationships are shown in Figure 6.4.

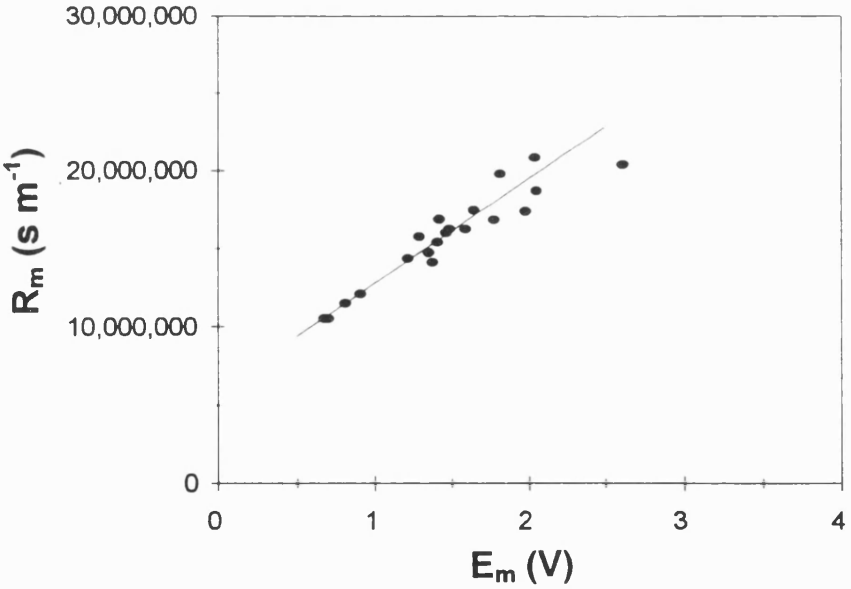

Figure 6.4: Membrane resistance to proton transport against membrane voltage drop for AW membrane showing curve fit

The scattered tail seen in Section 5.2.2 was not included in Figure 6.4 and the curve fit over the range indicated was given by:

$$R_m = 6.08\times10^6 + 6.71\times10^6 E_m \qquad [6.8]$$

AW membrane in nitric acid

$0.5 \le E_m(V) \le 2.5$

$C_c > 0.1M$

$j = 300\ mA\ cm^{-2}$

$T = 25°C$

6.1.2.2 Current efficiency evaluation

Prediction of E_m and R_m via the above relationships allowed determination of the membrane differential current efficiency, η_{DCE}, according to:

$$\eta_{DCE} = 1 - \frac{C_a\left[1+\frac{E_m\Im}{\Re T}\right] - C_c}{\frac{R_m j_{exp}}{\Im}} \qquad [6.9]$$

This relationship has the potential to become a very useful tool for use in electro-membrane process models. Providing that E_m and R_m can be determined over a range of conditions, the efficiency of membrane transport can be predicted. The experimental data source need not necessarily be from expensive pilot trials; simple membrane experiments are likely to be sufficient to determine the above parameters. Ultimately these factors might be determined from the theoretical relationships for acid sorption which is the current focus of fundamental

membrane research. As with all mathematical models, it is imperative that the range of validity of all relationships (theoretical or empirical) is clearly observed.

6.1.3 Other considerations

Having decided how to determine the electrochemical and membrane performance in the system, there remained some matters that needed addressing before a complete set of equations could be developed to describe the system.

6.1.3.1 Purge air stripping and vent gas

Due to the electrochemical generation of gases it was necessary to vent the electrolyte reservoirs to prevent a build-up. A purge-air stream was used to ensure that any hydrogen generated was present at concentrations less than its lower explosive limit. This required a considerable amount of air. The large air-flow gave rise to vapour stripping from the reservoir and therefore some electrolyte loss. In an industrial process de-misting, condensing or sorbing techniques or use of nitrogen blanketing would be employed to minimise vapour loss but these were not incorporated in the laboratory pilot rig. Consequently the process model had to include the effects of a purge-air stream.

It was assumed that all permanent gases went directly to the vent stream as the electrolytes would be close to saturation because of the continuous purge air flow. Vapour pressures were estimated using mean values for HNO_3 and H_2O over the range 0-40wt% taken from Perry (Perry, 1984) and the vapour pressure of NH_3 over NH_4^+ solutions at pH=8 (or below) from Pourbaix (Pourbaix,1974). The loss of vapours in the vent was estimated by assuming saturation. This would give an overestimate of electrolyte loss because in practice the purge-air would not reach complete saturation as it passed through

the headspace of the reservoirs and was not in intimate contact with the bulk liquid.

6.1.3.2 Membrane water transport

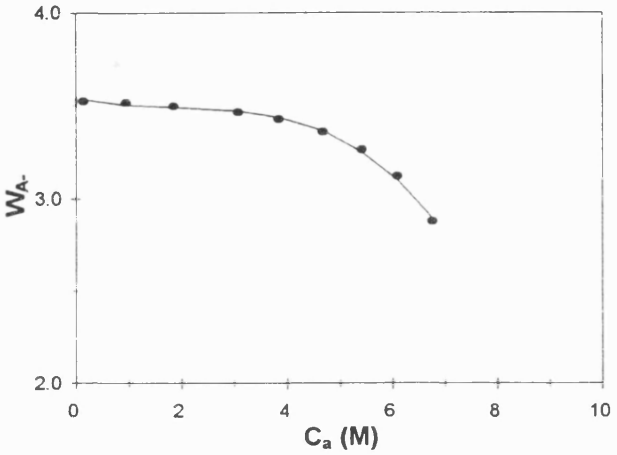

Figure 6.5: Variation of anion co-ordination number with acid concentration showing curve fit

Water transport through the membrane was determined by assuming constant proton co-ordination number ($W_{H+}=1.0$) and fitting a polynomial to the variation in anion co-ordination number shown in Figure 5.6. The curve fit is given by:

$$W_{A^-} = 3.543 - 0.068C_a - 0.029C_a^2 - 0.005C_a^3 \qquad [6.10]$$

6.1.3.3 Batch reactor model

As the residence time in the electro-membrane stack was much less than the reservoir residence time the system was approximated as a closed batch system. This assumption was shown to be valid providing that the ratio of reservoir volume residence time to cell residence time, $\tau_m/\tau_r > 20$ (Scott & Paton, 1993).

It should be noted that the ratio $\tau_m/\tau_r > 20$ is only a valid criterion for moderate values of current density (i.e. providing that the conversion per pass is low). The residence time ratios for the experimental rig were greater than this minimum criterion for both electrolytes and are tabulated below. τ_r was 0.56s in the cell and so a step-length of 0.50s was chosen for the model. In practice this step-length could probably be increased but as the computational time was small this was not undertaken.

Electrolyte	τ_m/τ_r
Anolyte	34
Catholyte	223

Table 6.1: Residence time ratios in experimental rig

τ_m reservoir residence time (s)

τ_r cell residence time (s)

6.2 Model system

Figure 6.6 illustrates the ion transfer system that was described by the model. For simplicity the representative reactions in the diagram are not stoichiometric and it does not show purge-air effects or the transport of water across the membrane. These factors were included in the model.

The complete set of differential equations used to describe the process are given in the sub-sections below.

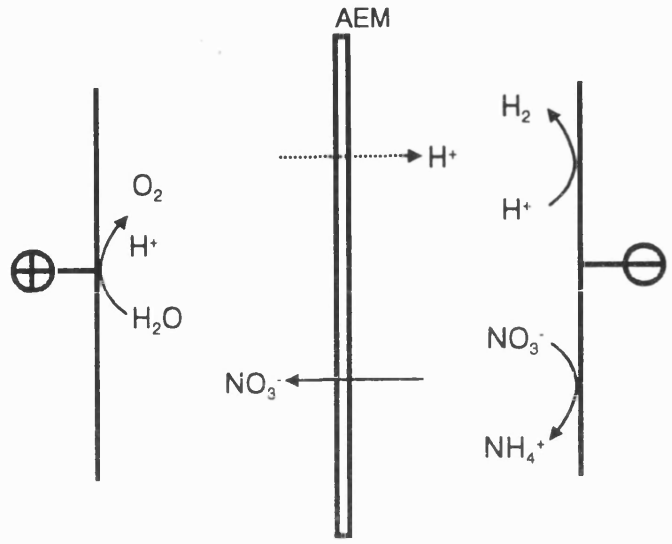

Figure 6.6: Illustration of system described by model (water transport not shown)

6.2.1 Electrode reactions

A single anode reaction was modelled according to Equation 6.11 but the cathode reactions were two competing reductions (of water and of nitrate), Equations 6.12 and 6.13 respectively.

Anode

$$^1/_2H_2O \rightarrow e^- + {}^1/_4O_2 + H^+ \qquad [6.11]$$

Cathode

$$H^+ + e^- \rightarrow {}^1/_2H_2 \qquad [6.12]$$

$$^1/_8NO_3^- + {}^{10}/_8H^+ + e^- \rightarrow {}^1/_8NH_4^+ + {}^3/_8H_2O \qquad [6.13]$$

6.2.2 Membrane transport

Three fluxes were considered to occur across the membrane: nitrate, protons and electro-osmotic water flux. The ionic fluxes were modelled using the differential current efficiency term and the water flux via co-ordination numbers that were estimated for each ionic species. These expressions are given in Equations 6.14 to 6.16.

$$J_{NO3-} = \eta_{DCE}\frac{j}{\Im} \qquad [6.14]$$

$$J_{H+} = -(1-\eta_{DCE})\frac{j}{\Im} \qquad [6.15]$$

$$J_{H2O} = \left[\eta_{DCE}(W_{A-}) - (1-\eta_{DCE})W_{H+}\right]\frac{j}{\Im} \qquad [6.16]$$

6.2.3 Electrolyte mass balance equations

Combination of the electrochemical and membrane transport equations produced a system of mass balance equations describing the variation of species in each electrolyte which are given by:

Anolyte

$$\frac{dN_{H2O}}{dt} = \left[-0.5 + W_{a-}\eta_{DCE} - W_{H+}(1-\eta_{DCE})\right]\frac{i}{\Im} \qquad [6.17]$$

$$\frac{dN_{O2}}{dt} = 0.25\frac{i}{\Im} \qquad [6.18]$$

$$\frac{dN_{H+}}{dt} = \eta_{DCE}\frac{i}{\Im} \qquad [6.19]$$

$$\frac{dN_{NO3-}}{dt} = \eta_{DCE}\frac{i}{\Im} \qquad [6.20]$$

Catholyte

$$\frac{dN_{H2O}}{dt} = \left[\frac{3\eta_r}{8} - W_{A-}\eta_{DCE} + W_{H+}(1-\eta_{DCE})\right]\frac{i}{\Im} \qquad [6.21]$$

$$\frac{dN_{NO3-}}{dt} = \left[-\frac{\eta_r}{8} - \eta_{DCE}\right]\frac{i}{\Im} \qquad [6.22]$$

$$\frac{dN_{H+}}{dt} = \left[-\frac{\eta_r}{4} - \eta_{DCE}\right]\frac{i}{\Im} \qquad [6.23]$$

$$\frac{dN_{H2}}{dt} = 0.5(1-\eta_r)\frac{i}{\Im} \qquad [6.24]$$

$$\frac{dN_{NH4+}}{dt} = \frac{\eta_r}{8}\frac{i}{\Im} \qquad [6.25]$$

6.3 Solution of model

A forward Euler technique was adopted to solve the differential equations used to describe the ion transfer paths illustrated in Figure 6.6 based on the set of equations presented above. Further work might employ a more efficient numerical solution method, such as Runge-Kutta, especially if incorporating fundamental electrochemical kinetic expressions. The solution algorithm for the

model is given in Figure 6.7 and a description of the Fortran code used for numerical solution is given in Appendix 6.

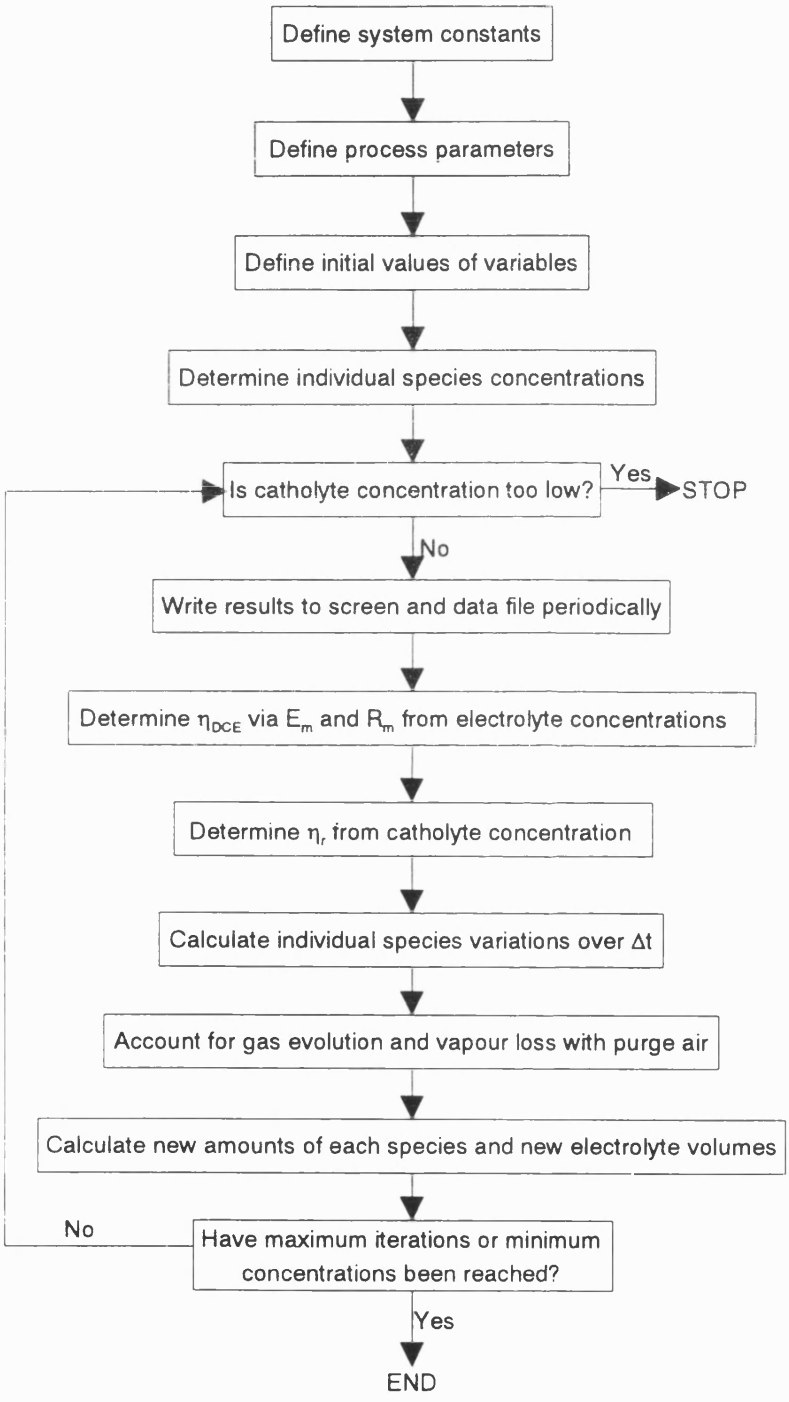

Figure 6.7: Solution algorithm used in numerical solution of the model

The model was tested to ensure continuity of the mass balances and that sensible predictions of current efficiency and nitrate reduction were generated. For instance, it was found for high initial catholyte concentrations (>2M), the H^+ could become depleted due to extensive nitrate reduction. In practice this would give rise to an increase in pH due to water splitting (or an alternative nitrate reduction mechanism) maintaining the current flow and, ultimately, this would lead to the evolution of ammonia gas as its vapour pressure becomes significant above pH=8. To include this phenomenon in the model, solvent decomposition would have to be added along with the effect of catholyte pH on various process parameters. This was not undertaken as such conditions were not reached in the comparative runs described below.

6.4 Comparison with experimental data

The runs AW1.5 and AW002 were chosen for comparison with the model because detailed species analysis (i.e. including NO_2^- and NH_4^+) had been undertaken during both of these experiments involving the AW membrane. Modelling results for both of these cases were similar and so only the data for the AW1.5 run are presented here. The AW002 data are given in Appendix 6.

The predicted ammonium concentrations are compared with the experimental data in Figure 6.8. A series of curves is seen which represent the effect of the factor X_s on the rates of competing reactions (Equations 6.3 and 6.4). A values of $X_s=1.0$ gives closest agreement with the experimental data which suggests that a switch between nitrate reduction and hydrogen evolution is most appropriate. A value of $X_s=1.0$ was therefore used to generate subsequent modelling results.

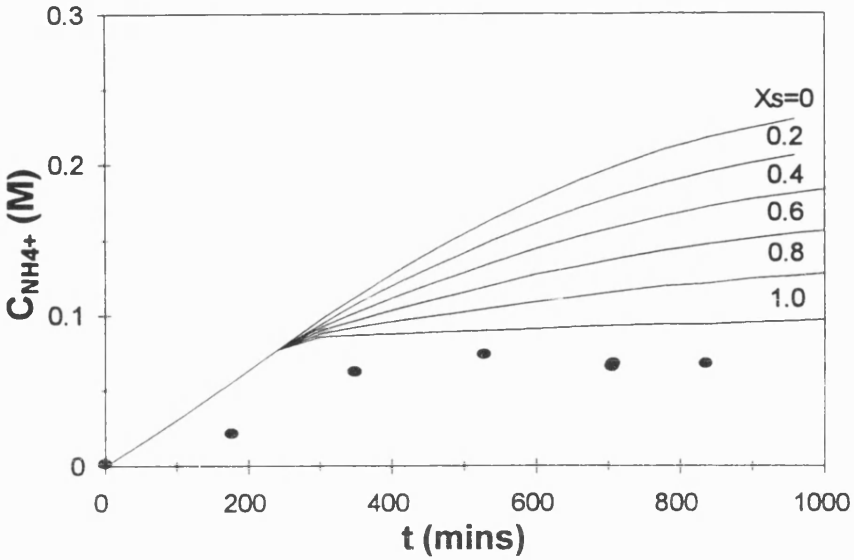

Figure 6.8: Comparison of measured and predicted ammonium concentration profiles (● C_{NH4+}, — model prediction)

It is interesting to note that the over-prediction of ammonium concentration at the end of the experiment might be attributed to the initial disagreement between the model and the experimental data. The predicted initial rate of ammonium evolution is greater than seen in the experimental data. If, however, a time lag were to be incorporated into the model before which no ammonium was produced, then the agreement would be closer. (For example, in Figure 6.8 the model curve would be displaced by +100 mins, -0.25M for an initial time lag of 100 mins.) The physical significance of a time lag is not clear as it suggests that prior to ammonium generation other reactions proceed to consume the current. The possibility of hydrogen evolution occurring is eliminated by the absence of gas bubbles in the experimental rig over this period. Consequently a nitrate reduction intermediate such as nitrite might be generated in this period. The absence of nitrite in all samples however tends to dismiss this concept and so additional experimental work is required in order to resolve the issue. This

would probably involve analysing many samples over the initial period of an experiment to study the species variations.

Having evaluated the nitrate reduction terms in the model it could be used to predict the membrane performance throughout an experiment. The measured and predicted current efficiencies are shown below.

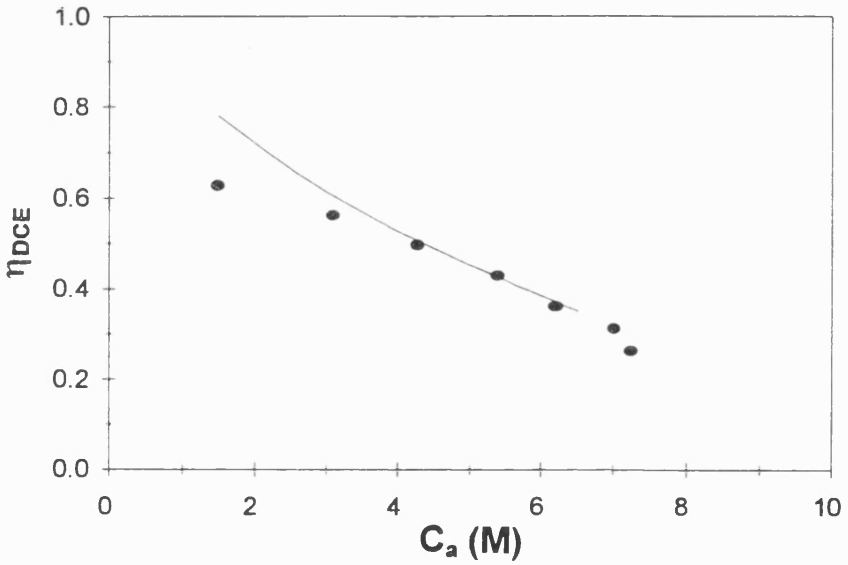

Figure 6.9: Comparison of measured and predicted current efficiency data (● η_{DCE}, —model prediction)

Current efficiency predictions were good but deviations were seen at the beginning of a run. This is because the initial estimates of membrane voltage drop are outside the region of validity for Equation 6.9 which leads to an over-prediction of current efficiency by the model until the membrane voltage drop enters the region of applicability (by the second experimental data point). The high current efficiency in the initial period over-predicts the amount of nitric acid transported across the membrane which gives rise to a high amount of water transport due to nitrate ion solvation. The net result of these over-estimates is a

reduction in the observed anolyte acid concentration which can be seen in Figure 6.10.

At the end of an experimental run the measured current efficiency included process limitations such as nitrate transport to the surface of the membrane. This could give rise to a higher prediction of current efficiency by the model which did not account for mass transfer limitations in this region. The deviation at the end of a run was more apparent in the AW002 data in Appendix 6.

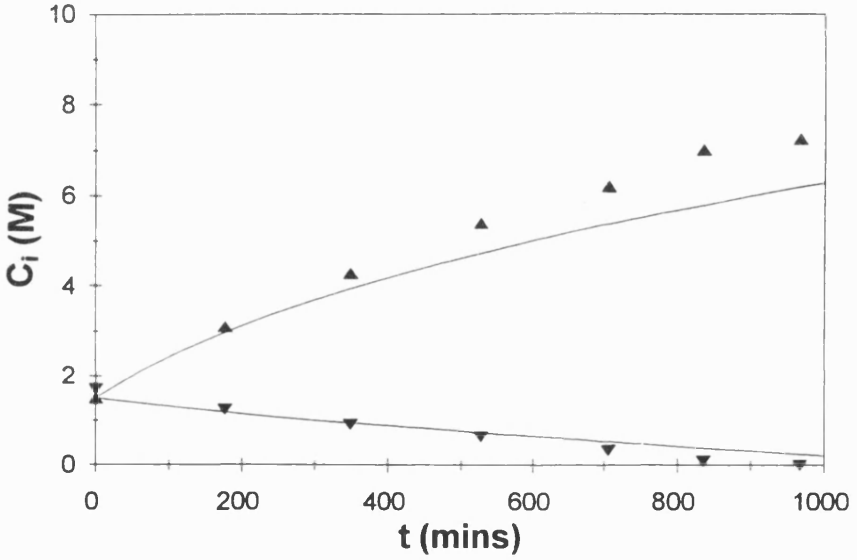

Figure 6.10: Comparison of measured and predicted acid concentration profiles ($\blacktriangle C_a$, $\blacktriangledown C_c$, — model prediction)

6.5 Example application of model

An engineering model can be used to evaluate the performance of a process which cannot be easily studied in practice or to employ it as a tool for process design. Detailed process optimisation is outside the scope of this thesis but the applicability of the model was exemplified by using it to study a base case nitric acid recovery via EED process described below.

$V_c(0)=1m^3$ $V_a(0)=0.1m^3$

$C_c(0)=1M$ $C_a(0)=1M$

$A_m=1m^2$

The above values are in similar ratios to those in the experimental rig. The membrane area was taken to be $1m^2$ based on a two-cell industrial electrolyser (e.g. ICI FM21 $A_m=0.42\ m^2$) and the flow and mass transfer characteristics were assumed to be identical to the laboratory FM01. Vapour losses via the vent were eliminated as these must be controlled in an industrial process. A combined chart of the data generated by the model for the above case is shown below.

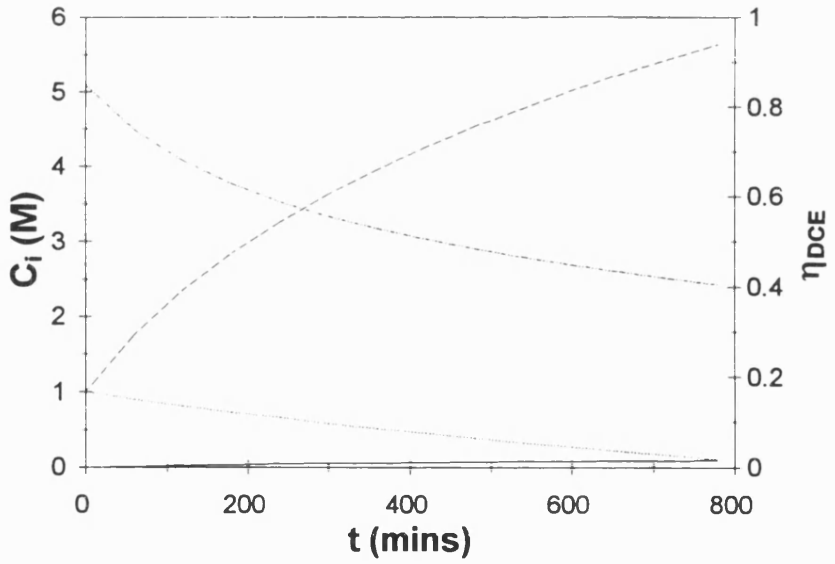

Figure 6.11: Species and η_{DCE} profiles predicted by the model for a base case industrial process
(- - C_a, ·· C_c, — C_{NH4+}, ···· η_{DCE})

The limitations of the model described in Section 6.4 still apply to the data in Figure 6.11. The observed performance trends were similar to those found during the experimental programme. Application of this model would allow

optimisation of membrane area and electrolyte volumes to be undertaken along with other considerations such as stage-wise processing. Detailed knowledge of the industrial electro-membrane stack configuration would allow overall voltage drop estimation and hence power requirements to be determined.

6.6 Conclusions of modelling

The basic model gave a good agreement with the experimental data although some deviations were seen. Given the assumptions made to develop the model, the deviations were not unexpected and could be explained as follows.

Nitrate reduction was over-estimated despite a complete switch from nitrate reduction to hydrogen evolution being shown to be most appropriate. It appeared that inclusion of a time lag term might yield an empirical improvement to this part of the model for use in process design. It would, however, be more useful to obtain detailed electrochemical kinetic data to allow inclusion of a fundamental model to represent this phenomenon. The inclusion of the effect of pH on the system (especially nitrate reduction) might yield a further improvement to the model.

Membrane performance was more successfully represented by the model and current efficiency predictions agreed closely with the experimental data over the range of validity. The form of the curves was similar to acid transport data reported by other workers, for example (Tugas et al, 1993), who undertook idealised fundamental membrane studies, in the absence of mass transfer limitations. Consequently their experimental conditions were closer to those of the model. Use of the re-arranged form of the Nernst-Plank equation to give the membrane resistance to proton transport was a very useful method of applying

the fundamental ion transport equation to a range of experimental data. This membrane performance model could be further improved as membrane understanding reaches a level where acid sorption and hence membrane transport properties can be accurately predicted for a given membrane and electrolyte system. New membrane modelling techniques, such as the parallel resistor-capacitor analogy discussed in Section 2.7.3, might prove useful for application in this area.

Although the model described in this chapter is elementary in nature, the data produced gave reasonable agreement with experimental results. The importance of generating a detailed complete process model not only for improved membrane understanding but as an engineering tool for electro-membrane process design was emphasised by the example application of the model in Section 6.5. The concept of combining electrochemical and membrane relationships in a detailed fundamental process model should be continued by further work in this area.

The industrial application of electro-electrodialysis as a nitric acid recovery technology is discussed in the next chapter.

Chapter 7:

Process evaluation

7. Process evaluation

The industrial application of electro-membrane processes for nitric acid recovery is discussed in this chapter. The first sections cover the main sources of waste nitric acid and conventional treatment technologies, whilst the remainder of the chapter focuses on possible cell and process configurations. Evaluation of each system is subjective and based on overall performance, fate of contaminants (metals and organics) and other process/ cost considerations. The optimum solution varies according to individual waste streams and treatment specifications and hence no single process appears superior for all applications.

7.1 Sources of waste nitric acid

There are many sources of waste acids but only the main sources of waste nitric acid are discussed in this section. The applicability of the processes to acids other than nitric would have to be considered on case-by-case basis as a result of further research.

The four main sources of nitric acid waste are listed below. By far the largest of these is the organic nitration industry which accounts for items 1 and 3 below.

1. Large-scale nitration processes.
2. Effluents from NO_x vapour scrubbing.
3. Small-scale/ speciality nitration processes.
4. Metal processing industry.

Conventional nitration processes employ either concentrated nitric acid or a mixed acid (nitric/ sulphuric) nitrating medium. Both of these systems give rise to an aqueous spent-acid waste stream containing a few percent nitric acid with possibly 70-80wt% sulphuric (Hammond, 1996). Effluent streams from NO_x removal systems or from speciality nitrations, such as those employing N_2O_5, could also contain similar concentrations of nitric acid (<5wt%).

It is difficult to quantify a 'typical' nitric acid waste as there is much variation in acid concentration and contaminants between different processes. The focus of this research was on waste resulting from speciality N_2O_5 nitration processes which would contain <5wt% nitric acid with trace large molecule organic nitrates as contaminants. Little/ no inorganic contaminants would be present.

A range of conventional technologies exist to recover waste nitric acid on the large-scales found in the nitration industry. These are highlighted below prior to discussing the applicability of electro-membrane processes in this area.

7.2 Conventional technology

Low concentration nitric acid streams are neutralised followed by dilute discharge to a suitable post-treatment process. Neutralisation processes generate sludge which must be disposed of carefully. This technology is strictly end-of-pipe and no attempt is made to recover the acid. Increasing environmental awareness, stronger legislation and higher costs has lead to such techniques becoming less favourable. Consequently, there is an increasing driving force towards acid recovery. The economic and social aspects of acid wastewater treatment technologies have been studied in detail (Richter, 1994).

The conventional nitric acid recovery processes operated in industry are based on distillation. A typical supplier of distillation equipment for these applications is Chemetics International Company Ltd, Vancouver (Ondrey & Shanley, 1993). Nitric acid forms a maximum boiling point azeotrope with water at 68wt% acid which makes direct recovery to 100% impossible. An extractive distillation process must be employed to break the azeotrope.

The two possible alternatives for extractive distillation of nitric acid use either magnesium nitrate or sulphuric acid to break the azeotrope. Often the magnesium nitrate is the most economical option, although there are often good arguments for employing sulphuric acid (Hammond, 1996). Intractable organics can decomposed at the higher temperatures used in the sulphuric acid process to increase product purity or reduce the build-up of waste organics. Additionally, if the waste emanates from a mixed acid nitration, the presence of sulphuric acid in the spent acid stream allows the sulphuric acid route to be followed as no additional chemicals have to be added. The choice between magnesium nitrate or sulphuric acid to break the nitric-water azeotrope depends, therefore, primarily on the amount of sulphuric acid present in the waste.

The role of electro-membrane processes in the field of nitric acid recovery is discussed in the remainder of this chapter.

7.3 General process considerations

The key factors relevant to industrial electro-membrane processes are highlighted here before discussing specific configurations in the subsequent sections.

7.3.1 Electro-membrane stack design

The electrochemical stack configuration used in the experimental rig was not satisfactory for an industrial process. For instance, the membrane-electrode distance was large resulting in excessive voltage drop across the bulk solution especially at low acid concentrations. This would have to be overcome in an industrial stack, for example, by using either 'lantern blade' or 'dished' electrodes to minimise the gap whilst enhancing mass transfer. Consequently, a detailed evaluation of commercial stacks would have to be undertaken when designing an electro-membrane process for acid recovery.

7.3.2 Electrodes and electrode reactions

Closely linked with stack design is the cell configuration which is discussed in detail later in this chapter. In electrodialysis (ED) electrodes operate in controlled electrode rinse streams whereas in electro-electrodialysis (EED) the electrodes must be capable of withstanding the process streams without any deterioration in performance. This is not always straightforward in practice because of many factors, for example, contaminants in the electrolyte can effect the performance and/or lifetime of electrocatalysts. Moreover the requirement for electrodes and electrocatalysts to withstand harsh process conditions can make them expensive.

7.3.3 Membrane fouling

In addition to electrode performance deterioration, membrane fouling can be a serious problem in a commercial electro-membrane process. Fouling can be either organic or inorganic (scaling). Organic fouling can be either as a result of large molecules obstructing the surface of the membrane or due to small molecules penetrating the membrane structure. Current reversal is undertaken

periodically in industrial electrodialysis stacks to minimise the effects of fouling. However, some fouling (such as small molecule organic penetration or metal hydroxide precipitation) can be practically irreversible. Consequently, the membrane lifetime under process conditions can be a critical factor when evaluating a process.

7.3.4 Contaminants

The effect of contaminants was not studied during the experimental programme which focused on a model nitric acid-water system. Contaminants can have a significant effect on an industrial process. Not only do they effect the purity of recovered acid, but they can be detrimental to other factors such as membrane fouling or electrocatalyst poisoning/ removal. The role of contaminants will vary according to individual species properties but the following characteristics were assumed in order to evaluate the electro-membrane processes. They were based on experience gained by other workers in the field.

Effect of contaminants

1. Metal ions are only transferred by CEMs
2. Large organics do not pass across ion exchange membranes
3. Small ionised organics can be transported by membranes
4. Inorganic fouling can occur on membranes
5. Polar or ionised organics can cause membrane fouling
6. Contaminants can effect electrode performance

7.3.5 Post-treatment

Acidic effluent from the experimental rig was neutralised prior to dilute discharge to drain. In an industrial process the choice of post-treatment

technique would vary according to the composition of the waste and final effluent specification. For example, it might be more desirable to discharge a near-neutral nitrate stream rather than a weak nitric acid effluent to a biological treatment process. The degree of further processing must therefore be considered when evaluating a particular process.

With these process considerations in mind the possible configurations of electro-membrane cells can be discussed.

7.4 Cell configurations

Alternative cell configurations have initially been restricted to the electro-electrodialysis process although this logically extends to electrodialysis during the discussion. Bipolar membranes or multi-stage electrochemical processes have not been considered. The configurations discussed start from the base-case EED configuration that was used throughout the experimental programme and increase in complexity as system constraints are included. The impact of metal ions and large molecular weight organic nitrates is considered according to the assumptions made in Section 7.3.4.

7.4.1 Two-compartment EED

Figure 7.1 shows the base-case EED configuration which involves a single anion exchange membrane (AEM) and intimate contact of the feed and product streams with their respective electrodes. Acid anions are recovered across the membrane with proton leakage decreasing the efficiency of membrane transport. Nitrate is reduced at the cathode giving rise to ammonium. This limits the amount of nitric acid that can be recovered and results in post-treatment being

required to process the ammonium nitrate effluent. The net electro-osmotic water flux is minimised by the oxidation of water on the anode giving rise to potentially higher acid product concentrations. All contaminants would remain in the feed and there is the possibility of recovering metals on the cathode.

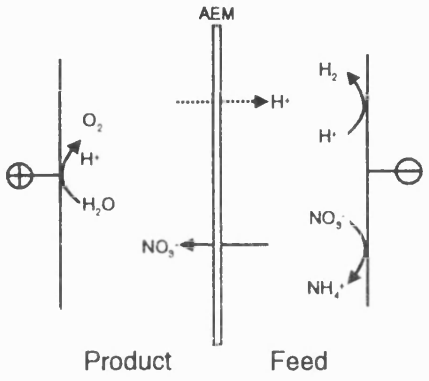

Figure 7.1: Two-compartment EED cell

7.4.2 Three-compartment EED

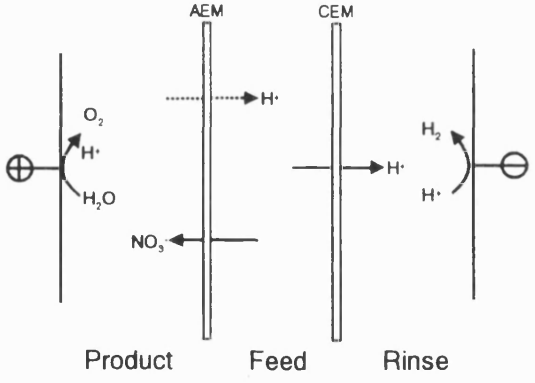

Figure 7.2: Three-compartment EED

Cathodic reactions such as the reduction of nitrate can be eliminated by the incorporation of an additional cation exchange membrane (CEM) and an electrode rinse stream. The CEM effectively prevents the feed from contacting

the cathode and thus stops any side reactions from occurring. Current is maintained by proton transport across the CEM into the rinse stream. The catholyte rinse maintains the flow of charge and sweeps away electrode gases. Thus many 'inert' electrolytes could be used for this purpose, for example sodium sulphate or sodium hydroxide. Organic contaminants would remain in the feed but metal ions would pass into the rinse stream from where they could be recovered. The acid anion transport and anolyte section of the cell operates identically to those in the two-compartment EED cell above where the product stream contacts the anode.

7.4.3 Four-compartment EED

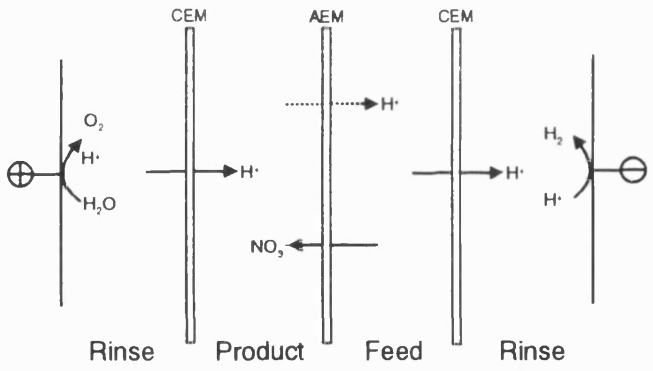

Figure 7.3: Four-compartment EED

Addition of another CEM and anolyte rinse stream could be employed to protect the anode. This configuration would be adopted if system contaminants such as fluoride were known to harm the electrocatalyst. If these contaminants were to pass across the AEM into the product stream they would not contact and damage the electrode. The net electro-osmotic water flux would not be minimised by anodic water oxidation in this configuration (and a water flux from the rinse stream to the product streams could occur) causing the maximum

product concentration to be lower than for the two- and three-compartment cells. Organic contaminants would be retained in the feed and metal ions could be recovered in the catholyte rinse stream. Neither the product nor the feed stream contacts the electrodes in this configuration which means that the electrodes do not have to withstand harsh process conditions. Current reversal could be employed in this configuration to minimise fouling. If a stack of repeated alternate membranes were to be built-up based on the CEM-AEM pair then an electrodialysis (ED) configuration would be obtained.

7.4.4 ED configuration

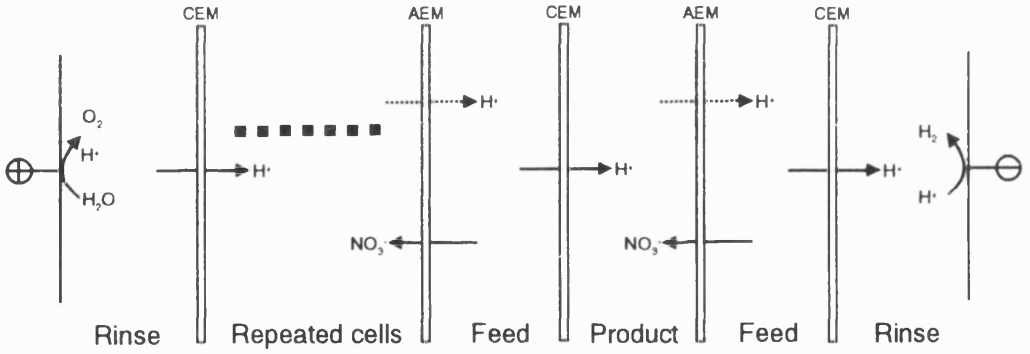

Figure 7.4: ED configuration

In electrodialysis many ions are transported per electrode reaction because of the 'domino' effect resulting from repeated unit cells. Despite this electrical advantage there are some disadvantages with the ED configuration. Firstly any contaminants that can cross an ion exchange membrane (AEM or CEM) will end up in the product stream. This can be advantageous if it is desirable to recycle contaminants to a process but not if a clean product is required. Additionally, transport of ions to the product stream through both membranes gives rise to a high electro-osmotic water flux (as in the 4-compartment EED

scheme) which reduces the maximum product concentration that can be attained.

7.5 Possible process configurations

The current efficiency of membrane transport was found to be relatively low compared to industrial electro-membrane processes such as chlor-alkali production. This results in a power cost that is substantially higher than would be obtained with a 100% efficient membrane. Taking typical efficiency values, along with proprietary capital cost data for industrial stacks, the recovered acid cost was estimated to be between £500 and £1000 per tonne of acid based on the experimental stack configuration (Hammond, 1995). Despite these high costs there are many environmental advantages associated with electro-membrane processes such as the ability to rapidly control processing to cope with feed variations and the fact that operation at ambient temperature minimises acid decomposition. Electro-membrane processes are therefore compared with distillation below.

In order to compare electro-membrane processes with distillation, a simple economic comparison of electrical costs to recover nitric acid against steam costs to remove the water was undertaken to estimate where the two processes might intercept (Hammond, 1995). This revealed that utility costs for EED would be less than those for distillation for nitric acid concentrations less than about 5wt%. This does not necessarily mean that either process is commercially viable at this concentration. In order to discuss possible hybrid configurations in this section, 5wt% nitric acid was taken to be the concentration beyond which distillation becomes economic.

Although the target of 30wt% nitric acid was set for this project in order to demonstrate technical feasibility, for re-use the acid product should preferably be over 50wt% and ideally above the azeotrope towards 100 wt%. Four schematic process flowsheets have been studied to illustrate the use of EED to recover nitric acid from aqueous streams containing metal ions and large organic nitrate molecules. These are listed below.

1. Weak nitric acid feed (<5wt%) to concentrated (azeotrope 68wt%) nitric acid product.
2. Weak nitric acid feed (<5wt%) to concentrated (azeotrope 68wt%) nitric acid product with no nitrate reduction.
3. Intermediate nitric acid feed (>5wt%) to concentrated (azeotrope 68wt%) nitric acid product.
4. Intermediate nitric acid feed (>5wt%) to 100% nitric acid product with electro-membrane breaking of azeotrope.

Cases 1, 2 & 3 generate a concentrated azeotrope product whereas case 4 represents an alternative technique for generating 100% nitric acid product. Recycles within the recovery processes are not shown in the flowsheets.

7.5.1 Case 1 - weak acid feed to concentrated product

The 2-compartment EED stack in Figure 7.5 recovers the nitric acid to 5wt% where it is passed to the distillation column to generate the concentrated acid product. Some nitrate would be reduced to ammonium which would limit the maximum amount of nitric acid that could be recovered. Metals and organics are retained in the feed stream which would be discharged along with ammonium at potentially near-neutral pH. Thus the 68 wt% acid product

would be relatively pure but a complex post-treatment process would be required to remove the other contaminants from the waste.

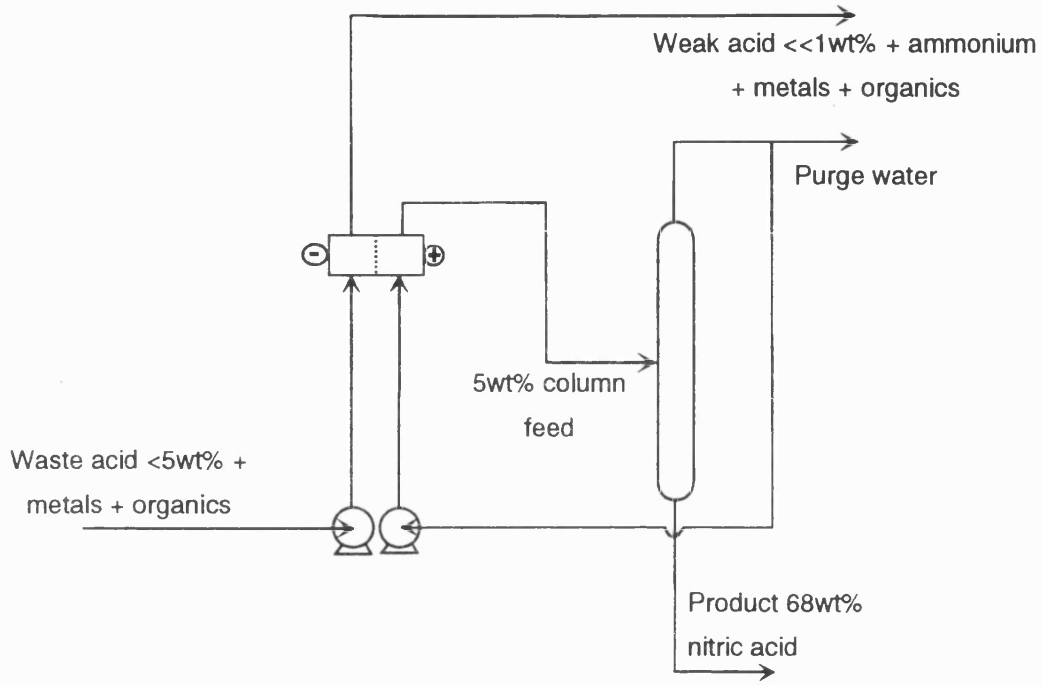

Figure 7.5: Flowsheet showing recovery of nitric acid via 2-compartment EED and distillation

7.5.2 Case 2 - weak acid feed to concentrated product

The flowsheet in Figure 7.6 is similar to that in Figure 7.5 except that a 3-compartment EED stack has been used, thus eliminating nitric acid loss to ammonium. It also allows metals to be simultaneously recovered in the catholyte e.g. by electrodeposition using proprietary cells such as: Chemelec, Envirocell or Porocell. This enhanced contaminant separation would simplify the post-treatment processes as two essentially binary effluents would be produced rather than a single complex mixture. The potential to recover metals might also enhance the economics of this process as metal removal is extremely important and expensive in effluent treatment applications because of the impact of heavy metals on the environment.

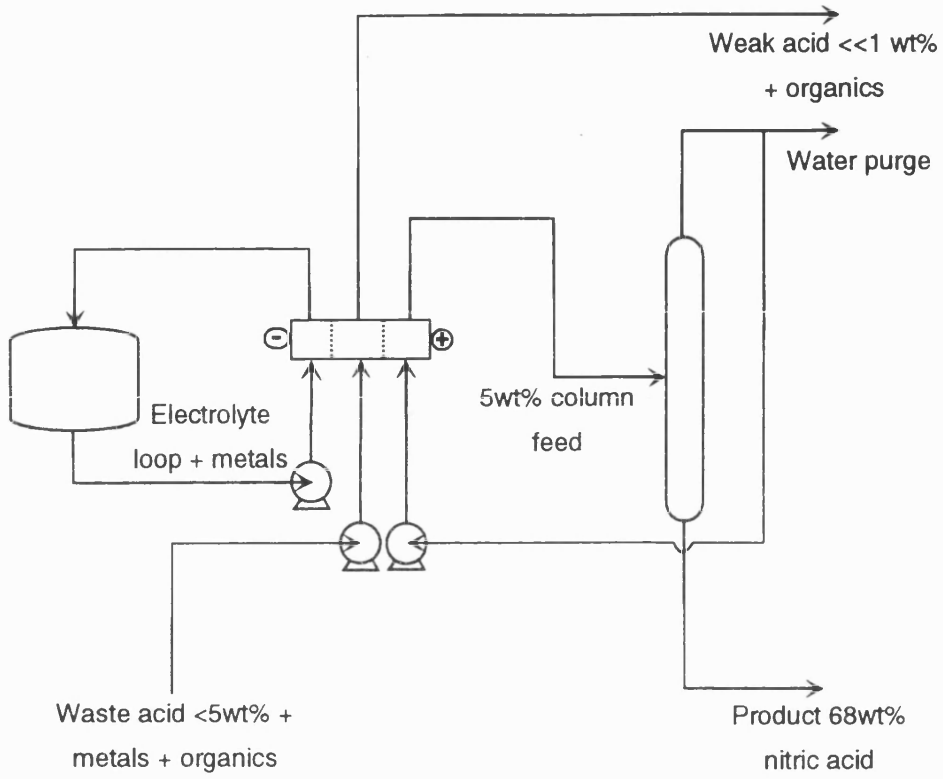

Figure 7.6: Flowsheet showing recovery of nitric acid via 3-compartment EED and distillation

7.5.3 Case 3 - intermediate acid feed to concentrated product

Figure 7.7 below illustrates how nitric acid might be recovered directly via distillation from an intermediate feed to concentrated nitric acid product. The most important observation is that contaminants are transferred to the product streams. Thus the concentrated nitric acid is likely to be less pure than that resulting from a hybrid electro-membrane-distillation process.

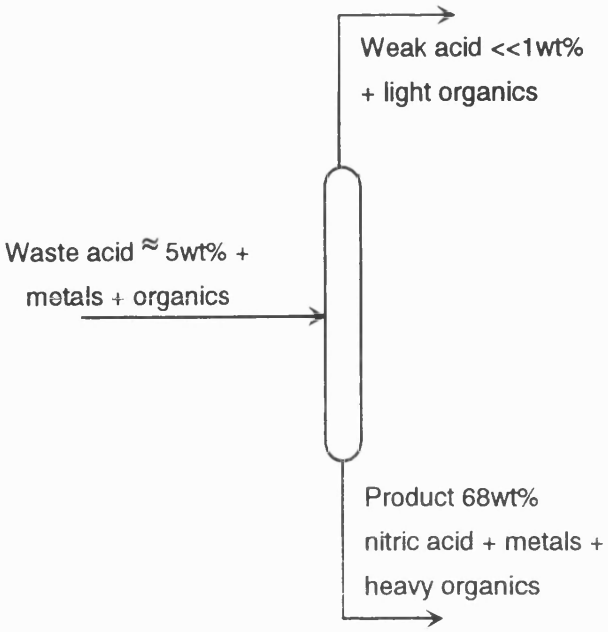

Figure 7.7: Flowsheet showing direct nitric acid recovery via distillation

7.5.4 Case 4 - intermediate acid feed to 100% product

As mentioned in Section 7.2 it is not possible to recover nitric acid directly to 100% because of the azeotrope at 68wt%. Conventionally, extractive distillation is used employing magnesium nitrate or sulphuric acid to break the azeotrope. A potential application of electro-membrane processes to high concentration nitric acid would be as a novel technique for breaking the azeotrope. As electro-membrane processes do not exploit vapour-liquid equilibria the azeotrope would be invisible allowing the mixture to be separated. This system would eliminate the requirement for additional chemicals and thus give the potential for higher purity products and a cleaner process. The electro-membrane process (EMP) could be ED, EED or even EED incorporating a cation rather than an anion exchange membrane (dehydration only). This concept is the focus of continuing new research.

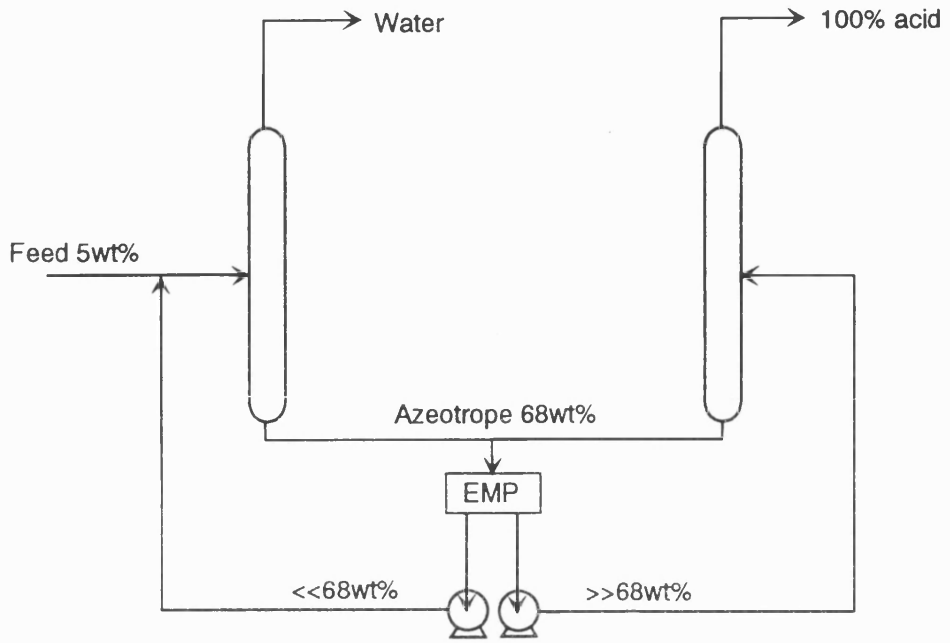

Figure 7.8: Flowsheet showing breaking of azeotrope by electromembrane process

7.6 Conclusions of process evaluation

It has been shown that the EED process studied during the experimental programme would not be commercially viable for recovering strong nitric acid. For example, it is unlikely that a low-efficiency process producing a significant amount of ammonium by-product would replace well optimised large-scale distillation units. However, where the scale of operation is small, or where there are other constraints, electro-membrane processes could be suitable for niche applications.

Notwithstanding the strong economic arguments, there are many environmental advantages associated with electro-membrane processes such as: the fate of (and option to recover) contaminants; the ability to rapidly control processing to cope with feed variations and the fact that operation at ambient temperature minimises acid decomposition.

The current stage of membrane performance appears to suggest that hybrid electro-membrane-distillation processes would be most suitable for recovering concentrated nitric acid from a weak acid feed. Various post-treatment techniques would need to be employed to attain a zero-discharge process. The economics of such a process might not be commercially favourable at present but they are likely to improve with increasingly severe environmental legislation and the drive for integrated pollution control.

Complete evaluation of process alternatives is difficult due to both the subjective nature of assessing environmental benefits and because of the lack of available commercial data for a detailed technical and economic comparison. An ongoing evaluation of both conventional and electro-membrane technologies should be undertaken to highlight best environmental options. These will change as membrane performance improves and environmental legislation strengthens. In all evaluations the total system, including post-treatment stages, should be studied to ensure adequate comparisons are made.

Chapter 8: Conclusions and recommendations

8. Conclusions and recommendations

Specific conclusions have been made throughout the course this thesis as part of the ongoing discussion. The main conclusions are summarised in this chapter along with the recommendations for further work. For clarity the conclusions and recommendations are summarised according to subject in the sub-sections below.

8.1 Nitrate reduction

Under the low pH conditions in the experimental cell an overall nitrate to ammonium reaction can be assumed with no nitrite intermediate being formed (Equation 4.14). When nitrate becomes mass transfer limited the common hydrogen evolution reaction prevails at the cathode and no nitrate reduction occurs. It is not clear why: i) a sharp rise in ammonium concentration was detected at the end of two of the five experimental runs where species profiles were measured or ii) there appears to be a time lag before ammonium production occurs in the experimental run. It is possible that i) corresponds to a sharp rise in pH at the end of an experimental run which enhances the rate of nitrate reduction. During the apparent time lag mentioned in ii), the cathode reactions could be forming intermediate nitrate reduction products such as nitrite or other cathode reactions such as dissolved oxygen reduction.

In order to further understand the nitrate reduction it would be necessary to undertake a fundamental electrochemical study of this phenomenon. A detailed study should allow the reaction mechanisms to be elucidated and may allow the anomalies describes as i) and ii) above to be further explained.

8.2 Membrane performance

Nitric acid was concentrated to 10 M (50 wt%) in the electro-electrodialysis process and this was dictated by experimental rather than membrane limitations.

The downstream (anolyte) acid concentration is a key parameter effecting the performance of anion exchange membranes. This can be demonstrated both empirically by comparing data from different experimental runs with the same membrane type and also by considering a modified form of the Nernst-Plank equation.

The performance of different anion exchange membranes follows the same trend in that current efficiency and water transport decrease with increasing acid concentration. The rate of decrease of these performance measures varies between different membrane types.

For a specific anion exchange membrane an interesting trade-off is observed in that both solvation of anions and membrane current efficiency decrease with increasing acid concentration. A balance must therefore be made between electrical cost and product concentration. This important phenomenon can be explained using a proposed heterogenous mechanistic model of the membrane which has been tested against observations reported in the literature.

Detailed analysis of a range of membrane performance data can be undertaken using a re-arranged form of the Nernst-Plank equation defining the membrane resistance to proton transport, R_m (Equation 5.8). This measure is useful both for improved membrane understanding and to allow semi-empirical

characterisation of the membrane performance for mathematical modelling. This model agrees well with the experimental data over its range of validity.

Future work should focus on the performance of anion exchange membranes and, in particular, should try to understand the variation of performance between different membranes. It would be interesting to use the new R_m parameter to characterise the performance of a range of anion exchange membranes and to determine whether any overall trends are observed. Additionally, improved experimental techniques might also allow unidirectional water fluxes to be determined to compliment improved understanding of ion transport.

The performance of electro-membrane processes over the range of nitric acid concentrations should also be evaluated. This would include both the very low concentration acid range (at near-neutral pH) and concentrated nitric acid (such as the azeotrope at 68wt%). Extension of the performance envelope to cover a wide range of acid concentrations could assist the development of viable electro-membrane technology.

8.3 Process evaluation

The cell configuration employed in the experimental programme is unlikely to be commercially viable at present because of the process inefficiencies and the high capital cost. Cell design should also be considered in future work as the key dimensions such as membrane-electrode distance were not optimised in any way in the experimental stack. A hybrid process containing, for example, both electro-membrane processes and distillation would be preferable for recovering nitric acid from low concentration effluents.

A detailed technical and economic comparison between electro-membrane processes and distillation should be made in order to identify the Best Environmental Options. This would require detailed cost data to be obtained from appropriate suppliers so that an accurate comparison could be made. The effect of acid concentration, contamination and flowrate of the effluent should also be studied as it is likely that the optimum process configuration will be dependent on these factors. The process evaluation should be ongoing and updated as the performance and costs of electro-membrane processes are improved or environmental legislation becomes tighter.

References

- Andres L J, Riera F A, Alvarez R, Coca J (1991) 'The application of the electrodialysis process to the selective separation of anions in a zinc electrolyte process' *Conference paper* University of Oviedo, Spain pp471-476
- Audinos R, Alvarez J R, Alvarez R (1989) 'Separation and concentration of sulphuric and nitric acids by electrodialysis' *Conference paper* Ecole nationale superieure de chemie, Toulouse, France pp369-375
- Audinos R, Nassr-Allah A, Alvarez J R, Andres J L, Alvarez R (1993) 'Electrodialysis in the separation of dilute aqueous solutions of sulfuric and nitric acids' *J. Memb. Sci.* 76 pp147-156
- Audran J, Baticle P, Letord M-M (1991) 'Recyclage d'acide chromique par électro-électrodialyse' *Industrie minérale - mines et carrières - les techniques* March pp139-141
- Baltazar V, Harris G B, White C W (1992) 'The selective recovery and concentration of sulphuric acid by electrodialysis' *Hydrometallurgy* 30 pp463-481
- Bard, Parsons, Jordan (1980) 'Standard potentials in aqueous solutions' USA: Mercel Dekker Inc. pp127-139
- Basset J, Denney R C, Geoffries G H, Mendham J (1978) 'Vogels textbook of quantitative inorganic analysis' Longmanns: London revised 4ed
- Bobrinskaya G A, Pavlova T V, Shatalov A Y (1985) 'Recovery of acids and sodium hydroxide from solutions of sodium sulfate and sodium chloride with the use of bipolar membranes' *J. Appl. Chem. of USSR* 58(4) pp711-714

- Boeteng D A D (1990) 'Membrane process for acid recovery' *US Patent* 603,053 October 25
- Boudet-Dumy M, Lindheimer A, Gavach C (1991) 'Transport properties of anion exchange membranes in contact with hydrochloric acid solutions. Membranes for acid recovery by electrodialysis' *J. Memb. Sci.* 57 pp57-68
- Boyoval P, Seta J, Gavach C (1993) 'Concentrated propanoic acid production by electrodialysis' *Enzyme Microb. Tech.* 15 pp683-686
- Brown C J, Pletcher D, Walsh F C, Hammond J K, Robinson D (1992) 'Local mass transport effects in the FM01 laboratory electrolyser' *J. Appl. Electrochem.* 22 pp613-619
- Brown C J, Pletcher D, Walsh F C, Hammond J K, Robinson D (1993) 'Studies of space-averaged mass transport in the FM01-LC laboratory electrolyser' *J. Appl. Electrochem.* 23 pp38-43
- Brown C J, Pletcher D, Walsh F C, Hammond J K, Robinson D (1994) 'Studies of three-dimensional electrodes in the FM01-LC laboratory electrolyser' *J. Appl. Electrochem.* 24 pp95-106
- Brunea J (1994) *Personal communication* (Solvay SA)
- Buche S (1996) *Personal communication* (University of Bath)
- Buck R P (1984) 'Kinetics of bulk and interfacial ionic motion: microscopic bases and limits for the Nernst-Planck equation applied to membrane systems' *J. Memb. Sci.* 17 pp1-62
- Chapatot A, Pourcelly G, Gavach C, Lebon F (1995) 'Electrotransport of proton and divanet cations through modified cation-exchange membranes' *J. Electroanal. Chem.* 386 pp25-37
- Chapotot A, Pourcelly G, Gavach C (1994) 'Transport competition between monovalent and divalent cations through cation-exchange

membranes. Exchange isotherms and kinetic concepts' *J. Memb. Sci.* 96 pp167-181

- Cherif A T, Gavach C (1988) 'Sulfuric acid concentration with an electro-electrodialysis process' *Hydrometallurgy* 21 pp191-201
- Cherif A T, Gavach C (1989) 'Electro-transport of sulphuric acid by electro-electrodialysis' *J. Electroanal. Chem.* 265 pp143-157
- Chiao Y C, Chlanda F P, Mani K N (1991) 'Bipolar membranes for purification of acids and bases' *J. Memb. Sci.* 61 pp239-252
- Clift R, Grace J R, Weber M E (1978) 'Bubbles drops and particles' London: Academic press
- Cohen T, Dagard P, Molenat J, Brun B, Gavach C (1986) 'Proton leakage through perfluorinated anion exchange membranes' *J. Electroanal. Chem.* 210 pp329-336
- Cohen T (1991) 'Recuperation des acides et des metaux par de nouvelles membranes echangeuses d'ions' *Journées d'études SEE* Gif-sur Yvette, France pp196-199
- Coleman D H, White R E, Hobbs D T (1995) 'A Parallel-plate reactor model for the destruction of nitrate and nitrite in alkaline waste solutions' *J.Electrochem. Soc.* 142 (4) pp1153-1161
- Coulson J M, Richardson (1986) 'Chemical Engineering' vol 6 Oxford: Pergamon Press
- Coulson J M, Richardson (1988) 'Chemical Engineering' vol 1 Oxford: Pergamon Press
- Cowan D A, Brown J H (1959) 'Electrodialysis cells' *Ind. & Eng. Chem.* 51(12) pp1445-1448
- Cox J L, Hallen R T, Lilga M A (1994) 'Thermochemical nitrate destruction' *Environ. Sci. Technol.* 28 pp423-428

- Cumming A (1995) *Personal communication* (DRA)
- Dukhin S S, Mishchuk N A (1993) 'Intensification of electrodialysis based on electroosmosis of the second kind' *J. Memb. Sci.* 79 pp199-210
- Elder G R, Waite M J (1995) 'Recent developments in electrochemical ion exchange for treatment of nitrate' *Electrochemical processing a clean alternative* Toulouse, France, April 1995
- Elmidaoui A, Belcadi S, Houdus Y, Cohen T, Gavach C (1992a) 'Perfluorinated anion exchange membranes: preparation and preliminary tests of dialysis' *J. Polymer Sci.* 30 pp1407-1412
- Elmidaoui A, Cherif A T, Brunea J, Duclert F, Cohen T, Gavach C (1992b) 'Preparation of perfluorinated ion exchange membranes and their application in acid recovery' *J. Memb. Sci.* 67 pp263-271
- Gavach C, Bribes J L, Chapotot A, Maillois J, Pourcelly G, Sandeaux J, Sandeaux R, Tugas I (1994) 'Improvements of the selectivity of ionic transport through electrodialysis membranes in relation with the performances of separation electromembrane processes' *Journal de Physique* 4 (Jan 1994) ppC1-233-C1-243
- Gavish B, Lifson S (1978) 'Membrane polarisation at high current densities' Dept of Chemical Physics, Weizmann Institute of Science, Rehovot, Israel
- Goldstein I S, Bayat-Makooi F, Sabharwal H S, Singh T M (1989) 'Acid recovery by electrodialysis and its economic implications for concentrated acid hydrolysis of wood' *Applied Biochemistry and Biotechnology* 20/21 pp95-106
- Graillon S (1995) *Personal communication* (CNRS Montpellier)
- Greben V P, Pivovarov N Y, Latskov V L (1988) 'Production of concentrated caustic soda and hydrochloride acid solutions from sodium chloride by electrodialysis with the aid of bipolar ion exchange membranes' *J. Appl. Chem of USSR* 61 (5) pp903-908

- Greben V P, Pivovarov N Y, Rodzik I G, Kovarskii N Y (1993a) 'Preparation of caustic soda and hydrochloric acid by electrodialysis using bipolar ion-exchange membranes at almost neutral pH of the sodium chloride solution' *Desalination* 90 (1-3) pp303-323
- Greben V P, Pivovarov N Y, Rodzik I G, Kovarskii N Y (1993b) 'Regeneration of sulfuric acid from sulfuric acid electrolyte for anodizing aluminium by electrodialysis using a combination ion-exchange membrane' *Russian J. Appl. Chem.* 66(2) pp229-232
- Gilroy D (1993) 'A process for the electrolytic destruction of nitrate in aqueous liquids' *UK patent application* GB 2 267 290 A
- Hammond J K (1995) *Personal communication* (Electrochemical Engineer)
- Hammond J K (1996) *Personal communication* (Electrochemical Engineer)
- Helfferich F (1962) 'Ion exchange' New York: McGraw-Hill (UMI reprint 1988)
- Hernandez D, Dotson R (1988) 'Electrochemical reduction of nitric acid to hydroxylamine nitrate' *UK Patent Application* GB 2 211 858 A
- Hobbs D T (1994) 'Electrochemical treatment of liquid nuclear wastes' *8th internationsl forum on electrolysis* Florida, USA, Nov 1994
- Hwang J-Y, Lai J-Y (1987) 'The effect of temperature on limiting current density and mass transfer in electrodialysis' *J. Chem. Tech. Biotechnol.* 37 pp123-132
- ICI (1993) 'FM01 data manual' ICI Chemicals & Polymers Ltd, Runcorn, UK
- Indusekhar V K, Trivedi G S, Shah B G (1991) 'Removal of nitrate by electrodialysis' *Desalination* 84 pp213-221

- Jiang, P-Y, Katsumura Y, Ishigure K, Yoshida Y (1992) 'Reduction potential of the nitrate radical in aqueous solution' *Inorg. Chem.* 31 (24) pp5135-5136
- Jörissen J, Simmrock K H (1991) 'The behaviour of ion exchange membranes in electrolysis and electrodialysis of sodium sulphate' *J. Appl. Electrochemistry* 21 pp869-876
- Judd S J, Solt G S, Wen T (1993) 'Polarization and back e.m.f. in electrodialysis' *J. Applied Electrochemistry* 23 pp1117-1124
- Kang Y S, Hong J-M, Jang J, Kim U Y (1996) 'Analysis of transport in solid membranes with fixed site carriers 1.&2.' *J.Memb. Sci.* 109 pp149-163
- Karlin Y V (1993) 'Simulation of ionic transport through the cation-exchange membrane during the electrodialysis of aqueous $NaNO_3$-$Ca(NO_3)_2$-HNO_3 solution using an explicit difference scheme' *Russian Electrochemistry* 6(29) pp950-955
- Kedem O, Maoz Y (1976) 'Ion conducting spacer for improving ED' *Desalination* 19 pp465-470
- Kedem O, Rubinstein I (1983) 'Polarization effects at charged membranes' *Desalination* 46 pp185-189
- Kessore K, Shaposhnik V A, Frolich P (1991) 'Transfer of nitrates through anion-exchange membranes in electrodialysis' *Sov. J. of Water Chem. & Tech.* 13 (12) pp63-65
- Kalinauskas G L, Elder G R, Hemmings R L (1992) 'Electrochemical ion exchange for removal and destruction of nitrates in water' *6th international forum on electrolysis* - Florida, USA, Nov 1992
- Kneifel K, Lührs G (1988) 'Nitrate removal by electrodialysis for brewing water' *Desalination* 68 pp203-209

- Kobuchi Y, Motomura H, Noma Y, Hanada F (1986) 'Application of ion exchange membranes to the recovery of acids by diffusion dialysis' *J. Memb. Sci.* 27 pp173-179
- Yoshida M (1979) 'Electrolytic processes for preparing nitrates' *UK patent application* GB 2 038 872 A
- Kononov A V, Ponomarev M I, Shkaraputa L N, Grebenyuk V D, Sklyar V T (1984) 'Removal of hydrochloric acid from waste waters containing organic synthesis products' *Sov. J. Water Chem. Technology* 6(1) pp89-91
- Koter S (1995) 'Influence of the layer fixed charge distribution on the performance of an ion exchange membrane' *J. Memb. Sci.* 108 pp177-183
- Kuppinger F, Neubrand W, Eigenberger G (1993) 'Fundamentals of electro-membrane processes' *Comett course 11-14 Oct 1993* Stuttgart: University of Stuttgart
- Lantagne G, Velin A (1992) 'Overview of the application of dialysis, electrodialysis and membrane cell electrolysis for the recovery of waste acids' *Conference paper* Hydro-Québec, Canada
- Leitz F B (1986) 'Measurements and control in electrodialysis' *Desalination* 59 pp381-401
- Li H-L, Chamberws J Q, Hobbs D T (1988a) 'Electroreduction of nitrate ions in concentrated sodium hydroxide solutions at lead, zinc, nickel and phthalocyanine-modified electrodes' *J. Appl. Electrochem.* 18 pp454-458
- Li H-L, Roberston D H, Chambers J Q (1988b) 'Electrochemical reduction of nitrate and nitrite in concentrated sodium hydroxide at platinum and nickel electrodes' *J. Electrochem. Soc.* 135 (5) pp1154-1158
- Lindheimer A, Boudet-Dummy M, Gavach C (1993) 'Electrodialysis of hydrochloric acid' *Desalination* 94 pp151-165
- Maeck M (1995) *Personal communication* (Université Libre de Bruxelles)

- Maletzki F, Rösler H W, Staude E (1992) 'Ion transfer across electrodialysis membranes in the overlimiting current range: stationary voltage current characteristics and current noise power spectra under different conditions of free convection' *J. Memb. Sci.* 71 pp105-115
- Mani K N, Chlanda F P, Byszewski C H (1988) 'Aquatech membrane technology for recovery of acid/base values from salt streams' *Desalination* 68 pp149-166
- Mani K N (1991) 'Electrodialysis water splitting technology' *J. Memb. Sci.* 58 pp117-138
- Mavrov V, Pusch W, Kominek O, Wheelwright S (1993) 'Concentration polarization and water splitting at electrodialysis membranes' *Desalination* 91 pp225-252
- McArdle J C, Piccari J A, Thornburg G G (1991) 'AQUATECH systems' pickle liquor recovery process - Washington Steel reduces waset disposal costs and liability' *Iron and Steel Engineer* May pp39-43
- McRae W (1993) 'Applications of ion exchange membranes, current state of the technology after 45 years' 3rd Int. conf. on effective memb. processes and new perspectives. Bath 12-14 May pp149-160
- Murphy A P (1991) 'Chemical removel of nitrate from water' *Nature* 350 pp223-225
- Narebska A, Koter S, Warszawski A, Le T T (1995) 'Irreversible thermodynamics of transport across charged membranes. Part VI. Frictional interactions and coupling effects in transport of acid through anion exchange membranes' *J. Memb. Sci.* 106 pp39-48
- Novalic S, Jagschits F, Okwor J, Kulbe K D (1995) 'Behaviour of citric acid during electrodialysis' *J. Memb. Sci.* 108 pp201-205

- Ogawa N, Yokoi K, Watanbe I, Ikede S (1992) 'Electrochemical reduction of nitrate ion at mercury electrodes in the presence of alkaline earth metal ions' *Denki Kagaku* 60 (1) pp26-31
- Okada T, Kjelstrup-Ratkje S, Moller-Holst S, Jerdal L O, Friestad K, Xie G, Holmen R (1996) 'Water and ion transport in the cation exchange membrane systems NaCl-$SrCl_2$ and KCl-$SrCl_2$' *J. Memb. Sci.* 111 pp159-167
- Ondrey G, Shanley A (1993) 'Making cents of acid recovery' *Chemical Engineering* Apr pp47-53
- Parykin V S, Vlasova S A (1988) 'The effectiveness of acid and alkali recovery from waste waters in electrodialysis plants with bipolar membranes' *Thermal Engineering* 35(2) pp100-103
- Perry R H (ed Green D) (1984) 'Perry's Chemical Engineers' Handbook' Singapore: McGraw-Hill
- Petrii O A, Safonova T Y (1992) 'Electroreduction of nitrate and nitrite anions on platinum metals: a model process for elucidating the nature of the passivation by hydrogen adsorption' *J. Electroanal. Chem.* 331 pp897-912
- Pourbaix M (1974) 'Atlas of electrochemical equilibria in aqueous solutions' 2ed pp493-503
- Pourcelly G, Boudet-Dumy M, Lindheimer A, Gavach C (1991) 'Transport of proton in polymeric ionic exchange membranes in relation with the dissociated sorbed acid' *Desalination* 80 pp193-209
- Pourcelly G, Tugas I, Gavach C (1994) 'Electrotransport of sulphuric acid in special anion exchange membranes for the recovery of acids' *J. Memb. Sci.* 97 pp99-107
- Praslov D B, Shaposhnik V A (1988) 'Selection of the distance between membranes in electrodialysis' *J. Appl. Chem. of USSR* 61(5) pp1051-1053

- Ramírez P, Aguilella V M, Manzanares J A, Mafé S (1992a) 'Effects of temperature and ion transport on water splitting in bipolar membranes' *J. Memb. Sci.* 73 pp191-201
- Ramírez P, Rapp H J, Reichle S, Strathmann H (1992b) 'Current-voltage curves of bipolar membranes' *J. Appl. Phys* 72(1) pp259-264
- Raucq D, Pourcelly G, Gavach C (1991) 'Comparative study of salt decomposition into acid and base by electro-electrodialysis and electrodialysis with bipolar membrane' *Conference paper* Lab. of phys-chem. of polyphasic systems. CNRS Montpellier, France pp363-368
- Raucq D, Pourcelly G, Gavach C (1993) 'Production of sulphuric acid from caustic soda from sodium sulphate by electromembrane processes. Comparison between electro-electrodialysis and electrodialysis on bipolar membrane' *Desalination* 91 pp163-175
- Reboiras M D (1996) 'Electrochemical properties of cellulosic ion-exchange membranes II. Transport numbers and electro-osmotic flow' *J. memb. Sci.* 109 (1996) pp55-63
- Richter M (1994) 'The treatment of acid wastewater - technology, economics and social aspects' MSc thesis. University of Bath. Aug 1994
- Rösler H W, Maletzki F, Staude E 'Ion transfer across electrodialysis membranes in the overlimiting current range: chronopotentiometric studies' *J. Memb. Sci.* 72 pp171-179
- Rubinstein I, Maletzki F (1991) 'Electroconvection at an electrically inhomogeneous permselective membrane surface' *J. Chem. Soc. Faraday Trans.* 87(13) pp2079-2087
- Salem K, Sandeaux J, Molénat J, Sandeaux R, Gavach C (1995) 'Elimination of nitrate from drinking water by electrochemical membrane processes' *Desalination* 101 pp123-131

- Samoilov O Y (1957) 'Structure of aqueous electrolyte solutions and the hydration of ions' New York: Consultants Bureau (1965 translation)
- Sanderson R (1996) *Personal communication* (University of Stellenbosch)
- Saracco G, Zanetti M, Onofrio M (1993) 'Novel application of monovalent-ion-permselective membranes to the recovery treatment of an industrial wastewater by electrodialysis' *Ind. Eng. Chem. Res.* 32 pp657-662
- Sata T, Yamaguchi T, Matsusaki K (1995a) 'Interaction between anionic polyelectrolytes and anion exchange membranes and change in membrane properties' *J. Memb. Sci.* 100 pp229-238
- Sata T, Yamaguchi T, Matsusaki K (1995b) 'Anion exchange membranes for nitrate removel from groundwater by electrodialysis' *J. Chem. Soc. Chem. Commun* pp1153-1154
- Scott K (1991) 'Electrochemical Reaction Engineering' London: Academic Press
- Scott K, Paton E M (1993) 'An analysis of metal recovery by electrodeposition from mixed metal ion solutions -Part 1. Theoretical behaviour of batch recycle operation' *Electrochimica. Acta.* 38 (15) pp2181-2189
- Shah P M, Scamehorn J F (1987) 'Use of electrodialysis to deionize acidic waste water streams' *Ind. Eng. Chem. Res.* 26 pp269-277
- Shah P R, Kovvali A S, Khan G Y, Khan A A (1993) 'Prediction of permselectivity of nitrate and acetate ions in the electrodialysis of aqueous solutions' *The Chem. Eng. Journal* 51 pp1-6
- Simons R (1993) 'Preparation of a high performance bipolar membrane' *J. Memb. Sci.* 78 pp13-23
- Spiegler K S, Laird A D K (1980) 'Principles of desalination' 2ed New York: Academic press

- Sridhar S (1988) 'Application of electrodialysis in the production of malic acid' *J. Memb. Sci.* 36 pp489-495
- Sridhar S (1989) German patent DE 3812183 A1 26 Oct
- Strathmann H (1985) 'Electrodialysis and its application in the chemical process industry' *Sep. and Pur. Methods.* 14(1) pp41-66
- Strathmann H, Bauer B, Rapp H J (1993)a 'Better bipolar membranes' *Chemtech* June pp17-24
- Strathmann H, Rapp H J, Bauer B, Bell C M (1993)b 'Theoretical and practical aspects of preparing bipolar membranes' *Desalination* 90 pp303-323
- Stulikova M (1991) 'Is nitrate really an inert electrolyte - a brief review' *Talanta* 38 (7) pp805-807
- Taniguchi I, Nakashima N, Matsushita K, Yasukouchi K (1987) 'Electrocatalytic reduction of nitrate and nitrite to hydroxylamine and ammonia using metal cyclams' *J. Electroanal. Chem.* 224 pp199-209
- Tenne R, Patel K, Hashimoto K, Fujishima A (1993) 'Efficient electrochemical reduction of nitrate to ammonia using conductive diamond film electrodes' *J. Electroanal. Chem.* 347 pp409-415
- Timashev S F 'Physical Chemistry of Membrane processes' (1991) pp177-218 Ellis Horwood Ltd, Chichester, UK
- Timashev S F (1996) *Personal communication* (Karpov Institute of Physical Chemistry)
- Torii S, Okumoto H, Satoh H, Minoshima T, Kurozumi S (1995) 'Electrochemical deamination of aromatic amines' *Synlett* May pp439-440
- Tugas I, Pourcelly G, Gavach C (1993a) 'Electrotransport of protons and chloride ions in anion exchange membranes for the recovery of acids Part I.

Equilibrium properties & Part II. Kinetics of ion transfer at the membrane-solution interface' *J. Memb. Sci.* 85 pp183-204

- Tugas I, Lambert J-M, Maillols J, Bribes J-L, Pourcelly G, Gavach C (1993b) 'Identification of the ionic species in anion exchange membranes equilibrated with sulphuric acid solutions by means of Raman spectroscopy and radiotracers' *J. Memb. Sci.* 78 pp25-33
- Urano K, Ase T, Naito Y (1984) 'Recover of acid from wastewater by electrodialysis' *Desalination* 51 pp213-226
- Valuev V (1996) *Personal communication* (Karpov Institute of Physical Chemistry)
- Velzen D v, Langenkamp H (1995) 'Electrochemical removal of nitrates from drinking water and effluents' *Electrochemical processing a clean alternative* Toulouse, France, April 1995
- Voortmann W J, Simpson A E, Kerr C A, Buckley C A (1992) 'Application of electrochemical membrane processes to the treatment of aqueoue effluent streams' *Wat. Sci. Tech.* 25(10) pp329-337
- Walsh F C (1993) 'A first course in electrochemical engineering' UK: Alresford Press
- Wišniewska G, Wišniewski J, Winnicki T (1993) 'Recovery of acid and water by membrane dialysis' *Desalination* 91 pp307-317
- Xing X, Scherson D, Mak C (1990) 'The electrocatalytic reduction of nitrate mediated by underpotential-deposited cadmium on gold and silver electrodes in acid media' *J. Electrochem Soc* 137 (7) pp2166-2174
- Xue T, Longwell R B, Osseo-Asare K (1991) 'Mass transfer in Nafion membrane systems: effects of ionic size and charge on selectivity' *J. Memb. Sci.* 58 pp175-189

• Yen Y-H, Cheryan M (1993) 'Electrodialysis of model lactic acid solutions' *J. Food Engineering* 20 pp267-282

Appendix 1

Appendix 1 - Spreadsheet model of cell

The spreadsheet model used to size the electro-membrane cell allowed input of cell and reservoir dimensions along with initial electrolyte concentrations and volumes. For a given operating current density the time taken to deplete the catholyte of nitric acid was determined using the optimiser tool in the Quattro Pro for Windows software.

Although the model was simplistic it allowed the effect of many factors to be considered in order to design the laboratory cell and associated hardware. An example of the spreadsheet model calculation can be seen in Figure A1.1. For this run the operating current density was set to 300 mA cm^{-2} and the cell configured as two-compartment EED. As a point of clarification the 'concentrate' and 'diluate' are equivalent to the 'anolyte' and 'catholyte' respectively. This discontinuity results from the different nomenclature used in ED and EED.

The results show that it would take 3.5 hours to reduce the concentration of a 10 dm^3, 1 M catholyte to 0.001 M using this configuration. It should be noted that this assumes 100% current efficiency and any deviations will increase the time taken to process the batch charge - on this basis it would take approximately 7 hours to process the same batch at 50% current efficiency. The maximum concentration of the anolyte was 5.47 M based on the assumed water transport numbers. The results also show that a flow of 26.5 dm^3 min^{-1} of purge air would be required to dilute the electrochemicaly generated hydrogen to safely below the lower explosive limit.

Basic model of ED/EED cell for rig sizing - batch operation

+++| w /c\d/c\d/c\d/c\d/c\d/ w |--- +++|c\d|---
w-wash, c-concentrate , d-diluate, +\ APM, /- CPM

Design data		ED/EED
No cells	1	0.5
Electrode	2	
Exch area	0.0064	m2
Total area	0.0128	m2
i density	300	mA cm-2
	3000	A m-2
Supply	38.40	A
@	20.00	V?
=	1536.00	W
Batch	3.5	hours
	12551	secs

Properties		
Mr Nitric	63	g mol-1
Mr water	18	g mol-1
Nitric	1.502	g cm-3
Water	1	g cm-3
Faraday	96484.563	A s mol-1
Solv shell	2	mol H2O / mol ion

Calculated movement		
Charge	481969	A s
Ions	9.99	moles (net nitric in conc)
Water	9.99	moles

Purge air		
Charge	481969	A s
F-mols	5.00	mol
H2	2.50	mol
O2	1.25	mol
rate H2	0.01194	mol/min
rate O2	0.00597	mol/min
STP H2	0.26745	dm3/min
STP O2	0.13373	dm3/min
Inert	26.5	dm3/min
% H2	1.00	%

Initial parameters	Conc	Dil	
Total vol	1.50	10.00	dm3
Conc	1.00	1.00	M
Vol frac	0.04	0.04	Acid
	0.96	0.96	Water
Conc	6.17	6.17	wt %
Moles	1.50	10.00	Acid
	79.84	532.25	Water

Final parameters	Conc	Dil		
Total vol	2.10	9.40	dm3	Spec ?
Conc	5.47	0.00	M	0.0010 M
Vol frac	0.23	0.00	Acid	
	0.77	1.00	Water	
Conc	30.93	0.01	wt %	
Moles	11.49	0.01	Acid	
	89.83	522.26	Water	

11.5 Vol error 11.5
0.00

Figure A1.1: Spreadsheet model of electro-membrane cell

Appendix 2

Appendix 2 - Estimation of cell power

In order to estimate the electrical power required by the electro-membrane stack a short-cut calculation was undertaken for both ED and EED configurations of the FM01 cell. The conductivity of electrolyte was taken to be equivalent to that of a 1M nitric acid solution. For this concentration a conductivity of 50 S m^{-1} was chosen. The conductance and hence resistance of electrolyte within a spacer compartment in the FM01 could be estimated from this conductivity estimate. In the FM01 the membrane electrode gap is approximately 7 mm and the cross-sectional area is 64 cm^2.

$$\text{Resistance} = \frac{\text{Thickness of compartment}}{\text{Cross - sectional area} \times \text{Conductivity}} \qquad [A2.1]$$

$$\text{Resistance} = \frac{7 \times 10^{-3}}{64 \times 10^{-4} \times 50} = 0.022\ \Omega \text{ per channel}$$

For operation at a current density of 300 mA cm^{-2}, the voltage drop across a channel can be estimated from the resistance using the formula:

$$\text{Voltage} = \text{Current} \times \text{Resistance} \qquad [A2.2]$$

$$\text{Voltage} = 38.4 \times 0.022 = 0.84\ \text{V per channel}$$

It was assumed that the cathode reaction was hydrogen evolution (E°=0V by definition) and the anode reaction was oxygen evolution (E°=1.23V). The voltage drop across a single membrane was assumed to be 1V and the

overpotentials at each electrode of the order of 2V. Using this information the total stack voltage drop could be estimated for both ED and EED.

For an eleven membrane ED stack the overall voltage drop will be of the order:

11 membranes	11V
Cathode	2V
Anode	3.23V
Channels (12)	10.08V
TOTAL	26.31V

Power
= voltage x current
= 26.31 x 38.4
= 1010 W

Similarly for a single cell EED stack:

1 membrane	1V
Cathode	2V
Anode	3.23V
Channels (2)	1.68V
TOTAL	7.91V

Power
= voltage x current
= 7.91 x 38.4
= 304 W

This data was used to specify a powerpack and to estimate the cooling requirements for the experimental rig.

Appendix 3

Appendix 3 - Nitrate reduction literature

A literature search of the publications on nitrate reduction was completed in order to establish what research had been undertaken in this area and to obtain a general background to the subject.

This literature review is by no means an exhaustive examination of all the relevant literature as it was intended only to give a broad overview of nitrate reduction. The literature search would need to be extended prior to commencing a detailed study of nitrate reduction.

For simplicity, the key features of the publications are presented in tabular form in Table A3.1 and the parameters relevent to this research project are also included in the table. The main conclusions of the literature review are summarised later in the appendix.

Reference	Focus of paper	Principle components	pH	T °C	Nitrate conc. M	Electrodes	Membrane type	Current density mA cm^{-2}	Relevant conclusions
Bard et al 1980	Standard reversible potentials	N species							Listed in Table end of appendix.
Pourbaix 1974	Detailed thermodynamic data	N species	range						Equilibrium equations useful for catholyte species.
Yoshida 1979	Preparation of nitrites	$NaNO_3$ NH_4NO_3	>4	5-95	0.1-2M	Hg, Pb, Sn, In	CEM		Only H_2 generated at pH>7.
Li et al1988	Destruction of nitrate and nitrite in NaOH	$NaNO_3$ $NaNO_2$	strong alkali	80		Pt, Ni	CEM	100	Nitrite intermediate peak observed. Ammonia major product at 500mAcm^{-2}.
Li & Chambers 1988	Reduction of nitrate in conc. NaOH	$NaNO_3$ $NaNO_2$	strong alkali		≈0.05	Zn, Pb, Ni		173	Significant nitrite intermediate peak noticed
Murphy 1991	Chemical nitrate reduction	$-NO_3$	>8	ambient	≈0.02	n/a	n/a	n/a	Al powder as reagent. 60-95% to ammonia product.
Pertii & Safonova 1992	Reduction of nitrate and nitrite	$NaNO_3$	>0.5	20	<0.1	Pt, Pd, Rh		low (polarisation curves)	Nitrier reduction more rapid than nitrate reduction.
Gilroy 1992	Electrolytic nitrate destruction	$-NO_3$	>11.5		<0.1	C	CEM	50	Ammonia product stripped from catholyte and oxidised in anolyte

cont'd...

Table A3.1: Summary of nitrate reduction literature

Kalinauskas et al 1992	Electrochemical ion exchange followed by nitrate destruction	$NaNO_3$					undivided		Bipolar cell converting nitrate to nitrogen
Hobbs 1994	Reduction of nitrate and nitrite	$-NO_3$	high	50	3.6M	Pt, Ni,C, Pb, Cu, 316SS	CEM		Liquid nuclear waste application.
Cox et al 1994	Thermochemical nitrate destruction	NH_4NO_3	range	>200 & 600-2800 psig		n/a	n/a	n/a	Optimise for N_2 product. Little/ no NO_2^- or NH_4^+.
Elder & Waite 1995	As Kalinauskas 1992			>70					
Velzen & Langenkamp 1995	Removal of nitrates from drinking water	$-NO_3$	7-12		≈0.1mM				Reduction to NH_4^+. Oxidation of NH_4^+ to N_2.
Coleman et al 1995	Model of nitrate destruction reactor	$NaNO_3$	alkali	25	≈2	Pb, Ni	none	250	reaction data from previous fundamental study
Jiang et al 1992	Measurement of reduction potential			20	1.5				Use of linear accelerator in experiments

cont'd...

Table A3.1: Summary of nitrate reduction literature

Tenne et al 1993	Nitrate to ammonia on diamond film semiconductors	$NaNO_3$ KNO_3	alkali			C (diamond) FeO doped	none	200-300	Suggest two-stage $NO_3 \rightarrow NO_2 \rightarrow NH_4$
Xing et al 1990	Reduction of nitrate in acidic media		>1		10^{-3}	Cd on Ag or Au	none		pH=3 nitrite product pH=1 beyond nitrite
Torii et al 1995	Electrochemical de-amination of aromatic amines			ambient		Pb			Reduction very efficient
Taniguchi et al 1987	Enhanced reduction using metal cyclams		10			Hg or Ag, Cu, Pb			Catalytic mechanism (cyclam structure similar to that of an enzyme active site)
Hernandez 1988	Production of NH_2OHHNO_3 (HAN)	HNO_3	1-1.6	5-50	0.1-1.2	Hg, Pb, Ga, Cd, Sn, Pt, Zn, In	CEM	<100	Controlled cell potential to minimise hydrogen gassing
Stulikova 1991	Reviews of nitrate as 'inert' supporting electrolyte								Metal ions can have a catalytic effect on nitrate reduction
Ogawa 1992	Reduction in presence of alkaline earth metals	$LiNO_3$	1-4		10^{-2}	Hg		≈20	Reduction very irreversible once initiated.

Table A3.1: Summary of nitrate reduction literature

The publications reviewed contained three recent conference papers and four patent applications from industrialists which clearly demonstrates that nitrate reduction is a topical research subject.

All the processes reviewed aimed to destroy rather than recover nitrate ions and consequently it was common to employ no cell separator or a CEM. AEMs were not used.

Many electrode materials were studied and those with a high hydrogen evolution overpotential favoured nitrate reduction.

Most studies were undertaken in alkaline media with all other studies conducted at pH>1. Nitrate concentrations were on the whole low (<<1.2M) for application to the water industry. Nitrate salts were more often used as the nitrate source rather than nitric acid.

Various mechanisms were proposed for the nitrate reduction pathway which increase in complexity with the presence of metal ions in the system. Despite the mechanisms being not fully understood, overall two key reduction products of nitrite and ammonium (or ammonia) were highlighted (although gaseous nitrogen compounds were also evolved under some conditions). Nitrite and ammonium are formed via the two simple equations:

$$NO_3^- + 2H^+ + 2e^- \rightarrow NO_2^- + H_2O \qquad [A3.1]$$

$$NO_2^- + 8H^+ + 6e^- \rightarrow NH_4^+ + 2H_2O \qquad [A3.2]$$

Some of the possible nitrogen half-cell reactions are given in Table A3.2 taken from Bard (Bard et al, 1980).

Reaction	**E° (V) vs SHE**
$O_2 + 4H^+ + 4e^- \rightarrow 2H_2O$	1.23
$2H^+ + 2e^- \rightarrow H_2$	0.00
$Na^+ + e^- \rightarrow Na$	-2.71
$K^+ + e^- \rightarrow K$	-2.92
$NO_3^- + 2H^+ + e^- \rightarrow {}^1/_2N_2O_4(g) + H_2O$	0.803
$NO_3^- + 2H^+ + 2e^- \rightarrow NO_2^- + H_2O$	0.835
$NO_3^- + 4H^+ + 3e^- \rightarrow NO + 2H_2O$	0.957
$NO_3^- + 5H^+ + 4e^- \rightarrow {}^1/_2N_2O(g) + 2{}^1/_2H_2O$	1.116
$NO_3^- + 6H^+ + 5e^- \rightarrow {}^1/_2N_2 + 3H_2O$	1.246
$NO_3^- + 10H^+ + 8e^- \rightarrow NH_4^+ + 3H_2O$	0.875
$NO_3^- + H_2O + e^- \rightarrow {}^1/_2N_2O_4(g) + 2OH^-$	-0.860
$NO_3^- + H_2O + 2e^- \rightarrow NO_2^- + 2OH^-$	0.010
$NO_3^- + 3H_2O + 5e^- \rightarrow {}^1/_2N_2(g) + 6OH^-$	0.250
$NO_3^- + 6H_2O + 8e^- \rightarrow NH_3 + 9OH^-$	-0.170
$NO_2^- + 2H^+ + e^- \rightarrow NO(g) + H_2O$	1.202
$NO_2^- + 3H^+ + 2e^- \rightarrow {}^1/_2N_2O(g) + 1{}^1/_2H_2O$	1.396
$NO_2^- + 4H^+ + 3e^- \rightarrow {}^1/_2N_2(g) + 2H_2O$	1.520
$NO_2^- + 8H^+ + 6e^- \rightarrow NH_4^+ + 2H_2O$	0.897

cont'd...

$NO_2^- + 7H^+ + 6e^- \rightarrow NH_3(g) + 2H_2O$	0.789
$NO_2^- + 7H^+ + 6e^- \rightarrow NH_3(aq) + 2H_2O$	0.806
$NO_2^- + H_2O + e^- \rightarrow NO(g) + 2OH^-$	0.460
$NO_2^- + 1\frac{1}{2}H_2O + e^- \rightarrow \frac{1}{2}N_2O(g) + 3OH^-$	0.150
$NO(g) + H+ + e^- \rightarrow \frac{1}{2}N_2O(g) + \frac{1}{2}H_2O$	1.590
$NO(g) + 2H+ + 2e^- \rightarrow \frac{1}{2}N_2(g) + H_2O$	1.678
$NO(g) + 6H+ + 5e^- \rightarrow NH_4+ + H_2O$	0.836
$NO(g) + 5H+ + 5e^- \rightarrow NH_3(aq) + H_2O$	0.727
$N_2O(g) + 10H^+ + 8e^- \rightarrow 2NH_4^+ + H_2O$	0.647
$N_2O(g) + H_2O + 8H^+ + 8e^- \rightarrow 2NH_3(aq)$	0.510
$N_2(g) + 8H^+ + 6e^- \rightarrow 2NH_4^+$	0.275
$N_2(g) + 6H^+ + 6e^- \rightarrow 2NH_3(g)$	-0.057
$N_2(g) + 6H^+ + 6e^- \rightarrow 2NH_3(aq)$	-0.092

Table A3.2: Nitrogen half-cell reactions

Appendix 4

Appendix 4 - Error analysis

It is useful to quantify the errors in the experimental techniques in order to assess the credibility of the results. The errors calculated in this appendix are those resulting from inaccuracies of the various measurements and they are evaluated for the three main measurements: total acid concentration, ammonium concentration and volume readings. The error evaluation technique for the specific water transport numbers is also show here.

Measurement errors

It was assumed that the concentrations of the reagents used in the analytical procedures were as specified (maximum error ±0.05% for Fischer Standard Laboratory Reagents) and that the volume measurement errors were as below:

Burette:	±0.05 ml
Pipette:	±0.04 ml ($\frac{0.05}{\sqrt{2}}$; diameter half that of burette)
Catholyte:	±50 ml
Anolyte	±25 ml

The analytical methods used in the experimental programme are discussed in detail in Section 3.2.3.

Total acid titration

The procedure for total acid determination was to add 25 ml of standard 2M NaOH to a 5 ml sample of acid electrolyte. This was then titrated with standard 1M HNO_3 to determine the acidity. The equation used to calculate acid molarity can therefore be expressed, including the measurement errors, as:

$$C_i = \frac{2\times10^{-3}(25\pm0.04)-1\times10^{-3}(x\pm0.05)}{1\times10^{-3}(5\pm0.04)} \qquad [A4.1]$$

x volume of standard acid added from burette (ml)

For a range of values of x, the maximum error can be evaluated from Equation A4.1 and this is tabulated below.

x ml	C_i M	Max. error %
10	8	1.13
20	6	1.24
30	4	1.46
40	2	2.12
49	0.2	13.91

Table A4.1: Total acid error analysis

It can be seen that the magnitude of the error increases with decreasing acid concentration which means that the ultimate values of the catholyte acid concentration could have errors of the order of ±15%, whereas the anolyte acid

concentrations will have decreasing errors throughout the course of an experiment.

Ammonium titration

The measurement errors in the ammonium titration can be quantified in a similar way to those described in the total acid analysis. In the ammonium analysis procedure a 5 ml sample is boiled with excess NaOH and the fumes absorbed into a 5 ml standard 1M HNO_3 solution. The resultant liquor is titrated with standard 0.1M NaOH solution. The error analysis equation for this technique is therefore given by:

$$C_{NH4+} = \frac{1\times10^{-3}(5\pm0.04)-1\times10^{-4}(y\pm0.05)}{1\times10^{-3}(5\pm0.04)} \qquad [A4.2]$$

y volume of standard alkali added from burette (ml)

For a range of values of y, the maximum error in the ammonium concentration can be evaluated from Equation A4.2 and this is tabulated below.

y ml	C_{NH4+} M	Max. error %
10	0.8	1.94
20	0.6	2.32
30	0.4	2.50
40	0.2	5.34
49	0.02	46.17

Table A4.2: Ammonium error analysis

The errors in the ammonium analytical technique increase with decreasing ammonium concentration and are greater than those described for the total acid analysis. It is worth noting that the ammonium concentrations were found to be less than 0.2M during the experimental programme and so the procedure should be revised in future work to improve the accuracy of the measurements.

Volume measurements

The errors in the volume measurements in terms of absolute volumes were small but could be large when determining volume changes for water transport measurements. The absolute volume errors are given below for both catholyte and anolyte volume readings based on the measurements errors listed above.

Catholyte dm^3	**Max. error** %	**Anolyte** dm^3	**Max. error** %
10.0	0.50	3.0	0.83
9.5	0.53	2.5	1.00
9.0	0.56	2.0	1.25
8.5	0.59	1.5	1.67
8.0	0.63	1.0	2.5

Table A4.3: Absolute volume errors

The errors when determining water transport in the anolyte reservoir are expressed in terms of the volume of water transported in the Table A4.4. The volume change errors can be significant. Consequently volume readings were typically only taken at 6 hour intervals so that the water transport between measurements was sufficient to reduce measurement errors.

Anolyte volume change ml	Max. error %
200	12.5
150	16.6
125	20
100	25
75	33
50	50
25	100

Table A4.4: Volume change errors

Specific water transport number

The specific water transport number is calculated from the water transport number and the integral current efficiency. In order to evaluate the errors inherent in the specific water transport number, the errors in the two other measurements were evaluated and then combined. First the error equation for the water transport number is given as:

$$t_{H2O} = \left[\left(V_f \pm 0.025\right) - \left(V_0 \pm 0.025\right)\right]\frac{1000}{18F} \qquad \text{[A4.3]}$$

Which can be simplified to be:

$$t_{H2O} = t_{H2O} \pm \frac{2.78}{F} \qquad \text{[A4.4]}$$

Similarly the integral current efficiency error equation can be expressed as:

$$\eta_{ICE} = \frac{(V_f \pm 0.025)C_f - (V_0 \pm 0.025)C_0}{F} \qquad [A4.5]$$

Which can be simplified to:

$$\eta_{ICE} = \eta_{ICE} \pm \frac{0.025}{F}(C_f - C_0) \qquad [A4.6]$$

The specific water transport number error equation is therefore obtained by combining Equations A4.4 and A4.6 to give:

$$n_{H2O} = \frac{t_{H2O} \pm \frac{2.78}{F}}{\eta_{ICE} \pm \frac{0.025}{F}(C_f - C_0)} \qquad [A4.7]$$

By comparing the error coefficients in Equation A4.7 it can be seen that:

$$\frac{0.025}{F} << \frac{2.78}{F} \qquad [A4.8]$$

Which simplifies the specific water transport number error equation:

$$n_{H2O} = \frac{t_{H2O}}{\eta_{ICE}} \pm \frac{2.78}{F} \qquad [A4.9]$$

This was used in the n_{H2O} plots given in Chapter 4. The variation of errors with Faradays of charge passed is shown in Table A4.5.

Faradays passed 'F'	Absolute error in n_{H2O}
5	0.56
10	0.28
15	0.19
20	0.14
25	0.11
30	0.09

Table A4.5: Absolute water transport errors

Appendix 5

Appendix 5 - Anolyte mass balance

A mass balance was carried on the anolyte to allow the increase in mass due to water transport across the membrane to be determined. The equations developed to describe this mass balance are described in this appendix. The overall mass balance can be described in words as:

Change in mass of anolyte	=	Change in mass of water	+	Change in mass of nitrate	+	Change in mass of protons

If the mass of the anolyte at a given instant, t, is given by M_t then the mass balance can be written as:

$$M_{t+1} - M_t = \Delta M_w - 0.5(F_{t+1} - F_t)18 + \eta_{DCE}(F_{t+1} - F_t)63 + (F_{t+1} - F_t)1 - (1 - \eta_{DCE})(F_{t+1} - F_t)1 \qquad [A5.1]$$

ΔM_w change in mass due to water transport (g)

which can be simplified to give:

$$M_{t+1} - M_t = \Delta M_w - 0.5(F_{t+1} - F_t)18 + \eta_{DCE}(F_{t+1} - F_t)64 \qquad [A5.2]$$

The differential specific water transport number is defined as the change in moles of water due to membrane transport per mole of acid that is transported across the membrane over a differential element of time. This gives rise to:

$$\tilde{n}_{H2O} = \frac{\Delta M_w}{18(F_{t+1} - F_t)\eta_{DCE}} \qquad [A5.3]$$

which relates the mass balance of Equation A5.2 to the specific water transport number. Solution of these equations to calculate the differential specific water transport number followed the algorithm:

1. Determine variation in total mass of anolyte from periodic volume and density measurements.
2. Mathematically fit polynomial curve to mass data such that $M_t = M(t)$.
3. Use M(t) and F(t) ('Faradays' passed) to calculate ΔM_w via Equation A5.2.
4. Calculate differential specific water transport number having evaluated all the unknowns in Equation A5.3.

The differential specific water transport number relative to proton transport could also be calculated in a similar way using:

$$\tilde{n}_{H2O/H+} = -\frac{\eta_{DCE}}{(1 - \eta_{DCE})}\tilde{n}_{H2O} \qquad [A5.4]$$

Appendix 6

Appendix 6 - Fortran model of process

The data from the AW002 experimental runs are compared with the model predictions in Figure A6.1, Figure A6.2 and Figure A6.3. Generally the observed trends agree with those of the AW1.5 run which was discussed in detail in Section 6.4.

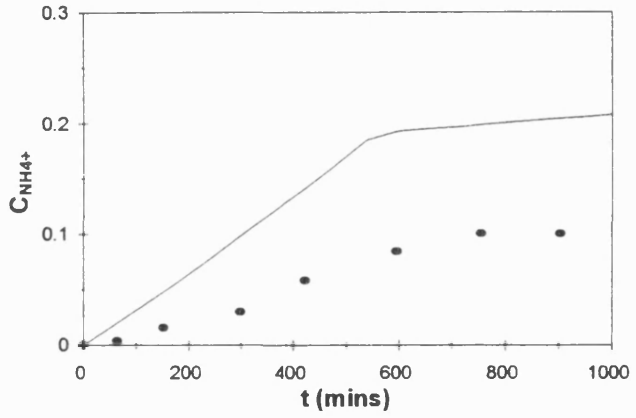

Figure A6.1: Ammonium concentration profile for AW002 run (● data, — model prediction)

The rate of ammonium generation in the AW002 experiment is less than predicted by the model as is shown in Figure A6.1. No gas bubbles were observed over the initial period of the experimental run and so the current must be consumed by liquid phase cathode reactions. As mentioned in Chapter 6 detailed electrochemical study of nitrate reduction is required if the model is to be improved by a non-empirical technique.

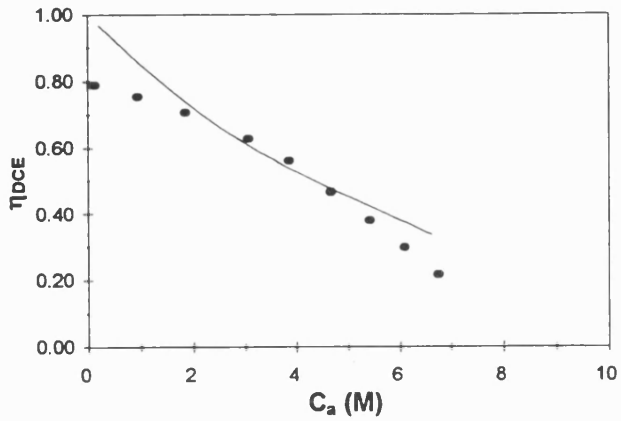

Figure A6.2: Differential current efficiency against anolyte acid concentration for AW002 run (● data, — model prediction)

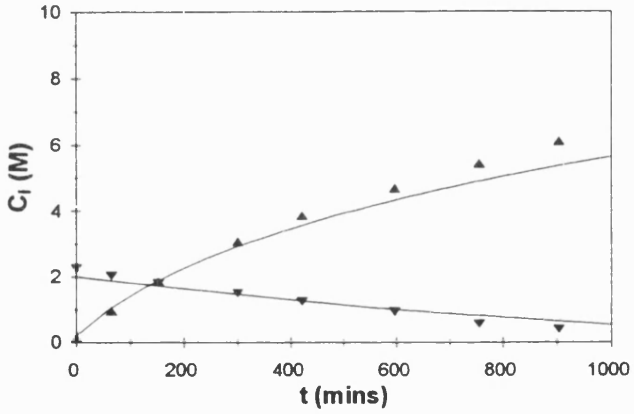

Figure A6.2: Concentration profiles for AW002 run (● data, — model prediction)

The Fortran code used to solve the mathematical model is listed below and additional comments have been made in bold text to enable the code to be more easily understood.

```
C    BRIAN J ROBBINS, UNIVERSITY OF BATH, SCHOOL OF CHEM ENG
C    MODEL FOR TWO-COMPARTMENT EED OF NITRIC ACID INCORPORATING
C    NITRATE REDUCTION AND ANION EXCHANGE MEMBRANE TRANSPORT USING
C    PARAMETERS DISCUSSED IN THESIS
C
C    SET-UP
C
     IMPLICIT REAL (A-Z)
     DIMENSION CA(6),CC(6),DELA(6),DELC(6),LOSSA(6),LOSSC(6),
    & NA(6),NC(6),RHO(6),Y(6),TVA(6),TVC(6)
     INTEGER M,N,REP
     COMMON F,I,KM,PA,PC,R,S,DT,TEMP,WA,WH,RHOG,X
     OPEN (1,FILE='C:\1BJR\CALCS\FORTRAN\RESULTS1.PRN')
C
C    DEFINE SYSTEM CONSTANTS
C    1=H20, 2=NO3-, 3=H+, 4=O2, 5=H2, 6=NH4+, A=anolyte, C=catholyte
C
     F=96485                    Faraday constant
     KM=3E-5                    Mass transfer coefficient
     RHOG=44.61E-3              Molar gas density (ideal)
     RHO(1)=997/18              Molar liquid densities
     RHO(2)=1504/63
     RHO(3)=1E6
     RHO(4)=1E6
     RHO(5)=1E6
     RHO(6)=618/17
     Y(1)=16.75/760             Vapour-liquid equilibrium constants
     Y(2)=0.058/760
     Y(2)=0
     Y(3)=Y(2)
     Y(4)=0
     Y(5)=0
     Y(6)=0
     Y(6)=1E-8
C
C    DEFINE PROCESS PARAMETERS
C
     I=39                       Operating current
     PA=3.33E-2                 Purge air flows
     PC=5.83E-1
     R=8.31451                  Ideal gas constant
```

```
      S=128E-4                          Membrane area
      DT=0.5                            Euler step length
      TEMP=298                          System temperature
      WA=3.5                            Co-ordination numbers
      WH=1.0
      X=0                               Nitrate reduction modifier
C
C     INITIAL VALUES OF VARIABLES
C
      VA=1.5                            Electrolyte volumes
      VC=10.0
      NA(2)=0.2*VA                      Species concentrations
      NA(3)=NA(2)                       A=anolyte
      NA(1)=(VA-NA(2)/RHO(2))*RHO(1)    C=catholyte
      NA(4)=0
      NA(5)=0
      NA(6)=0
      NC(2)=2.0*VC
      NC(3)=NC(2)
      NC(1)=(VC-NC(2)/RHO(2))*RHO(1)
      NC(4)=0
      NC(5)=0
      NC(6)=0
      REP=1                             Data report counter
      T=0                               Time
C
C     CALCULATION ROUTINE
C
      DO 555 M=1,300000
      DO 100 N=1,6
      CA(N)=NA(N)/VA
      CC(N)=NC(N)/VC
  100 CONTINUE
      WA=3.543-(0.068*CA(2))+(0.029*(CA(2)*CA(2)))-(0.005*
     & (CA(2)*CA(2)*CA(2)))             Variation of W_A- with C_a
      IF (CC(2).LT.0.1) THEN            Limit of correlation
      STOP
      ENDIF
      IF (REP.EQ.2) THEN                Write data to file & screen periodically
      TIME=T/60
    5 FORMAT (1F8.0,4F8.3,1F9.4,2F8.3,1F9.4)
```

```
      WRITE (6,5) TIME,DCE,NR,CA(2),CC(2),CC(6),VA,VC,WA
c7    FORMAT (2F6.2,6F8.4)
c     WRITE (6,7) TIME,NR,TVC(1),TVC(2),TVC(3),TVC(4),TVC(5),TVC(6)
6     FORMAT (1F8.0,1F8.3,5F8.3)
      WRITE (1,6) TIME,DCE,CA(2),CC(2),CC(6),VA,VC
c     & ,TVA(1),TVC(1),TVA(2),TVC(2),TVC(6)
      ENDIF
C
      CALL EFF(CA,CC,DCE)              Calculate membrane current efficiency
C
      CALL RED(CC,NR)                  Calculate nitrate reduction efficiency
C
      CALL DERIV(DCE,NR,DELA,DELC)     Calculate species derivatives
C
      CALL VENT(LOSSA,LOSSC,Y,DELA,DELC,TVA,TVC)
C                                      Calculate vent losses
      VA=0
      VC=0
      DO 200 N=1,6
      NA(N)=NA(N)+DELA(N)-LOSSA(N)
      NC(N)=NC(N)+DELC(N)-LOSSC(N)
      VA=VA+NA(N)/RHO(N)
      VC=VC+NC(N)/RHO(N)
200   CONTINUE
      T=T+DT                           Update time and report log
      REP=REP+1
      IF (REP.EQ.7200) THEN
      REP=1
      ENDIF
555   CONTINUE
      END
C
C     **********
C     CURRENT EFFICIENCY EVALUATION SUBROUTINE
C     **********
C
      SUBROUTINE EFF(CA,CC,DCE)
      IMPLICIT REAL(A-Z)
      DIMENSION CA(6),CC(6)
      COMMON F,I,KM,PA,PC,R,S,DT,TEMP,WA,WH,RHOG,X
      EM=0.83+(5.56*EXP(-0.50*CA(2)))  Membrane characterisation equations
```

```
      RM=6.08E6+6.71E6*EM
      DCE=1-(CA(3)*(1+(EM*F/R/TEMP))-CC(3))/(1E-3*RM*I/F/S)
      IF (DCE.LT.0) THEN
      DCE=0
      ENDIF
      END
C
C     ********************
C     REDUCTION REACTION SUBROUTINE
C     ********************
C
      SUBROUTINE RED(CC,NR)
      IMPLICIT REAL(A-Z)
      DIMENSION CC(6)
      COMMON F,I,KM,PA,PC,R,S,DT,TEMP,WA,WH,RHOG,X
      NR=KM*S*CC(2)*1000/(I/F)          Nitrate reduction efficiency based
      IF (NR.LT.0) THEN                 on assumptions in Chapter 6
      NR=0
      ENDIF
      IF (NR.GT.1) THEN
      NR=1
      ENDIF
      IF (NR.GT.0) THEN
      IF (NR.LT.1) THEN
      NR=X*NR
      ENDIF
      ENDIF
      END
C
C     ********************
C     DERIVATIVE EVALUATION SUBROUTINE
C     ********************
C
      SUBROUTINE DERIV(DCE,NR,DELA,DELC)
      IMPLICIT REAL(A-Z)
      DIMENSION DELA(6),DELC(6)
      COMMON F,I,KM,PA,PC,R,S,DT,TEMP,WA,WH,RHOG,X
      FA=I*DT/F                         Faradays per step
      DELA(1)=(-0.5+(WA*DCE)-(WH*(1-DCE)))*FA
      DELA(2)=DCE*FA                    d  derivatives for all species
      DELA(3)=DCE*FA                    dt
      DELA(4)=0.25*FA
      DELA(5)=0
```

```
      DELA(6)=0
      DELC(1)=((3*NR/8)-(WA*DCE)+(WH*(1-DCE)))*FA
      DELC(2)=((-NR/8)-DCE)*FA
      DELC(3)=((-NR/4)-DCE)*FA
      DELC(4)=0
      DELC(5)=0.5*(1-NR)*FA
      DELC(6)=NR*FA/8
      END
C
C     **********
C     VENT LOSS SUBROUTINE
C     **********
C
      SUBROUTINE VENT(LOSSA,LOSSC,Y,DELA,DELC,TVA,TVC)
      IMPLICIT REAL (A-Z)
      INTEGER N
      DIMENSION LOSSA(6),LOSSC(6),Y(6),DELA(6),DELC(6),TVA(6),TVC(6)
      COMMON F,I,KM,PA,PC,R,S,DT,TEMP,WA,WH,RHOG,X
      VENTA=(PA*DT*RHOG)+DELA(4)
      VENTC=(PC*DT*RHOG)+DELC(5)
      DO 300 N=1,6
      LOSSA(N)=Y(N)*VENTA          Determine vent losses from Yi's
      LOSSC(N)=Y(N)*VENTC
      VENTA=VENTA+LOSSA(N)         Revise vent flowrate as species calculated
      VENTC=VENTC+LOSSC(N)
300   CONTINUE
      LOSSA(4)=DELA(4)
      LOSSC(5)=DELC(5)
      DO 400 N=1,6
      TVA(N)=TVA(N)+LOSSA(N)       Take vent losses from electrolyte
      TVC(N)=TVC(N)+LOSSC(N)
400   CONTINUE
      END
```

Appendix 7

Appendix 7 - Completed publications

Table A7.1 shows a list of publications that have been completed during the course of the research contributing to this thesis. It includes poster presentations, oral presentations and a journal publication. Those papers highlighted with an asterisk were published in a refereed journal or conference proceedings with an ISBN number. Copies of them are included at the end of this appendix.

In addition to the publications listed in Table A7.1, I hope to complete two more papers before the end of my research. These are to be based on some of the areas discussed during the course of the thesis. The preliminary titles are likely to be:

1. Defining water transport in electro-membrane processes.

2. A novel and useful parameter for the performance characterisation of anion exchange membranes in acidic environments - definition and application to modelling.

Publications to date

Conferences

1. Robbins B J, Field R W, Kolaczkowski S T, Lockett A D (1995) 'Pilot studies of electro-membrane processes for acid recovery' *Electrochem '95 10-14 September 1995, University of Bangor*

2. *Robbins B J, Field R W, Kolaczkowski S T, Lockett A D (1995) 'Concentration and recovery of nitric acid via electrically enhanced membrane processes' *Euromembrane '95, ISBN 1 873703 69 4* pp I532-I535

3. Robbins B J, Field R W, Kolaczkowski S T, Lockett A D (1996) 'Evaluation of electro-membrane processes for acid recovery via laboratory pilot studies' *1996 IChemE Research Event 2-3 April 1996, University of Leeds* pp609-611

4. Robbins B J, Field R W, Kolaczkowski S T, Lockett A D (1996) 'Important considerations for ion exchange membranes in acid recovery' *ICOM '96, 18-23 August 1996, Yokohama, Japan* pp514-515

5. *Robbins B J, Field R W, Kolaczkowski S T, Lockett A D (1996) 'Laboratory pilot studies of electro-membrane processes for the recovery and concentration of nitric acid' *CHISA '96, ISBN 80 7080 263 4* ppP9.124

6. Robbins B J, Field R W, Kolaczkowski S T, Lockett A D (1996) 'The technical and economic impact of deviations from ideality in electro-membrane processing of nitric acid' *Electrochem '96, 16-19 September 1996, University of Bath*

Journal

7. *Robbins B J, Field R W, Kolaczkowski S T, Lockett A D (1996) 'Rationalisation of the relationship between proton leakage and water flux in anion exchange membranes' *J. Memb. Sci.* 118 pp101-110

Table A7.1: List of publications

Euromembrane '95

DP9 **Concentration and recovery of nitric acid via electrically enhanced membrane processes**

B J Robbins, R W Field S T Kolaczkowski, A D Locket
School of Chemical Engineering, University of Bath, Bath, *United Kingdom*

Keywords: *electrodialysis, electro-electrodialysis, acid recovery*

Abstract

Electromembrane concentration of dilute nitric acid using anion exchange membranes from Solvay SA is studied. Differential current efficiencies and water flux are determined for each system. Current efficiency decreases with increased concentration but the decline differs between membranes. The low volumetric water fluxes provide the potential for improved product concentration but this advantage is counteracted by relatively low current efficiencies.

1 Introduction

Many industrial processes generate low-grade acidic waste streams. Current treatment techniques are neutralisation followed by post-treatment and/or dilute discharge to water courses. With environmental legislation becoming tighter technology is required for current and developing processes to meet new legislative targets. Only recently have membranes become available allowing electromembrane processes to be considered for acid recovery (Cherif, 1988).

2 Electromembrane processes

Electromembrane processes combine the selectivities of ion-exchange membranes with electrochemical charge transfer at electrodes. Electromembrane synthesis is used on a large scale in the chlor-alkali industry whilst electromembrane separation is employed for potable water desalination. In this paper the electromembrane processes considered are: electrodialysis (ED) and electro-electrodialysis (EED). ED consists of alternating anion and cation permeable membranes forming many tens of unit cells between a single pair of electrodes. Ion transfer results in alternate channels of high and low concentration as the electrical field drives the species against the concentration gradient. Working electrodes do not contact the process fluid but operate in a controlled rinse stream as in figure 1.

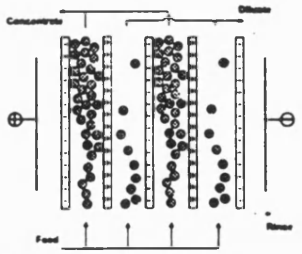

Figure 1 - schematic of ED process (adapted from Kuppinger, 1993)

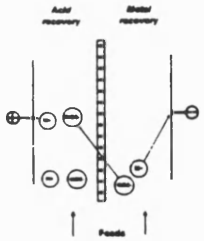

Figure 2 - EED ion movement showing metal plating

Unlike ED, EED utilises the electrochemical reactions at the electrodes. This requires a pair of electrodes for every unit cell which can increase costs significantly. Metals can be recovered on a cathode whilst acid is simultaneously transferred across the membrane (Cohen, 1991). Ion movement for EED of nitric acid is shown in figure 2. Fundamental studies have shown EED to be capable of achieving higher reconcentrated acid levels than ED (Elmidaoui, 1992) but with higher capital and operating costs. It has not been extensively studied as a demonstration/ pilot process for acid recovery.

2.1 Main theories

Ion movement in electromembrane processes is initiated by electrochemical charge transfer at the electrodes. As such the total number of moles of a species transferred is governed by Faraday's law. This is adapted in practice using an efficiency term, to account for non-idealities, to yield equation 1.

$$N = \eta \frac{it}{z\mathfrak{F}} \qquad [1]$$

Current efficiency relates the performance of a process to a maximum theoretical prediction and is therefore extremely useful for process evaluation. There are two definitions of current efficiency: integral current efficiency (ICE) and differential current efficiency (DCE). ICE relates the performance of a process over the duration of its operation and is appropriate for batch operation, whereas the DCE is an instantaneous current efficiency value (over a differential element of time). They are defined by equations 2 and 3. Although the ICE is only strictly valid for batch processing, it is most easily determined from experimental measurements. The DCE is very sensitive to small measurement errors and fluctuations; the error in terms of an absolute concentration may be slight but becomes significant with respect to concentration changes. To overcome this problem ICE data has been manipulated to derive credible DCE values. Ions passing through an ion exchange membrane are accompanied by a solvation shell of solvent molecules. Thus there is a water flux associated with ion transport. This is known as the electro-osmotic water flux. Volumetric flux (change with time) can be estimated using equation 4.

$$ICE = \frac{N(t) - N(0)}{F(t)} \qquad [2]$$

$$DCE = \frac{N(t+1) - N(t)}{F(t+1) - F(t)} \qquad [3]$$

$$V_{flux} = \frac{\Delta V}{F} \qquad [4]$$

3 Experimental

The electromembrane stack is based around an ICI FM01 laboratory electrolyser which can be easily configured to study the different processes and membranes. An industrial ED unit would have many more chambers and a smaller inter-membrane gap. Differences in module design will have to be considered during process evaluation. The unit is operated in batch recirculating mode.

One frame of the electromembrane unit has a working area of $64cm^2$ and so membrane area is a multiple of this depending on the process configuration. Temperature control is achieved using in-line heat exchangers and a refrigerated recirculating chiller. Chemical analysis of the system is

by titration with standard NaOH to determine total acid concentration. Further measurements are made using on-line digital density meters which are used to infer concentration changes during an experiment. Initial runs have been for an EED configuration at a current density of 300 $mAcm^{-2}$. To date a full set of data has been obtained for two membranes: ADP and ARA. Both supplied by Solvay SA, France.

3.1 Results and discussion

The concentration variations during an experiment are given in figure 3 for both membranes. Also shown are the associated voltage profiles which rise towards the end of a run as ions available for current transport become depleted. The voltage rises occur at different times but at similar diluate concentrations. Zero acid is not possible in the diluate as the electrolyte must retain some conductivity.

Using the assumption of linear volume variation between measurements the total moles of acid in the system can be determined. Hence the ICE is be determined using equation 2. Curves are fitted to manipulate the data to obtain DCE values. Both the ICE and the associated curve fits are shown in figure 4.

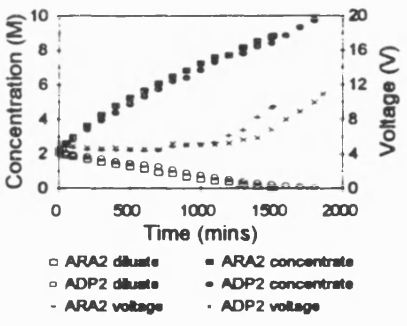

Figure 3 - concentration & voltage variation with time

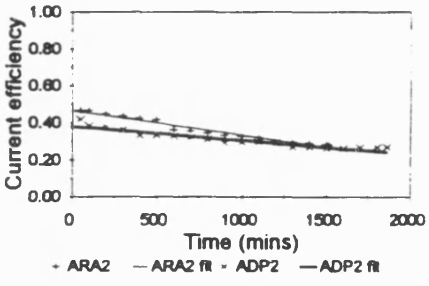

Figure 4 - ICE against time showing curve fits

Equations 2 and 3 can be combined with the curves fitted in figure 4 to generate DCE values. These can be seen plotted against the trans-membrane concentration difference in figure 5. Unlike ICE this relationship is not linear, especially at large concentration differences. When the DCE has a zero value no useful transport occurs across the membrane.

Volumetric water flux associated with ion transport is shown in figure 6. This flux will ultimately limit the maximum concentration of acid possible in the concentrate. It decreases with increased concentration difference which implies that the net water flux through the membrane is dictated by the external acid conditions. This interesting phenomenon is key to process performance and will be elaborated in future work.

4 Conclusions

DCE decreases with concentration difference which will probably be due mainly to proton leakage. For a low concentration difference ARA has the highest efficiency but ADP performs better at higher values. The values of current efficiencies are low compared to many industrial

processes. The membrane with highest current efficiency has associated with it the highest water flux which limits the maximum reconcentration level; in these runs ARA is most efficient overall but only achieves around 8.5M concentrate; ADP is less efficient but attains closer to 10M product. Water flux is low compared to other electrolytic processes but is counteracted by low current efficiencies which give rise to a high recovered acid cost. A balance between electrical cost and reconcentration level must be made.

Other process parameters, configurations and alternative membranes must also be studied in order for a complete process evaluation to be completed. Standard reference electrodes should also be included to develop a good cell model for use in module design.

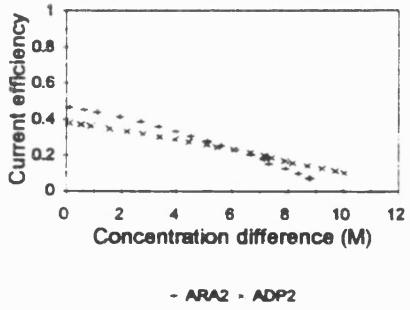

Figure 5 - generated DCE against trans-membrane concentration difference

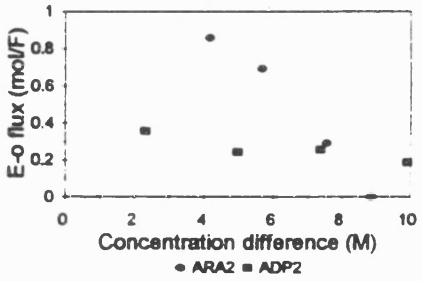

Figure 6 - volumetric flux against trans-membrane concentration difference

5 List of symbols

η	current efficiency	i	current (A)
$\mathfrak{F}$	Faraday constant (As mol^{-1})	N	moles transferred (mol)
ΔV	volume change in concentrate (m^3)	N(t)	number of moles at time t (mol)
V_{flux}	volumetric flux (m^3F^{-1})	t	time (s)
F	Faradays of charge passed	z	species valency
F(t)	number of Faradays passed at time t		

6 Acknowledgement

The authors would like to express their gratitude to the Defence Research Agency (Chemical Process Research) for funding this on-going project.

7 References

- Cherif AT, Gavach C, Cohen T, Dagard P, Albert L (1988) *Hydrometallurgy* 21 pp191-201
- Cohen T (1991) *Journées d'études SEE* Gif-sur Yvette, France pp196-199
- Elmidaoui A, Cherif A T, Brunea J, Duclert F, Cohen T, Gavach C (1992) *J. Memb. Sci.* 67 pp263-271
- Kuppinger F, Neubrand W, Eigenberger G (1993) *Comett course 11-14 Oct 1993* Stuttgart: University of Stuttgart

CHISA '96

Laboratory pilot studies of electromembrane processes for the recovery and concentration of nitric acid

Brian J Robbins, R W Field, S T Kolaczkowski & A D Lockett
University of Bath, School of Chemical Engineering, Bath, BA2 7AY, UK

Evaluation of electromembrane processes for nitric acid processing using a laboratory pilot rig is presented in this paper. The paper pays particular attention to the interesting process phenomena revealed during the research which includes deviations from ideality such as electrochemical side reactions and membrane leakage. In addition to improved theoretical understanding the technical and economic impact of these factors on the system is evaluated to give bottom-line process conclusions.

Many industrial processes generate low-grade acidic waste streams. Current treatment techniques are neutralisation followed by either post-treatment or dilute discharge to water courses. With environmental legislation becoming tighter, technology is required for current and emerging processes to meet new legislative targets. Only recently have membranes become available allowing electromembrane processes to be considered for acid recovery.

In order to study the new range of commercially available ion exchange membranes an experimental laboratory pilot rig was designed and built capable of studying processes such as electrodialysis (ED) and electro-electrodialysis (EED) over a range of operating conditions. The factor most affecting current efficiency in electromembrane acid processing is proton leakage through anion exchange membranes. In order to avoid the decoupling problems arising from using membrane pairs in ED and to focus on the performance characteristics of anion exchange membranes, an EED configuration was employed in the experimental work.

The simplest model of an EED stack processing nitric acid consists of nitrate transport across the membrane with hydrolysis reactions occurring on the electrodes. However in practice co-ion transport across the membrane and cathodic nitrate reduction reactions were found to be significant. This required a more detailed study of the process in order to understand the system. Analysis of both vent gas and the liquid phase along with other process measurements were used to quantify electrochemical transformations and membrane transport properties.

It was found, under certain conditions, almost all of the current went to nitrate electrochemistry rather than simple hydrolysis. This gave rise to the accumulation of nitrogen containing species (e.g. NH_4^+) which could not be transported across the membrane. Despite being a deviation from ideality these side reactions did yield some significant processing advantages. Membrane transport studies focused on two important factors: proton leakage and electroosmotic water flux. It was found that proton transport increased with increasing acid concentration but that the electroosmotic water flux decreased with a similar change in conditions. This meant that the same membrane operated less electrically efficiently had the potential to yield a stronger acid product. Thus a balance between electrical power consumption and recovered acid specification has to be made. This interesting phenomena lead to the development of a consolidated proton leakage and water flux model describing the performance of a membrane based on its state under various process conditions.

Whilst EED was found to be a high-cost low-efficiency process for high strength acids the data generated is being used laterally for further commercial electromembrane process evaluation.

The authors would like to express their gratitude to the DRA (Chemical Process Research) for funding this work

Journal of Membrane Science

ELSEVIER

Journal of Membrane Science 118 (1996) 101–110

journal of MEMBRANE SCIENCE

Rationalisation of the relationship between proton leakage and water flux through anion exchange membranes

Brian J. Robbins *, R.W. Field, S.T. Kolaczkowski, A.D. Lockett

University of Bath, School of Chemical Engineering, Claverton Down, Bath, BA2 7AY, UK

Received 31 July 1995; revised 15 February 1996; accepted 20 March 1996

Abstract

Electromembrane concentration of nitric acid using anion exchange membranes has been studied in a laboratory pilot rig. The main factor limiting acid concentration has previously been reported to be proton leakage but in the present work water flux is also shown to be significant. Differential current efficiencies and mean water transport numbers are determined for each system via mathematical manipulation of batch data. Water flux appears to be closely linked to proton leakage as an improvement in one of these leads to a deterioration of the other. Previous proton leakage theories have been developed further and a proton leakage and water flux model, based on sorbed species and their interactions within the membrane, has been postulated. It is suggested that the absolute amount of sorbed acid is more significant than the sorbed acid:water ratio. The model is validated by numerous cited publications, in addition to the data presented herein, to explain the performance variation of a given membrane when subjected to different operating conditions. Future work should consider water flux along with proton leakage as figures of merit for process evaluation, and investigate the applicability of the model to the comparative performance of different membranes when subjected to identical operating conditions.

Keywords: Electrodialysis; Electro-electrodialysis; Acid recovery; Proton leakage; Electro-osmosis

1. Introduction

Many industrial processes generate low-grade acidic waste streams. Current treatment techniques are neutralisation followed by post-treatment and dilute discharge to water courses. With environmental legislation becoming tighter technology is required for current and developing processes to meet new legislative targets. Only recently have membranes become available allowing electromembrane processes to be considered for acid recovery [1].

* Corresponding author. Tel.: +44 1225 826826, ext. 4840; Fax: +44 1225 826894; E-mail: cesrwf@bath.ac.uk.

2. Electromembrane processes for acid concentration: background

Electromembrane processes combine the selectivities of ion-exchange membranes with electrochemical charge transfer at electrodes. Industrially, electromembrane synthesis is used on a large scale in the chlor-alkali industry whilst electromembrane separation is employed for potable water desalination.

Electrodialysis (ED) consists of alternating anion and cation exchange membranes forming many tens of unit cells between a single pair of electrodes. Ion transfer results in alternate channels of high and low concentration as the electrical field drives the species

0376-7388/96/$15.00 Copyright © 1996 Elsevier Science B.V. All rights reserved.
PII S0376-7388(96)00095-6

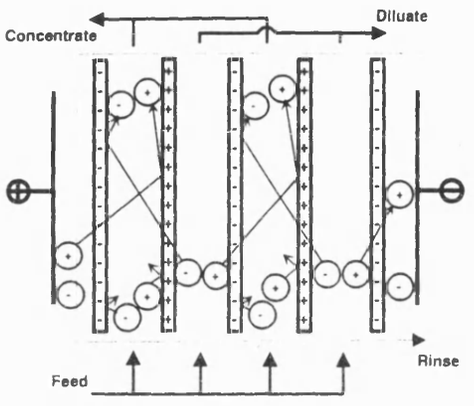

Fig. 1. Electrodialysis ion movement showing alternate concentrated and dilute channels.

against the concentration gradient. Working electrodes do not contact the process fluid but operate in a controlled rinse stream as in Fig. 1.

Unlike ED, electro-electrodialysis (EED) utilises the electrochemical reactions at the electrodes. This requires a pair of electrodes for every unit cell which can increase costs significantly. Metals can be recovered on a cathode whilst acid is simultaneously transferred across the membrane [2]. An example of ion movement for EED of nitric acid is shown in Fig. 2.

EED has been shown to be capable of achieving higher acid concentrations than ED [3]. This is due to the higher water flux in ED through both the anion and cation exchange membranes. However EED has higher capital and operating costs due to the increased number of working electrodes. EED has not been extensively studied as a demonstration/ pilot process for acid recovery.

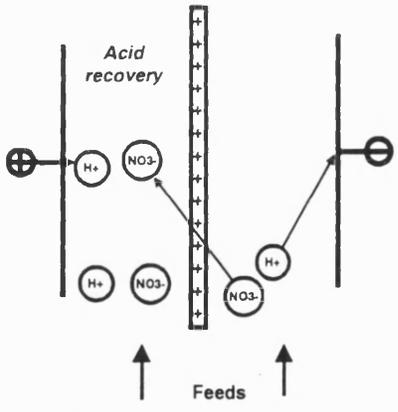

Fig. 2. Example of electro-electrodialysis ion movement for nitric acid recovery.

The two key parameters that determine the performance of an electromembrane acid concentration process are current efficiency and electro-osmotic water flux.

2.1. Current efficiency

Ion movement in electromembrane processes is initiated by electrochemical charge transfer at the electrodes. The Faradays of charge passed over in given time is defined by Eq. (1) the simpler form being applicable to constant current operation. This is applied using an efficiency term, to account for non-idealities, to yield the general Eq. (2).

$$F = \frac{\int_0^t i\,dt}{\Im} \equiv \frac{it}{\Im}\,(\text{constant current operation}) \qquad (1)$$

$$N = \eta\frac{F}{z} \qquad (2)$$

Current efficiency relates the performance of a process to a theoretical maximum and is therefore extremely useful for process evaluation. There are two definitions of current efficiency: integral current efficiency (ICE) and differential current efficiency (DCE). ICE relates the performance of a process over the duration of its operation and is appropriate for batch operation. It is defined mathematically by Eq. (3) and determined in practice using Eq. (4) where N is increasing with time.

$$\text{ICE} = \frac{Nz\Im}{\int_0^t i\,dt} \qquad (3)$$

$$\text{ICE} = \frac{N(t) - N(0)}{F(t)} \qquad (4)$$

On the other hand the DCE is an instantaneous current efficiency value over a differential element

of time. The mathematical formula for DCE is given by Eq. (5) and it is determined experimentally using Eq. (6).

$$\mathrm{DCE} = \frac{\mathrm{d}N}{\mathrm{d}t}\frac{z\mathfrak{F}}{i} \tag{5}$$

$$\mathrm{DCE} = \frac{N(t+1) - N(t)}{F(t+1) - F(t)} \tag{6}$$

Although the ICE is only strictly valid for batch processing, it is most easily determined from experimental measurements. The calculated value of DCE is very sensitive to small measurement errors and fluctuations. Whilst the error in an absolute concentration may be slight it can become significant with respect to small concentration changes. To overcome this problem ICE data has been manipulated to derive credible DCE values. This mathematical manipulation is given in Appendix A.

2.2. Electro-osmotic water flux

In aqueous systems ions passing through an ion exchange membrane are accompanied by a solvation shell of water molecules. Thus there is a water flux associated with ion transport. This is known as the electro-osmotic water flux. The net water flux was estimated using Eq. (7) where ΔV is the change in volume over a given time. From this the familiar water transport number can be estimated using Eq. (8).

$$V_{\mathrm{flux}} = \frac{\Delta V}{F} \tag{7}$$

$$t_{\mathrm{H_2O}} = \frac{V_{\mathrm{flux}}\,\rho}{M_{\mathrm{R}}} \tag{8}$$

3. Experimental

The combination of both anion and cation exchange membranes in ED makes decoupling of performance data to obtain different membrane attributes extremely difficult. EED utilises only a single ion exchange membrane and has the potential to achieve higher acid concentrations due to the smaller total electro-osmotic water flux. Consequently an EED configuration was adopted for the experimental work.

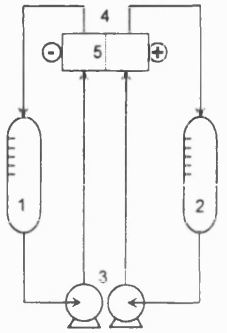

Fig. 3. Simplified schematic of experimental rig showing: 1, catholyte reservoir (10 dm^3); 2, anolyte reservoir (5 dm^3); 3, recirculating pumps; 4, EED stack; 5, anion exchange membranes (64 cm^2 multiple); (−) cathode and (+) anode.

The electromembrane stack was based around an ICI FM01 laboratory electrolyser which can be configured to study the different processes and membranes. Temperature control was achieved using in-line heat exchangers and a refrigerated recirculating chiller. Total acid concentration in the reservoirs was determined by volumetric analysis and further measurements were made using in-line digital density meters to infer concentration changes between samples. The experimental unit was operated in batch recirculating mode. A simplified schematic of the experimental rig is shown in Fig. 3.

As a result of proton leakage anion exchange membranes are the most significant source of inefficiency in an electromembrane process for acid recovery. Therefore performance assessment was made using various anion exchange membranes with nitric acid as a representative mineral acid. EED performance data at a current density of 300 mA cm^{-2} has been measured for the following anion exchange membranes: ADP, ARA, prototype AW (Solvay SA, France) and R5035 (RAI Research, USA). The results are discussed in Sections 3.1 and 3.2.

3.1. Results and discussion

Batch runs were started with equal anolyte and catholyte concentrations. Fig. 4 shows the typical concentration variations during an experiment for two runs both initially at 2 M. It should be noted that

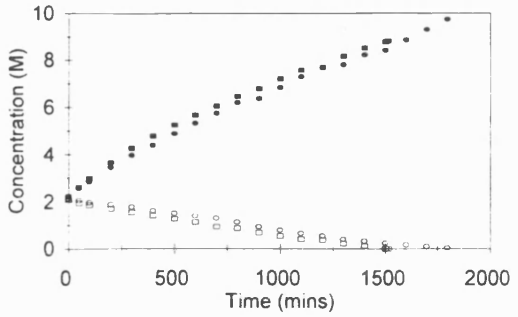

Fig. 4. Typical concentration variation with time for ADP and ARA membranes (□, ARA2 catholyte; ■, ARA2 anolyte; ○, ADP2 catholyte; ●, ADP2 anolyte).

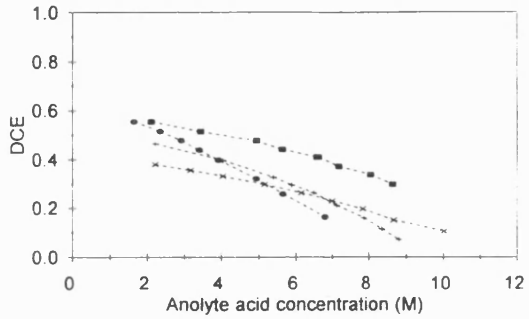

Fig. 6. Generated differential current efficiency (DCE) against acid concentration in anolyte for various membranes (■, AW2; ●, RAI2; +, ARA2; ×, ADP2).

ions must always be present in the catholyte in order to retain adequate conductivity for the process to operate.

Both the ICE and the associated curve fits are shown in Fig. 5. DCE values calculated using the method described in Appendix A are plotted against anolyte acid concentration in Fig. 6. The significance of the anolyte concentration is discussed in Appendix B. For all the membranes studied the DCE decreases with increasing anolyte acid concentration but the rate of decrease varies between membranes. If the DCE drops to zero no useful transport occurs across the membrane.

Previous work has focused on proton leakage as the limiting factor in acid concentration [4] and so has reported current efficiency as the main figure of merit. However a further important factor is the water flux associated with ion transport. Ultimately the maximum acid concentration cannot be greater than the concentration of acid being transported through the membrane. For example if a single mole of water is transported with every mole of acid, and if electrolytic water consumption is neglected, the mole-fraction of the product cannot exceed 0.5.

The mean water transport number is shown for different membranes and operating conditions in Fig. 7. Allowance for water oxidation at the anode has been made when determining these values. Osmotic flux has been considered to be small in comparison as zero current experiments showed little/no detectable water flux even at relatively high concentration differences. It is found that, for all membranes examined, the water transport number decreases with increasing anolyte concentration. This interesting phenomenon is key to overall process performance.

It should be noted that a change in current efficiency would be expected to alter the water transport number even if the mol water per mol acid remains

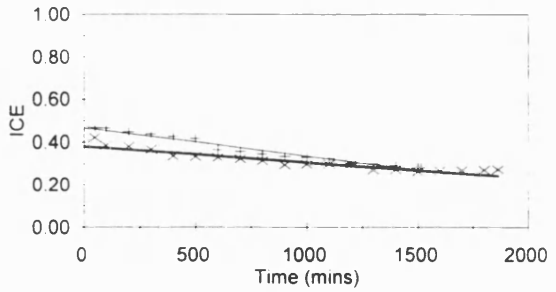

Fig. 5. Integral current efficiency (ICE) data against time showing mathematical smooth fits for ADP and ARA membranes (+, ARA2; —, ARA2 fit; ×, ADP2; —, ADP2 fit).

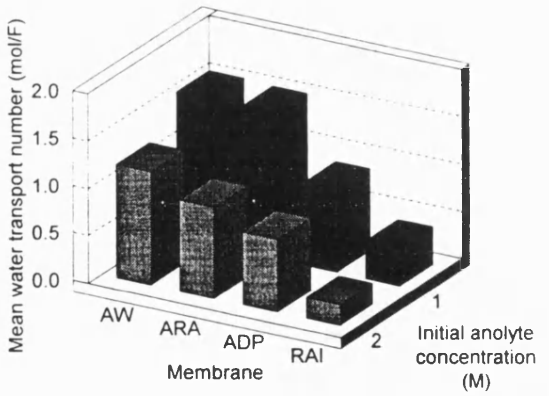

Fig. 7. Mean water transport numbers for various experimental systems showing variation of membranes and initial batch conditions.

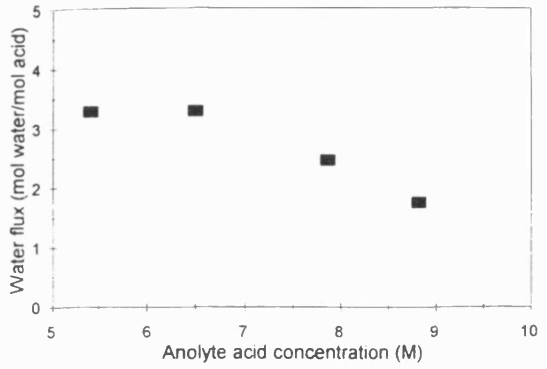

Fig. 8. Water flux in terms of mol water per mol acid against anolyte acid concentration for a typical experimental run (ARA2, ■).

unchanged. Fig. 8 shows how the water flux (in terms of mol water per mol acid) varies with anolyte concentration for a typical membrane. For this case the decrease in water transport with increasing anolyte concentration is greater than can be attributed solely to current efficiency, which suggests that the solvation shell is becoming smaller.

3.2. Summary of results

DCE decreases with increasing acid concentration in the anolyte. This is due mainly to proton leakage. The rate of decrease of efficiency varies between membranes. In addition to this a high efficiency membrane (such as AW) has a relatively high water transport number (≈ 1.1 mol F^{-1}) whereas a low efficiency membrane under similar operating conditions (such as RAI) has a much lower water transport number (≈ 0.2 mol F^{-1}). In acid recovery processes a low water flux gives rise to a higher concentration product but high acid strengths decrease the electrical efficiency. Therefore a balance between electrical cost and product concentration must be made.

4. Consolidated proton leakage and water flux theory

As mentioned in Section 3.1 previous work has focused on the importance of proton leakage through anion exchange membranes, but has largely ignored the impact of water flux. In order to understand the phenomenon of proton leakage detailed fundamental experimental studies were undertaken by other workers. Analysis of their work has lead to an improved understanding of the factors controlling transport through anion exchange membranes and has assisted the development of the consolidated proton leakage and water flux model given in this paper.

Important trends reported by previous workers are highlighted below and their conclusions have been compiled, in conjunction with new work, to postulate an explanation of the relationship between proton leakage and water flux. It should be noted that previous data was published for different membranes and acids. However the ion exchange membranes and inorganic acids that were studied were sufficiently similar to allow general conclusions to be drawn in order to reinforce the proposed mechanisms.

4.1. Previous work on proton leakage

An early study demonstrated that the amount of swelling water in a membrane increases linearly with increase in exchange capacity and found that in acid solutions the amount of sorbed acid depends on the water content of the membrane [5]. Further work [4] found that the amount of sorbed acid increased approximately linearly with increasing external acid concentration but different anions were sorbed in dissimilar amounts. More recent studies found that, for a given membrane, the amount of sorbed water decreased with increasing external (and hence sorbed) acid [6,7,10]. It was also noted that the electro-osmotic water flux decreased with increasing external acid concentration. Subsequent analysis of these results revealed that the total molar hold-up of sorbed species in a given membrane remained approximately constant ($\pm 10\%$). Recent work on cellulosic ion-exchange membranes also shows the electro-osmotic water flux to decrease with increasing electrolyte concentration [12].

Perhaps one of the most significant conclusions to date on the subject of proton leakage was that for three different membranes (1 cation and 2 anion) the loss of proton transport was attributed to an increase in the sorbed acid:water ratio [6]. Further work [7,8]

showed no undissociated acid to be present in the membrane. A mechanistic explanation of the effect of acid:water ratio was not proposed. It should be noted that the proton transport mechanism in anion exchange membranes must differ significantly to that found in cation exchange membranes which are specifically designed to transport protons via the active ion exchange groups. Additionally, the acid:water ratio appears to have little/no effect on proton transport when a given anion exchange membrane is subjected to different operating conditions [6,7,10].

It is unlikely that transport of protons is accompanied by the transport of water due to their extraordinary mobility via proton tunnelling [9]. Solvation decreases the mobility of an ion whereas proton leakage results from enhanced mobility. For example solvated cations such as Na^+ do not leak anywhere near as readily through anion exchange membranes as protons. It has also been shown that the ratio of ionic mobilities (H^+:Cl^-) in the membrane phase does not differ widely from that in water [10].

In summary proton leakage is affected both by the absolute and relative amounts of sorbed acid and water in anion exchange membranes.

4.2. Heterogeneous nature of anion exchange membranes

A simplistic model of an anion exchange membrane (e.g. based on a constant electro-osmotic water flux per mole of anions transported) would predict a decrease in water flux with increased proton leakage. However a more detailed understanding of the membrane structure is required in order to understand the mechanistic relationship between proton leakage and water flux.

Perfluorinated ion exchange membranes are currently regarded as heterogeneous in terms of polymeric and ion transport regions [10,11]. Detailed studies on cation exchange membranes [11] proposed an essentially two-phase model comprising a hydrophobic polymer backbone and hydrophilic ion exchange groups including sorbed water. A more recent study, specifically focused on anion exchange membranes [10], proposed a three-phase membrane model that incorporates co-ion leakage, comprising hydrophobic polymer, active ion exchange zone and interstitial sorbed acid zone. Sorbed water is divided between the active and interstitial zones. This representation of the membrane has been used to develop the consolidated model given in this paper and is illustrated in Fig. 9.

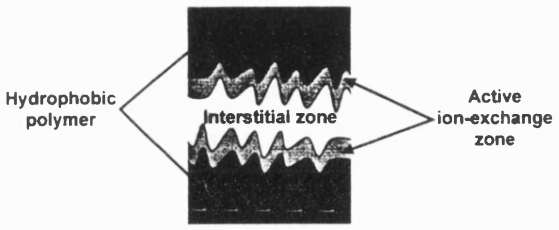

Fig. 9. Heterogeneous three-phase model of anion exchange membrane as proposed by Tugas [10] showing hydrophobic polymer, active hydrophilic ion-exchange zone and interstitial sorption zone.

In the proposed model it is assumed that sorbed water is partitioned between the active and interstitial zones of the membrane and that the degree of partition of the water between the zones is governed by interactions within the membrane between hydrophilic ion exchange sites, hydrophobic polymer matrix and solvation of the dissociated sorbed acid. It is this water partition which links proton leakage to electro-osmotic water flux.

In order to identify paths for ion transport it is useful to look at individual ion mobilities within the membrane. Using the three-phase membrane model, other workers have found the mobility of anions in the active zone of an anion exchange membrane to be greater than the mobility of anions in the interstitial zone [10]. Furthermore they found that, whilst the interstitial anion mobility remains approximately constant, the mobility of the active anions increases with increasing external acid concentration, and can be an order of magnitude greater than the interstitial anion mobility. Therefore it seems reasonable to assume that the majority of acid (anion) transport is via the active zone. On the other hand proton transport will occur mainly through the interstitial zone where repulsion by the ion-exchange sites is minimal and where protons can be exchanged with those already sorbed in the matrix. Consequently the electro-osmotic water flux will be governed primarily by the solvation of anions in the active zone whereas proton leakage will depend on the absolute acid sorption in the interstitial zone.

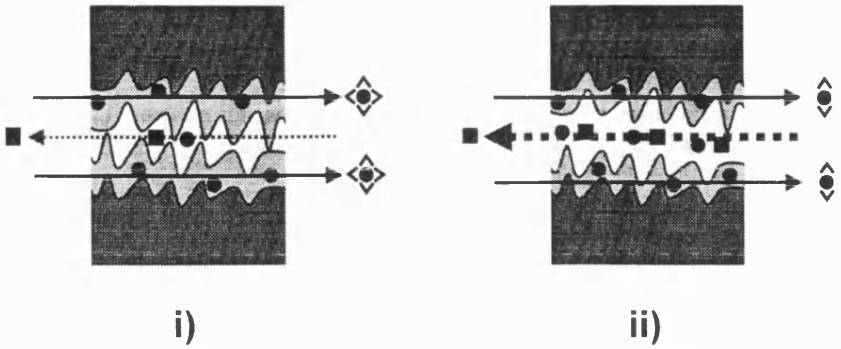

Fig. 10. Illustration of proposed consolidated proton leakage and water flux theory to explain the variation in performance of a given membrane under different external acid concentrations (●, solvated acid anion; ■, proton; key for zones as Fig. 9). (i) Low external acid concentration results in low acid sorption with low proton leakage. Water partition towards the active zone gives a high electro-osmotic water flux. (ii) High external acid concentration yields high acid sorption which enhances proton transport. Water partition towards interstitial zone due to solvation requirements of dissociated sorbed acid. Electro-osmotic water flux is smaller due to the low hydration of the active zone. There is no intention to represent the complex structure as a simple pore which may be indicated visually.

It is emphasised that the interstitial zone is neither a pore nor cylindrical in shape and may in reality be not continuous.

4.3. Consolidated model for proton leakage and water flux

Proton transport is governed by the absolute amount of sorbed acid in the interstitial zone. For a particular membrane, proton transport appears to be most strongly affected by absolute acid sorption but only minimally by variation in the acid:water ratio. For typical membrane data given in the literature $t_{H^+} \propto (n_{acid})^2$ appears to be a good approximation over a limited range of acid concentrations [10]. Electro-osmotic water flux is governed by the sorbed water in the active zone and hence the partition of water between the active and interstitial zones.

For a given membrane, as the external acid concentration is increased the acid sorption increases giving rise to a reduction in the overall sorbed water

Table 1
Validation of the main features of the consolidated proton leakage and water flux model using supporting citations

Feature	Characteristic and supporting citations
1. Membrane structure	Heterogenous three-phase model involving: hydrophobic polymer; active hydrophilic ion exchange groups and interstitial zones [10,11].
2. Water sorption	Linear relationship between water content and exchange capacity [5]. Water sorption decreases with increased acid sorption [6].
3. Acid sorption	Dependent on amount of sorbed water [5] and increases with increasing external acid concentration [4]
4. Total sorption (molar hold-up)	Remains approximately constant for a given membrane [6,7,10]
5. Water partition	Water partitioned between active and interstitial zones [10]. Partition varies with amount of sorbed species (hypothesis of model).
6. Proton transport	Increases with external acid concentration and increased acid sorption [10]. As a result of their enhanced mobility [9,10] proton transport does not involve a solvation shell.
7. Electro-osmotic water flux	Related to active anion (acid) transport. The smallest solvation shell coincides with the greatest mobility [10]. Electro-osmotic flux decreases with increasing external acid [6] because water associated with active anions decreases.

content. The sorbed water partition shifts towards the interstitial zone because of increased solvation requirements. This reduces the water content of the active zone, thereby increasing the active anion mobility, and decreasing the electro-osmotic water flux. The increase in sorbed acid significantly enhances proton transport. This is illustrated in Fig. 10.

It is difficult to visualise this interaction when comparing different membranes because of the multivariability introduced by not fixing the membrane. However, in general terms, reduced proton leakage would result from decrease in the absolute acid sorption in the interstitial zone. This in turn might be expected to give rise to increased active zone hydration and hence a greater electro-osmotic water flux.

4.3.1. Validation of consolidated model

In order to validate the proposed consolidated proton leakage and water flux model Table 1 lists its main features and the relevant supporting citations. Its applicability to different membranes is further reinforced by the results given in this paper.

4.3.2. Summary of consolidated model

The consolidated proton leakage and water flux model highlights the need to consider absolute acid sorption rather than sorbed acid:water ratio when assessing proton leakage for a given membrane. It draws together proton leakage theories and describes the relationship between proton transport and electro-osmotic flux via the variation of water partition between the active and interstitial zones of an anion exchange membrane. The consolidated model describes why the same membrane yields a stronger acid product when operated less efficiently.

Whilst the qualitative agreement between the consolidated theory and the numerous data sources is extremely strong when considering the change in performance of a single anion exchange membrane, at this stage it is only possible to hypothesise a relationship between different membranes because of the complexity of the problem and the lack of data in this area. Therefore the model has not yet been validated with fundamental measurements to explain the similar phenomenon that inefficient membranes appear to have a lower water flux than their higher efficiency counterparts. It nevertheless agrees with qualitative process measurements.

5. Conclusions

In many electrochemical processes it is important to consider the solvent flux across a membrane as this has a non-electrical effect on the overall process performance. This is certainly the case for acid concentration. Other process parameters, configurations and alternative membranes must also be studied in order for a complete process evaluation to be completed. For design purposes therefore, future work in this area should report water flux along with current efficiency as figures of merit for membrane evaluation.

The consolidated proton leakage and water flux model propounds that a reduction in proton leakage would lead to increased water flux which is found in practice. The theory has been validated to explain the variation in proton transport and water flux for a given membrane with different external acid concentrations. When the external concentration increases, proton leakage becomes more significant and current efficiency drops along with the water flux. Water flux is closely linked to proton leakage and an improvement in one of these leads to a deterioration of the other. The same membrane, when operated inefficiently, yields a stronger acid product. Extension of theory to cover the similar trend found between different membranes has yet to be validated with fundamental measurements.

6. List of symbols

η	current efficiency
$\Im$	Faraday constant (A s mol^{-1})
F	Faradays of charge passed
$F(t)$	number of Faradays passed at time t
$f(t)$	function fitting experimental ICE data
i	current (A)
M_R	molecular mass (kg $kmol^{-1}$)
N	moles transferred (mol)
$N(t)$	number of moles at time t (mol)
n_{acid}	amount of sorbed acid (mol g^{-1} dry membrane)
ρ	density of liquid (kg m^{-3})
t	time (s)
t_{H^+}	proton transport number (mol F^{-1})
t_{H_2O}	water transport number (kmol F^{-1})

ΔV volume change in anolyte (m^3)
V_{flux} volumetric flux (m^3 F^{-1})
z charge number

Acknowledgements

The authors would like to express their gratitude to the Defence Research Agency (Chemical Process Research) for funding this work and their continued investment in projects involving electromembrane processes for environmental applications. We are also grateful to Solvay SA for providing the new prototype AW membranes.

Appendix A. Mathematical smoothing of ICE data

It is important to be able to study the differential current efficiency of an electrochemical system if the figure of merit is not to be history dependant. Due to the practical problems associated with determination of DCE directly, as mentioned in Section 2.1, ICE values must be manipulated mathematically via a smoothing technique to derive credible DCE values. As this technique is a relatively new tool in the area of electro-electrodialysis, and has only recently been realised by workers in this field, it is given in this appendix.

The ICE is be determined using Eq. (2) from Section 2.1. Curves are fitted to manipulate the data to obtain DCE values as explained below: if a smooth function, $f(t)$, is fitted to the ICE data then it can be expressed by Eq. (A1) which when rearranged gives Eq. (A2).

$$\frac{N(t)-N(0)}{F(t)} = f(t) \qquad \text{(A1)}$$

$$N(t) = N(0) + f(t)F(t) \qquad \text{(A2)}$$

Eq. (A2) can be rewritten to give the value for $N(t+1)$ as in Eq. (A3). These expressions can be incorporated into the definition of DCE given by Eq. (3) in Section 2.1 to determine it using the smooth ICE curve, $f(t)$. This is shown in Eq. (A4).

$$N(t+1) = N(0) + f(t+1)F(t+1) \qquad \text{(A3)}$$

$$DCE = \frac{f(t+1)F(t+1) - f(t)F(t)}{F(t+1) - F(t)} \qquad \text{(A4)}$$

This approach was adopted to generate the data shown in Figs. 6 and 11. As a result the efficiency values plotted represent their values at a given instant rather than an average over the duration of the experiment.

Appendix B. Significance of anolyte (downstream) acid concentration

For the consolidated model to hold true the DCE values for a particular membrane under the same set of conditions should be close regardless of the initial batch starting concentration. That is for a given concentration on each side of the membrane the DCE values should be similar. This comparison has been made using the ARA membrane starting from both 1 and 2 M initial batch charges. Data from these runs can be seen in Fig. 11.

It can be seen that the DCE values for the ARA membrane are very close when plotted against the concentration of acid in the anolyte. The deviation of the curves can be easily explained. At the point where there is 2 M acid in the anolyte ARA1 has less than 1 M acid in the catholyte as it occurs at an instant during the run, whereas ARA2 has an equally strong catholyte as both experiments were started with zero trans-membrane concentration difference. Thus for a 2 M anolyte concentration the sorbed acid in the membrane in ARA1 will be less than the equivalent point during ARA2. Consequently the efficiency in ARA1 will be higher than that of ARA2 as the average amount of sorbed acid in the membrane will be lower.

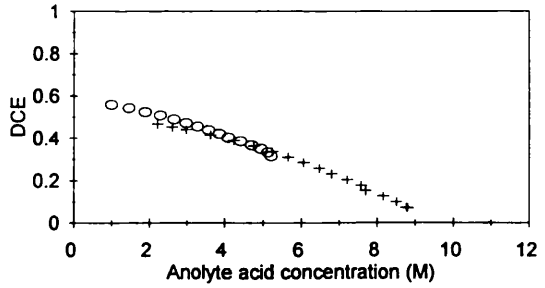

Fig. 11. Dependency of differential current efficiency on anolyte acid concentration for the ARA membrane with different initial experimental conditions (+, ARA2; O, ARA1).

The concentration of acid in the anolyte is most probably the most dominant factor for current efficiency as it is this face of the membrane through which proton leakage occurs (or is initiated). The dependence of DCE values on the average concentration and the trans-membrane concentration difference were also evaluated, however curves for runs ARA1 and ARA2 were distinct for apparently similar operating conditions indicating that absolute anolyte concentration is the most appropriate abscissa.

References

[1] A.T. Cherif, C. Gavach, T. Cohen, P. Dagard and L. Albert, Sulfuric acid concentration with an electro-electrodialysis process, Hydrometallurgy, 21 (1988) 191–201.

[2] T. Cohen, Recuperation des acides et des metaux par de nouvelles membranes echangeuses d'ions, J. Études SEE, (1991) 196–199.

[3] A. Elmidaoui, A.T. Cherif, J. Brunea, F. Duclert, T. Cohen and C. Gavach, Preparation of perflourinated ion exchange membranes and their application in acid recovery, J. Membrane Sci., 67 (1992) 263–271.

[4] A.T. Cherif and C. Gavach, Electrotransport of sulfuric acid by electro-electrodialysis, J. Electroanal. Chem., 265 (1989) 143–157.

[5] T. Cohen, P. Dagard, J. Molenat, B. Brun and C. Gavach, Proton leakage through perflourinated anion exchange membranes, J. Electroanal. Chem., 210 (1986) 329–336.

[6] G. Pourcelly, M. Boudet-Dumy, A. Lindheimer and C. Gavach, Transport of proton in polymeric ionic exchange membranes in relation with the dissociated sorbed acid, Desalination 80 (1991) 193–209.

[7] G. Pourcelly, I. Tugas and C. Gavach, Electrotransport of sulfuric acid in special anion exchange membranes for the recovery of acids, J. Membrane Sci., 97 (1994) 99–107.

[8] I. Tugas, J.-M. Lambert, J. Maillols, J.-L. Bribes, G. Pourcelly and C. Gavach, Identification of the ionic species in anion exchange membranes equilibrated with sulfuric acid solutions by means of Raman spectroscopy and radiotracers, J. Membrane Sci., 78 (1993) 25–33.

[9] F. Kuppinger, W. Neubrand and G. Eigenberger, Electromembrane processes, Comett Course Notes, 11–14 October 1993, University of Stuttgart, 1993.

[10] I. Tugas, G. Pourcelly and C. Gavach, Electrotransport of protons and chloride ion in anion exchange membranes for the recovery of acids. Part I. Equilibrium properties. Part II. Kinetics of ion transfer at the membrane–solution interface, J. Membrane Sci., 85 (1993) 183–204

[11] S.F. Timashev, Physical Chemistry of Membrane Processes, Ellis Horwood, Chichester, 1991, pp. 177–218.

[12] M.D. Reboiras, Electrochemical properties of cellulosic ion-exchange membranes II. Transport properties of ions and electro-osmotic flow, J. Membrane Sci., 109 (1996) 55–63.